Rheological Behaviour and Characterisation of Pitch-Based Carbon Precursors

Shatish Ramjee

Rheological Behaviour and Characterisation of Pitch-Based Carbon Precursors

by

Shatish Ramjee

A thesis submitted in partial fulfilment
of the requirements for the degree

Doctor of Philosophy (Chemical Engineering)

in the

Department of Chemical Engineering

University of Pretoria
Pretoria

February 22, 2015

SYNOPSIS

Pitch material is an important precursor in the production of carbon fibre, carbon composites and synthetic graphite. It has a complex transformation during pyrolysis which incorporates the separation of a liquid crystalline phase, known as mesophase. This thesis attempts to enhance the understanding of this change in composition, structure and its resultant behaviour.

In this study, two pitches, a coal-tar pitch (MP110) and a (SASOL) Lurgi-gasifier pitch, are pyrolised to produce material at different stages of mesophase development. These pitches produce mesophase of different mosaic type and therefore also resultant coke.

The MP110 was thermally treated up to a temperature of 437℃ and produced anisotropic pitch (which still contains significant particulate matter). The nucleated mesophase spheres did not coalesce to produce domains; this behaviour being attributed to the particulate material. The SASOL pitch produced a different type of mesophase material. The mesophase produced was of fine mosaic domains; a sample with continuous mesophase regions was also produced with a mesophase content of approximately 60% (by volume).

The aromatic starting material of MP110 produced higher quinolone and toluene insoluble (QI and TI) compounds after pyrolysis. This was also observed in the increase of C/H (molar ratio of carbon to hydrogen). The more aliphatic SASOL starting pitch showed similar trends to its MP110 counterparts with respect to QI (quinoline insolubles), TI (toluene insolubles) and C/H. The glass transition and associated temperatures of the pitches were analysed via thermal mechanical analysis (TMA), dynamic scanning calorimetry (DSC) and dynamic mechanical thermal analysis (DMTA). The techniques showed consistency between instruments, with TMA providing the likeliest reflection of the true thermodynamic glass transition temperature. The loss of volatile components was accompanied by an increase in glass transition temperature (observed in conjunction

with C/H and mesophase content). For anisotropic MP110 pitches, two relaxations were observed, one for the isotropic fraction, the other for the mesophase. No such behaviour was easily observed for the SASOL pitches.

Rheological measurements were obtained to understand the behaviour of the pitches. Measurements were limited to a specific viscosity range. The measurements of the samples were therefore made at different temperatures. The relation of the measurement temperature to the glass transition temperature is thus of extreme importance. The temperature governs the state of the structure; whether it be suspension, emulsion or gel.

Oscillatory shear experiments were undertaken for the pitch material. Predominantly isotropic material showed transition from viscoelastic solid to viscoelastic liquid as previously observed in pitch material.

The anisotropic MP110 pitches did not allow for the production of mastercurves due to non-linear viscoelastic effects caused by the softening of mesophase. This being the transition from a suspension of hard spheres to an emulsion of deformable droplets (depending on temperature).

For the higher mesophase content anisotropic SASOL pitches, mastercurves were produced; it had a similar shape to the isotropic pitches (at temperatures closer to the glass transition), but significantly increased elasticity was observed at higher temperatures. This phenomenon supported the hypothesis of a strong interaction between the components and phases of the pitch, and thus the possibility of gelled systems.

Rotational shear-rheometry was also utilised and showed that isotropic pitch material behaves as a predominantly isoviscous fluid.

The anisotropic MP110 pitches of approximately 30% mesophase showed high- and low-shear viscosity plateau fluid behaviour. This being caused by the breakup of agglomerated mesophase spheres. This was tested by the implementation of the Krieger-Dougherty suspension model. The possibility of droplet deformation was investigated for these samples by utilising a Krieger-Douherty based emulsion analogue, which confirmed suspension like behaviour (at the measured temperatures). MP110 samples with more mesophase were measured at higher temperatures. Their behaviour is more akin to Power-law shear-thinning behaviour. Being further away from the continuous isotropic phase glass transition temperature, the behaviour observed is similar to that of emulsions.

SASOL anisotropic pitches showed significant yielding upon shear, which is attributed to structure breakdown. This behaviour is appropriately described by a yield stress, shear-thinning model such as Herschel-Bulkley. Measurements of viscosity for these samples were made at temperatures significantly further from the glass transition temperature as compared to that of the MP110 pitches. This corroborates strong interaction between its components. The observed shapes of the curve, at temperatures of measurement, support the notion of a gel structure. This behaviour is first proposed via the complex structure observed (clusters of fine mosaic mesophase domains) and supported by strong

interaction of the components inferred from obtained rheological properties.

Keywords: pitch, mesophase, two-phase, mixture, coal-tar, Lurgi-Gasifier, characterisation, oscillation, rotation

ACKNOWLEDGEMENTS

This thesis is dedicated to my father, Mr. Harivadan Ramjee; without his guidance and sacrifice I would never have been in the fortunate position to produce this thesis. I would also like to thank my mother, Manorma, and two brothers, Preshant and Chetin, for supporting me through this endeavour.

I would like to thank Professor Brian Rand and Professor Walter Focke for the opportunity to partake in this project, as well as their guidance and supervision to help me through the unforeseen difficulties encountered.

A special thanks is attributed to Mrs Isbe van der Westhuizen and Mr Rainer Schumacher in providing assistance to focus on the project at hand. The help in producing the materials and running of equipment and instruments is greatly appreciated.

The support and communications of colleagues in the Institute of Applied Materials and the Department of Chemical Engineering at the University of Pretoria is also hereby acknowledged. The conversations have been stimulating and have allowed many a friendship to flourish. For this I am thankful.

This work is based upon research supported by the South African Research Chairs Initiative of the Department of Science and Technology (DST) and the National Research Foundation (NRF). Any opinion, findings and conclusions or recommendations expressed in this material are those of the authors and therefore the NRF and DST do not accept any liability with regard thereto.

CONTENTS

LIST OF FIGURES

LIST OF TABLES

NOMENCLATURE

$[\eta]$	Intrinsic viscosity	–
α_f	Thermal expansion of free volume relative to total volume	
δ	phase angle	rad
ϵ	strain	–
η	viscosity	$Pa.s$
η_0	zero-shear viscosity	$Pa.s$
η_c	Viscosity of continuous phase	Pa.s
η_d	Viscosity of dispersed phase	Pa.s
η_r	Reduced viscosity $\frac{\eta}{\eta_s}$	-
η_s	Viscosity of suspending fluid	$Pa.s$
η_T	Arrhenius Predicted Viscosity	$Pa.s$
η_T	viscosity at temperature T	$Pa.s$
η_∞	infinite-shear viscosity	$Pa.s$
η_{pl}	Plastic viscosity	$Pa.s$
η_{T_g}	viscosity at temperature T_g	$Pa.s$
γ	shear strain	–
ω	frequency	$rad.s^{-1}$

ϕ	Volume fraction of filler	$Pa.s$
ϕ_eff	effective volume fraction	–
ϕ_m	Maximum filler volume fraction	-
σ	shear stress	Pa
σ_B	Bingham yield stress	Pa
σ_{ST}	Surface tension	$N.m^{-1}$
τ	relaxation or retardation time	s
$\triangle H$	activation energy	$J.mol^{-1}.K$
a, b	Constants in the Doolittle equation	
a_t	shift factor	–
B	Fulcher, Tammamm and Hesse constant	K
C	Arrhenius Pre-exponential Constant	$Pa.s$
C_1^g, C_2^g	WLF constants at temperature T_g	
C_1	WLF constant 1	–
C_2	WLF constant 2	K
Ca	Capillary number	-
E	Modulus of elasticity in tension	Pa
E_η	Arrhenius Activation Energy	$J.mol$
f	fractional free volume	
f_g	fractional free volume at glass transition	
G	Modulus of elasticity in shear	Pa
G''	Loss modulus	Pa
G'	Storage modulus	Pa
G^*	Complex dynamic modulus	Pa
J	Creep compliance	Pa^{-1}

K	Viscosity ratio $\frac{\eta_d}{\eta_s}$	-
K_1	Power-Law Consistency Index	$Pa.s^{(n-1)}$
K_2	Herschel-Bulkley Consistency Index	$Pa.s^n$
K_3	Consistency Index	$Pa.s$
n	Behaviour Index	–
r	Droplet radius	m
T	Temperature	K
t	time	s
T_g	Glass transition temperature	K
T_R, T_r	Reference temperature	K
T_∞	Temperature at which viscosity approaches infinity	K
v	total volume per gram	
v_1, v_2, v_3	velocity scalars	$m.s^{-1}$
v_g	free volume per gram	
x_1, x_2, x_3	Euclidean co-ordinates	–

CHAPTER 1

INTRODUCTION

In the field of carbon research, there exists a subgroup dedicated to the processing, understanding and manipulation of material in the production of graphite. This involves the use of pitch as a binder or precursor material in the formation of carbon fibre, coke, carbon/carbon composites and graphite.

Pitch is a commonly available starting material, and is often the byproduct of other industrial processes. It can be thermally treated in a manner which results in graphite. During this process, the pitch transforms into mesophase (a liquid crystal material), which exhibits anisotropic properties. This carbonaceous mesophase upon further treatment, results in structurally fixed graphitisable coke. The final stage after coke, is thermal treatment to around 3000 ℃ and formation of the graphite structure.

Early stages in this transformation, from pitch to pure mesophase, is a complex topic. It is also vitally important to understand this, as many of the final graphite properties are influenced and fixed at this early stage. The manner in which the material transforms into mesophase, and its microstructure, properties and associated rheology are all linked. The study of the anisotropic pitches has previously been studied, and its composition and structure documented. The manner in which these systems interact is however not well understood. Rheology helps to give an insight into the interaction of the these two phase mixtures. This topic though is not as thoroughly documented. Studies have mainly been dedicated to dominant isotropic or mesophase materials. The partially anisotropic pitches lack information. This study attempts to fill some of this void. This is done by gathering some basic understanding of the composition and properties of the isotropic and anisotropic pitches. The resultant information used to guide the interpretation of rheological measurements; which is done in both rotational and oscillatory modes. Some modelling will also be attempted to try and corroborate and understand some of these results.

In this work, two pitches will be investigated: a locally (South African) available coal-tar pitch obtained from ArcellorMittal (given code: MP110), and a medium-temperature SASOL (Lurgi-gasifier) pitch (given code: SPAR). The pitch is thermally treated; resulting in pitches at different stages of transformation towards mesophase. These samples were chosen for two main reasons: they are from significantly different sources (thereby also different composition and properties), and produce different mesophase structure upon heat treatment.

CHAPTER 2

LITERATURE

Carbon precursors in the production of graphite, and other carbon composites, are often quite complex prior to carbonisation. Their chemical composition and physical properties are important in the production process; these properties contribute to the final properties of the graphite artefacts. Their rheological properties also affects the behaviour; as a result, in this document, more detail will be given to rheology.

Bearing this in mind, the literature study will be broken up into the following sections:

- Pitch Material and Mesophase Development
- Pitch and Mesophase Characterisation
- Concepts of Rheology
- Rheological Studies on Pitch and Mesophase Material

2.1 Chemistry Background

2.1.1 General Carbon Chemistry

Carbon has been utilised by man for a large part of human history, whether it be in the form of coal or graphite or one of its various other forms. In modern times though, the application and use of such materials has turned towards more technical aspects.

Carbon itself is a Group IV element that has various allotropes. The allotropes have both natural and synthetic states, eg. graphite and fullerene. The carbon atom has a valence of 4, with several covalent structures (Delhaes, 2001: 2):

- a tetrahedral arrangement, sp3 hybridisation with four bonds and neighbouring atoms which are that found in diamond (Figure 2.1) (Burchell, 1999: 4).
- sp2 hybridisation that has a trigonal planar arrangement, in the form of graphite, both π and σ bonds are present (Figure 2.2) (Burchell, 1999: 5).
- sp hybridisation which yield both single and triple bonds and referred to as carbynes (Burchell, 1999: 6).

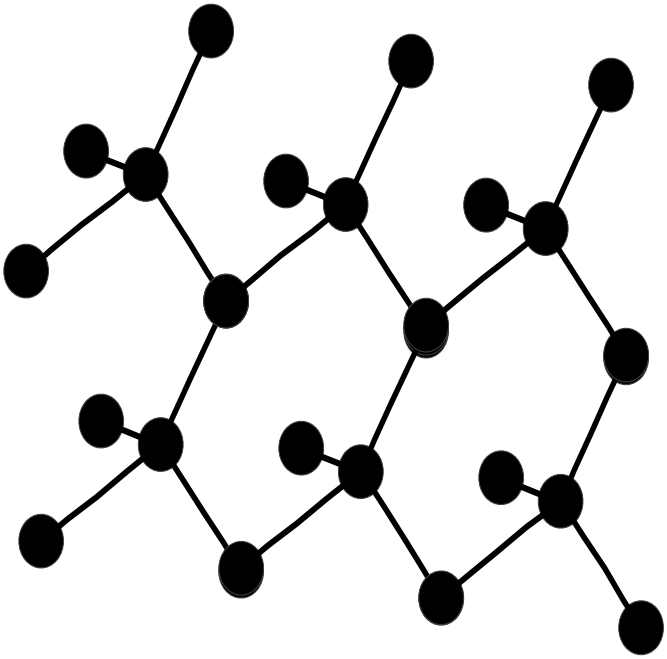

Figure 2.1: Structure of diamond via sp3 hybridisation

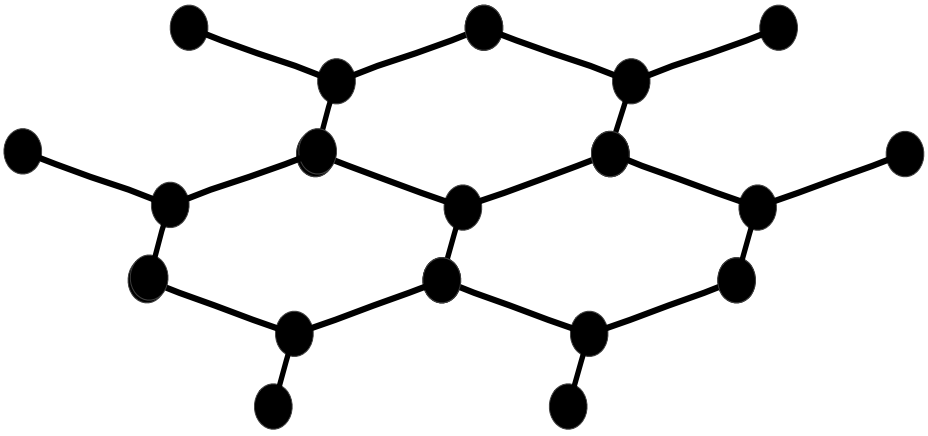

Figure 2.2: Structure of graphite via sp2 hybridisation

These carbon structures are all related to the crystal geometry by way of the different hybridisation. It is also possible to have a variability in hybridisation between different carbon atoms in the same molecule resulting in curvature in the structure. This has lead

to the rise in production and research of other allotropes of carbon such as nanotubes and fullerenes.

This is a very basic introduction to the different forms of carbon, Burchell (1999) and Delhaes (2001) have a thorough background in the thermodynamic and chemical properties of many of the natural and synthetic forms of carbon; there application, processing and structure.

2.1.2 Liquid Crystals

Liquid crystals are materials in a phase of state between a solid crystalline and an isotropic liquid. These materials flow like liquids, but they still have some structure associated with crystals (Stephen & Straley, 1974). The crystalline characteristic gives the material some order. An important characteristic, is that the molecules (referred to as mesogens), have order but still have freedom of movement. A graphical representation of this is shown in Figure 2.3.

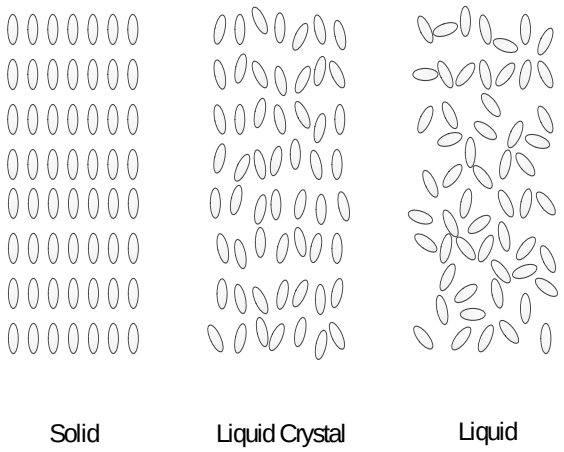

Figure 2.3: Simplified change in structure for different phases

The axis in which the mesogens are ordered is referred to as the director (Chandrashekhar, 1992: 85). In liquid state there is no order, and in the solid state it is highly ordered. Liquid crystals are anisotropic; and the extent of anisotropy is dependent on the average alignment of the director (in Figure 2.3, the director is vertical).

This liquid crystals, being anisotropic, results in other useful characteristics. The anisotropic nature allows for the change in electrical, optical and magnetic properties via manipulation of the orientation of the liquid crystals. Anisotropy of the liquid crystal also provided the manner whereby liquid crystals are categorised or classified into structures. Under polarised light microscopy conditions, the long range ordering is easily viewed. The polarised light only allows light from a single direction to pass through the lens; the orientation of phase is thus easily observed an this shows the presence of the liquid crystal.

There are different phases of liquid crystals and can be subdivided into thermotropic and lyotropic liquid crystals (Chandrashekhar, 1992: 1,10). Thermotropic liquid crystals are those that have a narrow temperature range within which they exist. They break down and become isotropic at too high temperatures, and form a crystalline solid at too low temperatures. Lyotropic crystal polymers are immiscible mixtures where the mesogens phase separate when the molecules reach a high enough concentration. This would be the case of an isotropic fluid acting as a solvent as it solubilises the mesogens.

Liquid crystals are generally classified into 2 classes based on shape: rod-like and disc-like mesogens. Discotic mesophase implies disc shaped mesogens. This is often caused by organic aromatic molecules. The liquid crystalline structure is likely a result of $\pi - \pi$ interactions (Chandrashekhar, 1992: 1,8) causing long range order. Liquid crystals also have positional order; they form the following phases (and can be seen in Figure 2.4):

- *nematic* - characteristic of long range orientation, but no long range direction. There is also no local direction.

- *smectic* - these liquid crystals are like nematic crystals with more orientation. They have positional order as well. They align in a layered structure, but not necessarily parallel to the director.

- *cholesteric* - similar to nematic phase, long range orientation with no long range order. The director however changes in a predictable manner. Cholesterics have a twist along the director axis. The distance over which the twist occurs, is referred to as the pitch. A nematic can be viewed as a cholesteric with an infinite pitch, however there is no interchange between these two phases. It is also referred to as chiral nematic liquid crystal.

- *columnar* - these liquid crystals are discotic and are stacked columns. They have the same long range ordering as nematics. There short range order is much more regular. These layered discs, in the shape of a beam when stacked, and viewed with low magnification, resemble worm-like structures.

Rod-like mesogens can have nematic, smectic and cholesteric structure; whereas disc-like can have nematic and columnar structure.

Liquid crystal technology has garnered higher status over the last few decades. They have found application in the fields of science and engineering and have therefore become more prevalent. Currently most application revolve around the use of liquid crystal displays (LCD's). They are also used in thermometers and other optical imaging devices. Recently the increasing use of polymer based, dispersed, liquid crystals have also caused an upsurge in research activity.

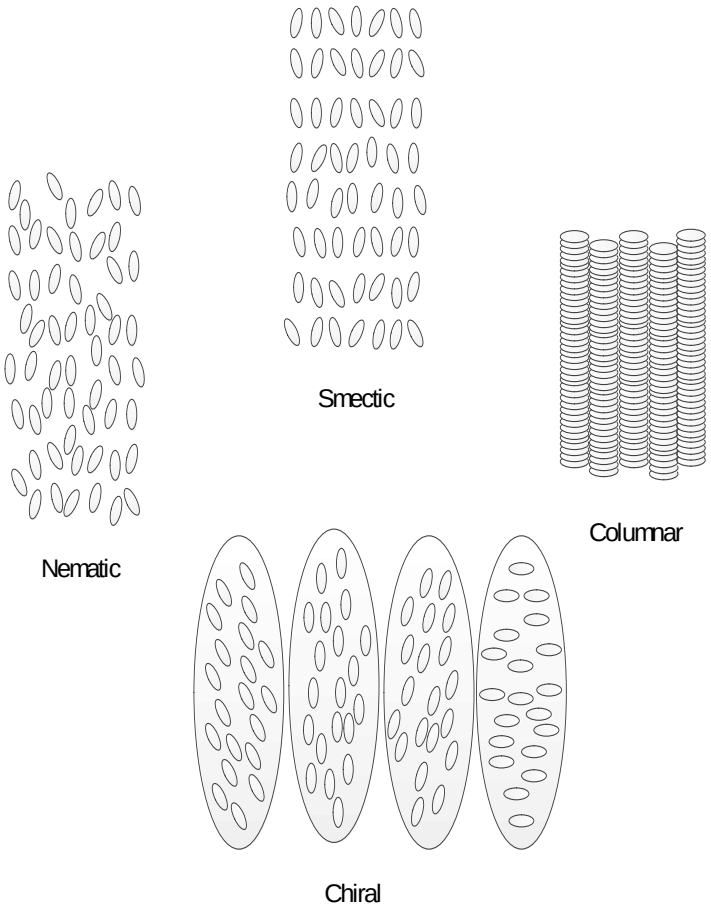

Figure 2.4: Different phases of liquid crystals

2.2 Pitch Material and Mesophase Development

The transformation of an organic precursor to graphite is complex. The original material is heat treated to form mesophase (a liquid crystal), carbonised to a coke and eventually converted to graphite at approximately 3300K. Carbon precursors can be distinguished by there ability to graphitise or not graphitise (Marsh & Menendez, 1988). Non-graphitic carbon material is that which cannot transform to graphite irrespective of heat and pressure (Marsh & Menendez, 1988). Graphitic carbon is organic material that can be transformed to graphite, and as such, non-graphitic carbon is that which cannot. A char is the product of a carbonisation with no fluid intermediary, whereas coke is (Marsh & Menendez, 1988). Coke is made of carbonised material that has passed through a liquid or liquid-crystalline state, and often contains material which is non-graphitic in nature (Marsh & Menendez, 1988). Semi-coke is an intermediate product between mesophase and coke as a result of incomplete carbonisation (Marsh et al., 1999).

This literature focuses primarily on the early stage graphitisation of organic material. Materials such as coal, heavy oils and their residues, pitches, cellulose, anthracene, organic polymers can be converted to graphite (Delhaes, 2001: 199). This study will concentrate on the pitch precursor.

Pitch

Pitches are organic materials produced via different low temperature pathways. It is a polyaromatic hydrocarbon (PAH) with various organic side chains. Pitch is a material that can be converted to graphite upon the requisite thermal treatment. It can contain both a graphitic and non-graphitic fraction. The various constituents make pitch a complex material. As a result, pitch has been separated into types of compounds based on their solubility in various solvents, in a sense fractionating the compounds (Rand et al., 2001: 125), for both characterisation and further processing. No two pitches are the same; the origin of the substance and the manner in which it is processed (its history) makes it unique. They have a broad range of molecular weights, both low and high; from low molecular weight aliphatic to high molecular weight aromatic compounds. This can be altered to a certain extent by a change in processing. Possible applications are in the production of graphite, coke, binder, carbon fibre and some forms of amorphous carbon. This allows for specific pitch to be used for specific applications (Rand et al., 2001: 125).

The important constituents of pitch are the benzene-based (aromatic) compounds and the asphaltene fractions; they are predominantly disc like in shape and are of significance with respect to the eventual properties of the pitch (Rand et al., 2001: 126) and its intended application.

Pitch and other similar precursors are also referred to as macromolecules (Delhaes, 2001: 201); they are PAH's connected by functional groups and behave like glass (viscoelastic) (Marsh et al., 1999). As discussed before, pitches come from various sources;

therefore they are classified based on their origins. Pitches have been divided into different classes, namely primary and secondary pitches (Rand et al., 2001: 126). The majority of primary pitches are coal-tar and petroleum pitches; secondary pitches are mainly from synthetic sources such as polymers and catalytically reacted smaller compounds (Rand et al., 2001: 126).

Coal-tar pitch

Coal-tar pitch is, as by name, a byproduct from coal. It is recovered via the thermal treatment and subsequent distillation of coal compounds. It is generally obtained from the coking process, during the formation of metallurgical coke. It is an aromatic pitch containing mainly carbon and hydrogen, and lower quantities of heteroatoms. The constituents of this type of pitch depends on the coal and its subsequent treatment (Rand et al., 2001: 127). The gases that are evolved from the coke-oven often contain residual coal dust, semi-coke or other particles.

Petroleum pitch

Petroleum pitch is a residue that is obtained from the distillation column of thermally treated petroleum precursors. Just like other pitches, origin and processing determines its constituents. For petroleum pitch, origins are much more varied because of the origins of the different fractions. This type of pitch also generally tends to be much more aliphatic than that of the coal-tar pitch (Rand et al., 2001: 127).

Heat-treatment to mesophase, molecular weight and oligomerisation

The thermal treatment of pitch leads to a change in physical and chemical characteristics. It is not always clearly understood. The organic matter forms pure carbon after the release of volatile hydrocarbons and heteroatom molecules (Delhaes, 2001: 199). The heat treatment process and carbonisation is controlled by kinetics; the pressure and temperature (heating rate, and time) affect the composition and reaction rate (Delhaes, 2001: 199).

Oil type substances, if not released, react and increase in molecular weight, they become solid and brittle, glassy-like materials (Delhaes, 2001: 200).

During pyrolysis, a break in the structure of the material results in its softening (Marsh & Menendez, 1988); it consists of BSU (Basic Structural Units) or elemental units in suspension (Delhaes, 2001: 202). BSU or elemental units are best described as the components that form the backbone of the graphite structure. They can react to form micelles or aggregates, commonly between 350℃and 450℃; these are building blocks for the mesophase material (Delhaes, 2001: 202) and grows as a new phase via homogenous nucleation (Marsh & Menendez, 1988). Figure 2.5 show the importance of this phase during its transformation to graphite; it graphically allows us to see how the original mesophase does eventually influence the final graphite structure.

This however is not always seen as a complete picture as Marsh et al. (1999) suggests that the liquid crystals self-assemble; the mesogens (molecules that make up the

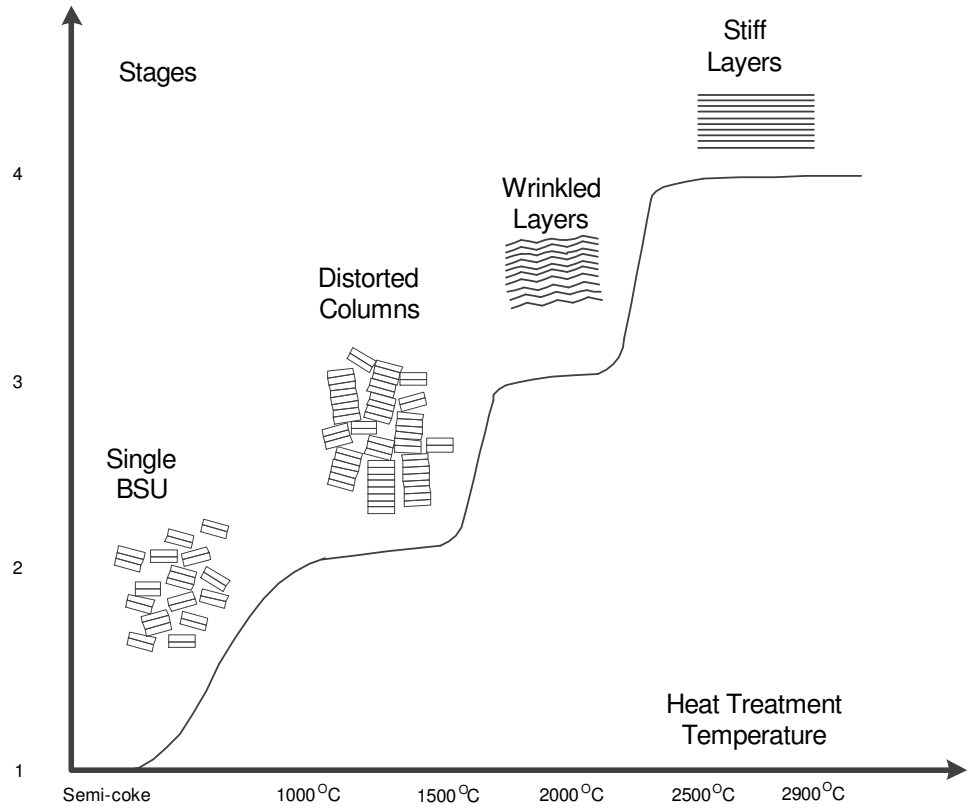

Figure 2.5: Change in ordering of BSU during thermal treatment

mesophase) are produced and then form the liquid crystal. Figure 2.6 visually shows the nucleation, growth and coalescence of the mesophase at different points of the heat treatment.

During heat treatment towards liquid crystal formation, condensation reactions occur. This competes with vaporisation reactions and can increase the softening and vaporising temperatures (Delhaes, 2001: 221); some volatile species remain in liquid phase which allow for condensation reactions or cracking reactions to occur (Delhaes, 2001: 222). Increased residence time in the liquid phase allows for the growth of molecules; this leads to higher molecular weight material via polymeric growth and/or fragmentation of molecules due to delayed vaporisation (Delhaes, 2001: 221). The soak time (time at heat treatment temperature) also increases the extent of these reactions and therefore the likelihood of producing mesogenic molecules (if an appropriate temperature is chosen). Some low molecular weight compounds therefore do not vaporise prior to primary carbonisation. This leads to the formation of only partially graphitic material upon graphitising temperatures; due to the presence of non-mesogenic species (Delhaes, 2001: 221).

One of the main reactions are dehydrogenation (Marsh & Menendez, 1988). This causes an increase in softening temperature, insolubility and changing the coking characteristics. The increase in molecular weight of its constituents leads to increase in its viscosity (Marsh & Menendez, 1988); this being caused by the formation of mesogens which separate to form the mesophase (Delhaes, 2001: 222). The molecular weight of

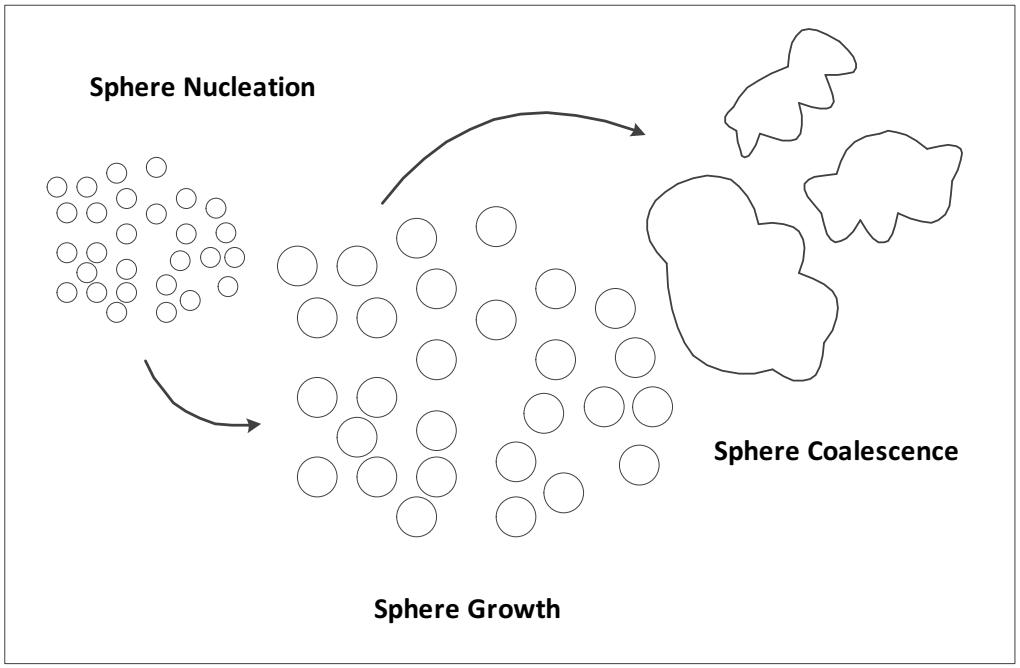

Figure 2.6: Different states of mesophase during pyrolysis

the mesophase itself does not increase, but the size of liquid crystal phase does, due to coalescence (Marsh & Menendez, 1988).

Mesophase has a broad molecular weight distribution. It might possibly mean that the smaller molecules are entrapped in the layered stacking of the mesogenic species; also that they act as a solvent (Delhaes, 2001: 223).

The spheres eventually coalesce until a continuous mesophase is formed. This flowable domain aligns which also causes disclinations and a decrease in viscosity which can form anisotropic regions (Marsh & Menendez, 1988). The mesophase with subsequent anisotropy allows for the carbonisation of coke with structure, and thus also a material which is graphitisable (Delhaes, 2001: 223). This is the manner in which the anisotropic structure is induced into the coke, graphite structure. Thus mesophase is understood to cause the eventual anisotropy that is associated with cokes (Marsh & Menendez, 1988).

Mesophase Formation and Coalescence

The main aspect of pyrolysis is to have a continuous mesophase, generated from the coalesced spheres (Marsh & Menendez, 1988). The coalescence increases viscosity and finally results in solidification (Delhaes, 2001: 204). The understanding of the mesophase has improved the knowledge base on the formation and production of coke (and graphite)(Marsh et al., 1999); this understanding has contributed significantly in the fields of carbon technology and resulting applications (Marsh & Menendez, 1988). This continuous liquid crystal phase, to a large extent, is responsible for the graphitic nature of the material and its eventual structure; this from a pre-graphitic, pre-carbonised material via heat treatment (Burchell, 1999: 24). Not all of the material from pitch passes through this liquid crystal region; they are generally excessively cross-linked and hence it

does not form a graphitic carbon upon high temperature treatment (Burchell, 1999: 24).

The most efficient shape for the mesogen species are planar and disc shaped polyaromatic molecules (with or without side chains) (Delhaes, 2001: 204) (Marsh et al., 1999). It has also been shown that the mesophase is liquid crystal which is discotic and nematic (as opposed to the more ordered smectic phase) (Marsh et al., 1999). They associate with each other and form there own localised structure. The mesogens would proceed to grow as long as they remain in the liquid state and the molecules are held together by there $\pi - \pi$ interactions (Marsh et al., 1999). The mesogens are held together, to form the liquid crystal phase, by physical forces and not chemical bonding (Marsh et al., 1999).

Mesophase is produced via PAH precursors, the mesogens themselves may not necessarily be planar due to the heteroatoms present (Marsh et al., 1999). Heteroatoms catalyse molecule growth to form the mesogenic compounds themselves, and thus vary significantly in shape and size; they thus still depend on the source of the precursor material (Marsh et al., 1999). The reactivity differs depending on the origin of the pitch and therefore there are as many mesophases as there are sources which produce this liquid crystal phase. This difference affects the manner in which the phase behaves, grows and coalesces; and therefore eventually the crystallinity and properties of the resultant coke and graphite (Marsh et al., 1999).

Discussing the structure of mesophase, it should be noted that the anisotropy of the mesophase allows for the liquid crystal domains to be visible clearly under polarised light. The local molecular structure and longer range of order contribute to this effect (Marsh & Menendez, 1988).

The mesophase can retain structure (Marsh et al., 1999) and this allows for orientation, and disclinations to be observed. In general, three orientations have been identified: columnar, distorted and nematic (Delhaes, 2001: 204). This is also in descending order of orientation. Columnar is a very structured rectilinear stacking of the disc-like molecules. Distorted columnar is stacking of the disc-like molecules into columns (can bend), but does not have any relation to the other columns. Nematic structure shows no columnar behaviour, only orientation of the discs in the same direction, therefore approximately parallel (Delhaes, 2001: 204).

Synthetic mesophase can also be formed; this being accomplished by catalyticaly reacting naphthenic-type species. This is a Friedel-Crafts type reaction normally catalysed by elemental potassium or aluminium chloride (Delhaes, 2001: 226). Mochida et al. (2000) does a thorough review on the topic of synthetically derived pitches, and is an excellent source should further reading on this topic be required.

Application of mesophase pitch has recently, largely centred in its use in the manufacture of carbon fibre. The choice of a suitable precursor and its processing, as with most pitch material, affects the properties that are best suited for spinnability of fibres (Delhaes, 2001: 229). There is a plentiful supply of articles that have addressed this

aspect and shall not be discussed here.

Types of Mesophase

Mesophase has been characterised in 3 different ways (Brooks & Taylor, 1965): referred to as A, B and C. The first is the Brooks and Taylor mesophase (Delhaes, 2001: 205). This type of liquid crystal tends to form spheres which are anisotropic, hence it has its own local molecular orientation, and has equatorial stacking (Marsh et al., 1999). A-type mesophase is synonymous with isotropic pitches from coal-tar or petroleum origins (Delhaes, 2001: 205). A distorted columnar arrangement is found to dominate within the sphere. Upon further heating, during primary carbonisation, the mesophase spheres coalesce and form a mosaic-like structure (Delhaes, 2001: 205) (Marsh & Menendez, 1988). The orientation of the structure changes and is determined primarily by the defects that are formed, ie. grain boundaries. This results in isochromatic regions, areas which have parallel orientation, most likely caused by the flow of the coalesced mesophase material (Delhaes, 2001: 206). Mosaics are further classified by size into coarse, medium or fine mosaics. Mesophase A is generally formed in the absence of large quantities of cross-linking heteroatoms.

Mesophase B and C tend to have more cross-linking agents; this tends to increase the softening point of the material and also leads to different forms of liquid crystals (Delhaes, 2001: 207). In general the local molecular orientation of the developed mesophase spheres has a larger deviation than that from mesophase A. They show misorientaion with other mesophase domains and do not show quite as homogenous regions. They do not have to form spheres, they could be ovoid or even cylindrical (Marsh et al., 1999). It has been observed that the local molecular orientation during coalescence is irregular as opposed to spherical. This leads to a much finer texture mosaic structure than those seen in mesophase A material (Delhaes, 2001: 207).

2.3 Pitch and Mesophase Characterisation

Properties of pitch and mesophase material discussed in section 2.2 have been characterised via different techniques. In this section some of these methods shall be addressed which allow for some of the important properties to be identified. Greater detail on the rheology of pitches will be discussed in section 2.5. Pitch-type materials have been characterised in many articles, and most deal with different processing techniques. The aim of most of these publications is not necessarily to investigate the use of different instrumentation, but use thereof in understanding the resultant product. The aim of this section is to identify the procedures necessary to describe the important properties and characteristics to understand the behaviour of the material.

Mesophase Content

The most often used technique to evaluate the mesophase content of pitch material

is via optical microscopy. As discussed in section 2.2, the mesophase material is easily observable under polarised light. Micrographs of the samples are obtained, upon which a particle count technique is employed to measure the mesophase content.

Another method of determining mesophase content is by volume of material that is successfully centrifuged. Vieira et al. (2011) and Singer et al. (1987) used this technique to successfully separate isotropic and anisotropic phases, mesophase content could be calculated by the amount of each phase via simple geometry (needed for tube in the centrifuge). There is a clear distinction between the two phases after separation, and this was shown via optical microscopy (Singer et al., 1987). This technique was believed to be superior to the particle count technique of optical microscope images to determine mesophase content, as the particle count is limited to a maximum mesophase concentration of 20% (Vieira et al., 2011).

Molecular Weight, Composition and Structure

An often used technique to help characterise pitch material is solubility. It assists in characterising the change in composition during primary carbonisation, until the formation of a semicoke material. Many people use solvent fractionation whereby the solubility is expressed in terms of $\alpha - \beta -$ and $\gamma - resins$ (Delhaes, 2001: 200), which give an indication of the type of compounds present. α-resin is the fraction of the material that is insoluble in quinoline. β-resin represents material which is soluble in toluene less that soluble in quinoline. Finally, γ-resin is the toluene soluble fraction.

Liedtke & Huttinger (1996) found that using tetrahydrofuran and N-methyl-pyrrolidine instead of toluene and quinoline result in similar solubility, and it is a less toxic alternative.

Quinoline is an important solvent when characterising pitches, as a large portion of the mesophase compounds are believed to be insoluble in this solvent (Delhaes, 2001: 213). In coal-tar pitches, the solid residue from the processing also forms parts of the QI, and is referred to as the primary QI. Secondary QI is the fraction related to mesophase formation.

Greinke & Singer (1988) characterised isotropic and mesophase fractions from the same parent petroleum pitch; they found that the molecular weight distribution of the mesophase did not change during any stage of transformation, however the isotropic pitch showed an increase. This was accomplished by the use of size exclusion chromatography. The constant molecular weight was explained by the continuous condensation reactions of the mesophase being counteracted by the transfer of smaller molecules from the isotropic phase.

Solubility tests identified the main component of mesophase spheres as being quinoline insoluble material (Kim et al., 1993). Just prior to, and from the point of phase inversion, mesophase has a constant quinoline insoluble content (Kim et al., 1993). The quinoline insoluble content of the isotropic phase increase was observed to almost linearly with

respect to soak time (at constant temperature for all samples) (Kim et al., 1993).

Blanco et al. (2000) also propose that primary quinoline insolubles (particulate matter), could support the selective transfer of high molecular weight compounds from the isotropic medium into the mesophase. This resulting in almost uniform sphere diameter of the mesophase, the phenomenon likely caused by inability of the nucleation of smaller spheres at the same point as growth or coalescence of others. This behaviour as a result of the continuous increase in molecular weight of the two phases.

Blanco et al. (2000) proposed the growth of mesophase being caused by the high uptake of β-resin from the isotropic phase. The C/H ratio was observed to be fairly constant (at 2) at all stages of mesophase growth, whereas the isotropic phase increases gradually; it however is never equal to that of the mesophase (Blanco et al., 2000) (Kim et al., 1993). This also showed larger molecular size, by condensation reactions of compounds in the mesophase (Blanco et al., 2000).

Panaitescu & Predeanu (2001) processed coal-tar pitch by solvent extraction and showed that the different types of toluene- and quinoline-insolubles and β-resin affect the type of mesophase formed, therefore also the texture of the resultant coke. Thus different components have a specific role in a the structure of the mesophase.

Bhatia et al. (1986) showed that the temperature of mesophase formation of the insoluble content of a coal-tar pitch could be lowered via solvent extraction. They attributed this to the higher average molecular weight of the (toluene) insoluble pitch material. The lower molecular weight material also has a much more significant contribution to the softening rather than the solidification of the pitch (Bhatia et al., 1986). The low-molecular-weight components increase both the softening and solidifying temperatures and also the rheology of the material (Bermejo et al., 1995).

Molecular-weight-distribution of pitches is known to play an important role in the behaviour of pitch. MALDI-TOF has successfully been implemented to obtain this data (Edwards et al., 2003). A caveat to this, has been the insolubility of high molecular weight pitch material in solvent; this was overcome by the use of a water-spotting technique in conjunction with tetracyanoquinodimethane for the particular pitch in their study. The presence of trimers and tetramers is found in high molecular weight material (Edwards et al., 2003).

Bermejo et al. (1995) used the techniques of elemental analysis, NMR, FTIR, microscopy and size-exclusion chromatography to study the role of low-molecular-weight components in pitch. Upon pyrolysis, these components reduce viscosity. The volatilisation of these compounds prior to pyrolysis results in higher temperatures at which the samples soften, harden and form mesophase. It does not however greatly affect the optical texture of the coke formed, but does remove some of the possible mesogen species which assist in the condensation reactions in the formation of mesophase compounds.

C/H ratio is also often used to characterise these different organic precursors (Delhaes,

2001: 200), this is more indicative of the aromaticity or average molecular weight. Only upon further heating, secondary carbonisation, is pure carbon formed (Delhaes, 2001: 200).

Pitch material can be transformed to mesophase by different preparation conditions that affect the composition and characteristics of the pitch. Perez et al. (2002) used the methods of distillation and heat treatment, and compared there findings. Their results showed that under the different conditions the pitch components change drastically. Pitch formed by distillation resulted in a high softening point pitch with predominantly aryl- and alkyl-substituted aromatic compounds; pitches formed by thermal treatment underwent increase in molecular size (via condensation reactions) and a large fraction of the starting aryl- and alkyl-substituted aromatic compounds were converted into planar aromatic compounds. Condensation reactions were more pronounced under distillation conditions, however the thermally treated material produced a higher amount and more developed mesophase (Perez et al., 2002). This was observed with the aid of data obtained via gas chromatography (GC) and Fourier-Transform-Infra-Red spectra.

In some pitches the degree of mesophase formation (achieved via pyrolysis) can be followed by adsorption peaks obtained via near-IR and UV-visible bandwidths (Ito, 1993). Three major groups were identified during transformation by Ito (1993): aliphatic, aromatic and lamellar. For pitches that form mesophase spheres and agglomerate, aromatic hydrocarbons are converted into lamellar structure. For mosaic type mesophase, the aromatic hydrocarbons are unstable and as a result, disordered carbon is formed (Ito, 1993).

Structural ordering of anisotropic pitch expected to change during transformation to mesophase. Such studies have been conducted and one technique used is that of Raman spectroscopy (Montes-Moran et al., 2002). Montes-Moran et al. (2002) produced a semi-coke material from a coal tar pitch, which was separated into its mesophase and isotropic components by hot filtration. The results obtained showed an increase in graphene-like orientation from the pitch to the mesophase, and an intermediate behaviour showed by the semi-coke material itself. This was confirmed by the relative intensities of the D and G Raman bands; the increase is however caused by a D band widening as opposed to a G band narrowing. This study confirms that mesophase formation can be monitored by Raman spectroscopy.

During carbonisation, mesophase components can also be detected by high temperature H-NMR before mesophase formation; an ESR spin probe is necessary and the phenomenon is monitoring the half-width of the resultant data. The change to mesophase occurs without a change in aromatic hydrogen concentration (Azami et al., 1989).

Another method, not often used is that of density. Similar to C/H and solubility, density of mesophase is also fairly constant. There is also an observed increase in density of the co-existing isotropic pitch (Kim et al., 1993).

Thermal Analysis

An important aspect to consider is the behaviour of the produced material under different thermal conditions. These techniques complement with the techniques described earlier. They give a better understanding to the behaviour of the material.

Alcan & Inorga (2001) determined that via the techniques of thermogravimetric analysis (TGA), differential thermal analysis (DTA) and Fourier-Transform-Infra-Red (FTIR) that different pitches can be identified, according to their industrial origins and method of preparation. The chemical components (or group of components) were identified via FTIR, and their interactions with dissimilar components (fractionated material) were observed via TGA and DTA.

Mesophase and isotropic pitch have distinctly different properties. Blanco et al. (2002b) characterised the pyrolysis behaviour of separated mesophase and isotropic pitch from coal-tar origins. This was done by TGA, differential thermogravimetry (DTG) and differential scanning calorimetry (DSC). TGA results show that mass loss in isotropic pitch is mainly attributed to distillation of light components, and in mesophase pitch it is attributed more to thermal reactions. DSC results show an endothermic region caused by distillation and two exothermic peaks (same results were obtained for the parent pitch). The mesophase pitch however only showed the first exothermic peak. Both exothermic peaks were attributed to condensation reactions: the first peak being associated to molecules that easily forms mesophase, and the second to molecules that do not easily form mesophase. Upon carbonisation of the separate phases, coke yielded from the parent and mesophase pitches showed an optical texture of coarse mosaic and small domains, while the isotropic fraction showed flow domains (Blanco et al., 2002b). Carbon yield and average molecular weight of the isotropic phase also increase with the thermal treatment (Blanco et al., 2000).

Another important measurement is that of softening and/or glass transition temperature. Glass transition temperatures (T_g) can be measured by both differential scanning calorimetry (DSC) and thermomechanical analysis (TMA) for pitch and mesophase material. For relatively pure component systems the DSC technique gives accurate results, however for mesophase-containing pitch systems (similar to mixed polymer systems) the TMA is preferred (Barr & Lewis, 1982)(Khandare et al., 1996). The TMA method is preferred for mesophase material due to the difficulties encountered in determining the T_g using DSC, TMA results are much more definitive. TMA analyses can be run in penetration mode for mesophase and isotropic pitch as done by Barr & Lewis (1982) or for more accurate dilatometry measurements, in expansion mode as done by Khandare et al. (1996). The T_g of the mesophase material can be related to fraction of high and low molecular weight fractions, as shown by the solubility of the mesophase-containing pitch material in pyridine, by Barr & Lewis (1982). Linear correlations between the glass transition temperature and Mettler softening point has also been observed (Barr & Lewis,

1982)(Khandare et al., 1996). The glass transition temperature increases with mesophase content; two linear regions are observed when the T_g is plotted against mesophase content. The temperature at which these two lines intercept is believed to be the phase-inversion point of the system (Liedtke & Huttinger, 1996).

Another interesting article which shows information on glass transition and softening is that by Mochida et al. (2002). In this paper the authors determine both glass transition and softening via different methods using both TMA and Dynamic Mechanical Thermal Analysis (DMTA). This is done on several mesophase pitches from different naphthalene-based precursors. In this study, they discovered that stacking height of the mesogen molecules in the mesophase is an important factor in determining the glass-transition temperature.

Anisotropic content in co-existing isotropic samples could be analysed via a micro-thermal technique using an atomic force microscope with thermal tip (Blanco et al., 2002a). Via this technique the two phases present in the sample could be identified via thermal expansion properties and therefore a topographic image similar to optical microscopy was produced. The technique also allows for localised heating which means that glass transition and softening could also be determined (Blanco et al., 2002a).

2.4 Concepts of Rheology

Rheology deals with the way in which material reacts to deformation. In most cases this is the manner in which liquids deform under flow; this also applies to "stiff" liquids or materials such as polymers, food and concrete, to name a few.

2.4.1 Viscoelastic Behaviour

A viscoelastic material is that which is neither solid nor liquid, it shows intermediate properties between these two states; properties of these phases will be outlined. In reality though, no solid is purely elastic and liquid is completely Newtonian. Simplified models over the time region of relevance are used to characterise materials.

A Newtonian liquid, is a fluid whose strain (normally represented by ϵ in tension and by γ when in shear) is proportional to strain rate (or velocity gradient), equation 2.1 (Ward & Sweeney, 2004: 54).

$$\begin{aligned} \sigma = \eta\frac{dv_2}{dx_2} &= \eta\frac{d\epsilon}{dt} \\ \sigma &= \eta\frac{d\gamma}{dt} = \eta\dot{\gamma} \end{aligned} \tag{2.1}$$

This liquid therefore always maintains the same fluid properties no matter what shear force is exhibited. A Newtonian liquid has no shape, deforms irreversibly and dissipates all energy when under external stress.

Fluids which do not obey this proportionality are said to be non-Newtonian. These fluids do not show the same proportionality observed with standard Newtonian fluids (Chhabra & Richardson, 2008: 5). This is shown in Figure 2.7.

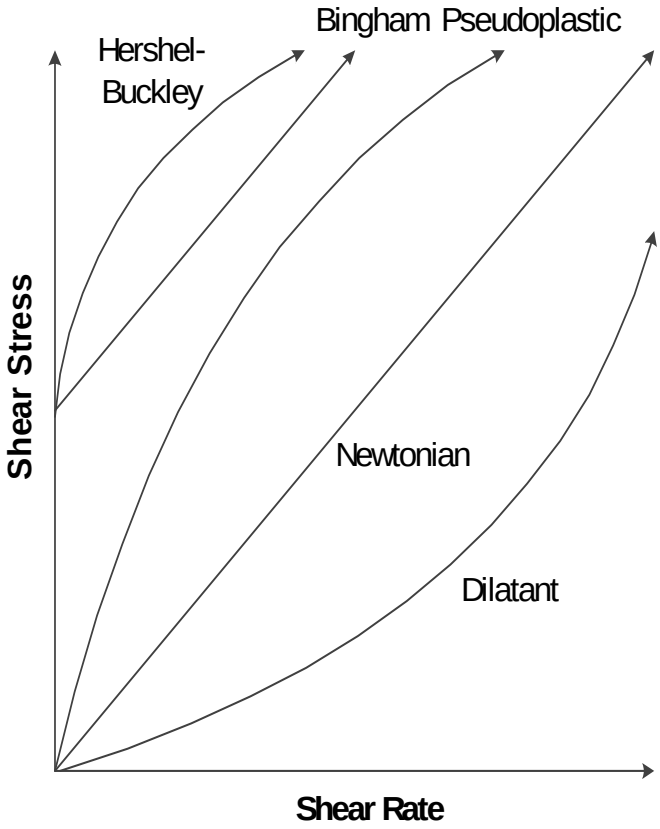

Figure 2.7: Stress-strain relationship for different types of Newtonian and non-Newtonian fluids

A Bingham plastic is a material that requires a certain amount of force before it flows. This inertial stress is called the yield stress. The sample shows solid-like properties until the yield stress is exceeded, after which it flows as a viscous liquid. The viscosity of the fluid during flow is termed the plastic viscosity. Materials normally behave as Bingham plastics if there is an initial structure which holds the sample together, like particles or large molecules. This is generally a weak structure which accounts for resistance to flow, and which may reform once the stress has subsided.

A thixotropic material is one that under increasing stress over time, reduces in viscosity. These substances require some amount of time to reach equilibrium viscosity. These are shear-thinning fluids. Other samples that "thin" with shear, but return to their initial state almost instantly once the stress is removed, are commonly referred to as pseudoplastic.

A rheopectic fluid is a material that has a time dependant viscosity. A thixotropic material is a time-dependent pseudoplastic. To help explain this, a simple diagram is shown in Figure 2.8.

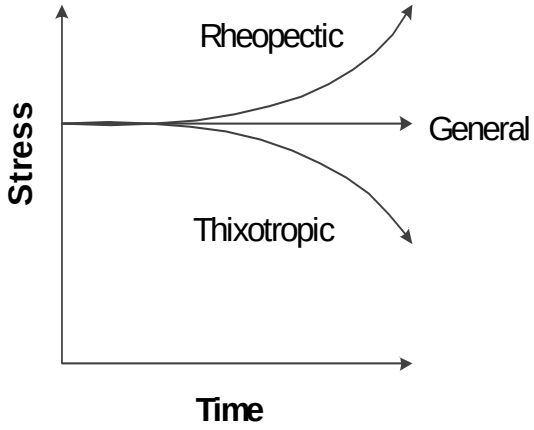

Figure 2.8: Stress-time relationship for different types of Newtonian and non-Newtonian fluids at a constant strain rate

Dilatant fluids are commonly referred to as shear-thickening. As the fluid is put under shear stress, the apparent viscosity of the material increases. This type of behaviour commonly occurs in suspensions which become stabilised under shear. The dispersion starts to floc which increases the mixtures viscosity. If once the shear force is released, and the material thins, it is also rheopectic.

On the other end of the spectrum from a Newtonian liquid, there is the Hookean solid. It is linearly elastic, whereby the stress is proportional to strain, equation 2.2(Ward & Sweeney, 2004: 55).

$$\sigma = E\epsilon = G\gamma \tag{2.2}$$

Equation 2.2 holds for loading of a material in the elastic range, prior to the yield strength. It is a solid that changes shape under an external force, but after subsequent removal of the force, returns instantaneously to its original state. The material therefore stores all the energy used during deformation to reverse the process.

This is a generalised version of Hooke's law, it is a measure of stiffness, and also applies to shear forces. In this case the constant of proportionality is referred to as the shear modulus.

An often used property of viscoelastic materials is creep (Ward & Sweeney, 2004: 56). This is a time dependant change in strain for a step disturbance in stress, which occurs over a short period of time. These substances recover after the removal of the stress to a residual strain. The manner in which this linear viscoelastic data changes, during and after the applied load, gives information on the state of the material. For polymers, an

increase in resistance to the stress is indicative of higher molecular weight or stiffness.

There are three stages of viscoelastic creep:

1. immediate elastic deformation (ϵ_1)
2. delayed elastic deformation (ϵ_2)
3. Newtonian flow (ϵ_3)

The strain is often shown by making use of the creep compliance and for these tests applying the Boltzmann superposition principle. (for a brief description of please refer to Dealy & Larson (2006: 91)) for linear viscoelastic data is(Ward & Sweeney, 2004: 56):

$$J(t) = \frac{\epsilon(t)}{\sigma_0} \tag{2.3}$$

$$= J_1 + J_2 + J_3 \tag{2.4}$$

This shows simply that creep is a function of the whole sample loading history. Each loading makes an independent contribution to the total loading history. The total final deformation is the sum of each contribution.

The creep compliance in equation 2.5 is associated with the different stages of deformation observed. At significantly high temperatures above the glass transition temperature (T_g), J_3 or ϵ_3, dominates, especially for amorphous linear polymers where there is no elasticity in the melt. However J_1 and J_2 are the major contributors in cross-linked and highly crystalline polymers.

Creep tests (compliance), can be used to obtain retardation behaviour which helps in inferring relaxation phenomena. For these tests however significant time is needed to ascertain the required data. This can be achieved also via several short tests by a technique called time-temperature superposition (to be discussed later).

Stress relaxation is another method whereby structural reorganisation is investigated. This phenomenon and its measurements also makes use of the Boltzmann superposition principle for this type of test. This test is a step in shear strain input, whereby the shear stress is measured as a function of time. In this case the stress relaxation modulus is given as (Dealy & Larson, 2006: 91):

$$G(t) = \frac{\sigma(t)}{\gamma} \tag{2.5}$$

Similar to creep, long time scales are often required to obtain information on relaxation; time-temperature superposition is then also implemented. Relaxation behaviour

gives information with respect to cross-linking, molecular weight distribution, molecular branching, etc. with respect to the structure of the material involved (in the case of polymers).

A key feature of both creep and relaxation behaviour is that of linear viscoelasticity. This implies, with respect to these tests, the original disturbance doubles in magnitude, so should the measured output. It shows that successive changes in the disturbances are additive.

The conditions for which the above behaviour is observed, are those of constant stress. An alternative method for experimental procedure are those of dynamic stress. A dynamic or periodic stress is that which undergoes oscillatory or vibrational motion.

Often small amplitude oscillatory shear is used in such experiments to avoid significant deformation of the microstructure of the fluid, it is different for common rotational shear and this is shown in Figure 2.9. Under such conditions the sample is oscillated homogeneously with sinusoidally varying shear stress or shear strain. This method is used to obtain linear viscoelastic behaviour.

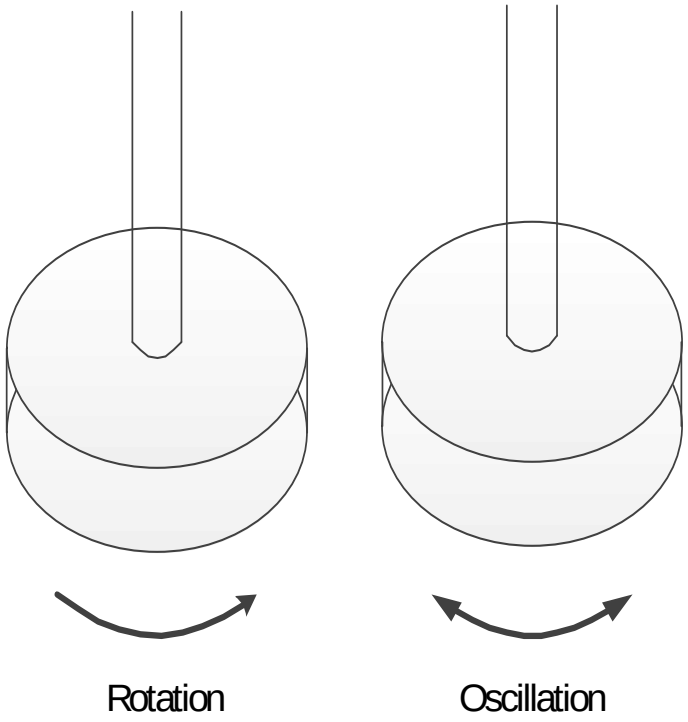

Figure 2.9: Movement of spindle during rotational and oscillatory disturbance

If the shear strain can be represented as the input in equation 2.6,then the shear stress can be represented by the output in equation 2.7 (Ward & Sweeney, 2004: 71).

$$\gamma = \gamma_0 \sin(\omega t) \tag{2.6}$$

$$\sigma = \sigma_0 \sin(\omega t + \delta) \tag{2.7}$$

A completely elastic material has an instantaneous response to disturbances; therefore with a sinusoidal input, the reaction is in phase ($\delta = 0°$ or $0rad$). The same is true of a purely viscous fluid. The response is out of phase where $\delta = 90°$ or $\frac{\pi}{2}rad$; this is a phase lag. If a material is viscoelastic, the phase lag is something between the mentioned outputs. This can be seen in Figure 2.10.

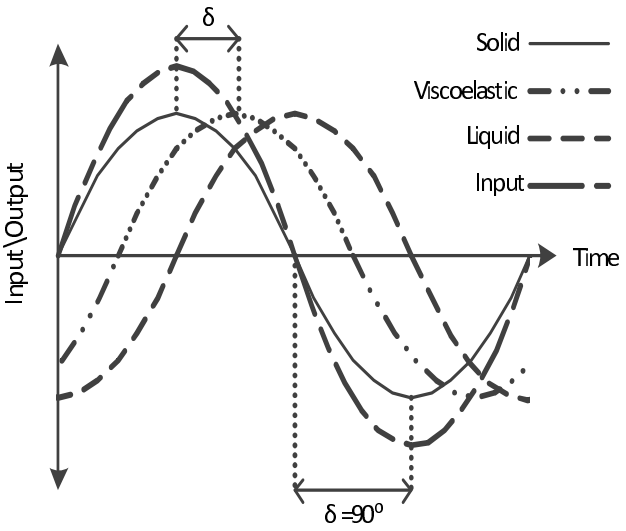

Figure 2.10: Input-output relationship during a sinusoidally varying disturbance

$$\sigma = \sigma_0 \sin(\omega t)\cos(\delta) + \sigma_0 \cos(\omega t)\sin(\delta) \tag{2.8}$$

The strain in equation 2.8 represents the distribution as from solid and liquid components; that which is in phase with the strain ($\sigma_0 \cos\delta$), and that which is out of phase with the strain ($\sigma_0 \cos\delta$). This can be rewritten in terms of shear moduli; the storage modulus (G') which is in phase and the loss modulus (G'') which is out of phase within the stress strain relationship of the material shown in equation 2.9, and can be pictured in figure 2.11.

$$\sigma = \gamma_0[G' \sin(\omega t) + G'' \cos(\omega t)] \tag{2.9}$$

The loss and storage moduli are components of the complex shear modulus. The storage modulus represents the amount of energy stored by the strain, and the loss modulus is that dissipated by the material. The relationship between the complex, storage and loss modulus is shown in equation 2.11.

$$\begin{aligned} G^* &= G^* \cos(\delta) + G^* \sin(\delta) \\ &= G' + G'' \end{aligned} \tag{2.10}$$

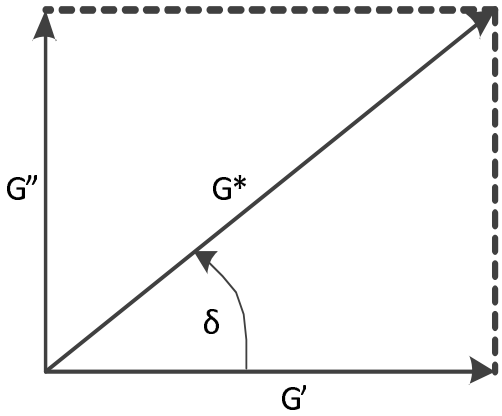

Figure 2.11: Breakdown of complex modulus into loss and storage modulus

A viscoelastic material shows mechanical properties between the two phases, and models of the behaviour are built upon a combination of the solid and liquid models. The most simple of these models are the Kelvin-Voigt and Maxwell models.

These are mechanical phenomenological models which are constrained to linear viscoelastic behaviour and application of the Boltzmann superposition principle. This principle states that the sum of the independent elastic and viscous components lead to the total deformation of the sample. It is common to have this behaviour diagrammatically shown as Hookean springs and Newtonian dashpots.

A Kelvin-Voigt model is spring and dashpot in parallel; this allows for the two units to be exposed to the same strain. A Maxwell model is a spring and dashpot in series; in this configuration the stress is the same for the two units. The Kelvin-Voigt model is better for expressing creep behaviour, whereas the Maxwell model describes relaxation behaviour of the material (Ward & Sweeney, 2004: 64). For these models

$$\tau_i = \frac{\eta_i}{G_i} \tag{2.11}$$

where τ_i is the relaxation time of a Maxwellian unit and the retardation time of a Kelvin-Voigt unit.

2.4.2 Glass Transition Region

The glass transition is the reversible change in properties of an amorphous material from a solid, brittle material into a viscoelastic material. The glass transition is not a first order change in state, and thus happens over a temperature range. Due to this, the transition cannot be measured by typical means; this is due to the fact that typical transitions such as melting and crystallising which show discontinuity in structure and properties (Rand, 1987).

Glass transition is a second order phase transition and the temperature is affected

by the kinetics of the transition. The structure and properties continuously change during transition (and therefore temperature). The main reason for the different kinetic behaviour is due to different relaxation times for the change in structure, and that for the rate of change of the temperature. Stronger bonds in liquid state would thus show a longer transition to the brittle solid phase. This would lead to a much longer temperature range over which enthalpy of melting would occur.

Figure 2.12 shows how some of the thermodynamic and physical properties change during the range of glass transition.

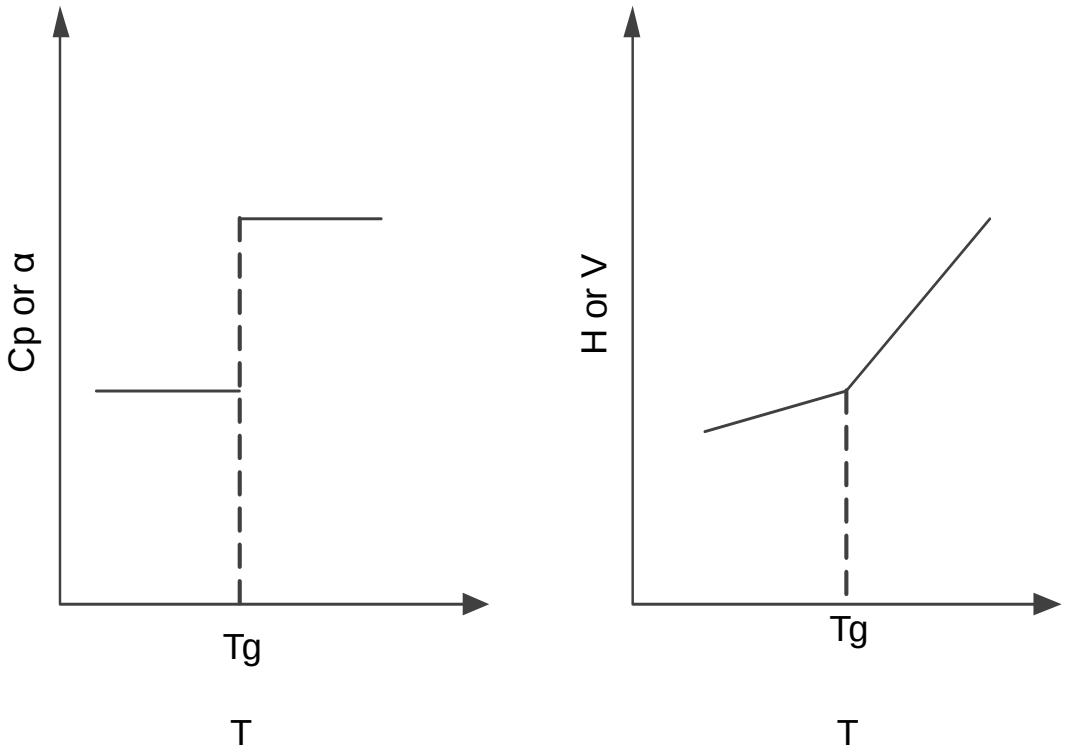

Figure 2.12: Change in some properties during glass transition

It is clear from Figure 2.12 that enthalpy and volume are continuous function of temperature, as opposed to typical solid liquid transition. The discontinuity for glass-formers is seen in the derivative of the aforementioned properties; specific heat and thermal expansion.

2.4.3 Time-Temperature Superposition

The effect of temperature on amorphous material is important because it causes a change in behaviour. This is especially true for polymers, when the viscoelastic properties during the transition from the glass-like state to the rubber-like state (Ferry, 1980: 264). There are two main reasons to investigate the temperature dependance (Ward & Sweeney, 2004: 95)

- from a practical point of view, it is not always possible to obtain the relaxation or retardation behaviour over the necessary time scale at a single temperature. It is therefore required to bring the mechanism or behaviour, to a time frame within which it is visible (This normally assumes that there is an interrelation between time and temperature).

- The other is the interpretation of molecular behaviour and transition; this occurs at elevated temperatures or experimental time scale. The molecular behaviour of a material can be affected by inclusions, crystals, molecular weight distribution, etc., and the mobility also shows us changes in glass transition temperature. This is especially true in polymers which show several relaxation phenomena.

Time-temperature superposition assumes that viscoelastic properties and behaviour of a material at a specific temperature, can be related to behaviour at another temperature, by a simple shift in time scale. It should be noted that most of these properties span decades (of the measurement unit involved) and also of duration over which they occur; and hence are represented by log-log plots. In these cases the viscoelastic properties can be superimposed by a horizontal shift from one temperature to another. This also occurs for dynamic measurements and a shift in frequency. The extent of deviation is represented by $\log(a_t)$, where a_t is the shift factor (Ward & Sweeney, 2004: 101).

With this technique, experimental measurements are made at several temperatures. These plots are then shifted horizontally to form a single curve. The plot at one of the temperatures stays constant, and the others move to superimpose onto that data. That temperature, whose data remains constant, is referred to as the reference temperature (Ward & Sweeney, 2004: 103). The single curve produced is commonly known as a mastercurve.

Many authors have suggested that some material properties also need to be adjusted to the reference temperatures. Notably the effects of temperature on density.

The underlying meaning of such shifts have generally fallen into two categories; one in which the shift factor is described by the Arrhenius relationship, the other being the Williams-Landel-Ferry relationship.

The Arrhenius model is based on a constant activation energy of the transition from one state to another controlled by the molecular rate process. The transitional states change is not dissimilar to that seen in reaction kinetics and equilibria; based on probability and Gibbs free energy (statistical thermodynamics) of the equilibrium states (Ward & Sweeney, 2004: 104).

The resistance to move from one energy state, to that of a state at a different frequency (state two), can to a relatively accurate degree be represented by an activation energy (enthalpy) (Ward & Sweeney, 2004: 104). Therefore

$$\omega = \omega_0 \exp(\frac{-\triangle H}{RT}) \tag{2.12}$$

and leads to

$$\log(a_t) = \frac{\triangle H}{R}\left(\frac{1}{T_2} - \frac{1}{T_1}\right) = \frac{\log(\omega_1)}{\log(\omega_2)} \tag{2.13}$$

for constant $\triangle H$

From equation 2.13, it is clear that a plot of $\log(a_t)$ vs $\frac{1}{T}$ will lead to the calculation of $\triangle H$. This will show that large changes in activation energy will lead to a similarly great change in frequency (Ward & Sweeney, 2004: 107).

The Williams-Landel-Ferry (WLF) equation, on the other hand, is based on the glass transition behaviour of the material. Williams, Landel and Ferry (after whom the equation is named) realised that after applying time-temperature superposition to several amorphous polymers, an approximate shift factor-temperature relationship was obtained for all the materials. They found empirically that

$$\log(a_t) = \frac{C_1(T - T_R)}{C_2 + (T - T_R)} \tag{2.14}$$

when the equation is applied to a suitable temperature for the polymer (Williams et al., 1955).

This lead to a curious notion to whether there was a fundamental meaning behind the WLF equation. Indeed there was, and this was based on the glass transition temperature and the concept of free volume.

By utilising the fractional free volume relation that

$$\begin{aligned} f &= f_g + \alpha_f(T - T_g) \\ where \quad f &= \frac{v_f}{v} \end{aligned} \tag{2.15}$$

an interpretation of the WLF equation can be obtained. Doolittle's equation relates the free volume of a liquid to its viscosity by:

$$\ln \eta = \ln a + \left(b\frac{v - v_f}{v_f}\right) \tag{2.16}$$

If the glass-type material is also modelled by Maxwellian units (equation 2.11), and if the change in elasticity with temperature is small in comparison with viscosity, then a shift factor can be approximated from T_g to T as

$$a_t = \frac{\eta_T}{\eta_{T_g}} \tag{2.17}$$

By substituting equations 2.15 and 2.16 into 2.17 and subsequent simplification, the following relationship is observed

$$\ln(a_t) = -\frac{b(T-T_g)}{\frac{f_g}{\alpha_f}+(T-Tg)} \tag{2.18}$$

or

$$\log(a_t) = -\frac{\frac{b}{2.303}(T-T_g)}{\frac{f_g}{\alpha_f}+(T-Tg)} \tag{2.19}$$

which is analogous to the WLF equation. When the WLF equation is written in terms of T_g instead of T_R, we have

$$\log(a_t) = \frac{C_1^g(T-T_g)}{C_2^g+(T-T_g)} \tag{2.20}$$

Equation 2.20 shows a discontinuity when $T = T_g - C_2^g$; whereupon the viscosity of the material is modelled to become infinite. It is in this regard that some authors have chosen to use this temperature (T_∞), where the discontinuity occurs instead of the measured glass transition temperature (T_g) to be of great importance to the nature of the material.

2.4.4 Continuum Shear Models

Rheological behaviour can be separated into Newtonian and non-Newtonian behaviour in terms of shear viscosity. Experimental Newtonian behaviour at constant temperature and pressure can be represented by the following characteristics (Owens & Phillips, 2002: 77):

1. Shear stress is the only stress generated in shear flow, normal stresses are zero.
2. Shear viscosity does not change with shear rate
3. Shear viscosity is constant no matter the stress (non-zero) and time of shear; even if the stress is stopped and re-applied.

Any liquid that deviates from the above mentioned behaviour is described as non-Newtonian.

The simplest model is that which maintains isoviscous behaviour yet is not a Newtonian fluid. This is the model representing a Bingham plastic. The equation representing this behaviour can be represented by:

$$\sigma = \eta_{pl}\dot{\gamma} + \sigma_B \tag{2.21}$$

There are also several models that are in literature that describes the behaviour of non-isoviscous fluids. In this section, we will briefly describe the ones used in this thesis.

The first model to be discussed is the Power-Law (or Ostwald de Waele) model. This is described by equation 2.22. The apparent viscosity is a function of the shear-rate or stress the fluid is subject to. It has no yield stress, and has a constant gradient between viscosity and shear-rate (on a logarithmic scale).

$$\eta = K_1 \dot{\gamma}^{n-1} \tag{2.22}$$

The behaviour index is classified in 3 ways:

- n>1, the fluid is shear-thickening
- $n = 1$, the fluid is Newtonian
- n<1, the fluid is shear-thinning

When $n = 1$, equation 2.22 simplifies to a constant, which is the behaviour of a Newtonian fluid. The larger the magnitude of n, the more shear-thickening the fluid is; and similarly, the smaller the magnitude of n, the greater the rate of shear-thinning.

This model is widely used but has its limitations. In general, the model is best valid for the shear-rates at which the viscosity changes with constant gradient (log-log plot). From the equation, any deviation towards a zero-shear or infinite-shear viscosity will result in poorer fits. Due to this constraint, the model is generally only applicable for a limited shear-rate range. The flow consistency coefficient index can also be viewed as the apparent viscosity at a shear-rate of 1; and this also shows the importance and choice of units required for collection of experimental data (Chhabra & Richardson, 2008: 9).

The next model discussed shall be the Herschel-Bulkley model (Herschel & Bulkley, 1926). This model is very similar to the Power-law model. This equation however incorporates the addition of a yield stress to the shear-thickening and shear-thinning behaviour; combination of Bingham plastic and Power-law behaviour. Due to this, the model is often written and fitted to the shear stress data for a sample as shown in equation 2.23.

$$\tau = \tau_0 + K_2 \dot{\gamma}^n \tag{2.23}$$

The next model to be described is the Cross model (Cross, 1965), equation 2.24. This is the first in the list to include zero-shear (η_0) and infinite-shear (η_∞) viscosity parameters. Inclusion of these parameters in the model are especially important in polymer engineering; in general they allow for much more variability in shape of curves to be analysed.

$$\frac{\eta - \eta_\infty}{\eta_0 - \eta_\infty} = \frac{1}{1 + K_3(\dot{\gamma})^n} \tag{2.24}$$

Cross (1965) initially included the time dependent parameter, λ, to describe the manner in which the structure of the material breaks down. If this constant is large, breakdown occurs at low shear-rates; as the value decreases, breakdown shifts to higher shear-rates.

Cross (1965) also fixed the flow behaviour index value to $\frac{2}{3}$, and believed this would be sufficient for most materials; however, it has generally been accepted to leave this as a variable as it allows for much more freedom and shape in the curve (Chhabra & Richardson, 2008: 11). This change allows for the slope of the curve, during transition between the two viscosity limits, to be modified.

The Bird-Carreau-Yasuda model is similar to Cross (1965) model, but instead contains an additional parameter to use for curve-fitting, 2.25 (Osswald & Menges, 2003: 139). This equation still has the two limiting viscosities, but contains another parameter used for fitting the transition behaviour. When this parameter, a, has a value of 2, it reduces to the Bird-Carreau model 2.26 (Osswald & Menges, 2003: 139).

$$\frac{\eta - \eta_\infty}{\eta_0 - \eta_\infty} = \frac{1}{\left(1 + (K_3\dot{\gamma})^a\right)^{\frac{n-1}{a}}} \tag{2.25}$$

$$\frac{\eta - \eta_\infty}{\eta_0 - \eta_\infty} = \frac{1}{\left(1 + (K_3\dot{\gamma})^2\right)^{\frac{n-1}{2}}} \tag{2.26}$$

2.4.5 Suspension Rheology

Suspensions are a mixture of a liquid containing solid particles. They occur in many practical applications from concrete to food, and their rheological behaviour is of value in understanding the mixture and its properties. Suspensions have been termed in the same breath as colloids and have been around as a scientific branch for the past few centuries. It is by no means a new concept, and with its applicability so evident in everyday life, it will continue to be so.

In the rest of section 2.4.5, the rheology of suspensions will be discussed; methods of modeling and predicting some of the rheological parameters will be described.

The measurement of viscosity is one of the main methods of understanding rheological behaviour. Continuum shear models and suspension models will be discussed.

Suspension models are based on the concept of the mixture viscosity, and the manner in which the viscosity of the suspending fluid is affected by volume of solid particles. Important aspects in this regard are an underlying understanding of the suspending fluid and knowledge of some of the physical characteristics of the solids (ie. shape, size and distribution).

The first form of the equation was that developed by Einstein, equation 2.27, which describes the viscosity of a suspension when a Newtonian fluid flows around a single sphere

(Larson, 1999: 265). Due to this limitation, the equation is only valid at extremely low volume fractions of filler.

$$\eta = \eta_s(1 + 2.5\phi) \tag{2.27}$$

Extension of Einstein's equation was incorporated by including terms of higher order, ϕ^2 and larger, which express the effects of hydrodynamic interactions on viscosity(Larson, 1999: 265). Further refinement of suspension models were done and many other equations proposed, but the important concept from these models was the property of intrinsic viscosity, $[\eta]$, which incorporates the shape of the filler particle. In the case of spherical particles, its value is 2.5. Many values of this paramater have been determined experimentally for different particles (Wildemuth & Williams, 1984). One such equation is shown, equation 2.28.

$$\eta = \eta_s(1 - \phi)^{-[\eta]} \tag{2.28}$$

The next most important concept is that based on particle crowding. This is a factor that comes to prominence at high volume fractions. It occurs when the filler is high enough so that maximum potential volume of particles during flow is approached and this causes significant increase in resistence to flow. Equation 2.29 is such an equation, it is a modified version of the Mooney equation (Wildemuth & Williams, 1984).

$$\eta = \eta_s \exp\left[\frac{[\eta]\phi}{1 - \frac{\phi}{\phi_m}}\right] \tag{2.29}$$

This leads to next stage of suspension rheology, whereby the afforementioned concepts are incorporated into an equation for a broad range of particles and liquids. This is equation 2.30, the commonly used Krieger-Dougherty equation (Krieger, 1972).

$$\eta = \eta_s\left(1 - \frac{\phi}{\phi_m}\right)^{-[\eta]\phi_m} \tag{2.30}$$

This is a robust equation which is used for a wide variety of fillers with different properties. These parameters when simplified often reduce to other equations when certain values are chosen. In the case of hard spheres, $[\eta] = 2.5$ and $\phi_m = 0.74$ (which is the closed packing value of spheres), leads to a $[\eta]\phi_m$ value of 1.85, that is close to the experimentally determined value of 2 (Krieger, 1972).

The Krieger-Dougherty equation is used extensively in suspension rheology, from food colloids to polymeric melts. The basis of such an equation, makes it a powerful tool for use in analysis of such mixtures and has garnered much popularity.

Another important variable which plays a role in suspensions is that of surface modification. Often dispersants are used to negate the effects of van der Waal's forces at close proximity; thus reducing the effective volume fraction of the system.

Another occurrence in dispersions and colloids is the presence of a non-Newtonian continuous phase. The local shear-rate, of a shear-thinning fluid, is not always indicative of the actual shear-rate measured, it is higher (Barnes, 2003). The viscosity therefore measured is higher than would be expected for such a suspension. With shear-stress however, no changes are needed due to the continuous nature within the fluid. Barnes (2003) therefore concluded that on shear-rate controlled experiments, with a power-law fluid, the Krieger-Dougherty equation need only be manipulated by the effect of the local stress. This is shown in equation 2.31, by addition of the power-law index in the exponent.

$$\eta = \eta_s \left(1 - \frac{\phi}{\phi_m}\right)^{-[\eta]\phi_m n} \tag{2.31}$$

A caveat of suspension rheology is the possibility of settling particles in the fluid (dependent on difference in densities of particle and fluid, and particle size), migration of particles across streamlines (at medium-high shear rates caused by small gaps and large particles) and difficulties accompanied with inertia (largely dependent on particle size and shear rate) (Larson, 1999: 264). In general to eliminate these problems, Barnes (2003) suggest that for moderate loadings, between $25 - 50\%$, that gap distance in the measuring geometry should be around 10 times larger than the particle size.

At low volume fractions, the viscosity does not change considerably; at higher concentrations however shear-thinning can occur at low shear-rates and shear-thickening at high shear-rates (Larson, 1999: 264).

2.4.6 Emulsion Rheology

Emulsions are connected to suspensions with regards to rheology; suspensions are limiting case of a dispersion of solid particles in liquid, and the particles act as droplets with infinite viscosity. These two mixtures are therefore related.

In analysing emulsion behaviour, it is therefore also useful to compare the behaviour to that obtained via suspension models. This will result in parameters which help describe the interaction between the continuous fluid viscosity and nature of the droplets (Barnes, 1994).

Due to this interaction, it is of interest to consider the following during emulsion rheology (Derkach, 2009):

- transition from non-deforming hard spheres to liquid drops (viscosity of the continuous and dispersed phases)

- the change in concentration, when it is necessary to take the interactions of the dispersed phase into account (hydrodynamics)
- the effect of the drop size and distribution

The qualitative rheology of such systems is much better understood. A manner in which to describe the quantitative change in variables is a much more difficult task to achieve with the models at present. To distinguish between the rate of droplet deformability and polydispersity for example is not a simple task (Barnes, 1994).

In rheological studies of emulsions the Krieger-Dougherty equation has also been adopted and is appropriate when the ratio of the viscosity of the dispersed phase to that of the continuous phase tends to infinity. When this is not the case, the viscosity ratio should be taken into account and the modified equation 2.32 is used (Pal, 2001).

$$\eta_r \left[\frac{\eta_r + 5K}{2 + 5K}\right] = \left(1 - \frac{\phi}{\phi_m}\right)^{-[\eta]\phi_m} \tag{2.32}$$

The capillary number (Ca) is also used to help determine the extent of the deformability of the dispersed phase. This number represents the extent of shear to interfacial resistance. This is shown in equation 2.33.

$$Ca = \frac{\eta_c \dot{\gamma}}{\frac{\sigma_{ST}}{r}} \tag{2.33}$$

The point whereby a mixture behaves as a suspension or emulsion is done by making use of the capillary number and viscosity ratio (Grace, 1982)(Jansen et al., 2001). Simultaneously can the effect of droplet break up be considered. Grace (1982) showed that for every viscosity ratio there is a critical capillary number above which an isolated drop will break.

As the viscosity ratio decreases, this critical capillary number increases. The critical capillary number asymptotically increases as the viscosity ratio tends to 4 upon increase. This is shown in Figure 2.13.

This implies that drops will not break up if the viscosity ratio is greater than 4 (Jansen et al., 2001). The interaction of droplets however, destabilises them, thus the critical number can be lower for concentrated emulsions. Jansen et al. (2001) proposed the use of a mean field capillary number for concentrated emulsions; here the viscosity ratio is composed of the emulsion viscosity as opposed to the original continuous phase viscosity. The minimum in the mean field critical capillary number with this modified viscosity ratio now moves progressively to higher values of the viscosity ratio as the dispersed phase concentration increases as shown in Figure 2.14.

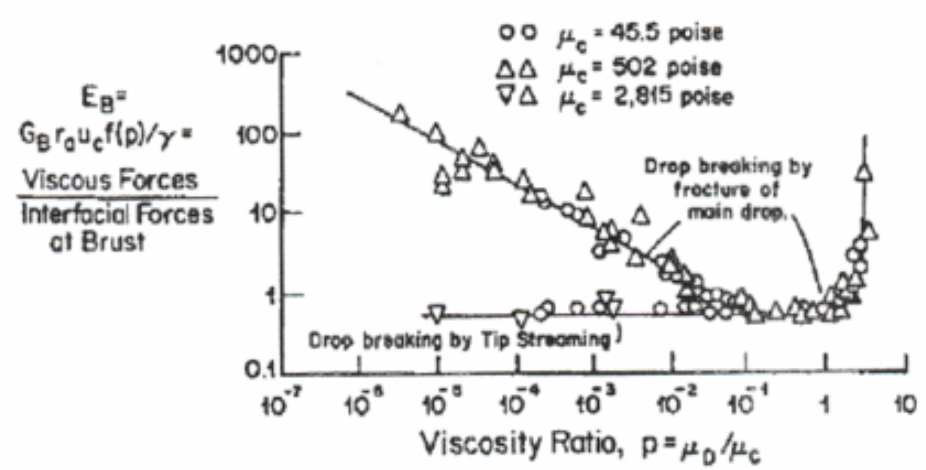

Figure 2.13: Capillary number relationship with viscosity ratio for droplet break up (Grace, 1982)

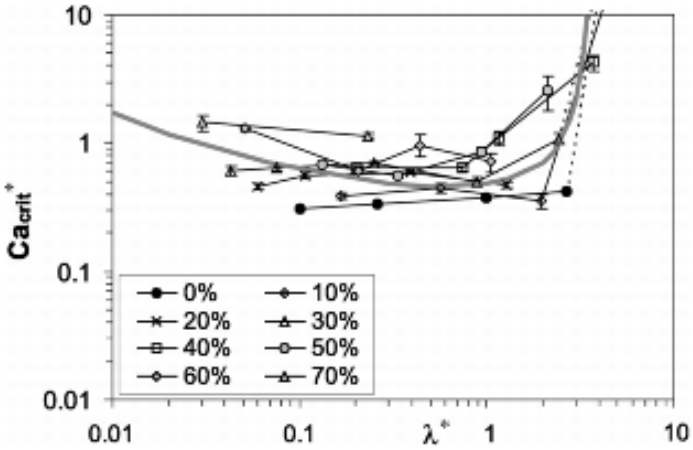

Figure 2.14: Capillary number relationship with mean field viscosity ratio for droplet break up (Jansen et al., 2001)

2.5 Rheological Studies on Pitch and Mesophase Material

Pitch-type substances are complex materials. The measuring of material properties cannot be described easily as they are viscoelastic. The formation of a liquid crystal structure adds further complexity to the mixture as it introduces anisotropy to the system.

Viscosity is an important variable during the production of mesophase as it plays a role in the texture of the coke formed from carbonisation. The viscosity of the system upon solidification is dependant on the chemical properties and constituents; at this point it determines much of the much of the final optical texture of the carbonised, and eventually graphitised product (Marsh & Menendez, 1988). The contribution of viscosity and other rheological properties are often not determined or well understood, and a review of literature which deals with this is necessary, especially since it is a major portion of this thesis. Those articles that pertain to this topic are outlined in this section.

2.5.1 Pitch Material

Bhatia et al. (1977) showed that all pitches show non-Newtonian behaviour under rotational conditions; they in fact behave like Bingham plastics which have a yield stress and plastic viscosity. This was found to be true for pitches with and without additives; additives tested were petroleum coke, carbon black and natural graphite (Bhatia et al., 1977). The pitches themselves are non-Newtonian, but this behaviour is enhanced by the additives. It was also showed that the yield stress as well as the viscosity of the pitch samples decreased with increasing temperature (for the temperatures tested - above the softening point).

Contradictory results were however obtained by Sakai (1979), who obtained Newtonian behaviour upon testing the viscosity of a molten coal-tar pitch. This conclusion was based on an isothermal test carried out at a temperature 30 °C above the softening point; as such Newtonian behaviour is not a surprising outcome. In the pitch-coke systems, and via the analysis of the creep compliance mastercurves, non-Newtonian behaviour was observed at high coke loadings. The higher coke content increased the elasticity of the sample. Shift factors for all the mastercurves produced were found to obey a single Arrhenius-type equation. This was true for all the experiments, at different temperatures as well as with different coke content. This showed that the viscoelastic properties of all the systems are governed by the pitch.

Rheological characterisation of air-blown pitches has also been studied. Menendez et al. (1998) were able to deduce, by the application of transient shear and oscillatory rheometry, that air-blown pitches are viscoelastic materials. A viscous parent pitch obtains stronger elastic properties with increased air-blowing time. This is caused by the

increase in molecular size and cross-linking of the pitch molecules.

Sakai & Inagaki (1981) continued on the determination of viscoelastic properties, this time by applying creep. A petroleum pitch and two coal-tar pitches were tested as well as mixtures of the two coal tar pitches. The measurement of the creep compliance clearly showed that all the pitches were viscoelastic in nature. It was also observed that the viscosity of the samples decreased with increasing temperature and the change in viscosity could be expressed by an equation of Arrhenius form (within the range of temperatures studied). Surprisingly, the creep compliance was found to be an increasing function of temperature, in contrast to polymer based materials. This behaviour was attributed to the non-linear softening behaviour of the pitch as a result of the inter- and intra-molecular interactions of the various constituents. Mastercurves were also produced from the creep compliance data and a linear relationship was obtained between creep compliance and temperature. A large difference was also observed for the mastercurves of the creep compliance from the coal-tar and petroleum pitches. This behaviour has been attributed to the vastly different origins of the pitches.

Measurement of the viscoelastic properties has thus far been limited to the measurement of viscosity and creep compliance. Another interesting and informative approach was also undertaken by Turpin et al. (1994). Controlled stress oscillatory rheometry was applied to characterise the behaviour of a commercially available petroleum pitch. The sample was tested at various temperatures from which loss and storage modulus data were obtained as a function of frequency. Over most of the temperatures tested, the loss modulus decreased with increasing temperature; at low temperatures the relaxation process which gives rise to the loss function is no longer the dominant feature and the loss modulus decreases.

Daji et al. (1999) also observed viscoelastic behaviour from an isotropic pitch. The pitch in question was a heat treated pitch and showed high elasticity and non-Newtonian behaviour at low frequencies. This has been attributed to the higher molecular weight of the material; as opposed to the notion that isotropic pitch can be viewed as a low molecular weight (not cross-linked) polymer. Significant scatter and break down of the time-temperature superposition was also observed for a coal-tar pitch at low frequencies, but no explanation was offered.

Controlled stress and controlled strain oscillatory results were found to be consistent; so were the results obtained by using parallel plate and cone and plate geometries (Py et al., 1997).

To complement the data obtained, time-temperature superposition was applied to produce mastercurves. Shift factors were obtained based on the loss modulus data, but all three mastercurves (loss modulus, storage and viscosity) showed satisfactory superposition. The shift factors of these master curves were adequately described by the Williams-Landel-Ferry (WLF) equation. With the constants obtained from this regres-

sion, the behaviour of the material at different temperatures (close to the glass transition temperature) could be predicted.

Py et al. (1997) showed that there is an α-relaxation mechanism that occurs. The α-relaxation temperature and peak $\tan(\delta)$ temperature (T_δ) were obtained for a petroleum pitch. It was showed that the applicability of the WLF equation is only strictly valid until T_δ. This is as a result of change in regime of the storage modulus shift factors. The characteristic relaxation time had been calculated and correlated with the Tammam-Vogel-Fulcher (TVF) equation within the investigated temperature range.

The same α-relaxation mechanism was observed in a coal-tar pitch (Daguerre et al., 1998). Daguerre et al. (1998) also importantly showed that density variation with temperature is negligible when applying the time temperature superposition principle. This being the case even though there is a linear temperature-density behaviour.

Daguerre et al. (1999) have also used this α-relaxation technique, with accompanying viscosity measurements to characterise raw pitch at a molecular scale. They were able to couple viscosity – temperature and α-relaxation time – temperature data with Stokes-Einstein relations to obtain hydrodynamical diameters. This technique was applied to two petroleum pitches and two coal-tar pitches (a coal tar pitch with primary QI, the other without primary QI). Size ranges observed were in the $9.5 - 20\mathring{A}$ range. This was in good agreement with results obtained by experimental means.

Softening point temperature has also often been used as a guide to some of the flow properties of pitches. Bhatia et al. (1977) investigated the behaviour of petroleum and coal-tar pitch with the same softening points; they concluded that petroleum pitch has a lower apparent viscosity than its coal tar counterpart with increasing temperature. This is not unexpected due to the more aliphatic nature of petroleum pitches. Traditional methods of measuring the softening point of a material is based on the ring and ball method, Sakai & Inagaki (1981) showed that this method leads to different values of viscosity for different materials at the softening point.

2.5.2 Mesophase Material

The study of mesophase material has lead to some interesting phenomena. Nazem (1980) was the first to show the non-Newtonian nature of the material. He studied samples from various pitch sources, and these materials had a very high mesophase content ($78 - 93\%$ mesophase). He showed that these were truly viscoelastic materials that exhibited the Weissenberg effect and die swell. Shear activation energies were calculated and were found to have similar values to polymeric materials.

The first joint microstructural and rheological study was conducted by Cato & Edie (2003) on the synthetically derived mesophase pitch. Flow curves were produced at several temperatures, and all showed similar behaviour; shear-thinning at low shear rates

which was followed by a sudden drop of viscosity to a predominantly Newtonian state. This sudden change in viscosity was dubbed as a "kink" in the flow curve. Samples were studied from the rheometer: before, during and after the "kink". The carefully cast samples showed a microstructural change from a mono-domain structure to a poly-domain structure; this was done via cross-polarised optical microscopy.

Cato et al. (2005) apart from confirming the non-existence of the tumbling effect predicted by most liquid crystal models, also investigated the response of mesophase pitch to transient shear. During transient start up, shear rate step up input, a large overshoot was observed in the shear stress response. A rapid decay was also observed when the step input was removed. The overshoot was shown to be dependant on the rest time between shearing.

The microstructural effects of synthetic mesophase pitch were studied further under different conditions. Kundu & Ogale (2006) studied the structure under shear flow. They found weak orientation of the sample in the radial direction when the sample is squeezed (during gap setting on the rheometer). They also found a flow-aligned fibrous structure during the transient shear flow. Kundu & Ogale (2007) also tested this pitch under oscillatory conditions. Fine and coarse textures were obtained prior to frequency sweeps; the cause of the different textures is as a result of the different sample history prior to oscillation. Four different pre-oscillation methods were investigated: no pre-shear, pre-shear at $1\,s^{-1}$, pre-shear at $10\,s^{-1}$ and large-strain preoscillation at $300\,rad\,s^{-1}$. Under no pre-shear conditions and slow pre-shear conditions, the results were those obtained from Kundu & Ogale (2006). At higher rates of pre-shear the flow-oriented microstructure developed was finer. For large-strain pre-oscillation there was no preferred orientation but the microstructure was round and significantly finer than the sample with no pre-shear. Frequency sweep analysis under the different preparation conditions left the loss modulus of the sample fairly unchanged. The storage modulus on the other hand did change, and this was dependant on the texture of the microstructure (fine texture - lower modulus). The preoscillated sample had similar behaviour to the finely textured pre-sheared sample at high frequencies, but had similar values to the no pre-sheared sample at low frequencies. Kundu & Ogale (2010) also made rheostructural studies of synthetic mesophase material at higher shear-rates via capillary rheometery; for the use of understanding flow orientation of pitch material during the carbon fibre spinning process; in this case, the radial orientation during flow of pitch through the die.

Cheung et al. (1995) investigated the behaviour of a synthetic mesophase material using controlled stress oscillatory rheometry. Mastercurves of loss and storage moduli, as well as the phase angle and dynamic viscosity were constructed. It was deduced that the material behaves elastically at high frequencies, close to the glass transition; with decreasing frequency they become viscoelastic (tending towards Newtonian behaviour), but at an even lower frequency range, the elasticity increased.

Mesophase pitches were also shown to obey WLF-type behaviour (Dumont et al., 2003). These results were based on apparent viscosity–shear-rate behaviour. Analysis based on WLF constants showed that methyl-naphthalene and naphthalene based synthetic mesophase pitches are differentiable. This is unsurprising as pitches from different sources tend to show different WLF behaviour.

WLF behaviour was also observed by Khandare et al. (2000). Shear activation energy was also modelled. It was observed that, as opposed to isotropic pitch, the shear activation energy of a mesophase pitch is shear-rate dependent. The shear activation energy was also calculated to be higher than isotropic pitch at all shear rates.

2.5.3 Anisotropic Pitch

Material Tested During Pyrolysis

Collett & Rand (1978a) investigated the rheological properties of two coal-tar pitches during its transformation to mesophase. This was done by obtaining the apparent viscosity during the thermal treatment of the pitch. They obtained Newtonian behaviour at lower temperatures, but non-Newtonian behaviour was observed at higher temperatures before mesophase formation. Shear-thinning was observed initially, followed by an increase in viscosity, after which the material shear-thinning was observed again (for every temperature). At a temperature which resulted in mesophase content above 25%, increasing viscosity was observed for a second time. Polymerisation was also observed at temperatures above 240℃. As a result of the method by which the experiment was conducted, both phases were always molten, resulting in an emulsion of mesophase in isotropic pitch or isotropic pitch in mesophase, depending on the temperature or composition of phase inversion. It was also shown by Collett & Rand (1978b) that under shear conditions the mesophase spheres change in shape to ellipsoids, therefore easily susceptible to deformation. Under reheating for a sufficient amount of time, these spheres revert back to there spherical shape. Reversible thixotropic loops were observed during reheating, and this reversibility is indicative of a physical phenomenon. It was suggested that the phenomenon was a coagulation of the suspended mesophase spheres which could be broken down at low shear.

The observation of intermediate maximum and minimum in the viscosity of samples upon heating was confirmed again by Balduhn & Fitzer (1980). They showed that this phenomena was true for various pitches and bitumen. The cause of these local maximum and minimum viscosity can be correlated to the temperature of mesophase formation of the respective pitch material. The temperature of mesophase formation was also found to be delayed by shear. The microstructure of the sheared material during heat treatment was similar to that associated with needle coke structure; similar to those of mesophase spheres under shear.

In a later publication by Fitzer et al. (1987), the local maximum and minimum observed in the viscosity during heat treatment was not observed. This was attributed to the inferior temperature control of older machines which were used to obtain measurements.

Material Test Under non-Reactive Conditions

Blanco et al. (1999) studied the rheology of partially anisotropic coal-tar pitches and the contribution of the isotropic phase on those results. Samples were studied with $10 - 46\%$ mesophase content. Flow-curves were obtained for all the samples. It was observed that all the samples were non-Newtonian in nature, behaving as a shear-thinning fluid. The isotropic phase was separated from the heat treated sample by hot filtration. At lower heat treatment times, and subsequent lower mesophase contents, difficulty in hot filtration was observed due to the release of volatiles. The isolated isotropic phase, showed similar behaviour to the heat treated sample. The material was also shear-thinning, but was of lower viscosity than its parent heat treated material. This behaviour is attributed to large molecules formed during the heat treatment that remain in the isotropic phase. It was also suggested that the heat treated pitches that contain mesophase spheres behave similar to suspensions.

Cheung et al. (1995) tested the behaviour of material with high mesophase content ($60 - 95\%$ mesophase) together with 100% mesophase material derived from synthetic means. Time-temperature superposition was implemented to obtain mastercurves and compare the samples. All the high mesophase content samples behaved in a manner similar to the synthetic mesophase sample; elastic behaviour at high and very low frequencies and viscoelastic in the intermediate range. The elastic response of the material is shown to be a non-linear response of the material at lower frequencies. In this frequency range, loss and storage moduli stop diverging; their curves decrease parallel to each other (on a logarithmic scale), and eventually start converging. This behaviour is more pronounced with higher mesophase content.

The most recent work on this topic was done by Braga et al. (2009) on partially anisotropic petroleum pitches. Rheometric softening points matched softening points obtained via conventional methods; increase in pitch viscosity was shown to be affected more by quinoline-insoluble content than it is by toluene-insoluble content. Pitch elasticity was found to be independent of mesophase content and that the elastic recovery is not always observed, even when the storage modulus is dominant over the loss modulus.

CHAPTER 3

EXPERIMENTAL

This section will give a description of the experiments carried out to:

- produce the different types of materials
- characterise the composition and structure of the materials, and the physical properties that result therefrom
- characterise the rheological properties of the materials produced

3.1 Materials Used

The MP110 pitch, obtained from ArcelorMittal, is known to be an aromatic pitch with an approximate softening temperature of 110 ℃ (Ring and Ball softening technique). The origin of this material is typical of coal-tar pitch as part of the coking process. It is also shown that this sample contains particulate material of approximately 10% (carbon particulate and/or inorganic material), determined by quinoline insolubility.

The SASOL pitch is from a lower temperature origin and significantly more aliphatic as compared to MP110. The by-product of the Lurgi-gasification process is a feed material to the delayed coker. The residue from the delayed coker is distilled to yield the pitch. It is liquid-like at room temperature and softens easily (often making it difficult to use for all the characterisation).

Given that these pitches are from such highly different processing backgrounds, make them ideal candidates for investigation in this study.

3.2 Heat Treatment of Material

MP110 and SPAR (SASOL pitch as received) were heated to different temperatures to produce material which contained mesophase. Approximately 600 g pitch was heat treated in a crucible within a vertical electrical tube furnace. A diagrammatic representation of the setup is shown in figure 3.1. The temperature of the furnace was controlled via a TOHO TTM-304 controller and the sample temperature measured via an immersed thermocouple. The furnace vessel is large, approximately 8 dm^3, and heated internally via convection. The pitch was not stirred (this being an unavoidable limitation). Heat treatment was conducted at different temperatures and varying times indicated in Table 3.1. The samples were heated at approximately 5 °C min^{-1}. In all cases a constant nitrogen flow of approximately 2 L min^{-1} was maintained. After thermal treatment the resultant pitches were ground and mixed thoroughly to produce a homogeneous powdered sample.

The furnace temperature was manually set by the operator and the sample temperature monitored throughout the heating process. A much slower and gradual change to soak temperature was enforced. Every 5–10 minutes, the furnace set temperature was changed manually in accordance to the monitored sample temperature. During this time, the sample temperature was continually monitored by the operator to observe if any fluctuations had occurred. For temperatures at 400 °C and lower, an overshoot in measured sample temperature of approximately 10 °C were encountered. Above these temperatures a much more conservative approach was undertaken whereby furnace set temperature was adjusted by smaller temperature increments to achieve the required sample temperature. Deviation in sample temperature did not exceed more than 3 °C than that of the required temperature. Once the soak temperature was achieved, the control of the sample temperature was maintained with greater ease.

The sample names are chosen to represent the heat treatment of the material. The name follows the following structure: name of original material, heat treatment temperature and heat treatment time. For example, MP110HT425T6, is made from pitch MP110; the material was heat treated to 425 °C for 6 hours. HT precedes the heat treatment temperature and T precedes the soaking time at the heat treatment temperature. If the soaking time is one hour the T code is not present in the sample name. SPAR in table refers to the as received (AR) SASOL pitch (SP).

The heat treatment temperature and soaking time used for each run was chosen to produce a material at different stages of mesophase formation. This was determined via optical microscopy where the structure of the material could be analysed.

Two containers were used for the production of the SASOL pitch. The first container produced samples SPAR, SPHT350, SPHT375, SPHT400, SPHT412 and SPHT425. Container two was used for SPHT400T3 and SPHT420T3. All MP110 pitch came from a

Table 3.1: Sample experimental conditions

Sample name	Pitch	Heat Treatment Temperature (℃)	Heat Treatment (Soaking Time) (h)
MP110	Mittal	N/A	N/A
MP110HT350	Mittal	350	1
MP110HT375	Mittal	375	1
MP110HT400	Mittal	400	1
MP110HT425	Mittal	425	1
MP110HT425T6	Mittal	425	6
MP110HT437	Mittal	437	1
MP110HT437T6	Mittal	437	6
SPAR	SASOL	N/A	N/A
SPHT350	SASOL	350	1
SPHT375	SASOL	375	1
SPHT400	SASOL	400	1
SPHT412	SASOL	412	1
SPHT400T3	SASOL	400	3
SPHT425	SASOL	425	1
SPHT420T3	SASOL	420	3

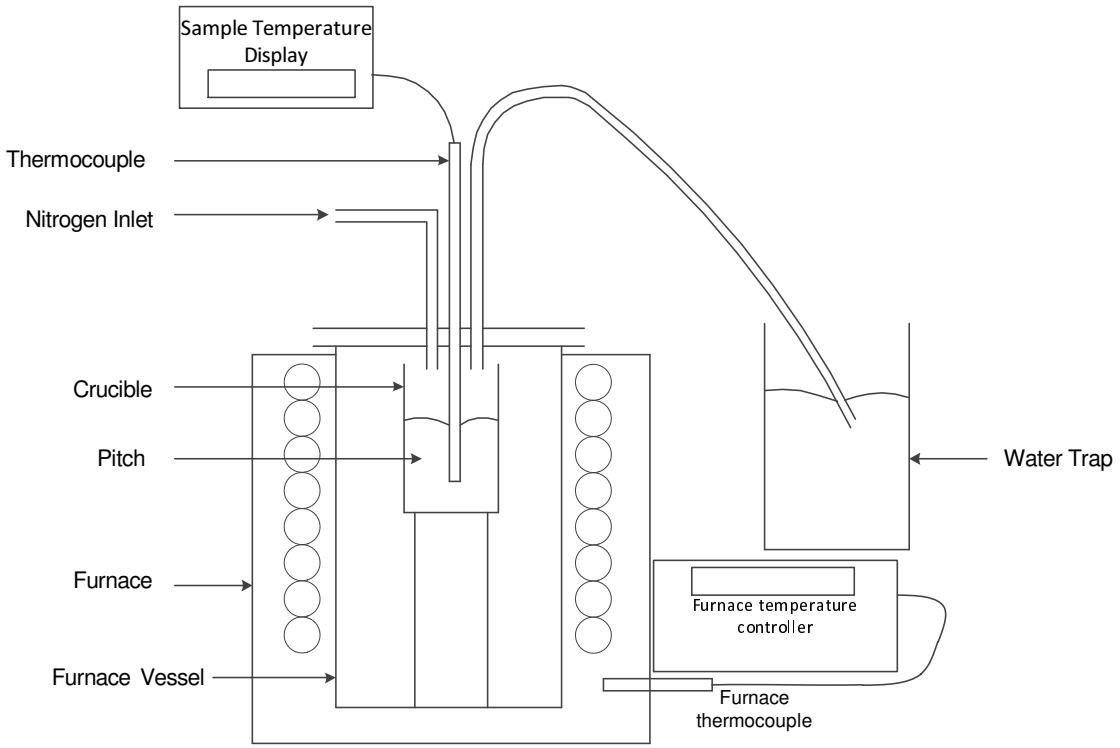

Figure 3.1: Setup to produce heat treated pitch material

homogenised material from a single batch.

3.3 Analysis Techniques

3.3.1 Optical Microscopy

Optical microscopy is used as a standard tool to determine the structure of pitch material during transformation to graphite; in this case, specifically in the transformation to mesophase. The structure viewed is often complex, and resolution to view finer details is not always possible.

The various materials produced from the thermal treatment were all prepared for analysis under the optical microscope. The powdered material was softened and cooled to form a glassy solid, at temperatures not exceeding 250 °C, to ensure no change in composition. The solid samples used were cast in a Struers EpoFix resin and cured with SpeciFix-40 curing agent. The resin and curing agent were mixed with a ratio of 2.5:1 (resin : curing agent). The mixture was poured onto the samples to be analysed in a vacuum environment to prevent excessive formation of air bubbles in the mounted material. The mounting cup (with sample and resin mixture), was cured in an oven at 50 °C for 4 hours.

Once removed from the mounting cup, the cured sample was then ground and polished with a Buehler Alpha 2-speed grinder-polisher. The grinding process was accomplished by successively grinding with silicon carbide based Bueler grinder paper with grit of P400, P600 and P1200. This was accomplished with constant flow of water over the grinding surface. The first stage of polishing was carried out using a ChemoMet soft synthetic pad with MetaDi 3 μm suspension fluid. The final stage of polishing was accomplished using a VerduTex soft cloth and a MasterPrep polishing suspension of 0.05 μm.

After the resulting preparation, the samples were viewed under a Leica DM2500M optical microscope connected to a Leica DFC420 digital camera. Micrographs were taken using Leica Materials Workstation Version V 3.6.1. The micrographs obtained were under polarised light with a 1λ retarder plate with a Fluotar 20X and/or a 50X oil immersion lens.

These micrographs were also used to help determine the mesophase content of the different pitch material. This was accomplished using MATLAB code generated. The micrograph obtained was converted into a grayscale image, shown in figure 3.2. A built-in filter function (based on gradient magnitude) was used to isolate the outline of foreground objects, essentially foreground markers. A morphological technique was used to locate the pixels inside the foreground markers. This is followed by finding markers in the background, and thereafter thresholding the image. The foreground material then appears white, whereas the background material appears black. The white pixels are an approximation of the mesophase material, an example is shown figure 3.3. The amount of white pixels in the image, divided by the total pixels in the image, gives the mesophase con-

tent of the sample. For the sample shown in figures 3.2 and 3.3, the mesophase fraction approximated was 45%. At least 7 images were used for calculating the content for each sample.

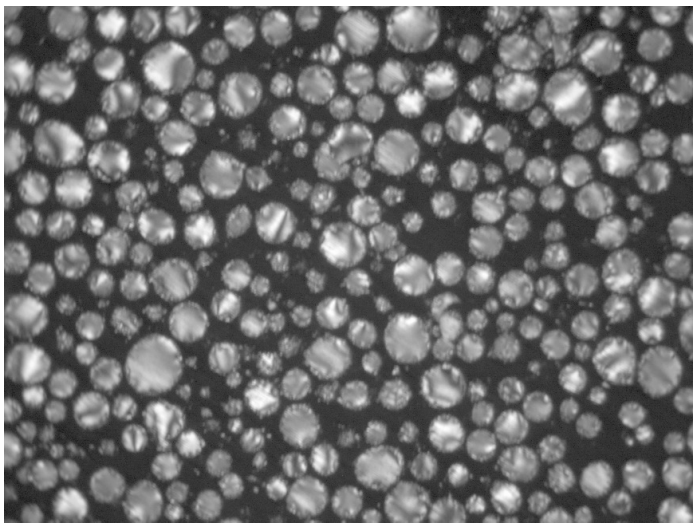

Figure 3.2: Grey scale image from micrograph of sample MP110HT425T6

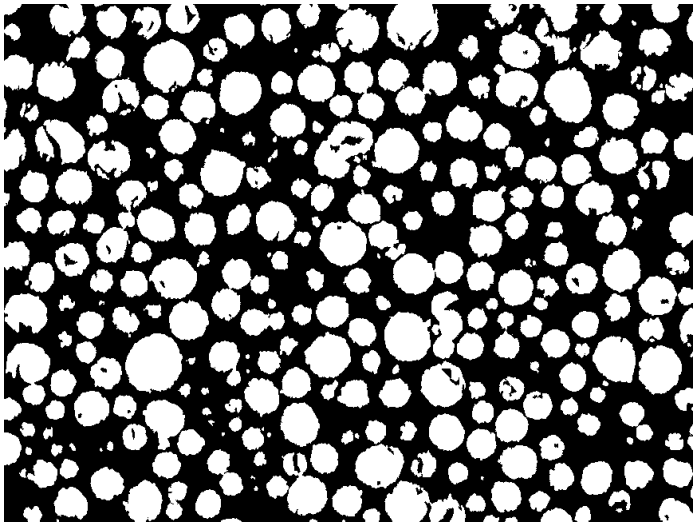

Figure 3.3: Mesophase approximated image from micrograph of sample MP110HT425T6

3.4 Elemental Analysis

This analysis was carried out Dr. Patricia Forbes with the Department of Chemistry at the University of Pretoria. Elemental analyses of the pitch samples were carried out using a Thermo Scientific Flash 2000 CHNS Elemental Analyser. Samples were placed

in a tin container and combusted in a reactor with a furnace temperature of 900 °C and a preheat oven temperature of 75 °C. A helium carrier gas of 130 ml min^{-1} and oxygen flow rate of 250 ml min^{-1} were used. After combustion the products were separated via a gas chromatography column and identified via thermal conductivity detector.

3.5 Solubility

Due to the many compounds found in tar and pitch-like material, the chemical composition is complex and varied. Solubility in different solvents differentiate between different pitches. It can assist in distinguishing the source of the material (petroleum, coal-tar), or following the change in composition of material during processing.

Many authors use this method to characterise their material, in the field of pitch and tar, and the technique chosen to be employed here is similar to that of Blanco et al. (2000). Solvents commonly used are toluene, quinoline, n-methylpyrrolidine and pyridine. In this thesis, the solvents used were toluene and quinoline.

For this experiment, 0.5 g of powdered pitch was used. 50 ml of solvent was refluxed via a Liebig condenser connected to a round bottom flask. The flask was raised to boiling point by a heating mantle. This was done continuously for 40 minutes. The solvent was then filtered whilst still hot through a Whatman No. 4 filter paper. It was re-washed with hot solvent and further with acetone. The filter paper was subsequently dried in an oven at 80 °C. The filter paper was measured before filtration, and then again after filtration and drying. The difference being the insoluble fraction of the sample.

3.6 Thermogravimetric Analysis

Thermogravimetric analysis (TGA) is a method whereby the mass of a sample is measured as a function of temperature (or time). This can be done with different temperature programs. The residual mass at the end of this experiment is an indication of the fixed carbon yield of the material. The derivative of mass loss can give information of the type of volatile matter present.

The instrument used in this work is a Thermal Analysis SDT Q600. Approximately 20 mg of material was used with a 50 ml min^{-1} flow rate of nitrogen. The temperature was ramped from room temperature to 1000 °C at a constant heating rate of 5 °C min^{-1}. The main reason for these experiments was to determine the coke yield of the samples. Two samples from each pitch product were run.

3.7 Differential Scanning Calorimetry

Differential scanning calorimetry (DSC) is a thermal technique whereby the heat flow required to increase the temperature of a sample is measured. The heat flow associated with thermal transitions is the major use of this type of equipment. It can measure glass transition temperature, heat of fusion, latent heat of melting, specific heat, heat capacity, as well as oxidation induction times. Pitch samples, being a glassy materials, were examined using this instrument in order to determine the glass transition temperature. This is often achieved by monitoring a step change in specific heat; a caveat is that it can often be difficult to see this transition. Due to this fact, the heat flow curve was used. The amorphous fraction of the material is often observed in polymers as a peak in the heat flow curve. Similarly in the pitch mixtures, the isotropic material would exhibit a peak and this in turn would be the measured glass transition.

For the experiments done on the pitch samples, a Perkin Elmer DSC400 was used. Sample mass used for these experiments are approximately 20mg. A constant nitrogen flow rate of $50\,\mathrm{ml\,min^{-1}}$ was maintained. The temperature increased from $20\,^{\circ}\mathrm{C}$ to $200\,^{\circ}\mathrm{C}$ at a rate of $10\,^{\circ}\mathrm{C\,min^{-1}}$. Samples were run at least twice to confirm results.

3.8 Thermal Mechanical Analysis

Thermal Mechanical Analysis (TMA) is a technique whereby the dimensions of a sample is measured as a function of temperature. Dilatometry is a version of analysis strongly related to TMA. This is where the sample dimension is measured with negligible applied force. In general, TMA incorporates the manner in which force is applied to the sample, and the load used to do so.

TMA can be run in both static and dynamic force situations. Static mode is with a constant load, whereas in dynamic mode the load is varied. Static zero load would relate to thermodilatometry. Sinusoidally varying force in dynamic mode would relate closely to dynamic mechanical thermal analysis (DMTA).

TMA can be used to determine softening and glass transition temperature, thermal expansion, compression modulus, and some phase transitions. For pitch samples, TMA was used in a manner to find the glass transition and softening temperature. This was done by using thermodilatometry. An example of the manner of calculation of the glass transition is shown in Figure 3.4.

Analysis was carried out using a Thermal Analysis TMA Q400 with a flat-ended macro-expansion probe. Approximately 20mg of powdered sample was placed in an alumina crucible and preloaded with a force of 1N to cause compression in the crucible. The temperature was ramped at $2\,^{\circ}\mathrm{C\,min^{-1}}$ under a nitrogen atmosphere. The change in length was measured, and subsequent thermal expansion calculated, as a function of

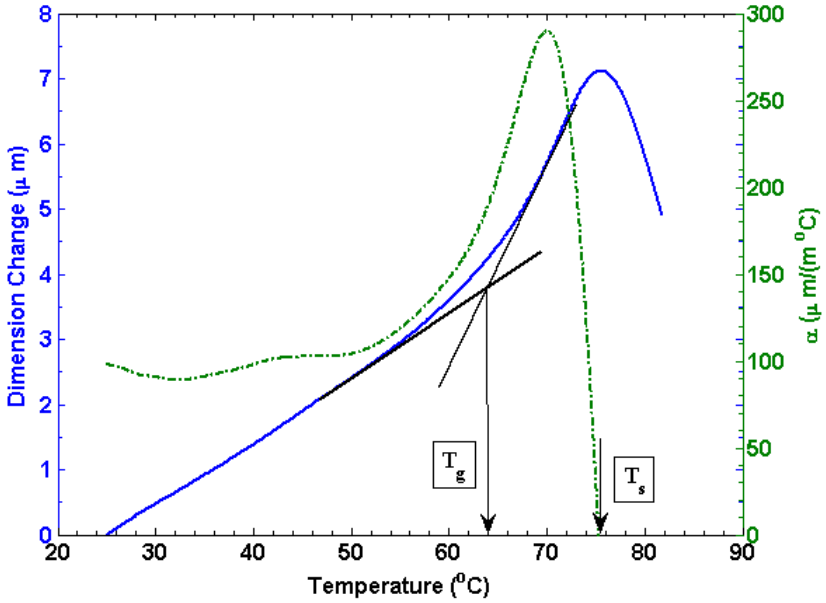

Figure 3.4: T_g and T_s calculation of samples via TMA

temperature. The glass transition temperature was determined by the classical method, as the temperature at which the thermal expansion coefficient changes (Rand, 1987). The softening temperature was measured as the peak of change in length before the probe penetrates the sample. The thermal expansion coefficient (α) is calculated using the TA Universal Software provided.

The point of maximum expansion is regarded as the temperature whereupon the sample only gets smaller, and can thus be viewed as the onset of softening. This can be easily seen via the thermal expansion coefficient curve, where $\alpha = 0$.

3.9 Dynamic Mechanical Thermal Analysis

Dynamic mechanical thermal analysis (DMTA) or dynamic mechanical analysis (DMA) is a technique whereby a sinusoidally varying disturbance (stress or strain) is applied to a sample. Variation with temperature is known as DMTA. The sample can be examined in tension, compression or shear. The instrument used normally allows for variation in temperature, frequency, stress or displacement.

Experiments can be run in different atmospheres and arrangements depending on the instrument available. Single/double cantilever as well as 3-point bending are also used depending on the setup. The result of a typical experiment is the variation of storage and loss modulus, as shown in section 2.4.1. This gives rise to determination of other phenomena typically associated with polymers (cross-linking, oxidation, rubber-transition).

For the pitch samples, temperature effects are of greatest concern. The glass transition

temperature and other temperature effects were investigated.

The viscoelastic character of the samples was determined on a Perkin Elmer DMA 8000 in a standard oven under nitrogen gas flow. The powdered sample was inserted into a metal jacket, and placed in a single cantilever configuration. The metal jacket allows for analysis of powdered material as its mechanical properties are not within the measurement range of the pitch material. Figure 3.6, shows the open jacket on the left, and closed jacket on the right which is used for analysis on the DMTA. The sample was oscillated at frequency of 0.1 Hz and the temperature was ramped at a rate of $1\,^{\circ}\mathrm{C\,min^{-1}}$. The data were analysed to provide storage modulus and $\tan\delta$ (refer back to section 2.4.1) as a function of temperature. The change in elastic modulus is not large (still in GPa), orders of magnitude higher than of a solid pitch material. The modulus approaches magnitudes more associated with that of a metal specimen. The jacket itself does not show any viscoelastic behaviour, and the elastic modulus of a solid is obtained when the jacket contains no pitch. Figure 3.5 is an example of a curve with pitch. The change in magnitude is directly as a result of the pitch within the metal jacket. The encasing of the pitch in the metal jacket thus allows the determination of qualitative change in modulus and $\tan(\delta)$. From this information, the glass transition was determined via a graphical method which is shown in figure 3.5. The onset of decrease in storage modulus was defined as the glass transition temperature.

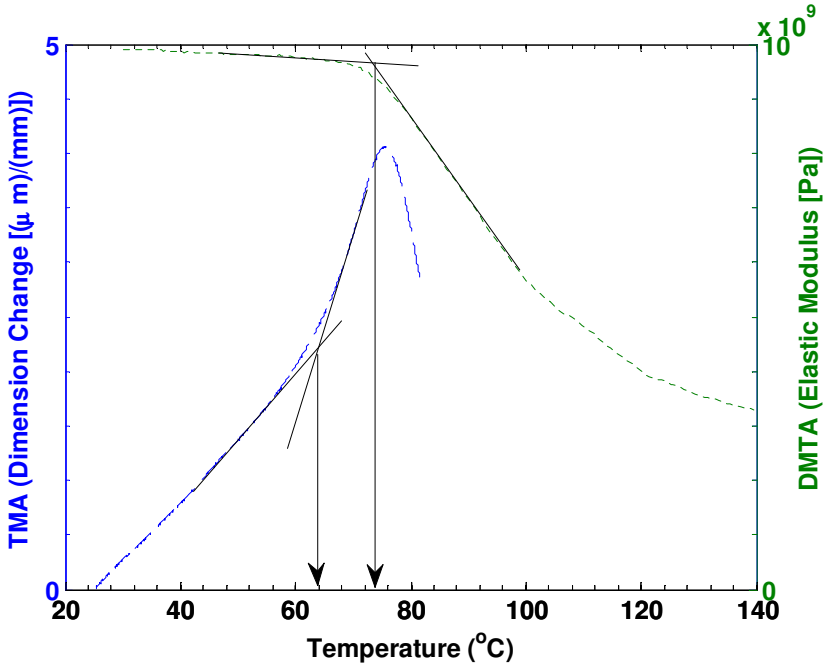

Figure 3.5: Determination of T_g via DMTA and TMA of sample MP110HT400

Figure 3.6: Metal jacket used for DMTA analysis

3.10 Pycnometry

Pycnometry is a measurement of density, via the measurement of volume, of solid material. In most cases this measurement is done by the use of gas in a closed chamber. The gas penetrates the pores of the sample until a specific pressure is reached in the container. The gas often used is helium. Boyle's law is used to correlate the relationship between pressure and volume. With the knowledge of the fixed volume of the container, prior to sample insertion, the volume of the sample can be measured.

For these experiments an AccuPyc II 1340 helium gas pycnometer was used. Approximately 3-5g of powdered sample was used for each experiment and placed in an 11.8 cm^3 cell; the volume was measured 5 times. The experiments were done at room temperature (approximately 25℃). The helium flow rate into the shell was 0.005 $psig\,min^{-1}$, until an equilibrium pressure of 19.5 $psig\,min^{-1}$ was attained. This high pressure forces the gas to fill the vacancies between the powder particles and any open pores present. Due to the implementation of 5 repetitions per sample, a highly accurate density measurement is obtained.

3.11 Rheometry

A study of rheology and the concepts thereof are explained in the section 2.4. Here, a brief overview on the rheometer itself is presented.

In this work, rheological data was obtained from an Anton Paar MCR301 rheometer, as shown in figure 3.7. This instrument unlike the previous generation of rheometers, has an air bearing to induce rotational or oscillatory movement of the spindle; as opposed

to a mechanical bearing. This change in design has a significant advantage as it reduces friction and therefore allows for an improvement in sensitivity and control of the device for the viscoelastic measurements. The machine also has the capability of operating under both controlled shear stress (CSS) or controlled shear rate (CSR) conditions.

Figure 3.7: Anton Paar MCR301 Rheometer with CTD600 convection oven attachment

A CTD600 convection hood attachment was connected to the Anton Paar rheometer. This allowed the sample to be placed in a convection oven to control the atmosphere and conditions of the system under measurement. The oven temperature was controlled via an externally connected TC30 controller device.

The measuring system used for these experiments was a 20mm parallel plate and base. This configuration provided the facilities to measure properties at low and high temperatures whilst also controlling the atmosphere. The pitch samples were investigated under inert atmosphere via a nitrogen gas flow into the convection oven.

The ideal environment to do any rheological tests would be to use a cone and plate measuring system. For use of the convection oven however, the suppliers had made it clear that for the higher temperatures (as the attachment is capable of 600 °C) sensors in the spindle would be damaged and therefore not work. The parallel plate used has no built in sensors, and was therefore sufficient. A further vindication of the use of this system was given by Py et al. (1997), who showed good agreement of results between both cone and plate as well as parallel plate systems.

Optimal conditions for measurements were discovered by implementing a procedure whereby the powdered material was heated to a sufficiently high temperature above softening to obtain a melt. Thereafter the parallel plate spindle lowered towards the pre-specified gap setting, and excess material trimmed away. The gap setting was set at 1 mm for all experiments. At this point, the temperature was adjusted to that at which the experiment was set. This procedure was implemented for all the experiments conducted on the rheometer.

3.11.1 Oscillation

In oscillation mode, the aim of the study was to obtain frequency based data. In order to obtain usable information, an amplitude which allowed the material to behave within a vicinity of constant properties was required. This meant that a linear viscoelastic region (LVER) needed to be identified.

The LVER was determined with a constant frequency, chosen as $10\,s^{-1}$, and the amplitude was varied. For a linear viscoelastic material, the loss and storage modulus remains constant. In most cases, after a large strain of amplitude is applied, the structure breaks, and results in a significant drop in both moduli. This is shown in figure 3.8.

The aim of this experiment was to use a low enough amplitude for oscillation to maintain linear viscoelasticity. This experiment is referred to as an amplitude sweep.

Having chosen an amplitude, a frequency sweep experiment is conducted. This is done when a constant amplitude is applied (throughout the experiment) and the frequency is varied. In this experiment, the amplitude is chosen based on the material and temperature of the experiment. The frequency is decreased from $100\,s^{-1}$ to $0.1\,s^{-1}$ on a logarithmic scale. These experiments were run isothermally at various temperatures.

3.11.2 Rotation

A much simpler process is involved for experiments run for rotational shear. The temperature of the sample is controlled to maintain isothermal conditions. The sample was exposed to increasing shear-rates on a logarithmic scale from $0.1\,s^{-1}$ to $100\,s^{-1}$ (occasionally, if possible, then higher). Often the experiments did not run until completion due to the inability to obtain steady-state results. Steady-state results occur when a constant

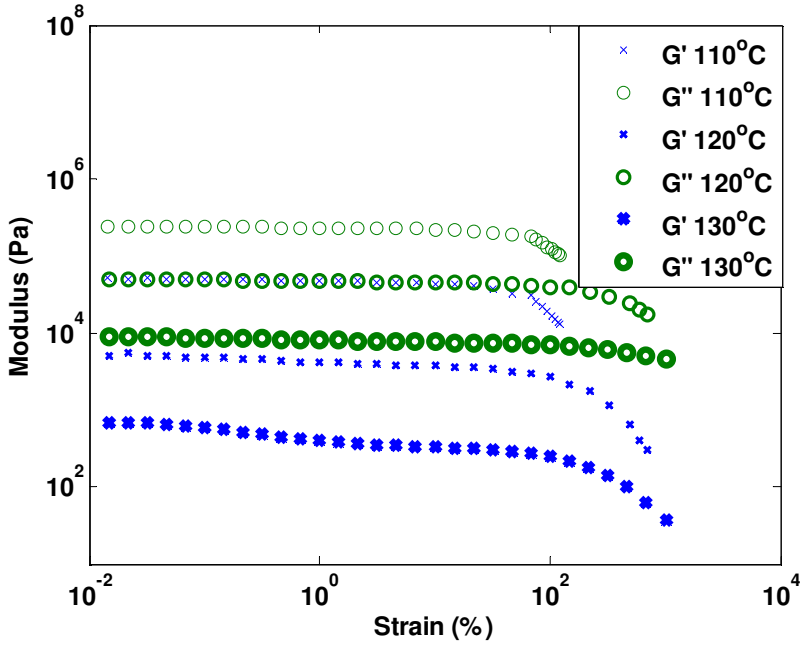

Figure 3.8: LVER measurements during amplitude strain for MP110HT375

torque is applied for a specific shear-rate. This is normally due to material properties, structure, slip conditions, and maximum torque values for the instrument being exceeded.

Rotational experiments were conducted under CSR conditions. This was chosen as shear-rates govern the deformation of structure of a material (even though the stress itself causes the deformation). The change in viscosity is only observed if the deformation is high enough to produce such results. Due to this phenomenon, CSR tests are more reproducible and are preferred for the pitch material.

CHAPTER 4

RESULTS: COMPOSITION AND STRUCTURE OF PITCH MATERIALS

This section contains a comparison of the MP110 and SASOL pitches after thermal treatment; the changes monitored via different analytical techniques. The composition of the heat treated pitch materials was analysed by LECO elemental analysis and solubility determined in toluene and quinoline. Carbon yield was also determined by TGA. The microstructure was studied with optical microscopy. The glass transition, softening and $\tan(\delta)$ peak temperatures were determined via TMA, DMTA and DSC. Density of the pitches were obtained via pycnometry.

The experimental method to produce the thermally treated samples was successful. This method was then implemented for Mittal pitch samples heat-treated at 450 ℃ for 1 and 6 hours respectively. These samples were ground, and mixed. Upon reheating, to soften the sample for preparation for optical micrsocopy, it was observed that the sample did not completely form a liquid. At this point, it was realised that a semi-coke product was produced. For optical microscopy, the samples needed to soften and form a glass-like solid upon cooling to ensure fluid characteristics and homogeneity. Similarly the SASOL pitch heat treated to 437 ℃ resulted in semi-coke product.

The MP110 and SASOL pitches were thermally treated and their yields at the respective heat treatment temperatures and soak times are indicated in Table 4.1.

The pitch yield tends to decrease as the heat treatment temperature and soak time increase. This is consistent with the release of volatile material during the pyrolysis process. MP110HT425 and SPHT400T3 are the only samples that did not conform to the trend expected (yield to severity of thermal treatment). These samples were still used in this study in an attempt to characterise the extent of thermal processing of the pitch not by the heat treatment temperature and soak time, yet be defined by their

Table 4.1: Sample experimental yield

MP110 pitches Sample name	Yield (%)	SASOL pitches Sample name	Yield (%)
MP110	-	SPAR	-
MP110HT350	95	SPHT350	56
MP110HT375	94	SPHT375	54
MP110HT400	86	SPHT400	46
MP110HT425	65	SPHT412	43
MP110HT425T6	79	SPHT400T3	53
MP110HT437	80	SPHT425	41
MP110HT437T6	76	SPHT420T3	35

composition and structure. Hence, the C/H ratio and mesophase content will be used to describe the sample. These properties are not necessarily unique for all pitch samples. It does however prove to be sufficient within the limited scope of this study. A better compositional parameter to accompany the C/H ratio would be the molecular weight distribution of the material, however this was not possible. Samples were not completely soluble in any known solvent to apply MALDI-TOF analysis (as the facility where analysis requested it be so) and attain the molecular weight distributions; this being the case even though an alternative technique is possible as described by Edwards et al. (2003).

4.1 Optical Microscopy

The purpose of microscopy was to follow the change in structure and the development of the mesophase during pyrolysis. This was accomplished by analysing micrographs under polarised light. A trial-and-error process, of different polariser angles, brightness, exposure time and colour saturation, was implemented to find the conditions for each sample. This was done to optimise conditions for the quantification of the mesophase fraction with the image analysis software. The polariser position was therefore adjusted to best view the mesophase; specifically for the analysis of mesophase content using greyscale images.

Figure 4.1 shows 20X magnification micrographs of MP110 derived samples with no appreciable mesophase visible. The as-received MP110 pitch contains no mesophase, but particulate matter is present, as seen in Figure 4.1(a). The black spots are the change in texture of the material around the particulate matter (Brooks & Taylor, 1965). MP110HT350 bears similarity to the as-received material. It is predominantly a light grey colour and therefore isotropic. MP110HT375 shows spherules of mesophase, seen as the brighter white spots in Figure 4.1(c). This point defines the beginning of mesophase development, the nucleated spheres. Figure 4.1(d) is a micrograph of sample MP110HT400. No structure is clearly visible at this magnification, although some white spots are present.

Figure 4.3(a) shows sample MP110HT400 at 50X magnification. Small mesophase spheres are present. The large scale sphere nucleation observed explains the many tiny white spots observed at 20X magnification.

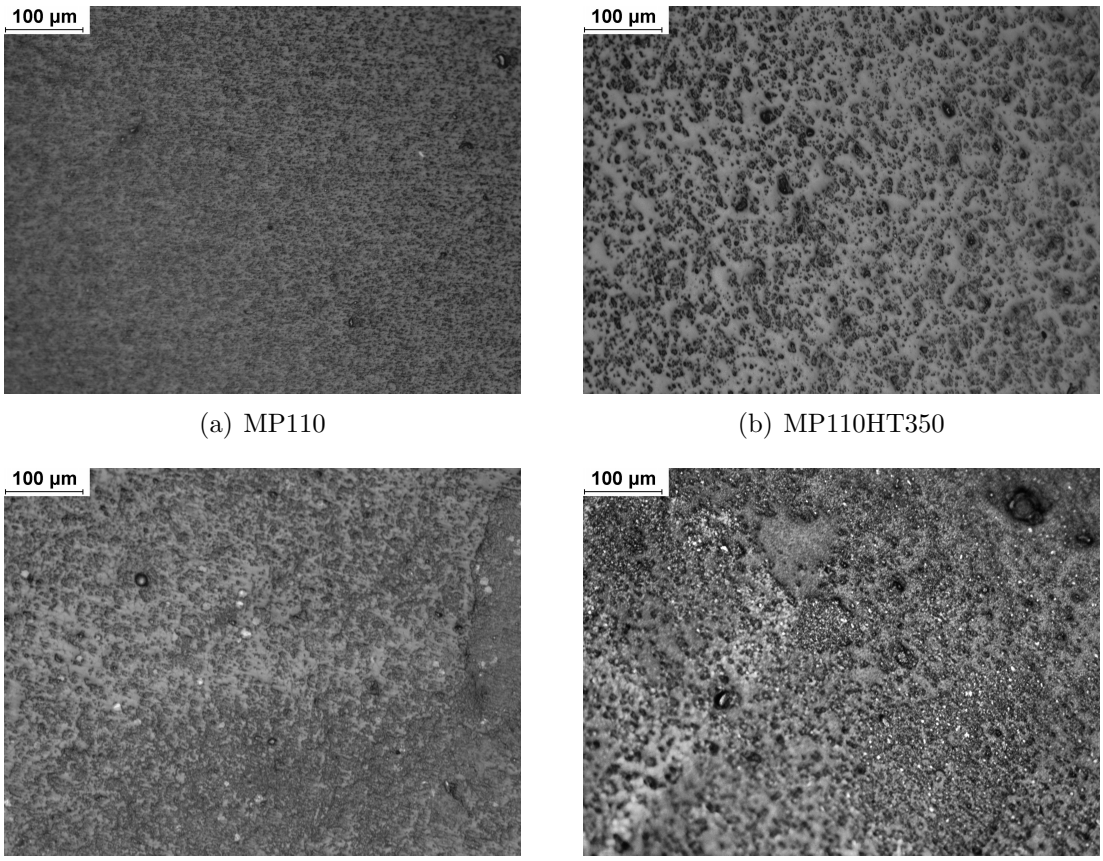

(a) MP110 (b) MP110HT350

(c) MP110HT375 (d) MP110HT400

Figure 4.1: MP110 pitches at 20X magnification showing negligble mesophase

Micrographs of MP110HT425, MP110HT437, MP110HT425T6 and MP110HT437T6 are shown in Figure 4.2. These show clearly the formation of mesophase spheres. Samples MP110HT425 and MP110HT437, shown in Figures 4.2(a) and 4.2(b), bear similar characteristics. They show the development (growth) of mesophase spheres throughout the sample. Continuous isotropic material is present as the major phase. There are many mesophase spheres, uniform in size possibly because no significant coalescence occurs. Samples MP110HT425T6 and MP110HT437T6 also show similarities; see Figures 4.2(c) and 4.2(d). The mesophase content has increased; the sphere size is slightly larger than in MP110HT425 and MP110HT437. Some coalescence may have occurred to produce the largest spheres visible.

Figures 4.3(b), 4.3(c) and 4.3(d) show large mesophase spheres with diameters between $20\,\mu m$ and $40\,\mu m$. There is darker material at the edge of the spheres; this is the particulate matter, this was similarly observed by Brooks & Taylor (1965). MP110HT425 and MP110HT437 have similar microstructures, and hence only the MP110HT437 mi-

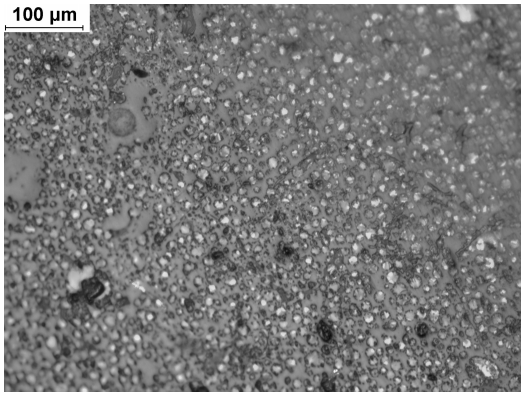

(a) MP110HT425

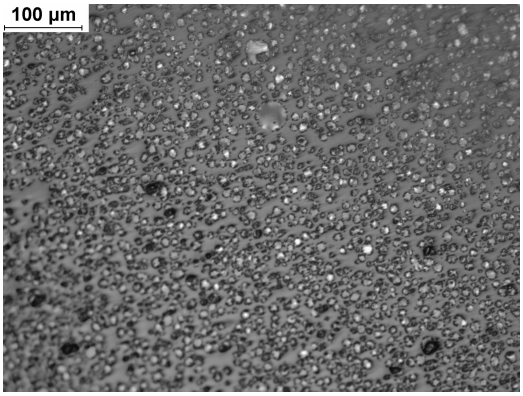

(b) MP110HT437

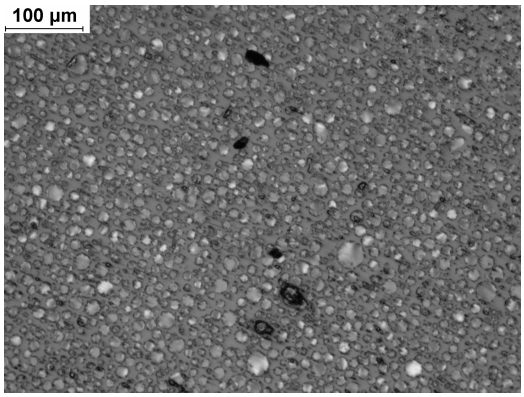

(c) MP110HT425T6

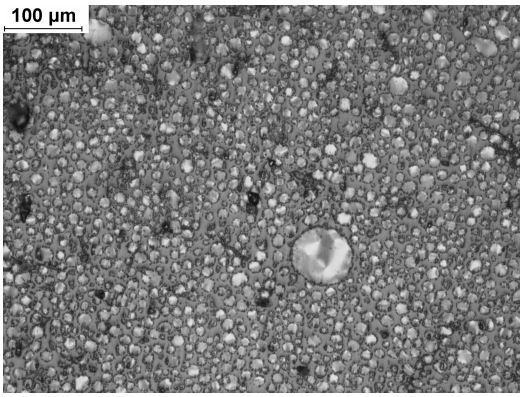

(d) MP110HT437T6

Figure 4.2: MP110 pitches at 20X magnification showing mesophase

crograph is shown at 50X. They have uniform spheres in an isotropic fluid dominated system. Sample MP110HT425T6, shows no significant sphere growth and coalescence. Figure 4.3(d), shows the particulates more clearly. A lack of larger spheres (50 μm and 100 μm) and domains, suggest that sphere growth is inhibited to some extent prior to the production of a semi-coke product. It suggests that there is a high surface tension between the two phases, and that the particulates stabilise the emulsion/dispersion; this the case since more coalescence would have been expected with high content mesophase. Samples MP110HT425T6 and MP110HT437T6 micrographs also show closer packing of the spheres which results in a more dense microstructure.

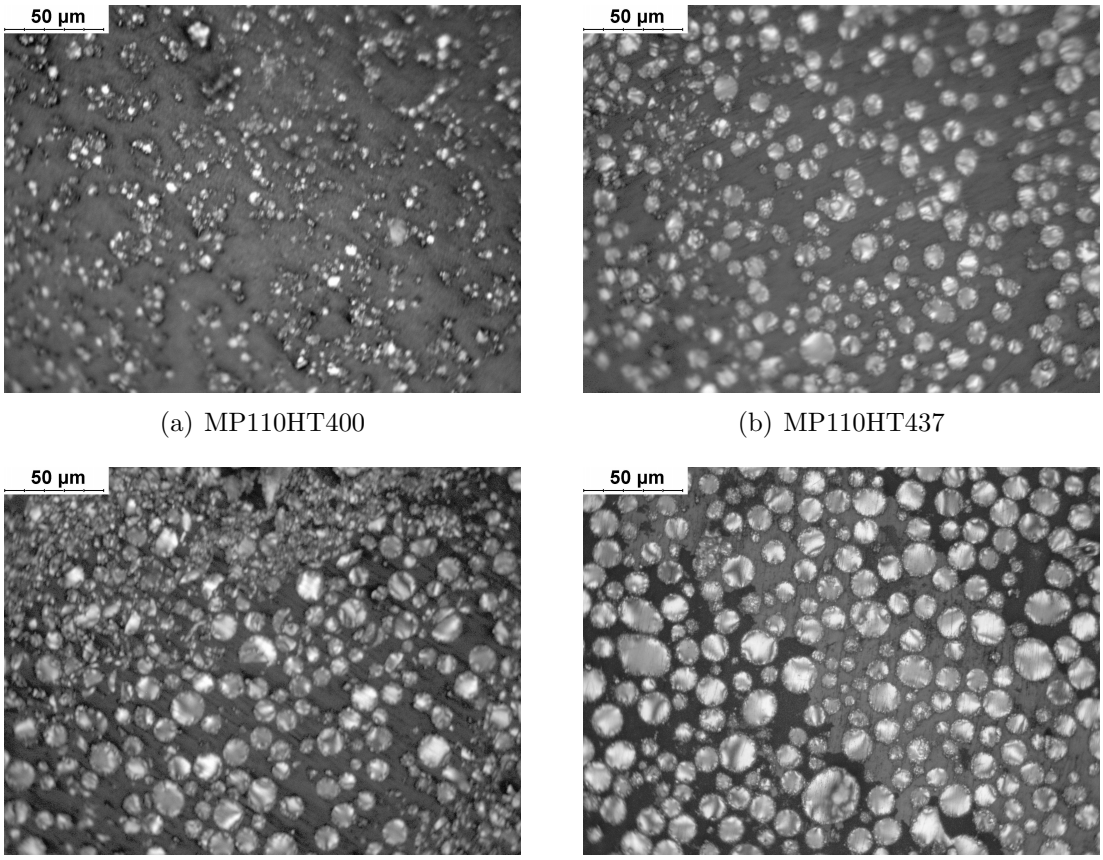

(a) MP110HT400 (b) MP110HT437

(c) MP110HT425T6 (d) MP110HT437T6

Figure 4.3: MP110 pitches at 50X magnification

From the micrographs obtained (at 50X magnification) the mesophase content was approximated via the technique described in Section 3.3.1; the mesophase fraction calculated is shown in Table 4.2. Vieira et al. (2011) showed the limitation of microscopy for attaining the mesophase content. In the attempt to avoid the constraints from the particle count technique, an approximation of mesophase content from mesophase area is made. Parks et al. (1991) also explored the use of NMR to determine mesophase content. Appreciable mesophase content is visible for heat treatment temperatures above 400 ℃. Mesophase spheres in sample MP110HT400 were estimated at 13 %. Samples pre-

pared at an extended soak time show the highest mesophase content. Pitches obtained at the same heat treatment temperature and extended soak time performed as follows: mesophase content increase from 26% to 38% for 425 °C and 27% to 49% for 437 °C. Samples MP110HT437 and MP110HT425 had similar mesophase content; followed by samples MP110HT425T6 and then MP110HT437T6 (in ascending order of mesophase content).

Table 4.2: Mesophase content of various MP110 Pitches

Sample	Mesophase Content (MC) (vol %)
MP110	0
MP110HT350	0
MP110HT375	0
MP110HT400	13
MP110HT437	27
MP110HT425	26
MP110HT425T6	38
MP110HT437T6	49

The pitches: MP110HT425, MP110HT437, MP110HT425T6 and MP110HT437T6, all contained mesophase spheres and did not feature any mesophase domains. This means that they will behave like a suspension or emulsion depending on the temperature.

MP110HT425 and MP110HT437 should show similar characteristics. However samples MP110HT425T6 and MP110HT437T6 should have different characteristics. This shows the beginnings of mesophase particle crowding. This is confirmed by deformed mesophase when spheres impinge.

The structural development of SASOL pitch was also investigated. The as-received SASOL pitch is not solid enough to be embedded in resin. As such, no micrographs were obtained. This was not the case for the pyrolised samples.

Micrographs of SPHT350 and SPHT375 at 50X magnification (Figure 4.4) show mesophase formation. Small spheres start to nucleate at these temperatures (Sima et al., 2003). However, it is difficult to measure the amount of mesophase present. No particulate matter is visible in these micrographs. It is clear that the microstructure starts to change at these temperatures, even if the material is almost completely isotropic. At this point, it is unknown as to whether this small amount of liquid crystal material, is significant enough to influence the material properties of the sample due to size and amount (less than 2%). Material heat treated to 400 °C for 1 hour, was the first to show a reproducible mesophase content. This microstructure is shown in Figure 4.4(c). Micrographs of samples with mesophase are shown in Figure 4.5. Sample SPHT400T3 showed early stage mesophase development (Figure 4.5(a)). Samples SPHT412 and SPHT425 (Figures 4.5(b) and 4.5(c)) show increased mesophase growth and sample MPHT420T3

shows coalescence of mesophase to produce continuous domains (Figure 4.5(d)). This is similar to the micrographs of the structure obtained during thermal treatment of the SASOL pitch as investigated by Sima et al. (2003).

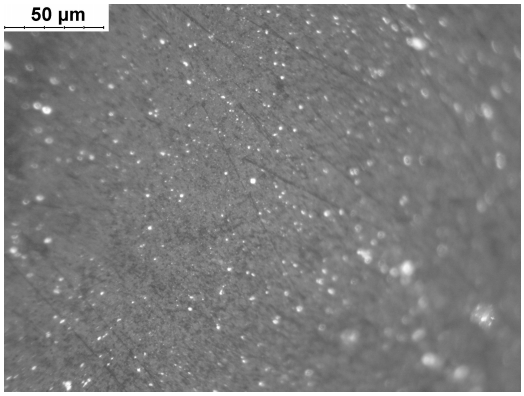

(a) SPHT350

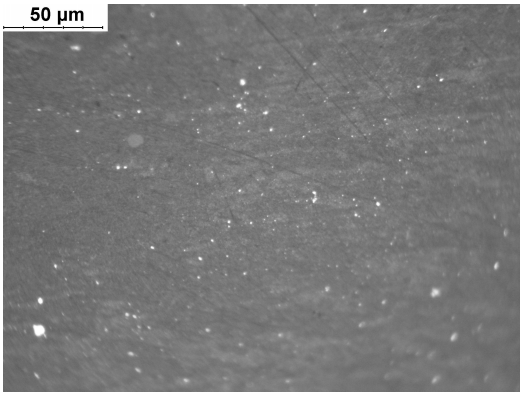

(b) SPHT375

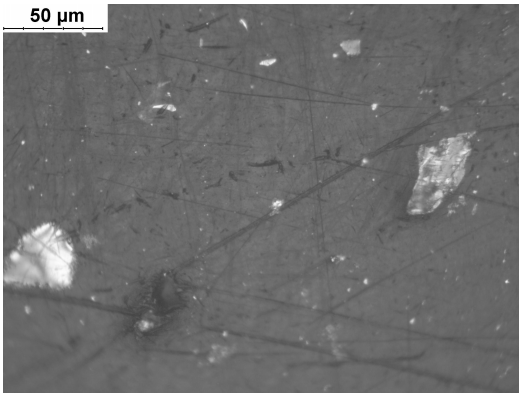

(c) SPHT400

Figure 4.4: SPHT350, SPHT375 and SPHT400 micrographs at 50X magnification

Figure 4.6 shows micrographs of SASOL pitch samples at 50X magnification. As the amount of mesophase increased, the size of the domains got bigger and mosaic structure developed. This shows the coalescence of the mesophase, and the possibility of flow domains when under external disturbance.

The domain size of the fine mosaic mesophase is between $20\,\mu m$ and $50\,\mu m$ for SPHT412 which form a more connected structure. SPHT425 showed domains which were larger than SPHT412. There is also a random shape to the mesophase domains, and seem to be strongly clustered (Sima et al., 2003). This would indicate that movement of these domains at higher temperatures is much more limited due to the irregular shapes and sizes. A more complex gel-like behaviour would be a possibility, due to this constrained mobility. SPHT420T3 possesses continuous mesophase domains; the mesophase is a major component in this sample and as a result will be the dominant aspect in the determination of sample composition and properties. The continuous nature of the mesophase also increases the probability of flow orientation when disturbed.

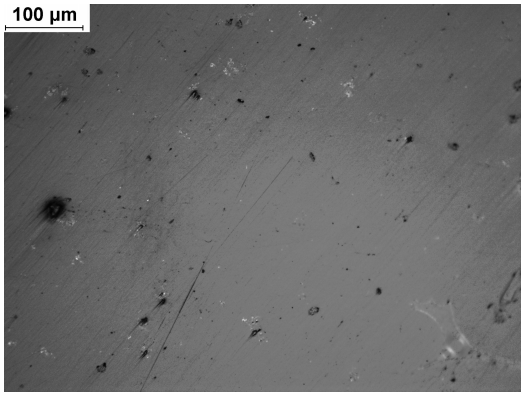

(a) SPHT400T3

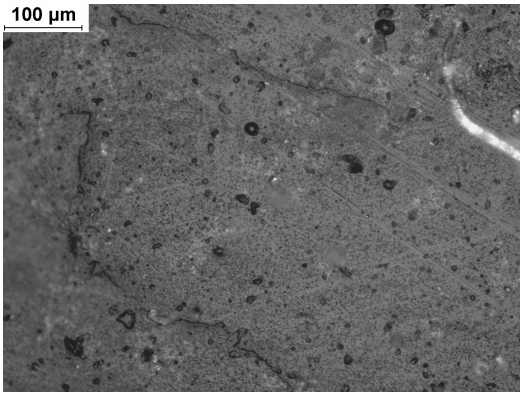

(b) SPHT412

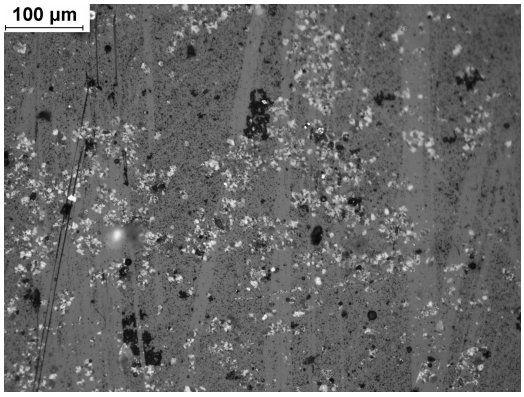

(c) SPHT425

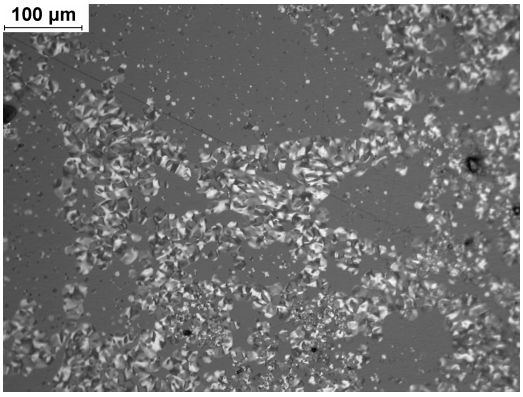

(d) SPHT420T3

Figure 4.5: SASOL pitches at 20X magnification showing mesophase

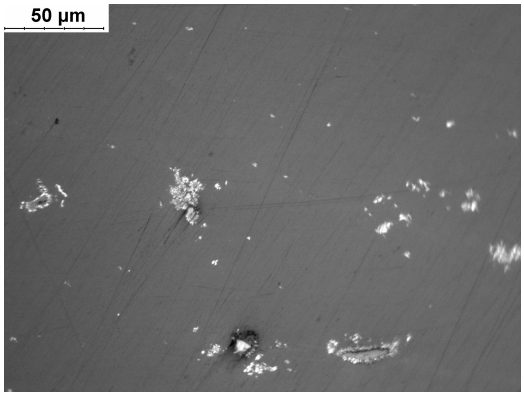

(a) SPHT400T3

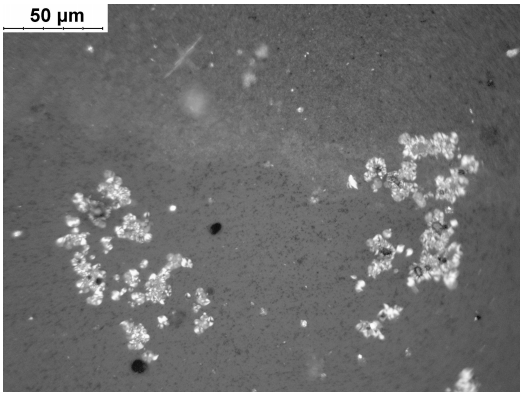

(b) SPHT412

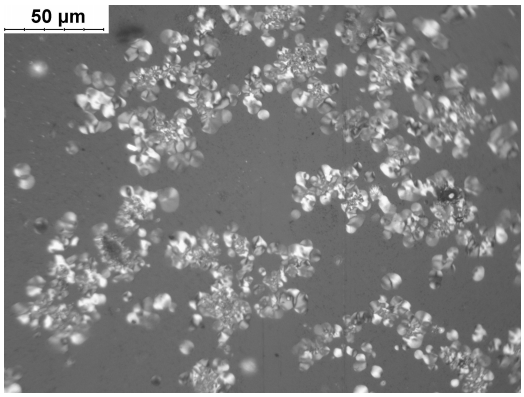

(c) SPHT425

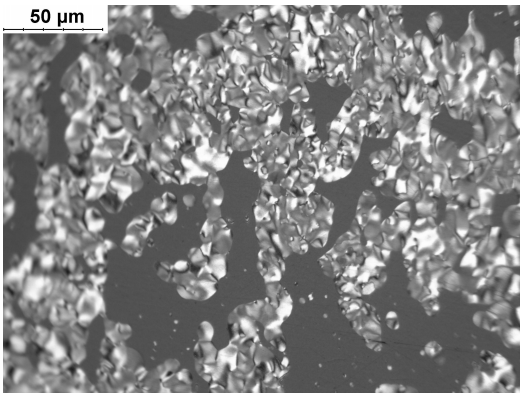

(d) SPHT420T3

Figure 4.6: SASOL pitches at 50X magnification showing mesophase

It is evident from the micrographs of the various pitches, that the mesophase formed is clearly different. MP110 pitch mesophase clearly shows the development of mesophase spheres, as well as their growth; however coalescence was not observed. A major contributing factor to this phenomenon is the particulate QI material. Each mesophase sphere also shows its own local molecular orientation. This seems to be a typical Brooks and Taylor mesophase type A material, from coal-tar origins (Delhaes, 2001: 205).

The SASOL pitches, do form spheres, but their local range of order appears different (irregular) to that of MP110 pitches. The mesophase domains themselves do not seem to be quite as homogeneous in structure. The SASOL pitches produce small spheres which easily coalesce to form larger spheres and small domains. With prolonged thermal treatment these domains become larger producing continuous domains, which are clearly not visible in the MP110 pitches. The mesophase domains themselves also have a fine texture. From these observations, it would appear that a Brooks and Taylor mesophase type B or C is formed (Delhaes, 2001: 207).

The amount of mesophase present in the SASOL pitch samples is shown in Table 4.3. The approximate values for mesophase content for these samples are slightly more difficult to measure since the shapes of the mesophase are ill defined and continuous, especially in the samples where coalescence is evident. Despite this, an approximation is possible and the software works well. The mesophase content determined ranges from isotropic material to 59 % continuous mesophase. There is significant increase in mesophase content between SPHT425 and SPHT420T3; this is likely to result in mesophase dominant characteristic and behaviour at elevated temperatures for SPHT420T3.

Table 4.3: Mesophase content of various SASOL Pitches

Sample	Mesophase Content (MC) (vol %)
SPAR	0
SPHT350	0
SPHT375	2
SPHT400T3	2
SPHT400	9
SPHT412	9
SPHT425	17
SPHT420T3	59

Larger standard deviation is observed for SASOL pitch samples as opposed to MP110 (see Figure 4.7). This is due to greater inhomogeneity of the sample on a micro-scale. MP110 show spheres over the majority of the image, whereas SASOL samples show areas of mesophase domains of irregular shape and varying size.

The evidence from the micrographs and the measured mesophase content indicates the SASOL pitch conversion to mesophase occurs in a narrow temperature window. The

mesophase content in the MP110 pitches is more homogenously dispersed (at micro-scale) due to the spherical nature, as opposed to the (small and large) continuous domains observed in the SASOL material.

4.2 Composition of Pitch Material

The composition of the material was characterised by the elemental composition, solubility and fixed carbon content. At first the elemental composition of the pitch will be investigated. The coal-tar pitch (MP110 pitch) is more aromatic, as compared to the more aliphatic nature of the SASOL pitch.

Table 4.4 shows the major elemental compositions in the different Mittal pitch samples. Analysis results are molar percentages, with oxygen calculated by difference.

Table 4.4: Elemental Composition of Various MP110 Pitches in molar percentage

Sample	C	H	N	S	O	C/H
MP110	63.0	34.4	0.8	0.0	1.8	1.83
MP110HT350	63.2	33.8	0.8	0.0	2.2	1.87
MP110HT375	64.1	34.0	0.7	0.0	1.2	1.88
MP110HT400	63.6	32.2	0.7	0.0	3.5	1.97
MP110HT425	66.0	31.6	0.7	0.0	1.7	2.09
MP110HT425T6	66.4	31.6	0.7	0.0	1.3	2.10
MP110HT437	65.8	32.1	0.7	0.0	1.4	2.05
MP110HT437T6	66.2	30.0	0.7	0.0	3.1	2.20

It is observed and expected that the heat treatment of the material does indeed change its composition. The general trend is an increased carbon and decreased hydrogen content with heat treatment. The severity of treatment (time and temperature) leads to greater changes in composition. The increase in carbon content is greater for samples heat treated above 400 °C. This suggests that condensation and dehydrogenation reactions are pronounced between 400 °C and 437 °C. These are also the samples that contain significant mesophase. Overall, there was no major change in the nitrogen content, which was low to begin with. The amount of nitrogen evolved is directly related to the compounds released, therefore a constant rate of nitrogen release. Interestingly there is no sulphur present in this sample, even though it is a coal-tar pitch with an approximate oxygen content of 2 % by mass. The oxygen was measurement by difference, and hence not the most accurate determination. Samples MP110HT400 and MP110HT437T6 are determined to have high oxygen content (around 3 %); this is suspected to be an error in measurement, and to not be true.

Sima et al. (2003) have done pyrolysis and characterisation on SASOL Lurgi-gasifier pitch. They discerned that the pitch contained high amounts of volatiles and that the mesophase was more prominently seen to grow at temperatures between 410 °C and 430 °C.

This was done in a reactor with 1 MPa pressurised atmosphere. The pitch had a low carbon yield and high volatile contents. The pitch had a high oxygen content, containing a large quantity of phenolic compounds and carboxylic acids. It was mainly aliphatic whilst having moderate content of polyaromatic hydrocarbons. This information was used to help understand the behaviour of the material in this study.

Similar to the MP110 pitch, the SASOL pitch samples result in higher carbon and lower hydrogen content due to higher and longer heat-treatment. This change in C/H ratio observed is common for heat treated materials. The elemental components of the many SASOL pitches are shown in Table 4.5. SPHT400T3 has a high carbon content but unusually high hydrogen content (comparatively to the other samples). This is caused by formation of larger components and re-condensation from volatiles that did not escape during the experimental procedure; this was caused by a blockage of the exhaust gas. It is also clear that the nitrogen content increased with heat treatment.

Table 4.5: Elemental Composition of Various SASOL Pitches

Sample	C	H	N	S	O	C/H
SPAR	52.2	45.2	1.0	0.0	1.6	1.15
SPHT350	53.1	42.8	1.1	0.0	3.1	1.24
SPHT375	55.6	40.4	1.1	0.0	2.8	1.38
SPHT400	58.5	37.9	1.2	0.0	2.4	1.55
SPHT412	58.9	37.4	1.2	0.0	2.5	1.57
SPHT425	59.8	36.6	1.2	0.0	2.4	1.63
SPHT400T3	58.0	38.1	1.3	0.0	2.6	1.52
SPHT420T3	61.3	34.8	1.4	0.0	2.5	1.76

The difference between the two pitches is the higher carbon content in the MP110 pitch, and higher hydrogen content in the SASOL pitch. Both pitches had low nitrogen content, with SASOL pitch higher than the coal-tar counterpart. Both materials had no detectable sulphur content. The oxygen is on average higher in the SASOL pitches (approximately 5 % by mass). This behaviour was observed by Sima et al. (2003). The authors suggest that the high oxygen content was responsible for the rapid change in the macromolecular structure and therefore mesophase formation at temperatures between 410 °C and 430 °C.

The large change in composition, of the SASOL pitch, is observed between 375 °C and 400 °C. This was also the range in which the pitch developed mesophase, and the coalescence of mesophase spheres to form small domains occurred. A similarly large change is observed for SPHT420T3 and the other SASOL samples.

From the elemental analysis, a ratio of carbon to hydrogen (C/H) can be calculated. This will be used to obtain an indication of the aromaticity of the material. Based on C/H ratio the MP110 pitch is more aromatic than the Lurgi-gasifier medium temperature SASOL pitch. The most severely heat treated SASOL pitch is still less aromatic and

has a lower carbon content than the parent MP110 pitch. This was unexpected since SPHT420T3 has such a high mesophase content. This corroborates the findings of Sima et al. (2003).

From this point, the C/H ratio will be used as the variable to monitor the extent or severity of heat treatment to the sample. This is done as a representative compositional characteristic. It is a better indication of the state of the material as opposed to the preparation conditions. Similarly the mesophase content will be used to indicate the structural change of the sample.

The C/H ratio showed that an aliphatic material can still form significant amount of mesophase. The SASOL mesophase separated and grew out of the aliphatic isotropic pitch over a narrow window of temperature. The molecular weight of mesophase is higher than the isotropic fraction. Mokoena et al. (2008) suggested that the condensation reactions of the SASOL pitch are caused by the crosslinking of different aliphatic structures which have reactive oxygen groups. From this point, the larger molecules then become more aromatic via dehydrogenation. The difference and rate of change in molecular weight (between the two phases), should lead to the phase separation; and its sharp transition. This is much more easily expressed via Figure 4.7.

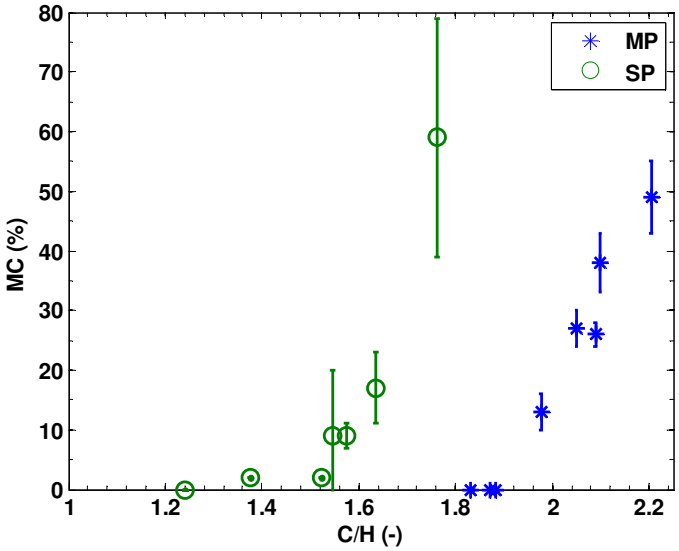

Figure 4.7: Mesophase content for the various pitches

MP110 has a higher C/H ratio than SPHT420T3 (C/H = 1.76), yet SPHT420T3 has the highest mesophase content. This confirms that an aliphatic material can produce a complex microstructure. The C/H ratio calculated for the thermally treated SASOL pitches is also comparable to some of those obtained from Sima et al. (2003). This suggests that some of the samples are at a similar point of transformation to mesophase.

A manner of approximating the change in molecular components of the material is by monitoring its toluene and quinoline insolubility. It is a measure of the change in

chemical composition of the material. For the Mittal pitch this is shown in 4.6.

Table 4.6: Solubility of Various MP110 Pitches

Sample	C/H (-)	MC (vol. %)	TI (%)	QI (%)	non-part. TI (%)	non-part. QI (%)
MP110	1.83	0	34	10	24	0
MP110HT350	1.87	0	38	14	28	4
MP110HT375	1.88	0	40	20	29	9
MP110HT400	1.98	13	47	23	36	12
MP110HT437	2.05	27	58	33	46	21
MP110HT425	2.09	26	60	34	45	19
MP110HT425T6	2.10	38	62	39	50	27
MP110HT437T6	2.20	49	68	41	56	29

The initial MP110 pitch had a quinoline insoluble content of 10%. This is expected since the material has particulate matter observed via microscopy. This material, being solid residue from the coking process, is believed to be composed of carbon and inorganic particles. It is also assumed that the pitch matrix itself, without particulate, contains no quinoline-insoluble material. The particulate-QI, calculated as 10% for the starting material, must remain as part of the yield ($particulate\% = \frac{10}{Yield of\, Pitch\%} \times 100\%$).

From the solubility experiments, the trend is of decreased solubility of samples in solvent as C/H ratio increases (severity of thermal treatment). It is also clear, that in all cases the toluene-insolubles is always higher than the quinoline-insolubles content. The solubility is determined predominantly by the shape, aromaticity, functional groups and side chains. The isotropic and mesophase components may have similar size, therefore some mesophase may still be soluble in a particular solvent (Marsh et al., 2000). This being the case even though Greinke & Singer (1988) showed that mesophase has a higher molecular weight than the isotropic phase. This is expected as with further heat treatment, the average molecular weight of the material is predicted to increase, however this is not a linear relationship with insoluble content (Marsh et al., 2000).

The relevant QI is that which does not contain particulate matter. This is associated with higher molecular weight compounds that form part of the mesophase.

The solubility of the SASOL derived samples was investigated and the amount of insoluble material obtained from filtration is shown in Table 4.7.

The SASOL pitch, unlike the Mittal material, initially contains no particulate matter from previous industrial processing. It was observed that for samples heat treated to 375 ℃, there was no formation of quinoline insoluble material. This agrees with the notion of smaller alkyl-aromatic compounds being the main constituents of the SASOL pitch (Sima et al., 2003) and indicates that the primary change in the pitch material is the release of volatiles. There is a general trend of increased insolubility with C/H. The exception is SPHT400T3 (C/H = 1.52), which has a much lower insolubility in

Table 4.7: Solubility of Various SASOL Pitches

Sample	C/H (-)	MC (vol. %)	TI (%)	QI (%)
SPAR	1.15	0	5[a]	0[b]
SPHT350	1.24	0	15	0
SPHT375	1.38	2	26	0
SPHT400T3	1.52	2	25	12
SPHT400	1.55	9	39	10
SPHT412	1.57	9	47	28
SPHT425	1.63	17	48	33
SPHT420T3	1.76	59	43	40

[a](Sima et al., 2003) [b]Papole (2012)

toluene but still has appreciable quinoline insolubles; this is different compared to other samples with similar toluene solubility. As explained above the behaviour observed in SPHT400T3 is due to the condensation of material back into the crucible. The results lead to the observation of increased aromaticity and possibly molecular weight in the material. Samples with more mesophase showed higher levels of insolubility. The trend with C/H ratio is still observed and reinforces the application of using this ratio as a characteristic of the material, and not the processing (ie. heat treatment temperature and time).

The pitches from the two sources also show overlap in the levels of insolubility in the solvents. MP110 is less soluble in both solvents, than is SPHT400 (although inherently, the particulate content contributes to this). This is unlike the elemental analysis, where no such overlap occurred. This suggests that during the thermal treatment, the small molecules that were present in the parent SASOL pitch formed larger macromolecules; it is not as aromatic as the Mittal material though.

The solubility tests show how important the heteroatoms are in forming larger structures which lead to mesophase formation. Sima et al. (2003) suggests that the SASOL pitch has low PAH content which produce larger crosslinked molecules; these compounds would also be less soluble in the solvents.

Figure 4.8 shows the variation of toluene insolubility for the various pitches. In this figure the trends from the two pitch sources are compared. It was observed that for the SASOL pitch, there is a steady increase until sample SPHT400 (C/H = 1.55) is reached. From this sample, the pitches with higher C/H vary between 40% and 50%. These are also samples that form small domains of mesophase.

There is a strong linear trend of C/H ratio with TI observed in the Mittal pitches. The TI material increased with increase in C/H ratio. This implies that the material constituents are still growing. A steady growth of TI compounds is observed; this trend is repeated for the QI, shown in Figure 4.9.

It is supposed that the original MP110 contains no QI (of a non-particulate nature).

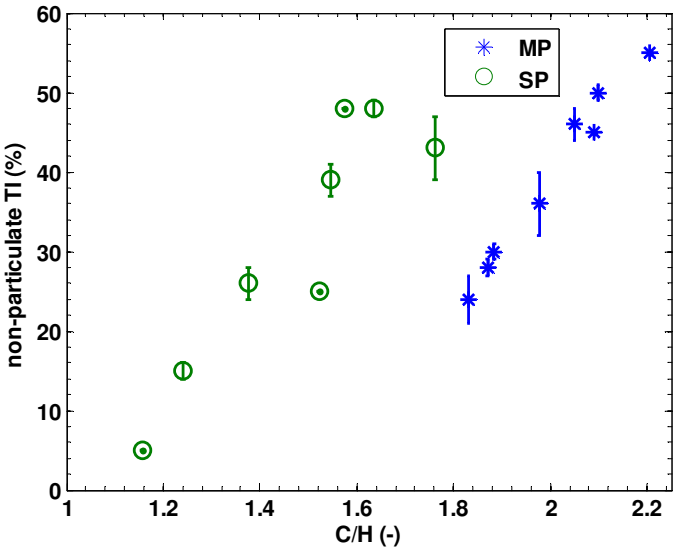

Figure 4.8: TI variation for the different pitches

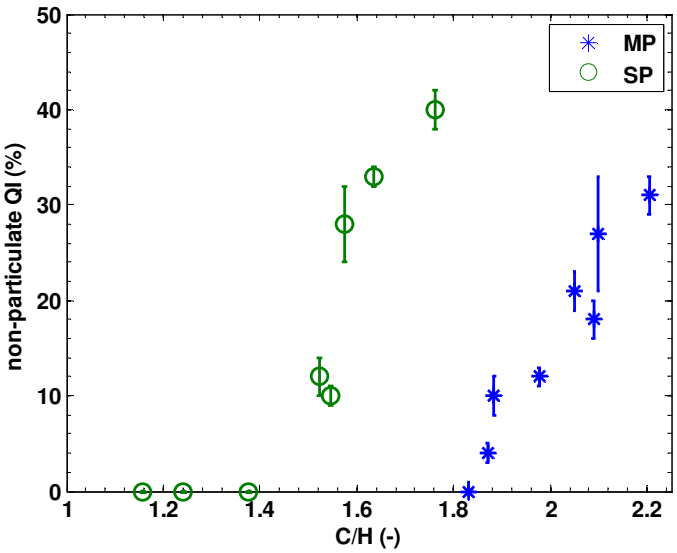

Figure 4.9: QI variation for the different pitches

The QI from this point continually increased with heat treatment. the structure of the raw MP110 is of a sufficient aromatic structure to produce more QI material; this is significant as it is a major contributor to the mesophase constituents (Blanco et al., 1999), this is unlike the SASOL pitch where the aromatic core needs to be developed and this occurs when the pitch is heat treated to 375 ℃ or C/H of 1.38 is reached. From a TI content of approximately 30 % the production of (secondary) QI was possible. This is more suggestive of series reaction route where, TS => TI => QI, in a mechanism similar to that proposed by Marsh et al. (1999). It is noticeable that there is also a sharp increase in the QI over a narrow region of C/H ratio for the SASOL pitch. This further supports the observed transition from isotropic material to mesophase within a narrow temperature range.

Given that the C/H ratio is significantly different for the two pitches, and similar insoluble measures were attained, the insolubles are likely also therefore of different C/H. As QI is a known important component of mesophase, this suggests that the composition of the mesophase is also similarly different. This supports the observation of formation of mesophase with different local molecular orientation; whereby the structure of the mesophase from the two pitches is significantly different. The variation of the non-particulate QI with mesophase content is shown in Figure 4.10.

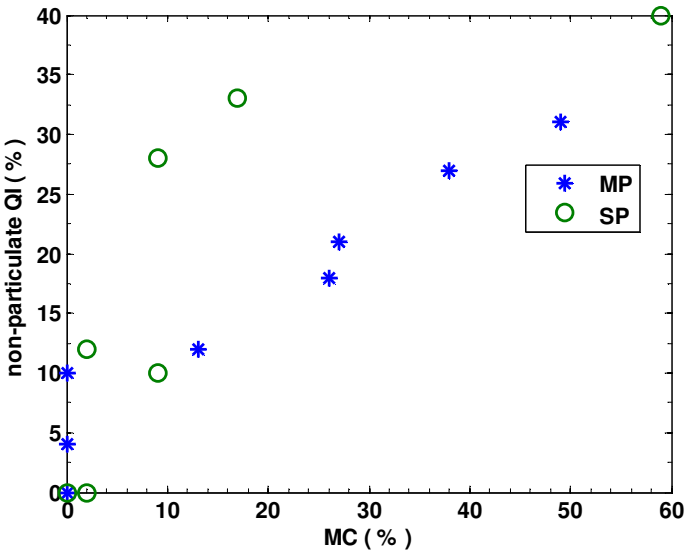

Figure 4.10: QI variation with mesophase for the different pitches

The MP110 pitch has a slightly different characteristic compared to the SASOL pitch. Both QI and TI increase in tandem as seen in Figure 4.11. The increase of QI with TI suggests that there is a direct proportionality between these two characteristics for the MP110 pitch samples. The as received MP110 pitch has the compounds required for increase in both TI and QI.

After evaluating the solubility of the samples, the next compositional parameter in-

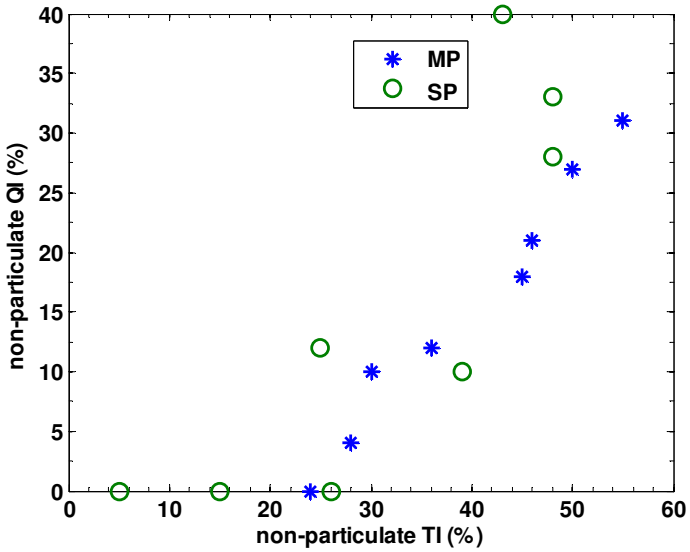

Figure 4.11: Quinoline and toluene insolubles relationship for the different pitches

vestigated was the fixed carbon content. This was done with TGA, and also provides information with respect to the volatile compounds present in the pitch. Figure 4.12 show the curves of mass loss for MP110 pitches upon carbonisation to 1000 ℃.

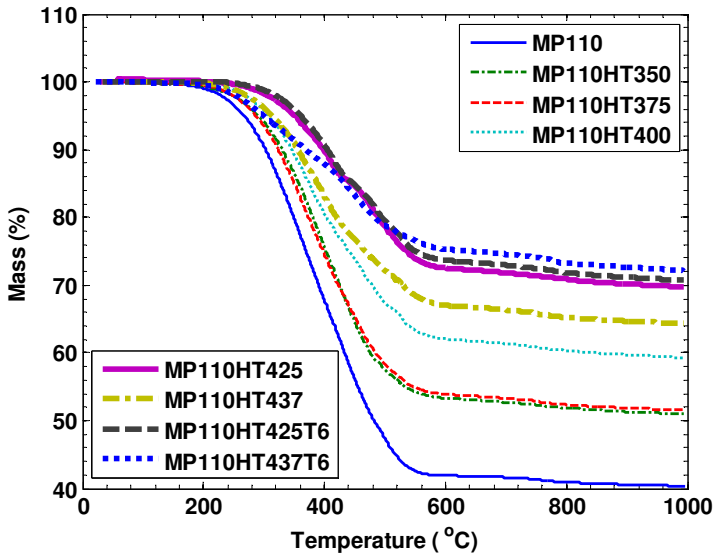

Figure 4.12: Mass loss curves from TGA for the different Mittal pitches

From the TGA curves obtained, each sample has been modified due to the heat-treatment. This is quantifiable by the amount of residue that remains after 1000 ℃ has been reached. This is termed the carbon or coke yield (CY), and is shown in Table 4.8. At these elevated temperatures, the volatile compounds after thermal treatment will be removed, resulting in a pure carbon product.

The change in fixed carbon has increased dramatically from 40%, for MP110 (C/H = 1.83), to 69%, for MP110HT437T6 (C/H = 2.20). The carbon yield is an important

Table 4.8: Carbon Yield for Various MP110 Pitches

Sample	C/H (-)	MC (vol. %)	Carbon Yield (%)	non-part. Carbon Yield (%)
MP110	1.83	0	40	30
MP110HT350	1.87	0	46	36
MP110HT375	1.88	0	48	38
MP110HT400	1.98	13	54	43
MP110HT437	2.05	27	61	49
MP110HT425	2.09	26	66	51
MP110HT425T6	2.10	38	66	54
MP110HT437T6	2.20	49	69	56

parameter to take into consideration when choosing a binder material for the production of synthetic graphite and/or graphite electrodes. The higher carbon yield allows for the release of less material during the carbonisation process. This allows fewer impregnation steps to be used and less change in structure caused by porosity and cracking.

Samples MP110HT350 and MP110HT375 show a small deviation from the raw material. This indicates that the heat treatment temperature difference was not significant enough to induce great change of volatile component composition. Above those temperatures a significant modification is observed. From Figure 4.12 it can be seen that samples MP110HT425 and MP110HT425T6, start to lose mass at a higher temperature compared to the other samples. This is unexpected; it was thought that with the higher thermal treatment and temperature of samples MP110HT437 and MP110HT437T6 (and C/H ratio for MP110HT437T6), the point of mass loss would largely increase accordingly. MP110HT425 and MP110HT425T6 both start losing mass at a similar temperature, as well as having similar C/H ratio and carbon yield, despite having a distinctly different mesophase content.

MP110HT437 and MP110HT437T6 seem to consist of compounds that are more volatile than the samples heat treated to 425 ℃; and despite this MP110HT437T6 still has a higher carbon yield. The shape of mass loss for this particular sample is also different compared to the other samples. It shows slightly different curvature that suggests some compounds present at 425 ℃ are cracked at higher temperatures to produce compounds that are more volatile. Benn (1989) also came to similar conclusions with high C/H ratio thermally treated pitches.

TGA results from the SASOL pitches are shown in Figure 4.13. They show similar trends to the MP110 pitches. Higher thermal treatment and temperature leads to higher carbon yields. This pitch has a starting material with very little carbonisable material, 20% (Table 4.9), and significant mass loss prior to carbonisation temperatures. The highly aliphatic nature of the pitch together with the low carbon yield, suggests that there is an abundant amount of volatile matter in the material. Similar conclusions were made by Sima et al. (2003). Together with the amount of material present at the end of the

experiment, a significant amount is also reacted within a narrow range of temperatures to increase the overall yield.

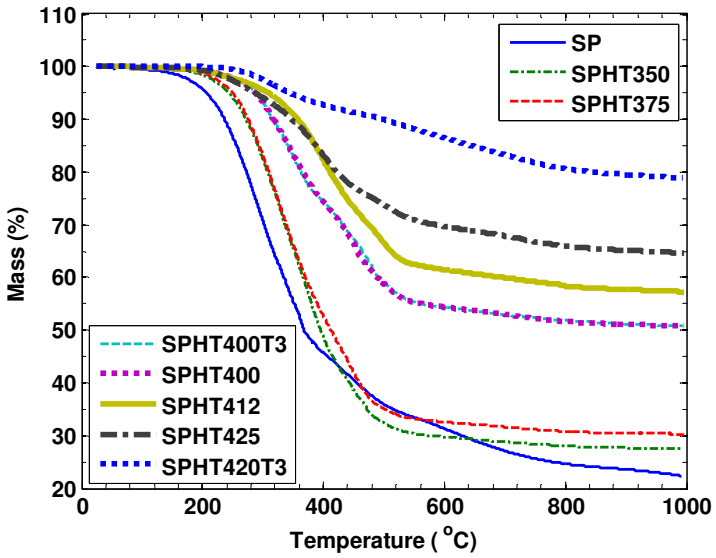

Figure 4.13: Mass loss curves from TGA for the different SASOL pitches

The results from Table 4.9 also show that the material has undergone a significant change to where the fixed carbon yield increases from 20% to 74%. This major change shows that a pre-treatment of the material could be a worthwhile consideration if a high coke yield was necessary (Sima et al., 2003). This would be purely from the release of volatile matter prior to any temperatures that would lead to any condensation reactions or mesophase growth (around 200 °C - 300 °C).

Table 4.9: Carbon Yield for Various SASOL Pitches

Sample	C/H (-)	MC (vol. %)	Carbon Yield (%)
SPAR	1.15	0	20
SPHT350	1.24	0	23
SPHT375	1.38	2	28
SPHT400T3	1.52	2	46
SPHT400	1.55	9	47
SPHT412	1.57	9	54
SPHT425	1.63	17	61
SPHT420T3	1.76	59	74

Table 4.10 shows the conversion of the carbon material produced after processing which is converted to coke. The Carbon Mass column refers to the amount of carbon as obtained from elemental analysis. This shows that a significant amount of the carbon that was uncarbonisible in the beginning, is either released or reacted, converted into a form that has the structure that will be obtained during the coking process.

Table 4.10: Elemental Carbon Properties for Various Pitches

Sample	C/H (-)	MC (vol. %)	non-part. Carbon Yield (%)	non-part Carbon Mass (%)	Carbon Conversion (%)
SPAR	1.15	0	20	88	23
SPHT350	1.24	0	23	86	27
SPHT375	1.38	2	28	87	32
SPHT400T3	1.52	2	46	93	49
SPHT400	1.55	9	47	88	53
SPHT412	1.57	9	54	88	61
SPHT425	1.63	17	61	88	69
SPHT420T3	1.76	59	74	93	80
MP110	1.83	0	30	81	37
MP110HT350	1.87	0	36	80	45
MP110HT375	1.88	0	38	82	46
MP110HT400	1.98	13	43	77	56
MP110HT437	2.05	27	49	80	61
MP110HT425	2.09	26	51	78	65
MP110HT425T6	2.10	38	54	81	67
MP110HT437T6	2.20	49	56	77	73

It is noticeable also that there is an increase in the conversion of the amount of initial carbon to carbonisable carbon from the different thermal treatments of the SASOL pitches. The conversion increases from 23% to 80%. This shows that not much of the material from the treatments is left unused when exposed to higher temperatures, which could lead to higher yields of graphite structured carbon. This is expected, due to such a high percentage volatile release from thermal treatment. Similar behaviour is observed for the MP110 pitches.

From the previously discussed information, we can also approximate the extent of condensation reactions. This is done considering the starting material, its thermal processing (yield) and finally the carbon yield at 1000 ℃ from TGA. This is indicated by an increase in the carbon yield conversion to 25% (for SPHT420T3). MP110 pitch samples continually increase to a 53% conversion of the starting material (43% if non-particulate matter is taken into account). From both the MP110 pitch and the SASOL pitch samples, it is evident that the major factor in producing a higher carbon yield starting material is the release of volatile matter.

The relationship of C/H with coke yield (CY) is shown in Figure 4.14. The trends observed for the Mittal pitch and the SASOL pitch is slightly different.

The SASOL pitch appears to have two linear regimes in Figure 4.14. Up to C/H of 1.38 there is a single gradient, above this ratio there is an increase in the gradient of the carbon yield. This indicates a change in behaviour of the material, due to the change in composition. The initial region is the isotropic pitch that has major volatile release, and

Table 4.11: Elemental Carbon Yield based on Process

Sample	C/H (-)	MC (vol. %)	non-part. Carbon Yield (%)	Yield (%)	Yield Conversion (%)
SPAR	1.15	0	20	-	-
SPHT350	1.24	0	23	56	13
SPHT375	1.38	2	28	54	15
SPHT400T3	1.52	2	46	53	24
SPHT400	1.55	9	47	46	22
SPHT412	1.57	9	54	43	23
SPHT425	1.63	17	61	41	25
SPHT420T3	1.76	59	74	35	26
MP110	1.83	0	30	-	-
MP110HT350	1.87	0	36	95	34
MP110HT375	1.88	0	38	94	36
MP110HT400	1.98	13	43	86	37
MP110HT437	2.05	27	49	80	39
MP110HT425	2.09	26	51	65	33
MP110HT425T6	2.10	38	54	79	43
MP110HT437T6	2.20	49	56	76	43

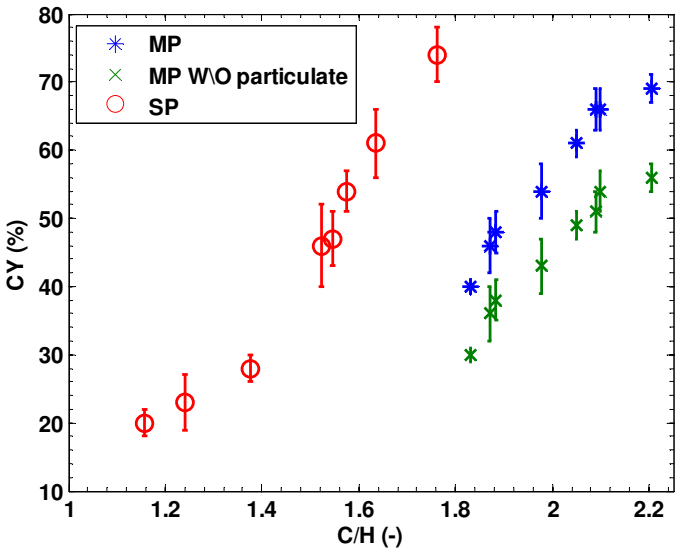

Figure 4.14: Carbon Yield of the different pitch samples

secondary steeper gradient coincides with the samples that develop and have mesophase. The change in structure and presence of larger molecules, possibly QI, affect the coking characteristics of the material. This is visible in Figure 4.15.

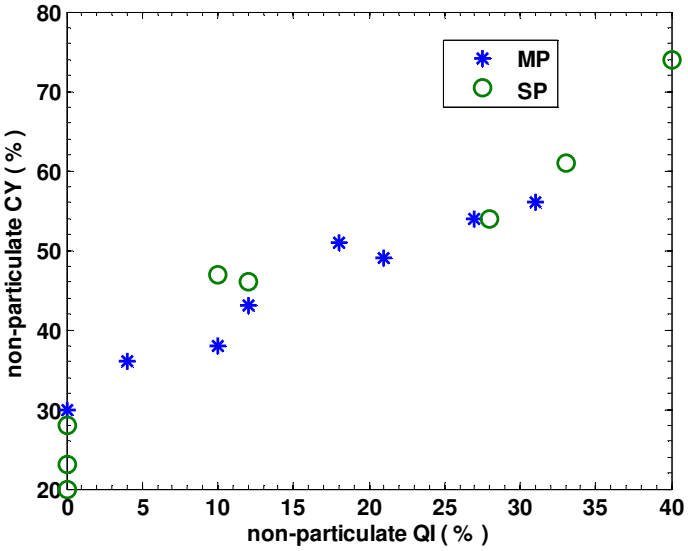

Figure 4.15: Quinoline insoluble content in carbon yield

The most striking feature is the direct proportionality between these two parameters. This suggests that there is a link between the final carbonisable and the non-partculate QI. This may be as the structure of carbon material in the form of non-particulate QI (and mesophase), is responsible for the increase in coke yield.

This implies that there is approximately 30% carbonisable material in the original pitch which is soluble in quinoline, and that any further carbonisable material would have to be insoluble in the solvent (for MP110). For the SASOL pitch, the carbonisable carbon needs to first be developed to approximately 30 %, before any additional carbon in the form of QI (which is carbonisable) is produced.

4.3 Glass Transition and Softening Behaviour

The glass transition temperature of the samples was determined via thermal mechanical analysis and dynamic mechanical thermal analysis. Dynamic scanning calorimetry was also used to attain additional transition information.

4.3.1 TMA

The first technique used to observe the glass transition of the samples was TMA. Dilatometry was used to graphically obtain the glass transition temperature as shown in Figure 3.4. The softening temperature in this section is determined at the point of maximum

length, this being the temperature after which, upon heating, the sample length (height) only decreases. Barr & Lewis (1982) and Liedtke & Huttinger (1996) have also previously obtained glass transition temperatures of pitch materials via TMA.

In polymers, the softening point is generally assumed to be around 50 ℃ above the T_g. Using the TMA, only the first glass transition and softening behaviour was visible. The change in dimension and thermal expansion of the different MP110 pitches is shown in Figures 4.16 and 4.17.

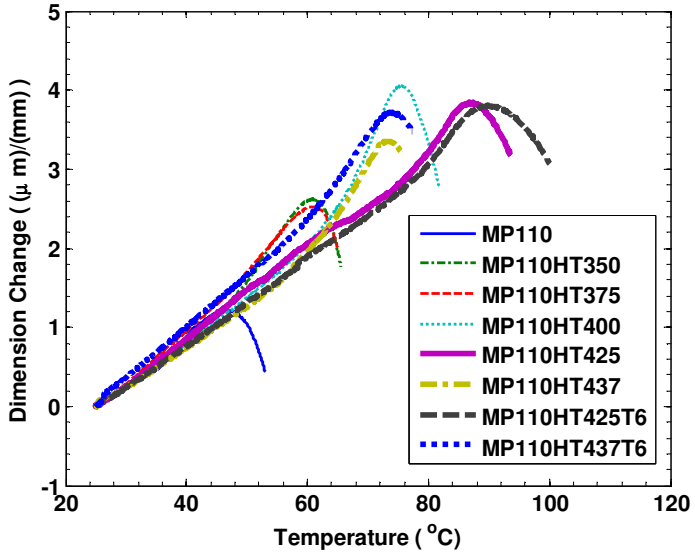

Figure 4.16: Dimension change curves from TMA for the different Mittal pitches

The dimensional change of the samples has two linear regions prior to maximum length, this allows for calculation of T_g.

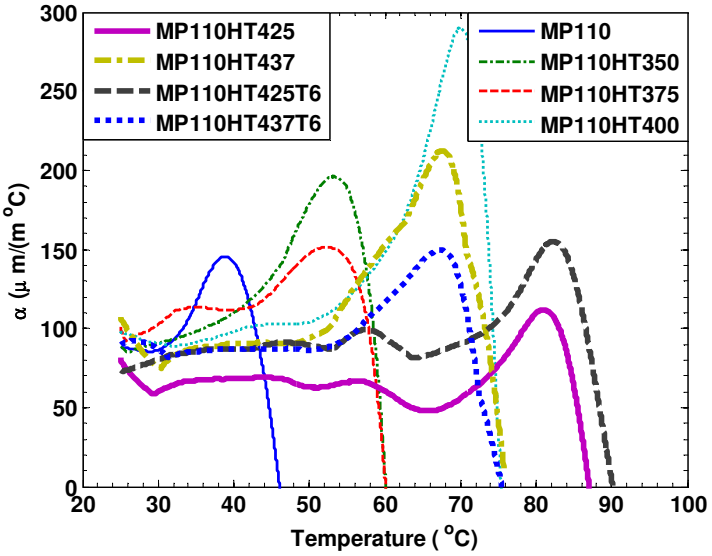

Figure 4.17: curves of thermal expansion from TMA for the different Mittal pitches

Thermal expansion coefficient (α) curves also shows that most samples have a clear

initial linear region. The shape after this region, is a transient curve with slow increase and a sharp decline. The softening temperature is determined at the point of maximum length; this is the point where the thermal expansion coefficient is zero. Glass transition and softening temperatures determined for the MP110 pitches are showed in Table 4.12.

Table 4.12: TMA Properties for Various MP110 Pitches

Sample	C/H (-)	MC (vol. %)	T_g (°C)	T_s (°C)
MP110	1.83	0	37	46
MP110HT350	1.87	0	47	59
MP110HT375	1.88	0	50	59
MP110HT400	1.98	13	65	73
MP110HT437	2.05	27	65	73
MP110HT425	2.09	26	76	84
MP110HT425T6	2.10	38	77	87
MP110HT437T6	2.20	49	64	73

Compounds which are volatile at lower temperatures are related to the compounds that soften at lower temperatures; therefore also have lower glass transition temperature. From the TGA curves, there is a change from samples heat treated to 425 °C and to 437 °C. Samples heat treated to 437 °C lose mass at lower temperatures.

From the calculated glass transition temperatures, an upward trend is observed with respect C/H ratio, until C/H of 2.10 (sample MP110HT425T6) is reached. At the higher temperature of 437 °C for 6 h, there is a drop in glass transition temperature. This trend of volatile release and T_g is thus observed.

It should be noted here, that the T_g determined for these pitches are that of the continuous phase. In the case of the Mittal pitches, this is observed to be the isotropic phase (see Section 4.1).

MP110HT400, MP110HT437 and MP110HT437T6 also have similar glass transition temperatures. This would imply that the structure and composition of the isotropic phases of these samples are closely related; similar behaviour of their isotropic fractions would be expected. The same argument can be made for MP110HT425 and MP110HT425T6.

From this analysis, it is clear that the softening temperature is not appreciably higher than the glass transition. The two temperatures are approximately 10 °C apart as compared to 50 °C often used in polymers.

The dimension change and thermal expansion curves for the SASOL pitches are shown in Figures 4.18 and 4.19.

The shape of these curves are similar to the pitch samples from the Mittal material. The most distinct feature in these figures is the dominance of SPHT420T3 (C/H = 1.76) and hence is showed separately in Figure 4.20. From this sample it is difficult to measure

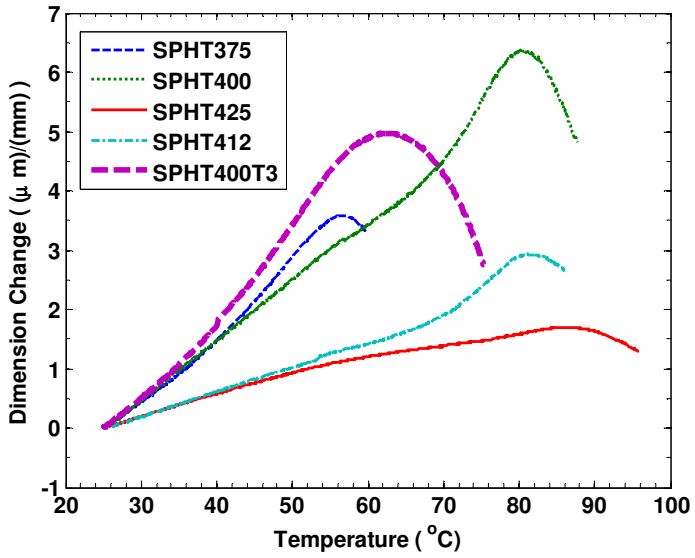

Figure 4.18: Dimension change curves from TMA for the different SASOL pitches

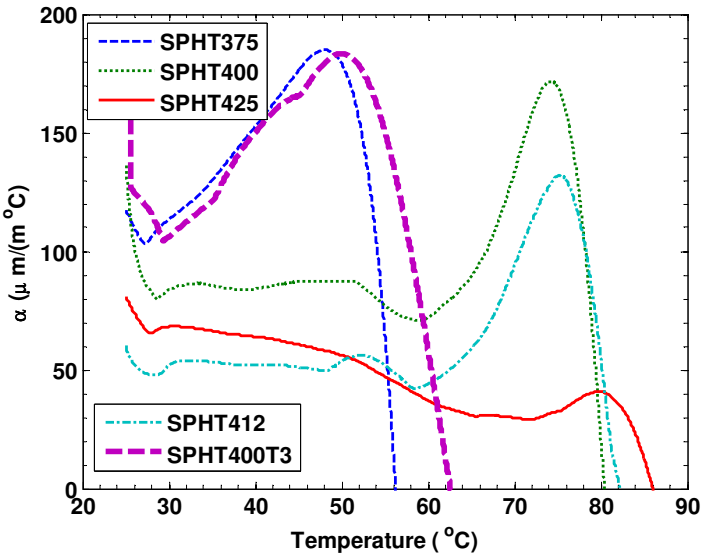

Figure 4.19: Curves of thermal expansion from TMA for the different SASOL pitches

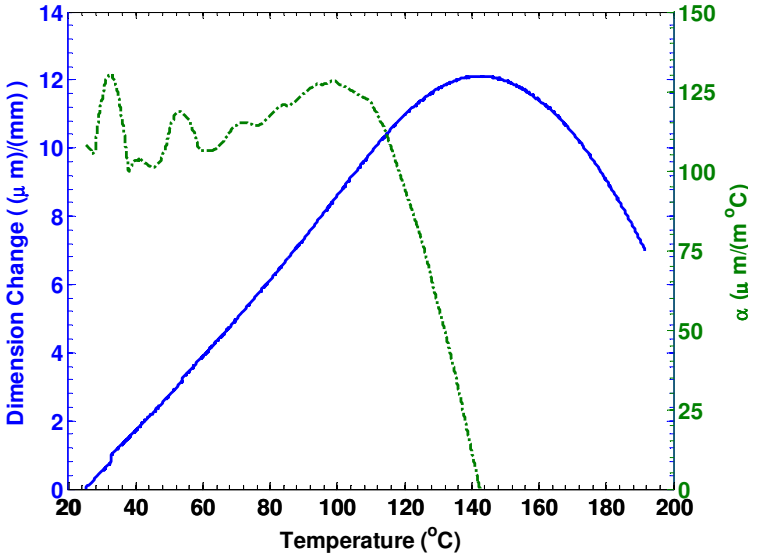

Figure 4.20: Curves of thermal expansion and Dimension change from TMA for the SPHT420T3

T_g. This sample has high mesophase content. This suggest a complex structure with a slow relaxation. This is thus a sample whereby the mesophase dominates the behaviour. The measurement of an isotropic transition was not possible due to dominance of the mesophase relaxation. The glass transition and softening temperature of the SASOL samples are shown in Table 4.13.

Table 4.13: TMA Properties for Various SASOL Pitches

Sample	C/H (-)	MC (vol. %)	T_g (℃)	T_s (℃)
SPAR	1.15	0	-	-
SPHT350	1.24	0	-	-
SPHT375	1.38	2	46	57
SPHT400T3	1.52	2	51	65
SPHT400	1.55	9	72	80
SPHT412	1.57	9	69	80
SPHT425	1.63	17	77	85
SPHT420T3	1.76	59	-	140

The glass transition and softening temperatures follow the trend of increasing temperatures with C/H ratio. This observed trend was explained earlier with respect to volatile release. No T_g value was determined for SPHT420T3.

The glass transition temperatures of these pitch samples are shown in Figure 4.21. The samples have different C/H ratios, similar solubility (associated with composition), from the two parent sources, yet have similar T_g values. This implies that the structure developed is different, which is confirmed via microscopy, and is shown here as a change in physical properties. This proves that the structure and composition of the samples

must be known to understand the mechanism by which physical behaviour is observed.

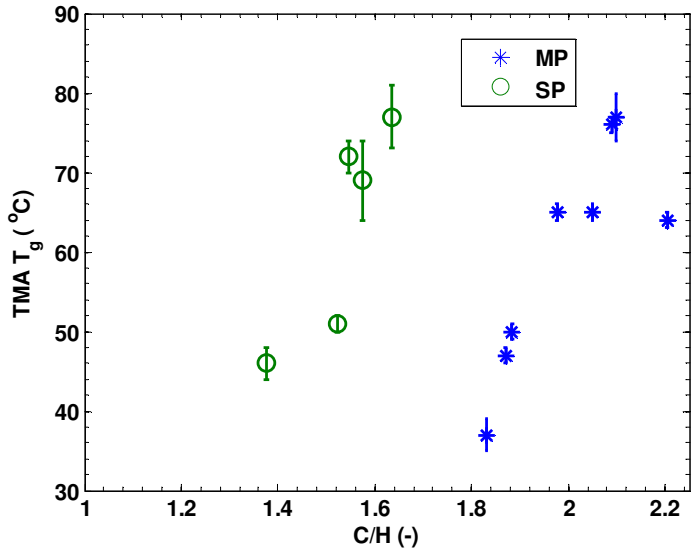

Figure 4.21: TMA T_g variation for the different samples

The softening temperature has a similar trend with C/H as the glass transition temperature and is observed in Figure 4.22. An interesting trend is that of the variation of the glass transition and softening temperatures which is shown in Figure 4.23.

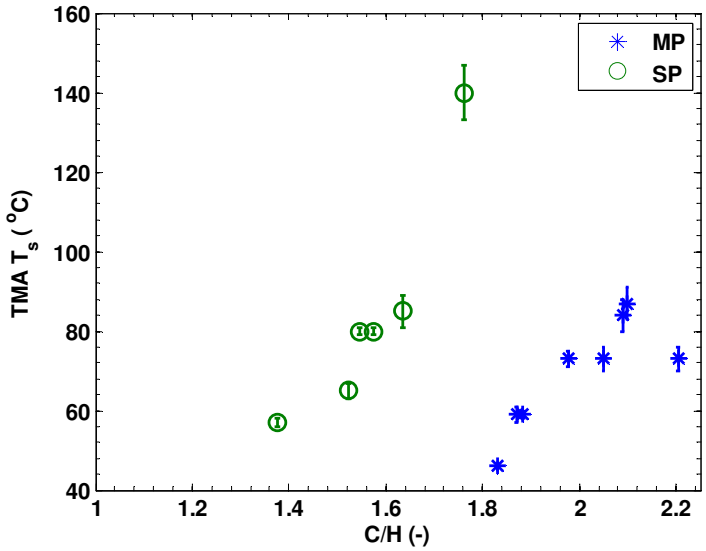

Figure 4.22: TMA T_s variation for the different samples

The samples show a linear trend of glass transition temperature to softening temperature. The significance of these trends, is the constant offset of 10 ℃. This shows that for all the samples that have clearly isotropic fractions, the softening temperature is predictable given that the T_g is known.

A significant point about the figure 4.23 is that both series (pitches from both sources) lie on a common line. This being the case despite their contrasting compositions. This

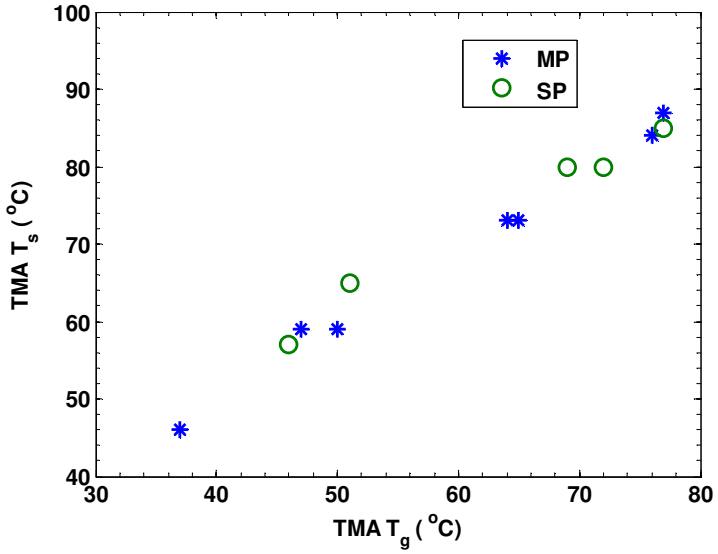

Figure 4.23: The relationship of T_g with T_s

suggests that the reason for the observed trend is likely a result of the manner of measurement, both temperatures being determined from the expansion curves of TMA. This technique would thus produce a good correlation between T_s and T_g for isotropic continuous pitch of low T_g.

4.3.2 DMTA

DMTA curves were obtained to determine the T_g of the pitch; the tan(δ) curves are often used in polymers, the peak resembling the transition temperature. For the pitch samples in this study, a qualitative shape of the curve is used to help characterise the material. This is normally done using dog-bone or similarly shaped samples. A metal jacket is used in these experiments as a powdered material and not a solid bar was the state of the sample. This manner of technique is also used by Royall et al. (2005).

In this work, the T_g was calculated as the onset of decay of modulus (as a function of temperature), and not the peak in tan(δ) as is used in most polymer systems. The determination of T_g from the modulus is shown in Figure 3.5. The onset of decay, is the beginning of the loss of solid (elastic) properties; the deviation away from the solid glass state. The temperature at which this occurs is much closer (or similar) to the temperature of the glass transition. The curves of the normalised storage modulus and tan(δ) are shown in Figures 4.24 and 4.25 with T_g of samples determined via DMTA shown in Table 4.14. The trend of transitions is similar to that measured via TMA.

The peak of tan(δ) is strongly associated with a transition from viscoelastic solid to viscoelastic liquid. This transition is thought to be a relaxation that occurs upon softening. Relaxation of the sample is clearly visible via a distinctive change in tan(δ), as is shown in Figure 4.25. The metal jacket does not affect the temperature dependence

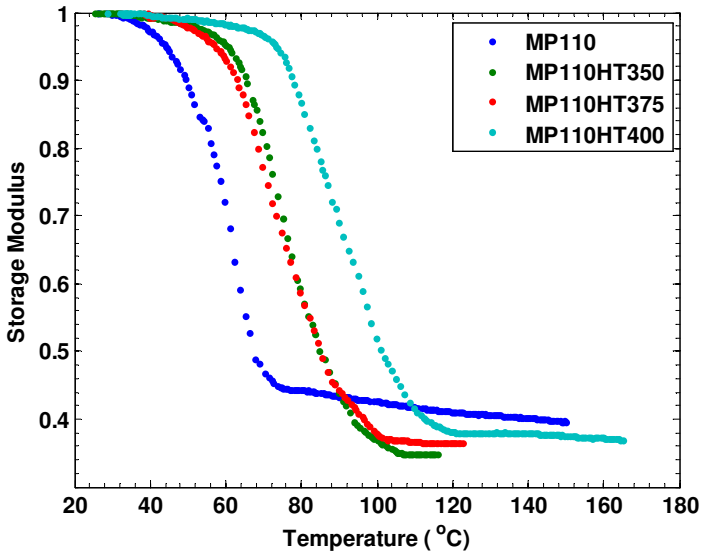

(a)

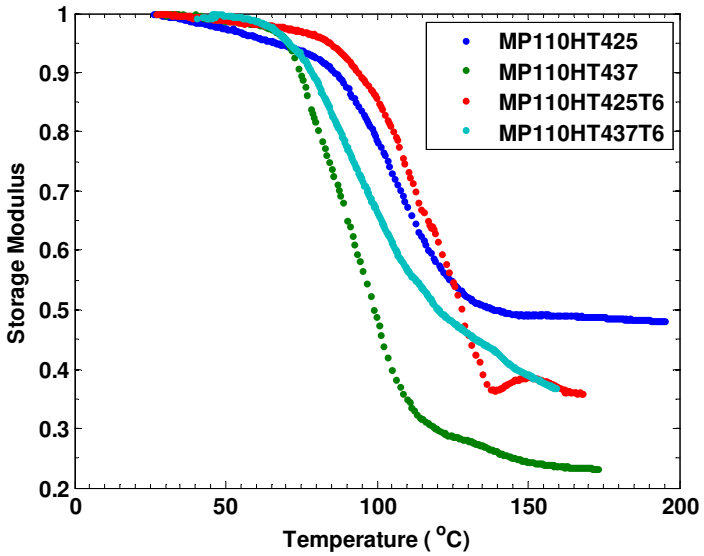

(b)

Figure 4.24: Normalised storage modulus for MP110 pitches

Table 4.14: DMTA Properties for Various MP110 Pitches

Sample	C/H (-)	MC (vol. %)	T_g (°C)	T_δ^{one} (°C)	T_δ^{two} (°C)
MP110	1.83	0	49	58	-
MP110HT350	1.87	0	59	77	-
MP110HT375	1.88	0	60	75	-
MP110HT400	1.98	13	72	95	-
MP110HT437	2.05	27	70	96	135
MP110HT425	2.09	26	86	111	-
MP110HT425T6	2.10	38	91	118	140
MP110HT437T6	2.20	49	76	100	138

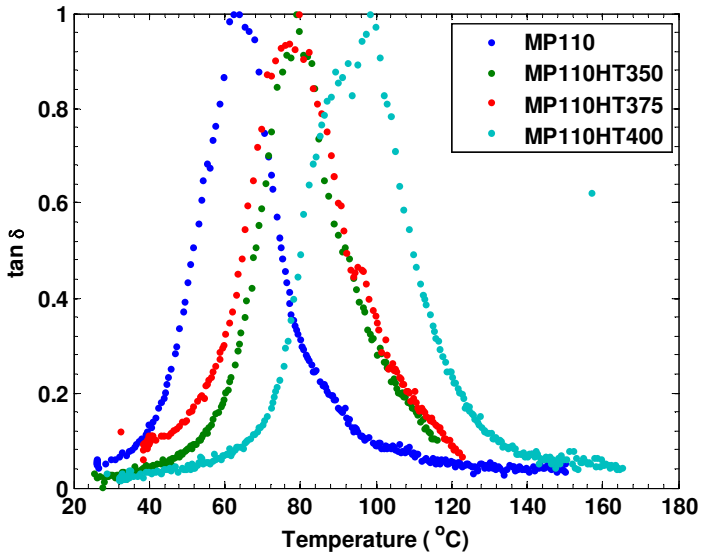

(a)

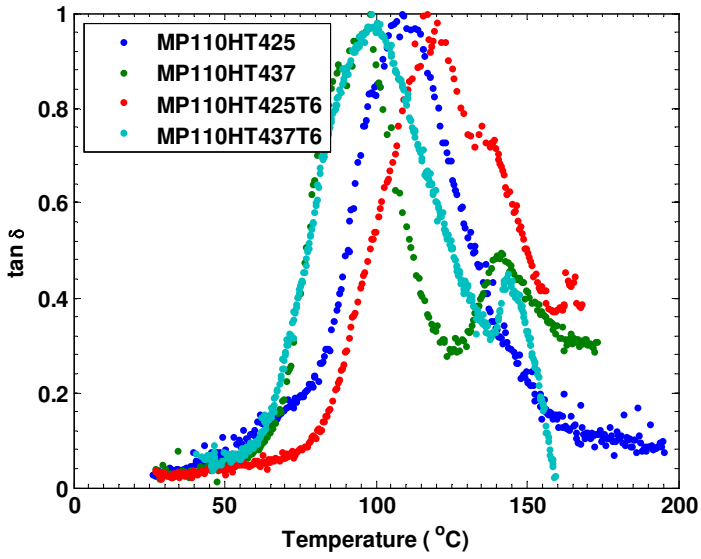

(b)

Figure 4.25: Normalised $\tan\delta$ for MP110 pitches

of these results as it does not show any change in its mechanical behaviour at these temperatures.

All samples showed at least one relaxation. This first peak is assumed to be the relaxation of the isotropic phase. These temperatures can be seen in Table 4.14. The trend of T_δ^{one} with C/H ratio is similar to that observed with T_g.

Some samples also show a distinct second peak or a shoulder protruding from the first. An example of this can be seen in Figure 4.26. This phenomenon was only visible in samples containing mesophase. This second relaxation was thus attributed to the transition of the mesophase. This shows that DMTA is sensitive enough to pick up transition of immiscible phases, given that the two relaxations are far enough apart in temperature. The transition of the mesophase also appears to be constant for all the samples at approximately 140 ℃. Unfortunately, due to the method of measurement, a direct measure of the T_g of the mesophase in the material is not possible. If need be, an approximation can be inferred via the relationship between the T_g and T_δ^{one} obtained from the isotropic phase. Assumptions for such a case would imply that the relaxation mechanism of glass transition and softening would be similar for both isotropic and mesophase material.

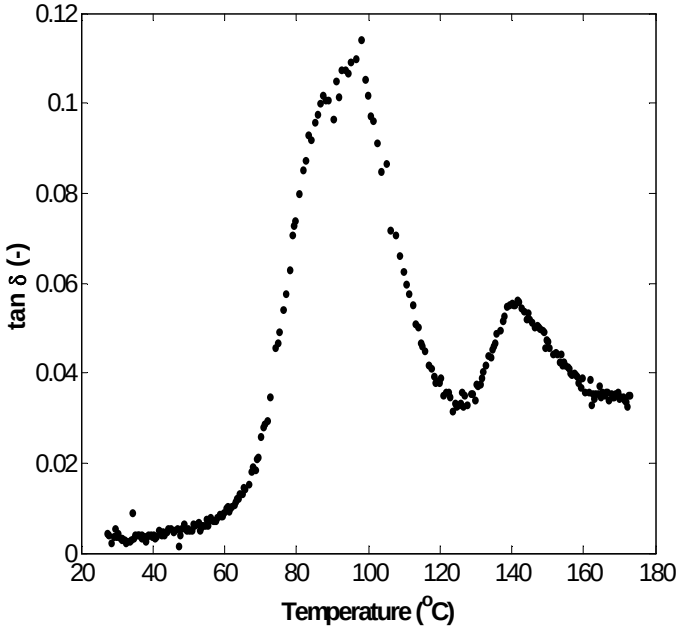

Figure 4.26: DMTA $\tan\delta$ curve showing two peaks for MP110HT437 (C/H = 2.05)

The DMTA results for the SASOL pitch provided the required information to produce T_g and T_δ temperatures. The shape of the curves obtained are similar to those of the Mittal pitches, and are shown in Figures 4.27 and 4.28, with determined temperatures shown in Table 4.15.

Analysis showed samples with some mesophase material might be developing a shoul-

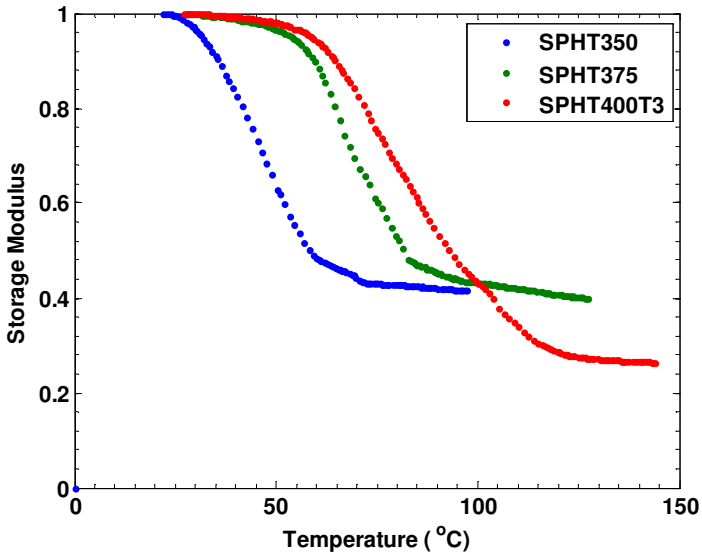

(a)

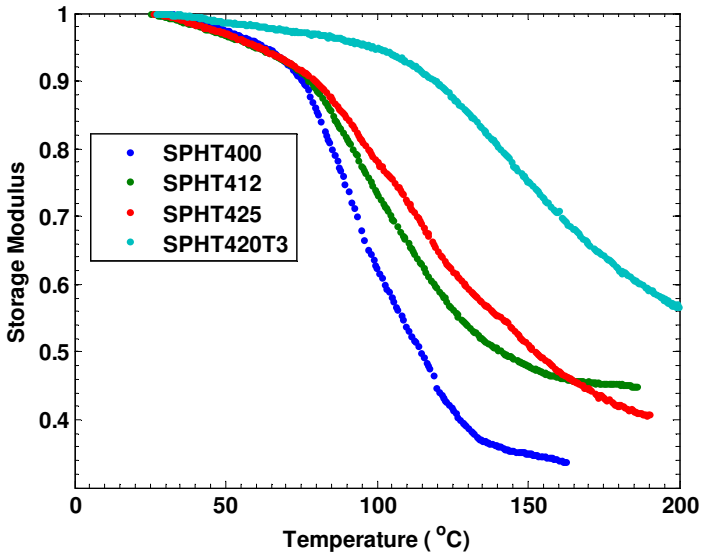

(b)

Figure 4.27: Normalised storage modulus for SASOL pitches

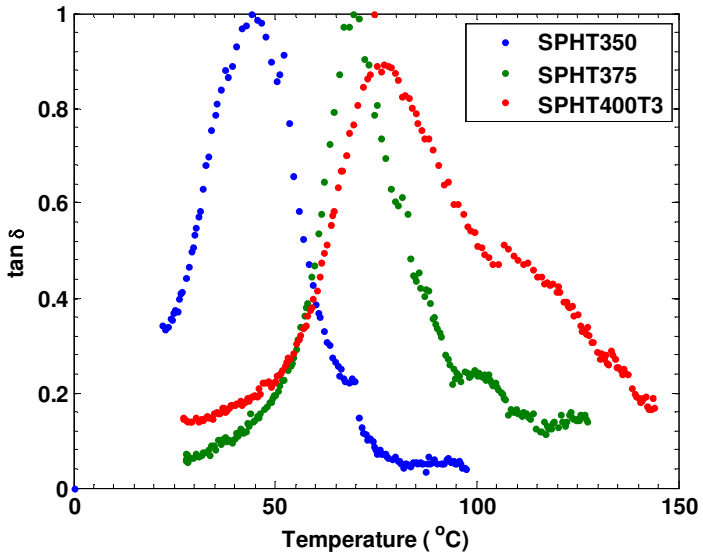

(a)

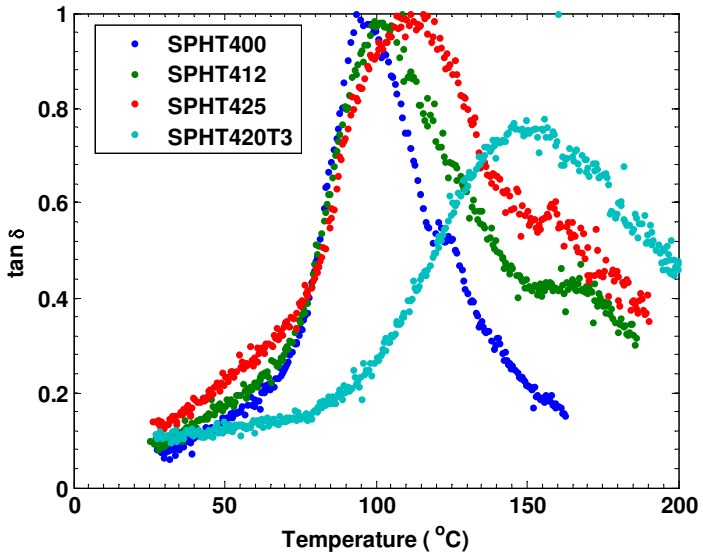

(b)

Figure 4.28: Normalised tan δ for SASOL pitches

der in their tan(δ) curves, but no definitive second peak was observed. This suggested the possibility of an influence of mesophase, but it certainly was not as distinct as the Mittal pitches. These shoulders were not as reproducible and as such are not presented as second tan(δ) temperature peaks. Tentatively, a more complex structure is present in these samples, with possible variation in mechanical properties at temperatures above or around 140 ℃. SPHT420T3, clearly has two phases, but only a single peak is evident. For this sample, it was expected to observe two clear peaks, as was observed in some of the anisotropic MP110 pitches. The reason for this behaviour is likely as described before, dominant mesophase where measurement of the isotropic phase is masked by mesophase relaxation. This indicates that the relaxation of the SASOL samples is controlled by a structure with a single dominant phase; either isotropic, mesophase (for SPHT420T3) or a gel.

Table 4.15: DMTA Properties for Various SASOL Pitches

Sample	C/H (-)	MC (vol. %)	T_g (℃)	T_δ (℃)
SPAR	1.15	0	-	-
SPHT350	1.24	0	32	43
SPHT375	1.38	2	55	68
SPHT400T3	1.52	2	64	79
SPHT400	1.55	9	72	97
SPHT412	1.57	9	76	104
SPHT425	1.63	17	83	118
SPHT420T3	1.76	59	110	157

The transition temperatures calculated follow the trends of the C/H ratio for the two sources. The more aromatic the material becomes, the higher the respective transition temperatures. This expected and the values obtained are similar to those obtained via TMA. DMTA does however prove to be a much easier and reliable instrument when quantitative behaviour, such as transition temperatures, need to be calculated. This is mainly due to robustness of the technique compared to possibility of other variables involved (packing density, thermal history, sensitivity, particle size distribution); other instruments are generally much more sensitive, but require a much better understanding of the component structure and composition.

The variation of glass transition temperature of the different samples observed via DMTA is shown in Figure 4.29. The trend of pitch glass transition temperature is similar to those obtained via TMA.

This trend in glass transition observed for both pitches is repeated for the T_δ determined. The notable exception being a second tan(δ) peak observed. The T_δ^{two} observed is however lower than the peak observed for SPHT420T3. This suggests the possibility that the structure of SPHT420T3 requires a higher amount of energy to relax. The peak

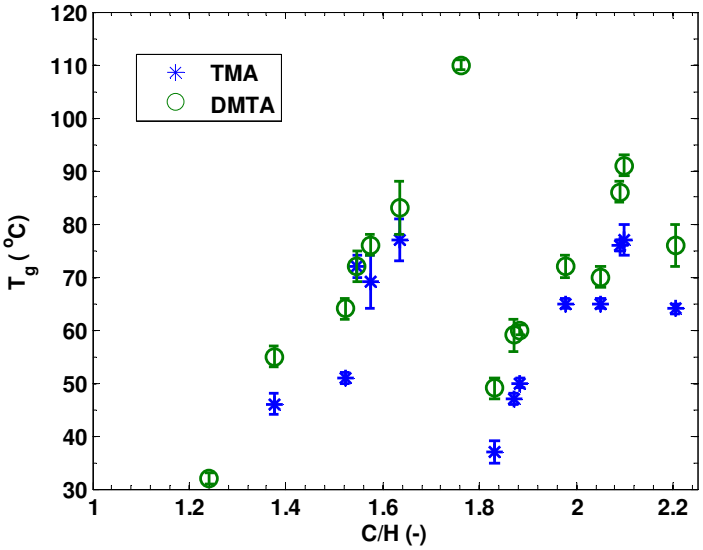

Figure 4.29: DMTA T_g variation for the different samples

is also much broader, which indicates that it is also a much slower process as opposed to the mesophase observed from MP110. This gives an indication of a more interconnected isotropic-mesophase structure of SPHT420T3, and the possibility of a gel-like material.

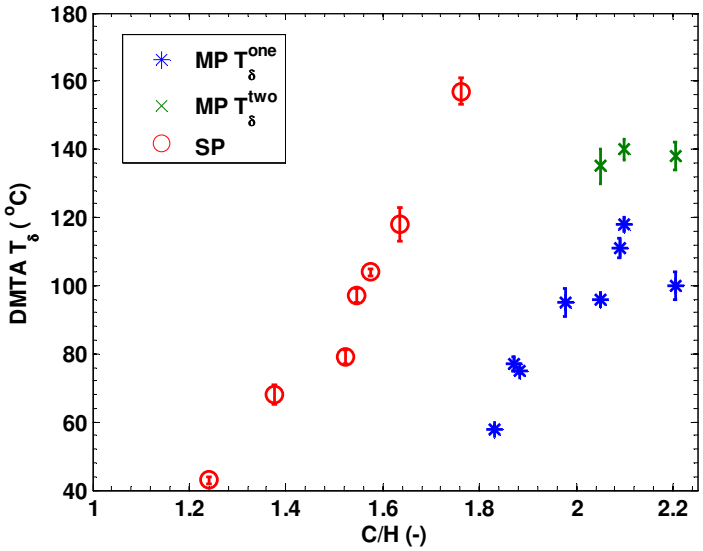

Figure 4.30: T_δ variation for the different samples

The T_g and the T_δ are also believed to be related. A pattern between these variables does exist as observed by linearity between the variables; this is shown in Figure 4.31. More scatter is observed at higher glass transition temperatures; there is a strong correlation between T_g and T_δ.

Given that both TMA and DMTA were used to obtain temperatures of significance from the samples, it would be of interest to compare these temperatures determined. Figure 4.32 shows us data between these two instruments.

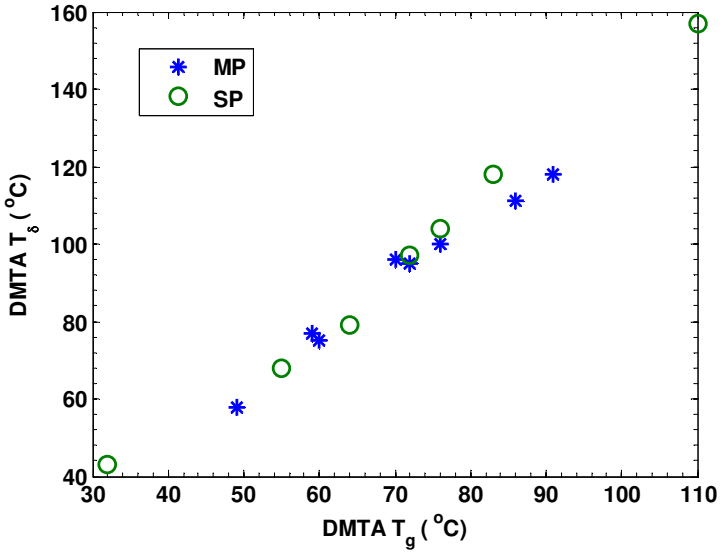

Figure 4.31: Relationship of T_g with T_δ

From Figures 4.32(a) and 4.32(b) linear trends are observed. This shows that there is consistency between the temperatures determined from the two instruments. It is observed that the determined temperatures, based on instrument and method of determination, are always higher on the DMTA.

4.3.3 DSC

Dynamic scanning calorimetry (DSC) heat flow curves were used to help characterise the pitches produced. Similar studies have been attempted by Barr & Lewis (1982). These are shown in Figures 4.33 and 4.34.

All the curves show endothermic peaks; they resemble that of melting crystals. This peak is observed easily on first heating. This peak was also observed by Blanco et al. (2002b). Reheating of the sample directly after first heating was attempted. This pronounced peak was then not observed. This pitch behaviour is similar to amorphous polymers as explained by Barr & Lewis (1982), and their origins are not completely understood. Upon heating, the amorphous powders soften, due to their low thermal conductivity, an exaggerated change in specific heat is observed via a larger input in heat flow. When cooled, the sample material reorganises into a state where a change in specific heat (and therefore heat flow) is not easily seen upon second heating; Barr & Lewis (1982) were able to observe a small change in specific heat and heat flow which was the glass transition. The original transition observed is a function of the nature of the material and the manner in which it is organised; in this case the major contributors are the cooling of the pitch after heat treatment and grinding via pestle and mortar. The strong endotherm is the process to reduce the surface energy from a powdered state to a single fused solid state. Due to the exaggerated change, the first heating peak will be

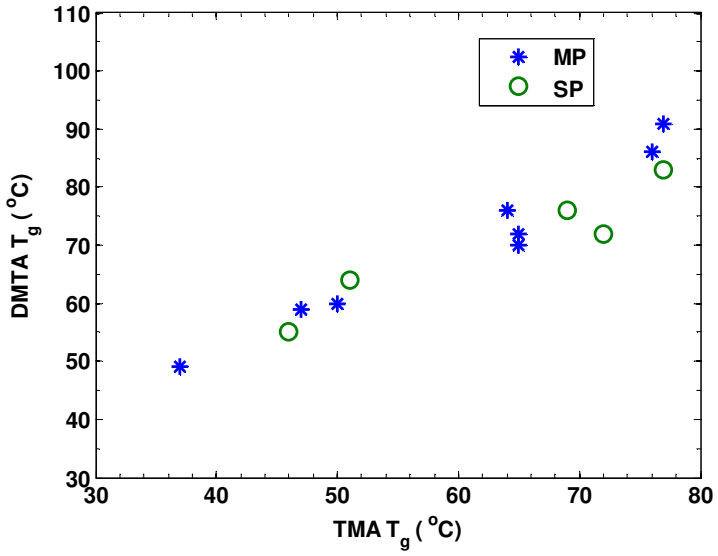

(a) T_g from TMA and DMTA

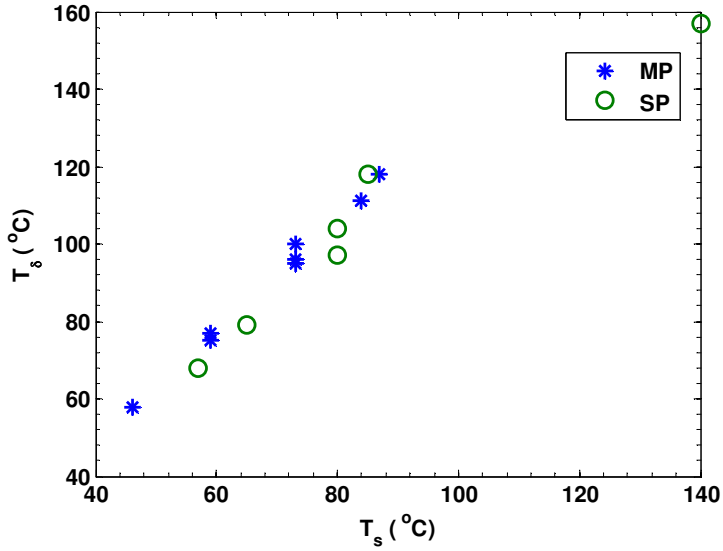

(b) T_s and T_δ

Figure 4.32: Comparison between determined temperatures from TMA and DMTA

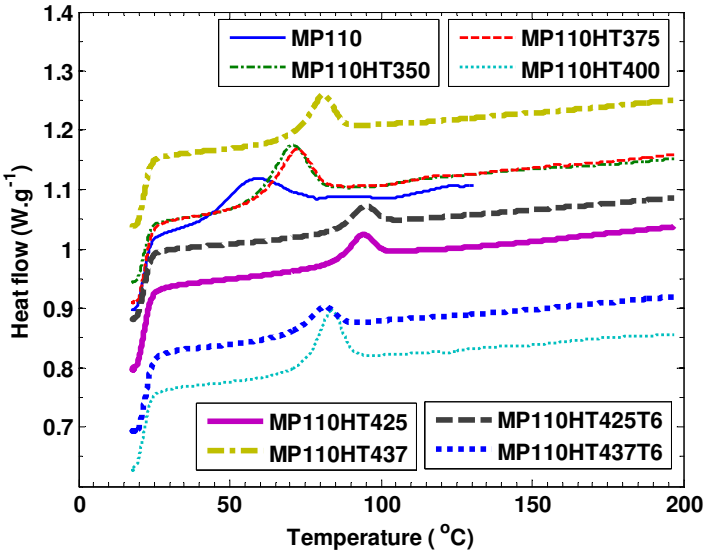

Figure 4.33: Heat flow curves from DSC for the different Mittal pitches

used to characterise the material, and is representative more of a softening temperature (similar to the peak in thermal expansion). These softening temperatures are determined and shown in Table 4.16.

Table 4.16: DSC Softening Temperatures for Various MP110 Pitches

Sample	C/H (-)	MC (vol. %)	T_s^{DSC} (°C)
MP110	1.83	0	59
MP110HT350	1.87	0	64
MP110HT375	1.88	0	66
MP110HT400	1.98	13	81
MP110HT437	2.05	27	78
MP110HT425	2.09	26	92
MP110HT425T6	2.10	38	91
MP110HT437T6	2.20	49	77

The observed solid-like to liquid-like change with C/H ratio, is the same as that observed via TMA and DMTA. This behaviour is expected and the three analytical techniques corroborate the behaviour observed as it is consistent for all the samples.

It is also evident from the curves that no appreciable change in heat flow occurs after the endothermic peak, suggesting no discernible melting (or other transition) can be detected by this instrument with this method.

The SASOL pitches possess similar endothermic peaks to that of the MP110 pitches. This is shown in Figure 4.34. The unmodified SASOL pitch and SPHT350 are not present in this figure. The SASOL pitch itself is already soft, liquid-like, at room temperature and was not tested. For SPHT350 the curve obtained was not usable or reproducible, due to similar characteristics as that of SPAR.

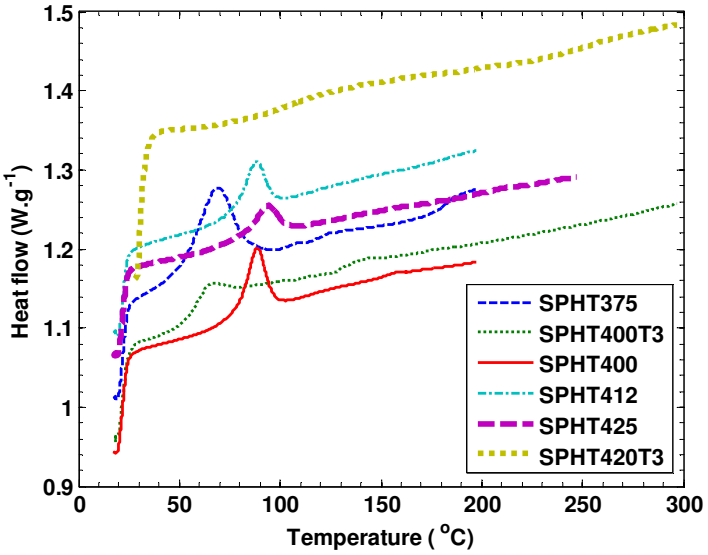

Figure 4.34: Heat flow curves from DSC for the different SASOL pitches

The softening temperatures for SASOL pitches are shown in Table 4.17. SPHT420T3 is the sample in this group that behaves anomalously. It does not show a clear endothermic peak, and the result is viewed as a much more broad peak; as a result no temperature of softening was determined. DSC curves for pure mesophase pitches as obtained by Khandare et al. (1996) and Barr & Lewis (1982) also show broad peaks. They observed much more pronounced heat flow endotherms and transitions as compared to SPHT420T3. A possibility is that the structure is not similar to the previously mentioned amorphous fraction of an anisotropic pitch. This suggests that the material relaxes over a wider range of temperature, and a simple conclusion to its behaviour is not offered purely via DSC. It is possible that this may be attributed to the high mesophase content and gel-like structure postulated earlier from optical microscopy, TMA and DMTA.

Table 4.17: DSC Softening Temperatures for Various SASOL Pitches

Sample	C/H (-)	MC (vol. %)	T_s^{DSC} (°C)
SPAR	1.15	0	-
SPHT350	1.24	0	-
SPHT375	1.38	2	70
SPHT400T3	1.52	2	73
SPHT400	1.55	9	90
SPHT412	1.57	9	89
SPHT425	1.63	17	95
SPHT420T3	1.76	59	-

The softening temperatures has a trend with C/H ratio; the same as observed with determined temperatures via TMA and DMTA. This is shown in Figure 4.35.

From these analyses, it is clear that DSC cannot be the sole instrument to gauge the

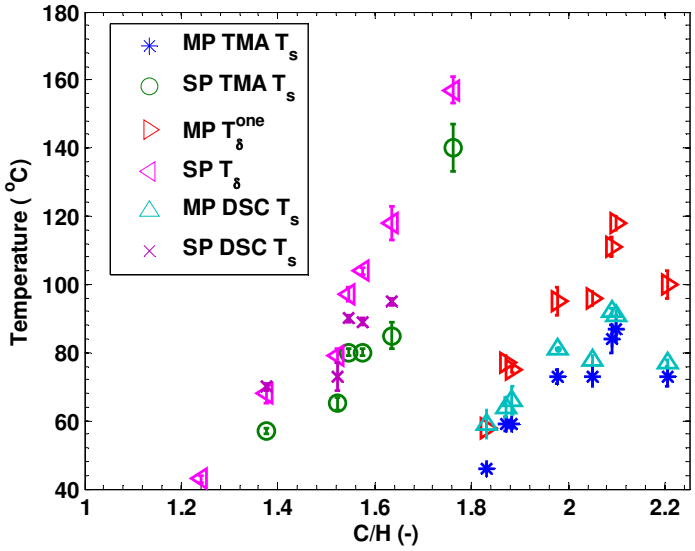

Figure 4.35: DSC T_s variation for the different samples and other cahracteristic temperatures

transition behaviour of the material. The DSC observed the isotropic phase change, but no behaviour is obtained with respect to the mesophase. The trend of the amorphous softening behaviour however, is the same as the trend of the transition temperatures observed via TMA and DMTA. The temperatures determined via DSC are consistently lower than the T_δ from the DMTA and higher than the T_s calculated via TMA.

4.4 Density

One of the few properties that is measurable and able to link the two-phase nature and structure of mesophase containing pitches and its chemical composition is the density. This technique is a method whereby properties of both phases are measured simultaneously. The density of the samples measured and their respective values are shown in Table 4.18. The samples show an increase in density as the C/H increased.

Table 4.18: Density for Various MP110 Pitches

Sample	C/H (-)	MC (vol. %)	Density ($kg.m^{-3}$)
MP110	1.83	0	1336
MP110HT350	1.87	0	1349
MP110HT375	1.88	0	1353
MP110HT400	1.98	13	1368
MP110HT437	2.05	27	1379
MP110HT425	2.09	26	1386
MP110HT425T6	2.10	38	1392
MP110HT437T6	2.20	49	1394

A significant increase in density was observed (with heat treatment and C/H), this still being considerably lower than the density of graphite (approximately 2200 $kg\,m^{-3}$). The isotropic phase changes composition whilst the mesophase properties are predominantly constant as observed by Greinke & Singer (1988). The change in density is therefore caused by a change in isotropic phase density and concentration of mesophase.

The density of the different SASOL pitches were measured and the results obtained are shown in Table 4.19.

Table 4.19: Density for Various SASOL Pitches

Sample	C/H (-)	MC (vol. %)	Density ($kg.m^{-3}$)
SPAR	1.15	0	-
SPHT350	1.24	0	1229
SPHT375	1.38	2	1273
SPHT400T3	1.52	2	1289
SPHT400	1.55	9	1301
SPHT412	1.57	9	1306
SPHT425	1.63	17	1323
SPHT420T3	1.76	59	1330

The SPAR sample was not tested for skeletal density as it was fluid, and the instrument needs a solid sample. The material does however have a significant increase in density over the treatment range. The densities are within the ranges expected of a pitch; initially quite low, probably due to the highly aliphatic nature. Similar to most of the other trends observed, the major changes occur between samples SPHT375 (C/H = 1.38) and SPHT400T3 (C/H = 1.52), and SPHT425 and SPHT420T3.

The samples have released volatile matter during heat treatment; this has been accompanied by an increase in molecular weight and hence a change in density. Figure 4.36 shows the manner in which the different samples vary with density. The dominant feature here is the linearity of the change in density with C/H. Previously, all other parameters had shown a change in measured property with C/H only being observed for pitch from a single source. For density, this is observed for the data of both sources combined. The implication is that the density is not directly influenced by the mesophase content of the samples. A more complex relationship which comprises the isotropic phase, mesophase, C/H ratio and molecular weight exists. However, all of these parameters are influenced by the molecules that influence them; hence the possibility that the constituent components directly influence the density.

It is also known from density measurements done by Kim et al. (1993), that the density of mesophase pitch remains relatively constant. An increase in density is caused by the components being much more tightly packed. This being the case, the lower C/H ratio SASOL pitches, have compounds that do not pack tightly together. A possible

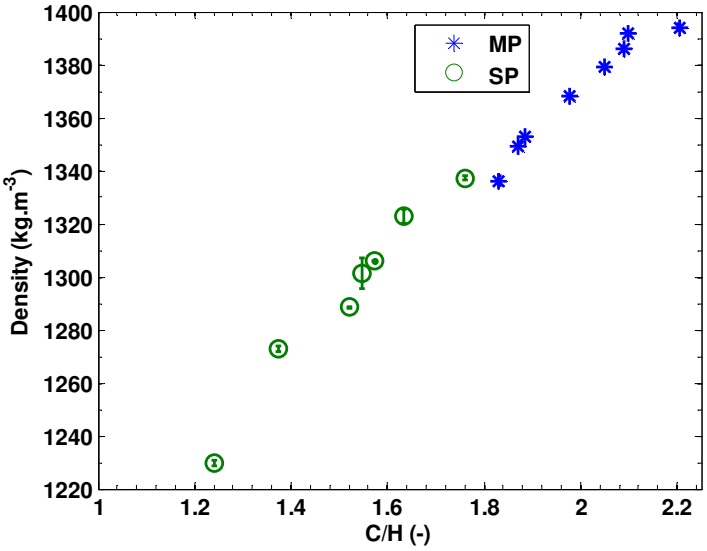

Figure 4.36: Variation of density for the different pitches

reason for this behaviour is that the SASOL pitches have compounds that have a varied stereochemistry. This being a result of the compounds being crosslinked into a shape that is not planar. These compounds do not necessarily stack as easily as the planar aromatic hydrocarbons of the Mittal pitches and therefore do not form as dense a structure. Another effect is that of the growth of mesophase, and structure of these mesogens.

4.5 Summary

A final summary of the pitches studied will be made here, and a table of compositional characteristics can be seen in Table 4.20, and its associated transition temperatures in Table 4.21.

The thermal treatment resulted in release in volatiles. This caused a change in composition; both by release in volatiles and condensation reactions. A change in structure is observed by the formation of mesophase. This was monitored by the change C/H, MC, QI, TI and CY. Similarly the composition and structure affect the measured glass transition temperature and density.

From the information gathered, the Mittal pitch is an aromatic precursor. It has a considerable particulate content. Heat treatment resultant in mesophase formation. Brooks and Taylor type A mesophase spheres were formed whereby coalescence was prevented by the particulate content. This being the case even though 49 % mesophase content pitch was produced. Both isotropic and mesophase transitions were determined. The mesophase relaxing at higher temperatures. The resultant pitches are therefore expected to behave as suspensions or emulsions when heated to temperatures that do not result in further volatile release.

Table 4.20: Compositional and structural characteristics of the pitches

Sample	C/H (-)	MC (vol %)	Particulates (%)	TI (%)	QI (%)	CY (%)	Density ($kg.m^{-3}$)
SPAR	1.15	0	0	5	0	20	-
SPHT350	1.24	0	0	15	0	23	1229
SPHT375	1.38	2	0	26	0	28	1273
SPHT400T3	1.52	2	0	25	12	46	1289
SPHT400	1.55	9	0	39	10	47	1301
SPHT412	1.57	9	0	47	28	54	1306
SPHT425	1.63	17	0	48	33	61	1323
SPHT420T3	1.76	59	0	43	40	74	1330
MP110	1.83	0	10	34	10	40	1336
MP110HT350	1.87	0	10	38	14	46	1349
MP110HT375	1.88	0	10	40	20	48	1353
MP110HT400	1.97	13	11	47	23	54	1368
MP110HT437	2.05	27	12	58	33	61	1379
MP110HT425	2.09	26	15	60	34	66	1386
MP110HT425T6	2.10	38	12	62	39	66	1392
MP110HT437T6	2.20	49	13	68	41	69	1394

Table 4.21: Glass transition and associated temperatures of the pitches

Sample	C/H (-)	MC (vol %)	T_g^{TMA} (°C)	T_g^{DMTA} (°C)	T_s^{TMA} (°C)	T_s^{DSC} (°C)	T_δ^{one} (°C)	T_δ^{two} (°C)
SPAR	1.15	0	-	-	-	-	-	-
SPHT350	1.24	0	-	32	-	-	43	-
SPHT375	1.38	2	46	55	57	70	68	-
SPHT400T3	1.52	2	51	64	65	73	79	-
SPHT400	1.55	9	72	72	80	90	97	-
SPHT412	1.57	9	69	76	80	89	104	-
SPHT425	1.63	17	77	83	85	95	118	-
SPHT420T3	1.76	59	-	110	140	-	157	-
MP110	1.83	0	37	49	46	59	58	-
MP110HT350	1.87	0	47	59	59	64	77	-
MP110HT375	1.88	0	50	60	59	66	75	-
MP110HT400	1.97	13	65	72	73	81	95	-
MP110HT437	2.05	27	65	70	73	78	96	135
MP110HT425	2.09	26	76	86	84	92	111	-
MP110HT425T6	2.10	38	77	91	87	91	118	140
MP110HT437T6	2.20	49	64	76	73	77	100	138

The SASOL pitch is from a much more aliphatic origin, with high volatile content. Thermal treatment resulted in the formation of a finely textured mesophase. Small clusters of mesophase formed as opposed to the spheres observed in the Mittal pitches. This is likely a result of the aliphatic nature and higher oxygen content which resulted in rapid mesophase formation at temperatures between 410 °C and 430 °C. SPHT420T3 was the only pitch that produced a pitch with continuous mesophase. The pitches produced showed dominant isotropic or mesophase systems. These pitches, under higher temperatures, are expected to behave as a single phase material. It is possible that due to the mesophase clusters formed, low to medium mesophase content samples will affect the system response under external disturbances.

The manner in which these very different (SASOL and Mittal) anisotropic systems interact under both temperature and disturbance, will thus be investigated via rotational rheometry.

CHAPTER 5

RESULTS: SHEAR RHEOMETRY

From Chapter 4, it has been established that the MP110 and SASOL derived pitches are of significantly different physical structure. The spherical mesophase and the finely textured clustered mesophase are expected to behave differently. The rheological behaviour of these samples will thus also be different. The mechanical stresses applied from the apparatus limited the rheometry measurements between 1×10^1 Pa s and 1×10^6 Pa s for the viscoelastic fluid. Rheological behaviour is also dependent on temperature; for the pitch samples the glass transition temperature is an important characteristic to consider. Since samples have different T_g, they therefore will also have different measurement temperatures.

5.1 Isotropic Pitch

For all the samples, flow curves were obtained at several temperatures. For MP110 the shear-rate versus viscosity relationship at different temperatures is shown in Figure 5.1.

MP110 shows predominantly isoviscous behaviour at the shear-rates tested. This behaviour has previously been observed by Sakai (1979). The material maintains isoviscous behaviour; therefore there was no significant change to the microstructure. This sample showed a slight decrease in viscosity at higher shear-rates with an increase in temperature. This is an isotropic pitch suspension with particulate QI filler.

The flow curve obtained at 130 ℃ showed deviation from stable isoviscous viscosity measurements. This can be explained by the particulate content in the material; at this temperature, the non-particulate material behaves as a low viscosity Newtonian fluid. The particulate material in a low viscosity fluid makes a large contribution to the rheological properties; hence influence the measurement of the pitch.

The flow curves of MP110HT350 and MP110HT375 (C/H = 1.88) are shown in Figure

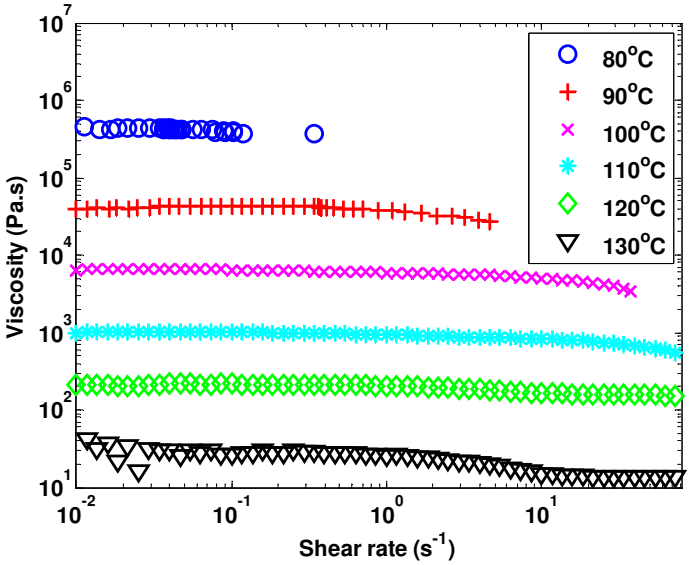

Figure 5.1: Flow curves for MP110 pitch (as received) (C/H = 1.83)

5.2 and 5.3. The flow curves obtained are dominated by isoviscous behaviour. These curves graphically show more shear-thinning over the range of shear-rates, as opposed to MP110; this is not a substantial increase in the shear-thinning effect. In these samples, the behaviour could possibly be the particulate material changing the manner in which the suspension behaves. This would suggest the change in the isotropic pitch has now allowed for the particulate content to more strongly influence the underlying behaviour. If initially the particulate QI has to some minor extent formed small clusters of particulates, then at higher temperatures and shear-rates, these clusters have been broken and dispersed to form a homogenous high-shear phase. This would also explain the level of scatter shown by MP110 at 130 °C. This suggest that the isotropic pitch is a weak non-Newtonian fluid. This behaviour will only be observed at low isotropic phase viscosity (or higher solids content).

The flow curves of MP110HT400 (C/H = 1.97, MC = 13%) is shown in Figure 5.4. The flow curves are still predominantly isoviscous, with minor shear-thinning. At the higher temperatures of measurement, the sample viscosity is transitioning to that of a high shear plateau. This is observed in material when structure is changed, rearranged to lower its resistance to flow (when no compositional changes occur).

MP110HT400 though has some mesophase material. The mesophase has a T_δ of approximately 140 °C and is thus in the process of softening between 120 °C and 170 °C (temperatures of measurement). Given that the T_δ^{one} of the isotropic fraction is 96 °C, the mesophase is expected to be at a much higher viscosity than the isotropic material (due to much higher T_δ). In emulsions, if there is a large difference in viscosity between the two phases, the droplet phase (mesophase) is less deformable. In this case the particulates would also prevent mesophase deformation. This emulsion would thus more likely act as

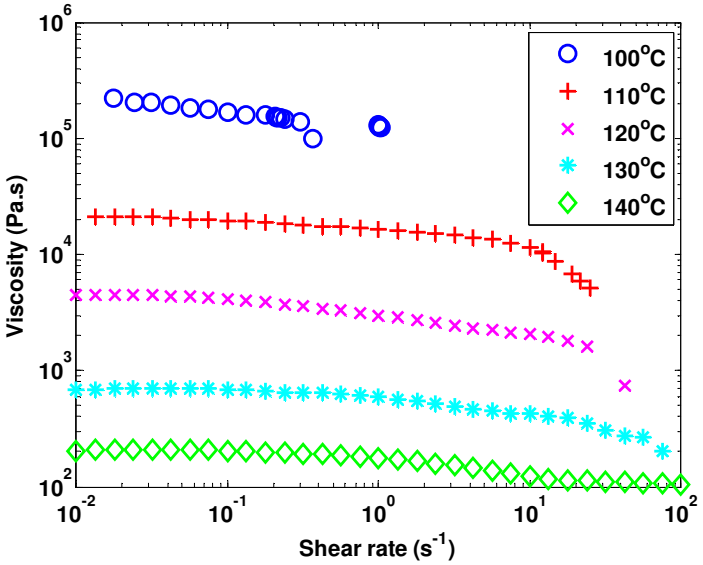

Figure 5.2: Flow curves for MP110HT350 (C/H = 1.87)

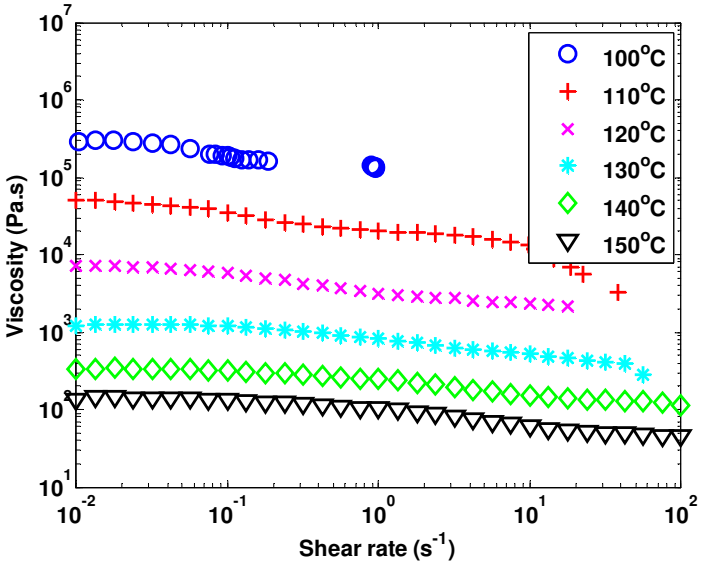

Figure 5.3: Flow curves for MP110HT375 (C/H = 1.88)

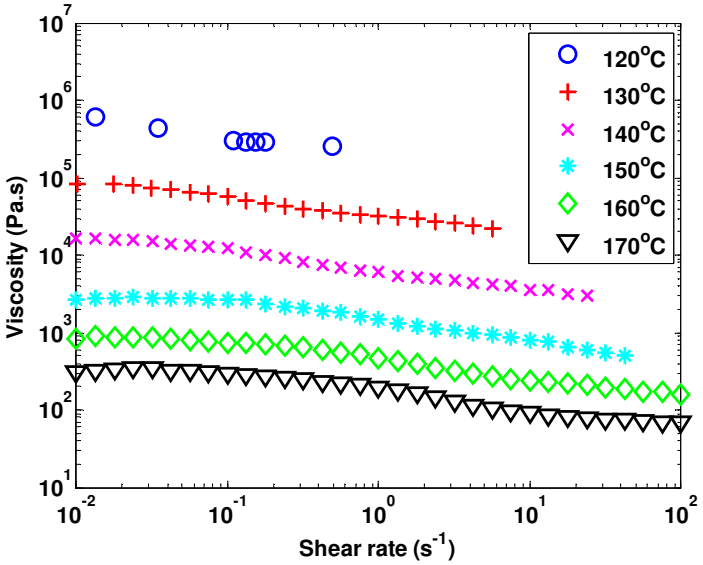

Figure 5.4: Flow curves for MP110HT400 (C/H = 1.97, MC = 13%)

a suspension (emulsion droplet phase with infinite viscosity).

From this sample, the change in viscosity and rate of shear-thinning has increased. This shows the effect of change in microstructure and higher solids (and solid-like) content on rheology. There is a higher shear-thinning component to this sample, but only in comparison to the samples with lower solid content (only particulate). It is a weak non-Newtonian fluid with slight shear-thinning; none of the experiments have yet yielded a fluid that has changed isothermal viscosity by a single decade (over the range of shear-rates tested). The underlying behaviour is still dominated by the isotropic phase, and a slight shear-thinning is expected as has been shown by Blanco et al. (1999). Sample MP110HT400 is not a purely isotropic pitch, contains 13% mesophase, but its behaviour resembles that of the isotropic pitches. For this reason it is included in this section.

For the isotropic Mittal pitches, at temperatures closer to the T_g, the viscosity of the continuous pitch is high and this characteristic dominates its behaviour. At temperatures further away from T_g, the sample softens, with low viscosity continuous phase and particulate matter; this contributes to the minor deviation away from isoviscous behaviour.

For SPAR the flow curves are shown in figure 5.5. The curves are clearly isoviscous at these temperature and at this stage of development. The material behaves as a high viscosity liquid at low temperatures and a low viscosity liquid at high temperatures. No non-Newtonian behaviour was observed.

Figures 5.6 and 5.7 show the flow curves of SPHT350 and SPHT375. Similar to SPAR, the flow curves are isoviscous, showing no major change in behaviour. At high temperatures and low shear, slight shear-thinning is observed. The only difference between SPHT350 and SPHT375 is the higher temperatures needed for the experiments due to higher T_g.

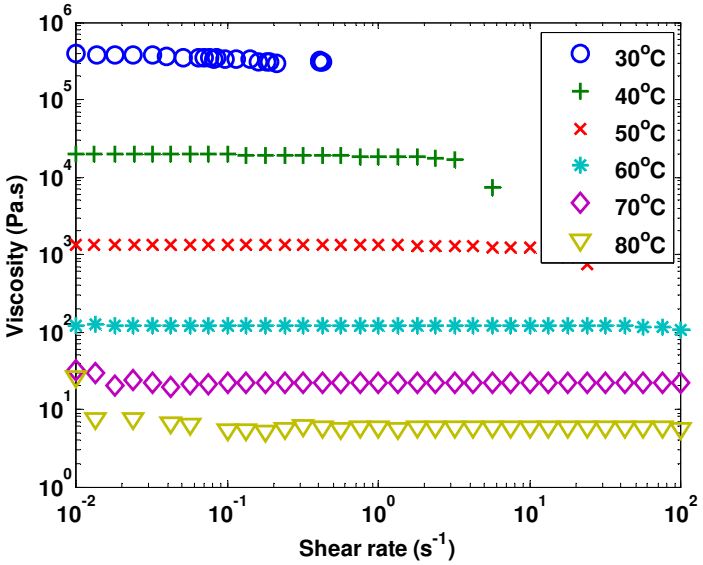

Figure 5.5: Flow curves for SASOL pitch (as recieved) (C/H = 1.15)

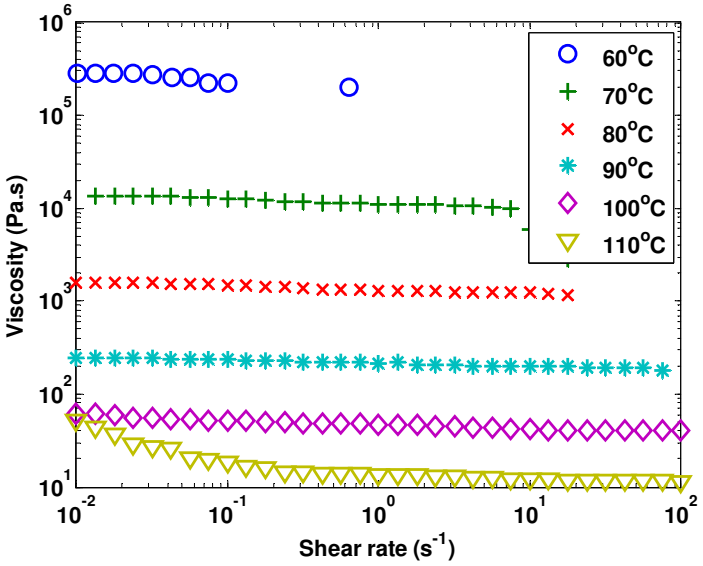

Figure 5.6: Flow curves for SPHT350 (C/H = 1.24)

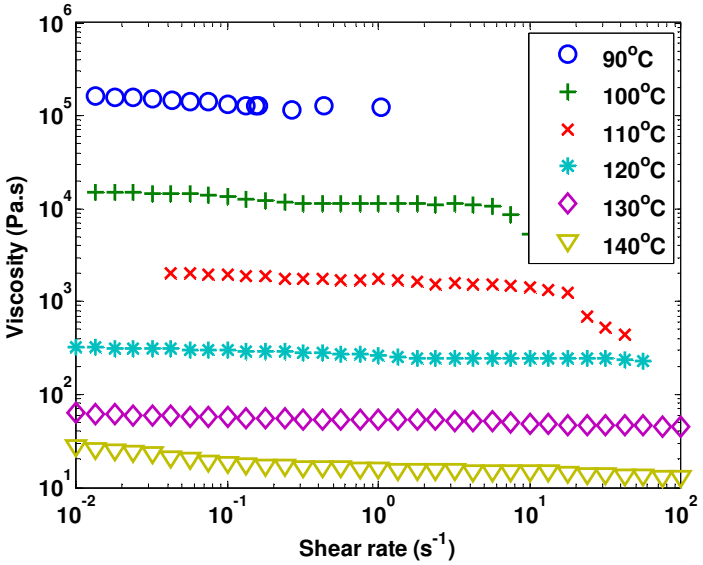

Figure 5.7: Flow curves for SPHT375 (C/H = 1.38)

The flow curves for SPHT400T3 are shown in Figure 5.8. The behaviour for this sample is slightly different to the previous samples, with weak shear-thinning at low temperatures (measured).

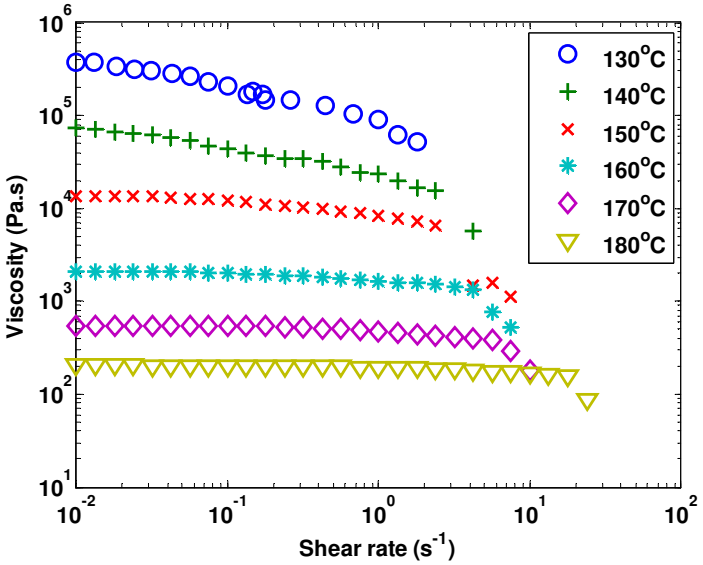

Figure 5.8: Flow curves for SPHT400T3 (C/H = 1.52)

5.2 Anisotropic Pitch

MP110HT437 (C/H = 2.05, MC = 27%) flow curves are shown in Figure 5.9. The shape of this curve is different from the isotropic pitches; shear-thinning behaviour is accentuated. The shape resembles the transition zone of an S-curve (mirrored).

This is unsurprising since this sample contains mesophase spheres of a much larger size, the underlying microstructure, and hence would have a much larger influence on behaviour. These spheres might be expected to move or deform in the sample as a result of shear and temperature. With a DMA $\tan(\delta)^{two}$ peak at around 140 ℃ relaxation of the spheres would occur and thus also possible deform. However the extent of this phenomenon depends on the difference in viscosity between the continuous phase and the particle/droplet phase as described in section 2.4.6. At lower temperatures, the mixture is expected to behave as a suspension, due to high viscosity (almost solid) of the mesophase compared to the isotropic pitch. Another major factor is the role of the solid particulates at the interface. Their presence at the sphere surface has prevented coalescence of similar viscosity spheres. These particles are likely to restrict the effect of external disturbance to the stable sphere state. This should assist in some form, the reduction of possible sphere deformation, which will be discussed in section 6.3.

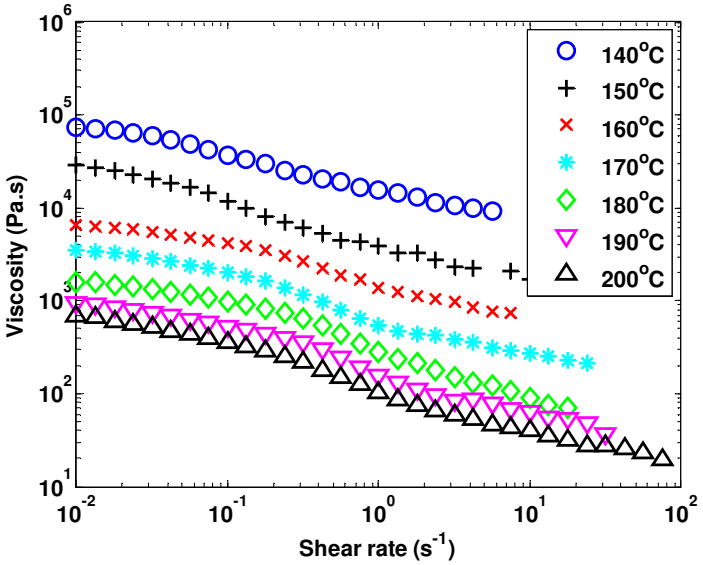

Figure 5.9: Flow curves for MP110HT437 (C/H = 2.05, MC = 27%)

The flow curves of sample MP110HT425 (C/H = 2.09, MC = 26%) with mesophase content similar to that of MP110HT437 are shown in Figure 5.10. Due to both samples having ±27% mesophase, it is anticipated to show a similar behaviour.

The major difference between the two samples is the higher temperature at which similar viscosity flow curves were obtained. MP110HT425 has a higher continuous isotropic T_g as compared to MP110HT437. Both samples have similar mesophase content, and therefore the change in T_g is the cause for higher measurement temperatures. The shape of these curves can be divided into three regions: low shear-rate tending towards zero shear plateau (evident at the higher temperatures), mid shear-rate region with a steeper gradient, and high shear-rate towards infinite shear plateau. This shape is similar to the kink-shape observed by Cato & Edie (2003) and Cato et al. (2005). The flow curves

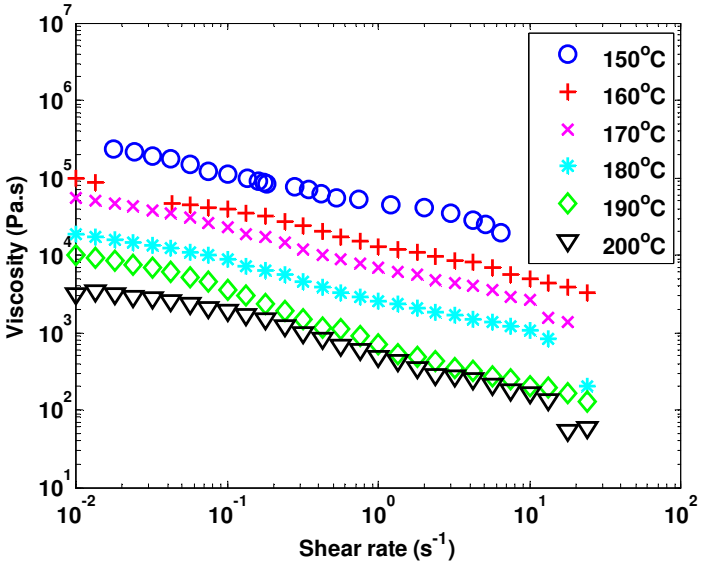

Figure 5.10: Flow curves for MP110HT425 (C/H = 2.09, MC = 26%)

obtained for those curves were based on synthetic mesophase material. Their reason for the kink-type behaviour is attributed to the change of the mesophase from a poly-domain structure to a mono-domain structure. This is not the case in this coal-tar pitch samples as no continuous mesophase material is observed.

The flow curves of MP110HT425T6 (C/H = 2.10, MC = 38%) are shown in Figure 5.11. It is difficult to obtain good data at high shear-rates. There is a significant shear-thinning aspect to these curves. This phenomenon is much more appreciable in this sample as compared to MP110HT425 (C/H = 2.09, MC = 26%) and MP110HT437 (C/H = 2.05, MC = 27%). This is due to two major aspects: the higher mesophase content, and higher temperatures at which viscosity was measured. This leads to the sample being measured at a higher temperature above T_g (as compared to MP110HT425 which has a similar T_g). This implies that there is a lower isotropic viscosity as compared to lower C/H Mittal pitch samples. Higher temperature also results in lower viscosity mesophase; possibly more susceptible to deformation. The particulates should remain unaffected and are expected to continue to restrict deformation. The higher dispersed phase content will also increase the viscosity of the mixture.

The change of this suspension/emulsion is due to a change in the underlying microstructure; possible mesophase sphere deformation. There is a high probability that the sample measurements are made in the region where the mixture transitions from suspension-like to emulsion-like behaviour.

The shape of these curves is that of a dominant monotonically decreasing viscosity (with shear-rate); with no observable transition to or from a viscosity plateau. This phenomenon is still apparent in the flow curves of MP110HT437T6, shown in Figure 5.12.

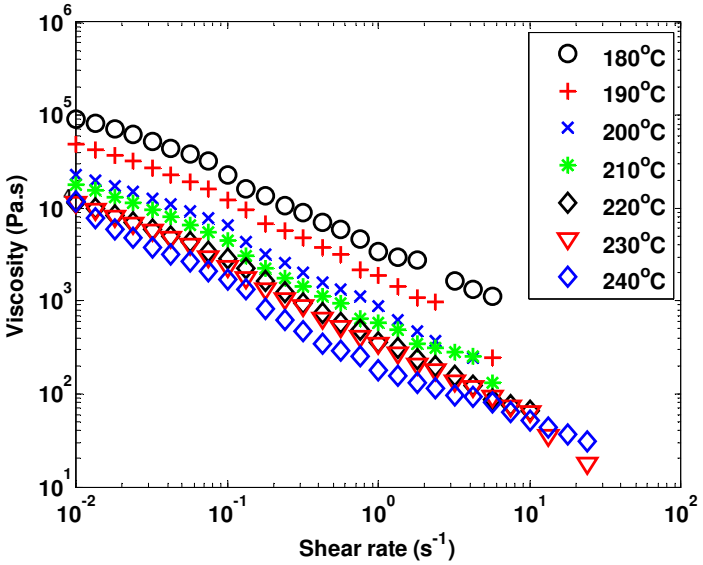

Figure 5.11: Flow curves for MP110HT425T6 (C/H = 2.10, MC = 38%)

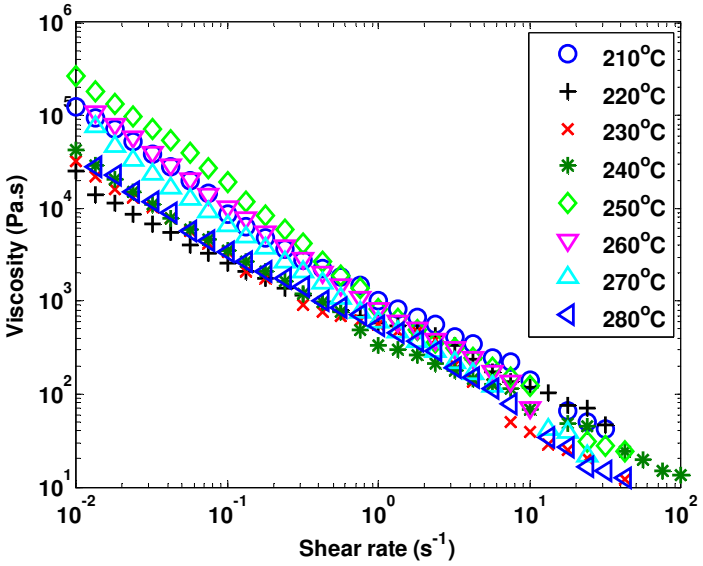

Figure 5.12: Flow curves for MP110HT437T6 (C/H = 2.20, MC = 49%)

This sample has the strongest shear-thinning characteristic. In this respect it is similar to MP110HT425T6 by not being dominated by a single distinguishable feature (measurement temperature and mesophase content). This behaviour is largely attributed to the mesophase material present. At the temperatures at which experiments were conducted, a significant drop in viscosity of the mesophase is expected. The spheres are expected to show more deformation. They are likely to form ellipsoids and to some extent, coalesce, to reduce the viscosity of the mixture (Collett & Rand, 1978a)(Collett & Rand, 1978b).

At these temperatures the continuous isotropic phase is significantly above its T_g. The isotropic fluid has a much lower viscosity. The low viscosity of the suspending medium means that the effect of concentration and viscosity of the droplet or dispersed mesophase is a greater contributor to the mixture behaviour. This is believed to be the case as there is no significant change in viscosity with respect to temperature. The change in viscosity is largely a result of change in mesophase content.

The two important features of the mixture viscosity are: the viscosity of the two phases, and their concentrations. In this sample, the isotropic phase has a low viscosity whereas the mesophase has a much higher viscosity (still deformable). The high concentration of dispersed mesophase is the dominant feature of this mixture. The isotropic phase has such a low viscosity, that the concentration of mesophase drastically changes the mixture viscosity. A fresh sample is used for every flow curve, and therefore each result may be based on a slightly different mesophase concentration. At the high temperature above the isotropic T_g, this deviation in mesophase concentration is amplified. Due to these phenomena, there is no obvious pattern with respect to temperature. It should be noted, that in this crowded mesophase state, the particulates still play a role. It slows down the mechanism of structural change; this being deformation and/or coalescence.

The investigation continues to the anisotropic SASOL pitches. The flow curves for SPHT400 are shown in Figure 5.13. At lower temperatures closer to the T_g, flow curves show slight shear-thinning. For experiments conducted at higher temperatures, appreciable shear-thinning is observed at lower shear-rates with viscosity plateaus evident at higher shear-rates. This is likely a state whereby a small portion of the material is rearranged; possibly the coalescence and/or alignment of mesophase. Similar shaped flow curves were observed for pure petroleum mesophase pitches by Dumont et al. (2003).

The shear-thinning behaviour is also observed in the rotational flow curves of SPHT412 and SPHT425, shown in Figure 5.14 and 5.15.

The behaviour of SPHT412 and SPHT425 are similar to SPHT400. At higher temperatures, low shear-rate shear-thinning is observed. The higher shear-rates tend towards a viscosity plateau. High shear-rate data (above $10\,s^{-1}$) was not obtained. These three samples have similar microstructures, low to moderate mesophase content, with coalesced mesophase clusters.

The higher temperature data resemble curves that can be described by a Bingham

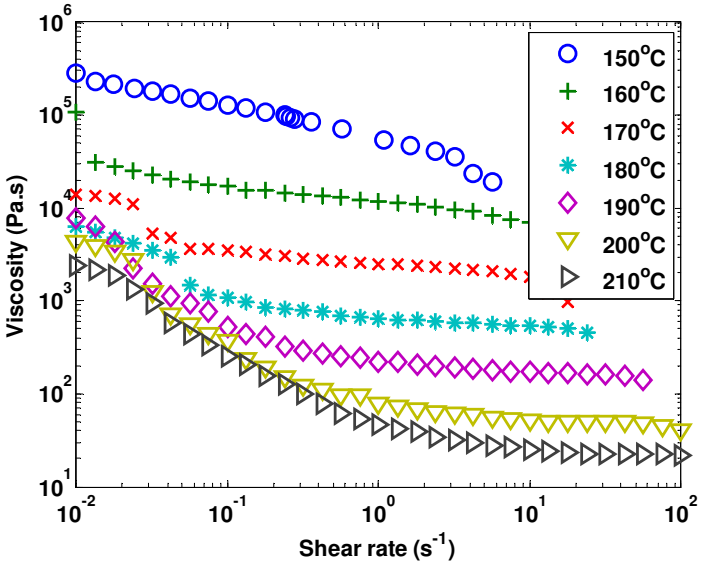

Figure 5.13: Flow curves for SPHT400 (C/H = 1.55, MC = 9%)

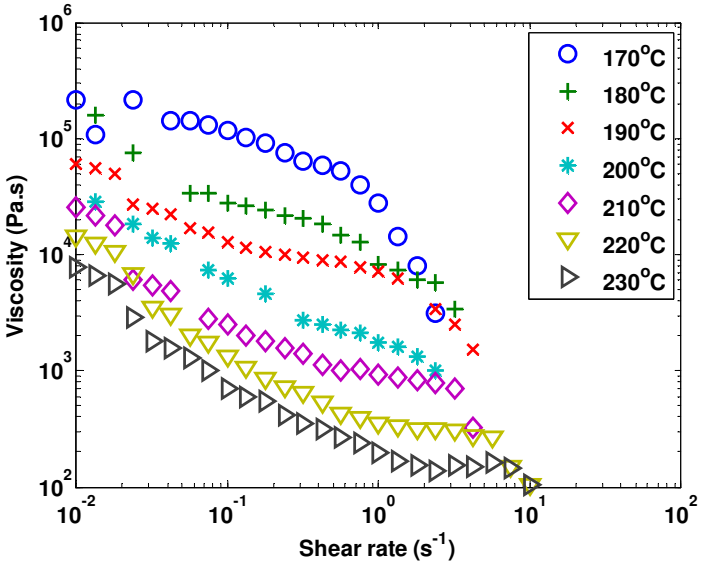

Figure 5.14: Flow curves for SPHT412 (C/H = 1.57, MC = 9%)

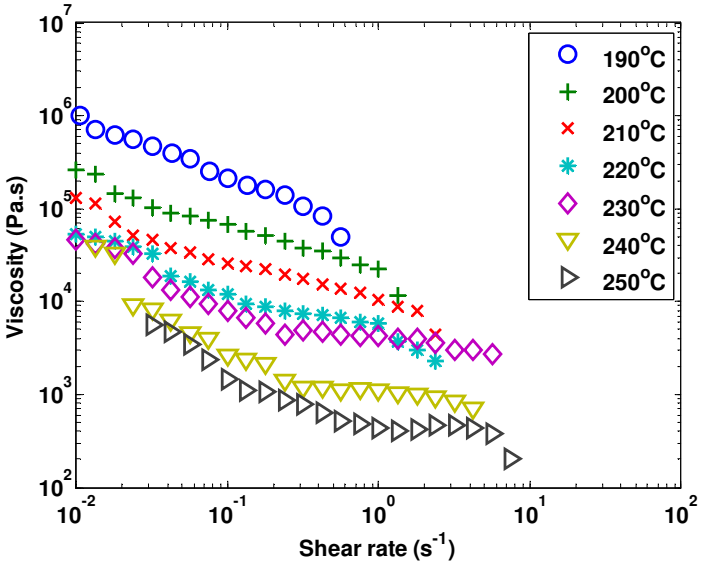

Figure 5.15: Flow curves for SPHT425 (C/H = 1.63, MC = 17%)

plastic model. The yield stress is the force required to reorganise the structural components of the sample to its final state. An important note of consideration for these samples is the temperature at which measurements are made. Flow curves are obtained at temperatures much higher than that of the softening temperature. This is noteworthy since there is not a substantial mesophase content. The shape of the curve and temperature of measurement suggest that the sample has a structure composed of components that have a strong interaction. This is similar to that of a weak gel or viscoelastic liquid (Saravanakumar et al., 2012).

The rotational shear results of SPHT420T3 (C/H = 1.76, MC = 59%) are shown in Figure 5.16. These flow curves show shear-thinning over the entire range of shear-rates over which measured viscosity was obtained. It is unlike previous samples as there is no indication of a high shear-rate plateau viscosity. This implies that the structure is still in a state of change. This shape of curve bears some similarity to SPHT425 (C/H = 1.63, MC = 17%), as they share shear-thinning characteristics. This sample however, has a much higher mesophase content. The cause of the shear-thinning is more likely due to deformation and or orientation of the mesophase. The entrapped isotropic phase is unlikely to be the major contributor to the observed behaviour.

For samples with moderate to high mesophase content in the anisotropic SASOL pitches, high-shear rate data were not attainable. This would indicate that there is a significant change occurring within the material which prevents the accurate measuring of the viscosity.

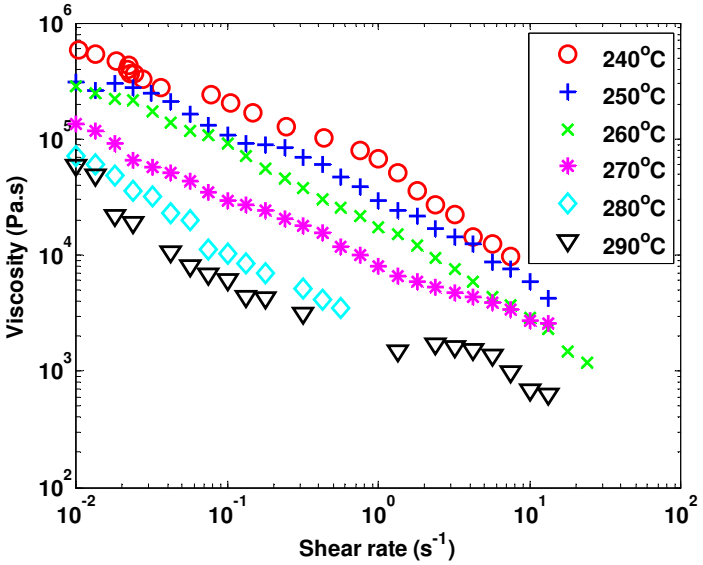

Figure 5.16: Flow curves for SPHT420T3 (C/H = 1.76, MC = 59%)

5.3 Discussion

The pitches go through different stages of mesophase development as shown in Chapter 4. The effect of the evolution of the properties and microstructure dictates the behaviour of the material under controlled shear rotational rheometry.

The pitch, being a glassy substance is expected to behave as such. The behaviour of the pitch samples were investigated around the softening temperature, or as close to it as possible. This is done within machine limits and where usable data points can be obtained.

MP110 (C/H = 1.83) is an isotropic pitch with particulate content. It is an isoviscous material at the shear-rates investigated and region of viscosity measured. This behaviour is also observed for the isotropic heat-treated MP110HT350 (C/H = 1.87) and MP110HT375 (C/H = 1.88) pitches. Behaviour of the material showed there is decreasing isoviscous viscosity with an increase in measured temperature. This is behaviour expected in most materials (especially fluids).

The 13% mesophase content of MP110HT400 retains the isoviscous nature of isotropic material. The main difference in behaviour observed from these samples is the temperature used for measurement. The measured viscosities are at higher temperatures for higher C/H samples; this is as a result of the higher glass transition temperatures. The viscosity measured still remains within the same region.

The relatively consistent isoviscous behaviour shows that this is a glassy substance with not much long range order. At high shear-rates, there is shear-thinning behaviour as well. This can either be attributed to the particulate quinoline insoluble material in the sample which changes the viscosity (low resistance to flow at the temperatures tested); or there is slip between the spindle and material which gives rise to the anomalous results.

Samples MP110HT437 (C/H = 2.05, MC = 27%), MP110HT425 (C/H = 2.09, MC = 26%), MP110HT425T6 (C/H = 2.10, MC = 26%) and MP110HT437T6 (C/H = 2.20, MC = 49%) all contain significant mesophase material. The first obvious difference in these samples (compared to predominantly isotropic pitches) is the change to non-Newtonian fluid behaviour. It is also observed that the temperatures used during these tests are temperatures much higher than that of the isotropic glass transition temperatures measured. These samples will behave as either suspensions or emulsions at the temperature of measurement.

The higher temperatures required for experimentation are as a result of the additional mesophase present. The liquid crystals have a higher glass transition temperature than the isotropic material. The microstructure of the samples, show that the mixture behaves like that of a suspension (and thereafter emulsion) at temperatures tested; the viscosity of the material is significantly increased. This changes the flow behaviour of the mixture.

Flow curves deviate further from Newtonian behaviour with change in composition and/or concentration of the mesophase. For MP110HT437 and MP110HT425 at low shear-rates, the viscosity shows minor change; at higher a shear-rates a steep slope, and then a shallower decrease in viscosity is observed. It is graphically seen that the sample continually decreases in viscosity with shear; it is a shear-thinning mixture. There appears to be kink-type behaviour in samples MP110HT425 (MC = 27%) and MP110HT437 (MC = 26%). This is attributed to the effect of the presence of mesophase spheres in the mixture. This is likely caused by the mesophase particle-particle interaction; a phenomenon which will be investigated in more detail in Chapter 6. Sample MP110HT425T6 (MC = 38%) and MP110HT437T6 (MC = 49%) are almost entirely monotonically decreasing. The probable reason for this is that the mesophase spheres dominate the behaviour of these systems. The mesophase in these samples are likely at a temperature whereupon the mixture is in a state of transition from a suspension to that of an emulsion; possible mesophase deformation may occur. This is likely the cause of the change in shape of the flow curves obtained; mesophase deformation to form ellipsoids and possible coalescence.

Choosing appropriate shear models, discussed in Chapter 6, the temperature dependence of the different samples was also investigated. The effect of temperature on viscosity was modelled using the common form of the Arrhenius equation:

$$\eta_T = C \exp^{-\frac{E_\eta}{RT}} \tag{5.1}$$

The procedure of obtaining the activation energy for the different samples is as follows:

- each flow curve is modelled with respect to shear
- viscosity at several shear-rates for each temperature was collected

- the viscosity at each shear-rate at several temperature was fitted using the Arrhenius equation (to obtain E_η)
- an average E_η value was used to represent the sample

Each separately heated treated material was modelled in the above mentioned manner, and an approximate activation energy was obtained for each sample. This is only possible as the flow curves of each sample (at their different measured temperatures) are predominantly parallel to each other. This therefore allows E_η to be independent of shear. C is a shear dependent parameter and will not be shown. The E_η values are showed in figure 5.17(a).

Each sample is represented by its respective C/H ratio. This shows the material shear activation energy varying with thermal treatment. A noticeable feature from this figure is the information for sample MP110HT437T6. Its magnitude and variance does not change with temperature. This is due to the behaviour of the sample; weak function of temperature, as opposed to concentration at the temperatures tested.

The samples with the lower C/H ratios: MP110, MP110HT350, MP110HT375 and MP110HT400, show a decrease in shear activation energy with increase in C/H. The viscosity of these four samples are in a similar range and are at temperatures of comparison (measured temperature relation to glass transition temperature); shown in Figure 5.17(b). The glass transition temperature used for these measurements are those obtained via DMTA.

This trend suggests that the material becomes less sensitive to temperature. In this case the composition of the aromatic isotropic phase loses volatile matter, increases in aromaticity and higher molecular weight (Greinke & Singer, 1988). This forms a structure comprised from a slightly narrower distribution of material and needs more energy to produce a similar change in viscosity; for this case, a higher temperature (in relation to T_g) is required. For heat treated isotropic pitch, higher temperatures are required to process the material. During processing there would be less fluctuation in viscosity due to change in temperature of the pitch as a result of lower E_η.

Figure 5.17(b) also shows how high above the continuous isotropic glass transition temperature the measurements for the anisotropic pitches were made. The mesophase and isotropic phase have an approximate difference of 50 ℃ difference in $\tan(\delta)$ and similar difference would be expected of the glass transition. For the anisotropic mixtures ($C/H \geq 2.05$) The measured temperatures are above what would be the glass transition temperature of the mesophase. MP110HT437 (C/H = 2.05, MC = 27%) and MP110HT425 (C/H = 2.09, MC = 26%) are measured at temperatures where the mesophase is expected to be a high viscous fluid. MP110HT425T6 (C/H = 2.10, MC = 38%) and MP110HT437T6 (C/H = 2.20, MC = 49%) are at measured at temperatures where a more significant softening and low viscosity fluid is expected. Hence the belief

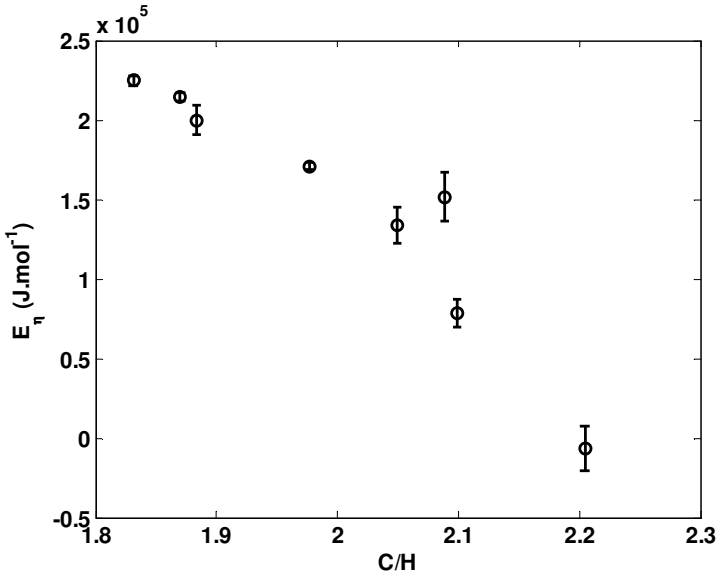

(a) Arrhenius activation energy for different Mittal samples

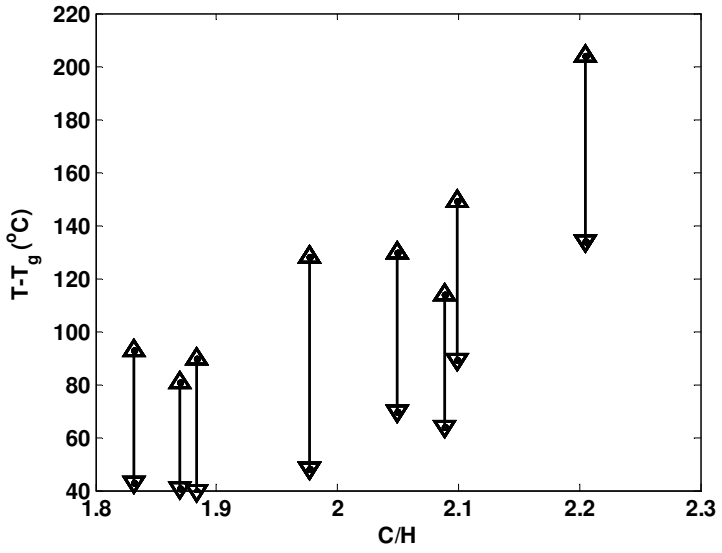

(b) Relative measurement temperatures for different Mittal samples

Figure 5.17: Temperature and viscosity effects of Mittal pitches

that MP110HT437 and MP110HT425 behave more as suspensions, MP110HT425T6 is transitioning towards an emulsion and MP110HT437T6 is an emulsion. The effect of the particulates should not be neglected.

The isotropic SASOL pitches show similar behaviour with respect to temperature as the MP110 pitches. Dominant isoviscous behaviour is observed. This pertains to SPAR, SPHT350, SPHT375 and SPHT400T3. Some shear-thinning behaviour of SPHT400T3 is seen at lower temperatures.

For the higher C/H ratio SASOL pitches non-Newtonian behaviour is observed. With the change in composition, C/H ratio, the samples tend to have increased shear-thinning at lower shear-rates and higher measurement temperatures (above T_g) for SPHT400, SPHT412 and SPHT425. This is indicative of polymer melts where, upon use of the entanglement model, the chains are uncoiled to a state where they cannot change anymore, eventually leading to an infinite-shear viscosity (which is also observed). This is not the case with respect to the pitch samples as the molecular weight distribution of its components are not high enough (Greinke & Singer, 1988); the chains are too short to cause behaviour expected of a material which has entanglement.

The sample would act as a suspension/emulsion (depending on the temperature) or weak gel. A possible explanation is the reorganising of coalesced regions upon shear; this is however not likely since the mesophase content of the SPHT400 and SPHT412 is still low. This suggests that the formation of a gel-like structure with stronger interaction is a more likely possibility. The initial yielding observed is a result of the breakdown of this structure. The possibility of this structure is likely since there would be strong intermolecular forces between its components (possibly isotropic pitch and mesophase); this is likely as a result of the higher oxygen content (Sima et al., 2003)(Mokoena et al., 2008) and stronger hydrogen bonding.

SPHT420T3, which has a significant amount of mesophase shows continuous shear-thinning over the entire range of shear-rates tested. This would be indicative of initial structure change, as also observed in SPHT425. Mesophase deformation and possible alignment would lead to continued shear-thinning at these temperatures.

Sample SPHT425 and SPHT420T3 do not show significantly different rotational rheology results; despite the large change in mesophase content and subsequent structure. This suggests that the mesophase is significant to the properties of the underlying microstructure. The behaviour is much more like that of a weak-gelled system; with SPHT425 being a weaker gel than SPHT420T3. This is observed by the drastic change in $T - T_g$ or T_s of SPHT425 compared to the other samples as shown in Figure 5.18(b). This supports the notion of a strong interaction between the two phases and its components; a single dominant structure for the SASOL pitch as opposed to the mesophase spheres and isotropic pitch of the MP110 anisotropic pitches.

In the same manner as the MP110 was modelled to the Arrhenius equation, this

method was applied to the SASOL pitches. The calculated Arrhenius energies are shown in Figure 5.18(a). A feature of this material is that the isotropic pitch samples has an almost constant activation energy. The large deviation of these E_η values of the anisotropic SASOL pitches are a result of the different shapes of the curves at the temperatures measured due to the gel-like structure postulated earlier. To have a constant and reliable value, parallel flow curves are necessary. The result of this implies that higher C/H samples Arrhenius activation energies cannot be used to characterise the material behaviour. This is different from the MP110 pitches where we have a decrease in activation energy with an increase in $T - T_g$ and C/H.

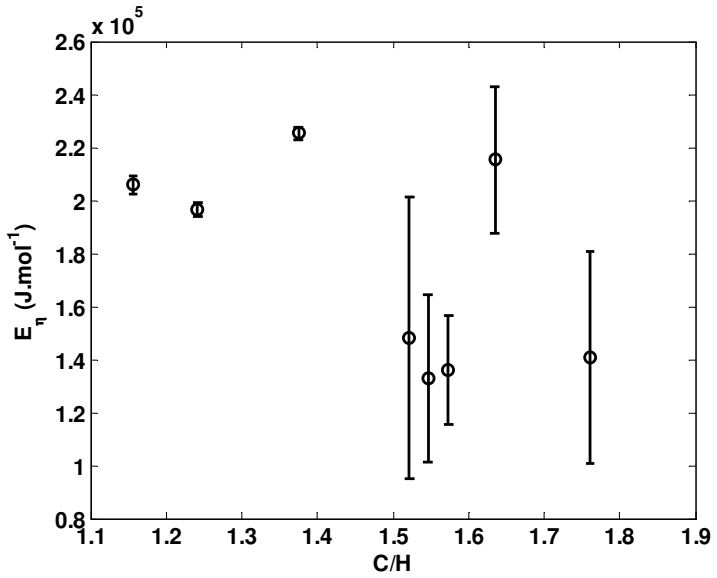

(a) Arrhenius activation energy for different SASOL samples

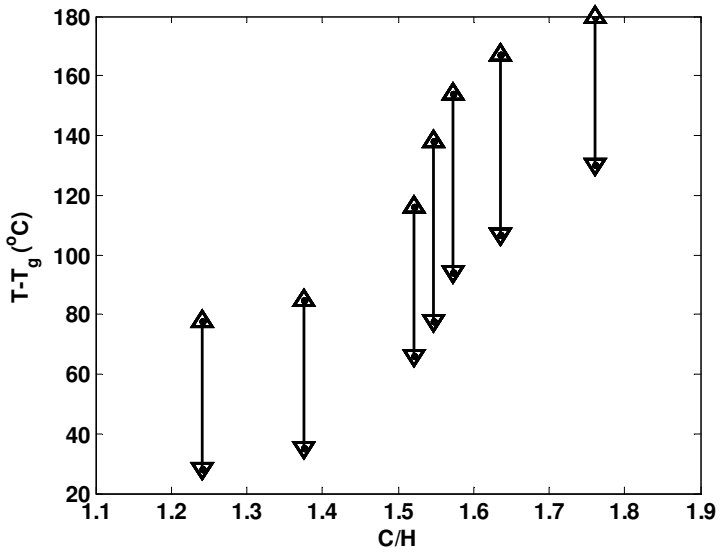

(b) Relative measurement temperatures for different SASOL samples

Figure 5.18: Temperature and viscosity effects of SASOL pitches

The viscosity of a sample has also been used to indicate properties of a sample; mainly to approximate the softening and glass transition temperature of a sample. This can be a dangerous path to follow as it has been shown that non-Newtonian behaviour is observed, and therefore isoviscous temperature for a sample is not always possible.

If a 1000 Pa s is used to describe the softening temperature of MP110 (C/H = 1.83), it would be approximately 110 ℃, yet for sample MP110HT437 (C/H = 2.05) it would be between 140 ℃ and 180 ℃. So using an isoviscous temperatures to help predict behaviour should be made with caution.

CHAPTER 6

RESULTS: MODELLING OF ROTATIONAL SHEAR DATA

In this chapter the rotational shear data presented in Chapter 5 will be modelled with continuum models discussed in Section 2.4.4:

- Cross (Cross)
- Bird-Carreau (Bird)
- Bird-Carreau-Yasuda (CY)
- Hershel-Bulkley (HB)
- Power-Law (PL)
- Bingham plastic (BP)

The models have been separated into those that have zero and infinite viscosity plateaus (Cross, Bird, CY), and those that do not (BP, PL, HB).

These models were curve-fitted by an algorithm programmed in the MATLAB environment built on some optimisation concepts. The basics of the curve-fitting technique employed is as follow:

- sorting of experimental data
- choosing initial parameters for the model
- calculate predicted model viscosity values with initial parameters and independent variable (shear-rate or stress) as input

- optimise parameters for model from an appropriate objective function (normally a least squares error)

Further detail on the numerical procedure shall not be discussed, but these concepts are important to remember when trying to improve the fitting parameters from a model.

The application of some of the data to suspension/emulsion rheology will also be attempted; this is done by using the Krieger-Dougherty equation (and its modified emulsion equivalent).

6.1 Zero and Infinite-Shear Viscosity Models

The Cross, Bird and CY models are two plateau models. These are expected to predict the shape of all of the viscosity data, or to fit the data better than the other models in Section 6.2. This is expected since it is assumed that the parameters would reduce to a form of a simpler equation where necessary. The differentiation between these models is the manner in which the transition between the upper and lower shear limits is mathematically expressed.

The fit of the Carreau-Yasuda model to MP110 (C/H = 1.83) is shown in Figure 6.1. The fit of the model is good across the range of temperatures. This can be observed via the R^2 values calculated and shown in Table 6.1. The fits of the Bird and Cross models are similar to that of the CY model. This is also observed together with similar R^2 values. This trend is seen with all the samples. The isotropic pitches fit well, and observed with the fit and R^2 values for SPHT350 (C/H = 1.24) shown in Figure 6.2 and Table 6.2.

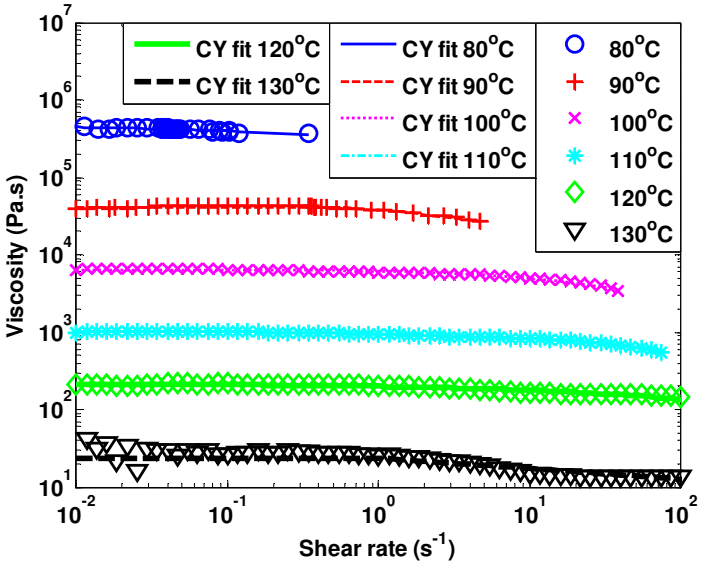

Figure 6.1: Flow curves for MP110 pitch (C/H = 1.83) with Carreau-Yasuda fit

Samples SPAR, SPHT375, SPHT400, MP110HT350, MP110HT375 and MP110HT400 are all predominantly isotropic pitches that have strong isoviscous characteristics; this

Table 6.1: R^2 values for the plateau model applied to MP110 (C/H = 1.83)

Temperature (°C)	Cross	Bird	CY
80	0.771	0.787	0.776
90	0.936	0.940	0.940
100	0.982	0.945	0.983
110	0.978	0.931	0.979
120	0.944	0.927	0.944
130	0.771	0.763	0.725

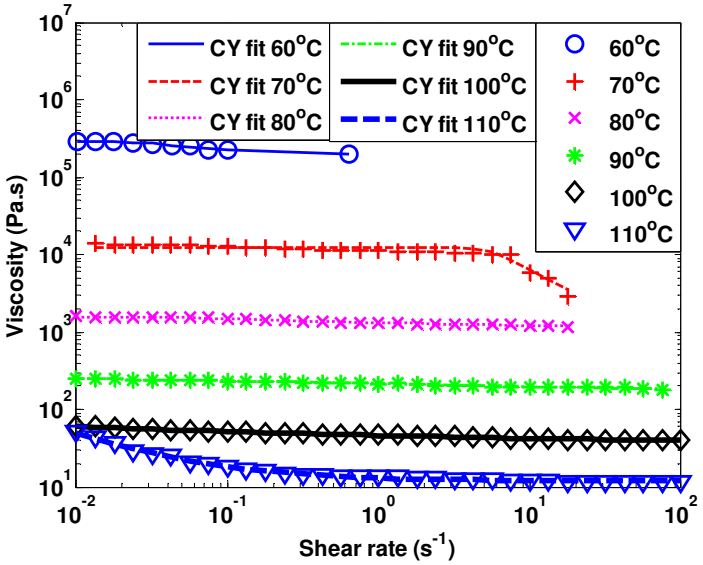

Figure 6.2: Flow curves for SPHT350 (C/H = 1.24) with Carreau-Yasuda fit

Table 6.2: R^2 values for the plateau model applied to SPHT350 (C/H = 1.24)

Temperature (°C)	Cross	Bird	CY
60	0.885	0.901	0.985
70	0.944	0.902	0.921
80	0.980	0.973	0.988
90	0.985	0.984	0.985
100	0.985	0.987	0.987
110	0.993	0.993	0.994

results in good fits for the plateau models. These excellent fits are still seen in sample MP110HT425 (C/H = 2.09, MC= 29%), Figure 6.3 and Table 6.3. This sample has a different shape, and is still excellently fitted via these two plateau viscosity models. This occurs as a result of the shape of the curve suiting the manner in which the model is constructed. The flow curves for these samples appear to be tending towards an isoviscous high and low-shear viscosity limit. The R^2 values for this sample are extremely good and better than the fits for the isoviscous isotropic samples. The excellent fits continue with MP110HT437 (C/H = 2.05, MC = 27%) and MP110HT425T6 (C/H = 2.10, MC = 38%). The two plateau models were also chosen as they were believed to help understand the manner in which the mesophase spheres act and change in their different structural states under shear.

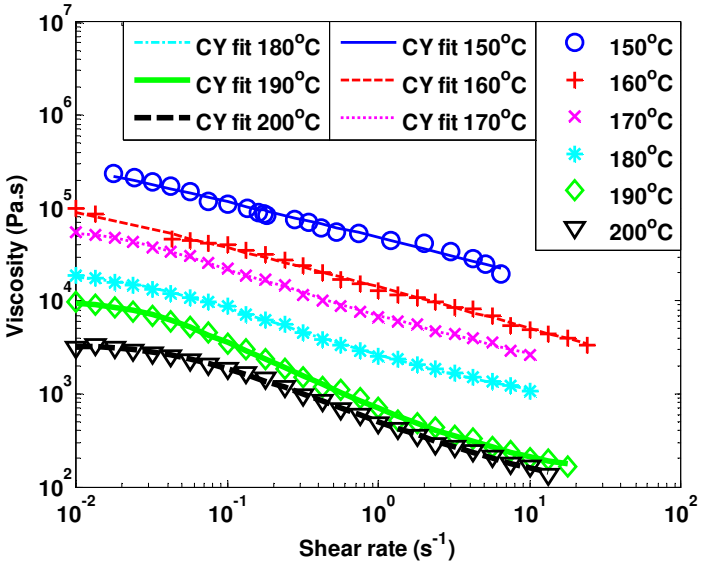

Figure 6.3: Flow curves for MP110HT425 (C/H = 2.09, MC = 26%) with Carreau-Yasuda fit

Table 6.3: R^2 values for the plateau model applied to MP110HT425 (C/H = 2.09, MC = 26%)

Temperature (°C)	Cross	Bird	CY
150	0.988	0.989	0.986
160	0.996	0.996	0.996
170	0.998	0.999	0.999
180	0.999	0.999	0.999
190	0.999	0.999	0.999
200	0.999	0.999	0.999

SPHT400 has a very different set of flow curves for the temperature range over which the experiments were carried out. The lower temperatures resemble a power-law and/or isoviscous curve shape, and the higher temperatures show low shear-rate shear-thinning

which tends towards an isoviscous range. This is different as compared to the MP110 anisotropic pitches where the same shape was observed for all the temperatures. These three models fitted all of these curves well. This shows the versatility of this type of model to be applied to different shapes of curves. The shape of curves is similar for SPHT412 (C/H = 1.57, MC = 9%) and SPHT425 (C/H = 1.63, MC = 17%); hence similarly good fits are obtained.

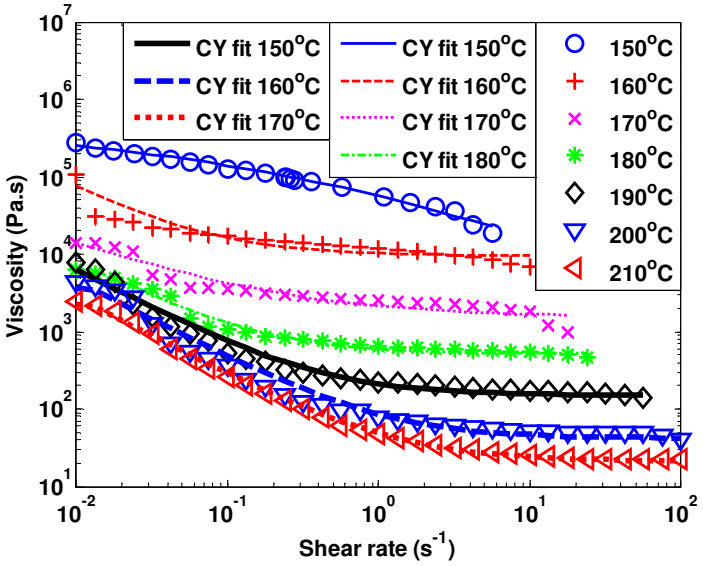

Figure 6.4: Flow curves for SPHT400 (C/H = 1.55, MC = 9%) with Carreau-Yasuda fit

Table 6.4: R^2 values for the plateau model applied to SPHT400 (C/H = 1.55, MC = 9%)

Temperature (°C)	Cross	Bird	CY
150	0.986	0.978	0.988
160	0.808	0.803	0.805
170	0.893	0.893	0.893
180	0.981	0.977	0.979
190	0.990	0.973	0.973
200	0.989	0.973	0.973
210	0.998	0.997	0.997

Samples SPHT420T3 (C/H = 1.76, MC = 59%) and MP110HT437T6 (C/H = 2.20, MC = 49%) are the two samples with the most mesophase present. The shape of SPHT420T3 at low temperatures is that of transition away from a low-shear isoviscous limit. At mid-range temperatures it transitions to a monotonic shear-thinning power-law fluid; and at high temperatures the curves are shear-thinning towards a high-shear plateau limit. The model predicts all of these flow curve viscosities, Figures 6.5 and 6.5.

Figure 6.6 and Table 6.6 continue to show the robustness of this type of model (via fit and R^2). These models simplify to the power-law model over the entire temperature range.

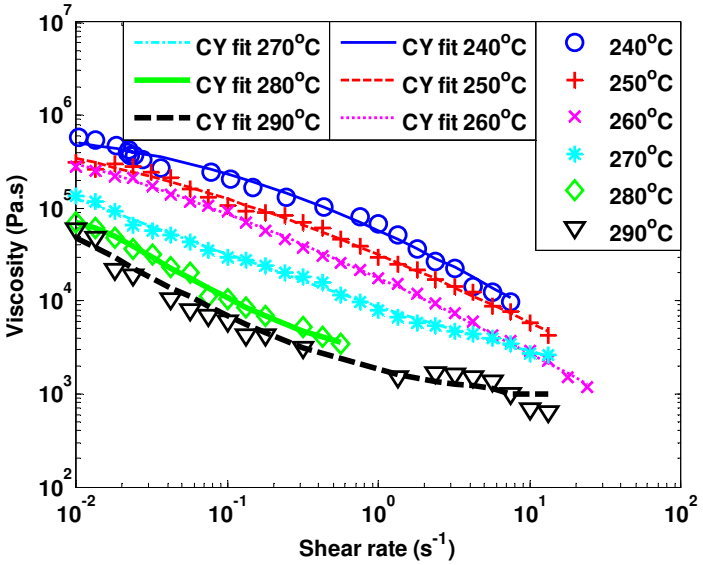

Figure 6.5: Flow curves for SPHT420T3 (C/H = 1.76, MC = 59%) with Carreau-Yasuda fit

Table 6.5: R^2 values for the plateau model applied to SPHT420T3 (C/H = 1.76, MC = 59%)

Temperature (°C)	Cross	Bird	CY
240	0.988	0.979	0.991
250	0.996	0.994	0.996
260	0.998	0.997	0.999
270	0.997	0.997	0.997
280	0.994	0.994	0.994
290	0.964	0.964	0.967

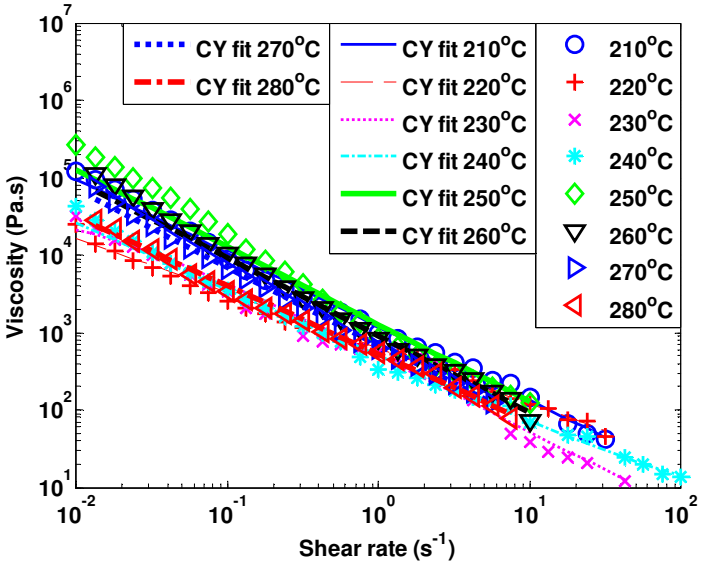

Figure 6.6: Flow curves for MP110HT437T6 (C/H = 2.20, MC = 49%) with Carreau-Yasuda fit

Table 6.6: R^2 values for the plateau model applied to MP110HT437T6 (C/H = 2.20, MC = 49%)

Temperature (°C)	Cross	Bird	CY
210	0.995	0.995	0.995
220	0.989	0.989	0.991
230	0.978	0.978	0.984
240	0.995	0.995	0.994
250	0.999	0.968	0.973
260	0.997	0.991	0.991
270	0.999	0.993	0.996
280	0.995	0.995	0.996

The result of the good fit for all these models, is to show the versatility of this type of equation to predict the viscosity, of all of these curves, despite the different shapes observed. The model is an excellent tool to use to retro-fit the data to possibly be used in further applications.

The difficulty in the use of these models is that the four/five variables used for curve fitting do not systematically change in any particular manner. This is not necessarily a problem for the isoviscous samples, as there are no interpretable parameters; but does prove more difficult for the anisotropic pitches. The anisotropic samples do not have a single set of curves that have a constant shape. This tends to increase the difficulty in obtaining parameters which can be used for interpretation of the underlying microstructure and its behaviour. The shape of the curves were initially believed to allow for these parameters to follow a pattern. The interaction between these variables did not allow for this to occur. This is shown in the parameters obtained for MP110HT425 (C/H = 2.09, MC = 26%) and SPHT400 (C/H = 1.55, MC = 9%) in Tables 6.7 and 6.8 where λ,a and n do not change in any systematic way. Due to no definable pattern, the two plateau viscosity models prove to be nothing more than a curve fitting tool.

Table 6.7: Carreau-Yasuda model parameters for MP110HT425 (C/H = 2.09, MC = 26%)

Temperature (°C)	η_0 (Pa.s)	η_∞ (Pa.s)	λ (s)	a (-)	n (-)	R^2 (-)
150	1.30×10^7	1.73×10^2	9.45×10^3	1.40×10^2	4.86×10^{-1}	0.986
160	1.41×10^7	3.87×10^2	1.95×10^2	1.02×10^{-1}	2.90×10^{-1}	0.986
170	5.53×10^4	1.04×10^3	5.78×10^1	2.72	4.57×10^{-1}	0.996
180	2.03×10^4	6.48×10^2	4.02×10^1	1.31	3.78×10^{-1}	0.999
190	9.81×10^3	1.14×10^2	3.68×10^1	2.05	2.19×10^{-1}	0.999
200	3.35×10^3	6.54×10^1	2.01×10^1	1.56	3.26×10^{-1}	0.999

Table 6.8: Carreau-Yasuda model parameters for SPHT400 (C/H = 1.55, MC = 9%)

Temperature (°C)	η_0 (Pa.s)	η_∞ (Pa.s)	λ (s)	a (-)	n (-)	R^2 (-)
150	4.75×10^5	7.78×10^{-5}	6.40×10^{-1}	2.73×10^1	1.01×10^{-5}	0.988
160	1.37×10^6	9.68×10^3	2.07×10^3	8.14×10^2	1.55×10^{-5}	0.805
170	8.79×10^4	1.56×10^3	1.79×10^3	1.75×10^1	3.13×10^{-1}	0.893
180	6.04×10^3	5.16×10^2	7.02×10^1	1.03×10^1	1×10^{-5}	0.979
190	1.08×10^4	1.50×10^2	1.75×10^2	7.97×10^1	6.28×10^{-5}	0.973
200	3.77×10^3	4.20×10^1	8.40×10^1	8.39×10^1	1×10^{-5}	0.973
210	2.26×10^3	2.13×10^1	8.14×10^1	7.88×10^1	1.11×10^{-5}	0.973

6.2 Herschel-Bulkley Derived Models

The next model investigated, the Herschel-Bulkley model, incorporates both yield stress and power-law functionality, Equation 2.23. This equation is chosen, as it has parameters that are easier to interpret.

$$\tau = \tau_0 + K_2\dot{\gamma}^n \tag{2.23}$$

With simple modification this equation simplifies into the form of the power-law equation, Equation 2.22, when $tau_0 = 0$.

$$\eta = K_1\dot{\gamma}^{n-1} \tag{2.22}$$

The Herschel-Bulkley equation also easily simplifies to the Bingham plastic equation, Equation 2.21, when the power-law index tends to 1.

$$\sigma = \eta_{pl}\dot{\gamma} + \sigma_B \tag{2.21}$$

So the Herschel-Bulkley equation still possesses some freedom to fit different shaped curves, with three adjustable parameters, but can be constrained to a much simpler form to allow for different interpretation. The fit of this equation to MP110 is shown in Figure 6.7 and the parameters obtained from the fit are in Table 6.9.

Table 6.9: Herschel-Bulkley model parameters for MP110 (C/H = 1.83)

Temperature (°C)	τ_0 (Pa)	K_2 $(Pa.s^n)$	n (-)
80	0	3.47×10^5	0.94
90	0	3.72×10^4	0.96
100	0	5.64×10^3	0.95
110	0	8.96×10^2	0.95
120	0	1.89×10^2	0.95
130	0	2.27×10^1	0.89

The parameters of the Herschel-Bulkley model for MP110 reduce to the parameters

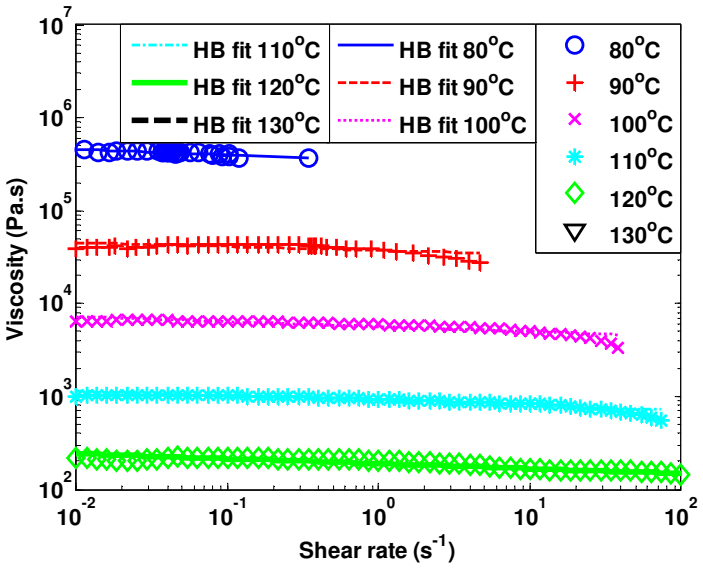

Figure 6.7: Herschel-Bulkley fit for MP110 (C/H = 1.83)

for the power-law equation ($\tau_0 = 0Pa$). This trend continues with all the isotropic samples at almost all temperatures, both MP110 and SASOL derivatives. High power-law indices also account for weak shear-induced characteristics; this is expected since strong Newtonian behaviour is observed. Due to this behaviour, the isotropic Mittal and SASOL pitches simplify to a similar form. The almost isoviscous nature of these samples are the main attribute that allows for good fits.

The fit of the Herschel-Bulkley model to the anisotropic Mittal pitches was also implemented. The MP110HT425 (C/H = 2.09, MC = 26%) fit is shown in Figure 6.8 and the parameters from this fit are shown in Figure 6.10.

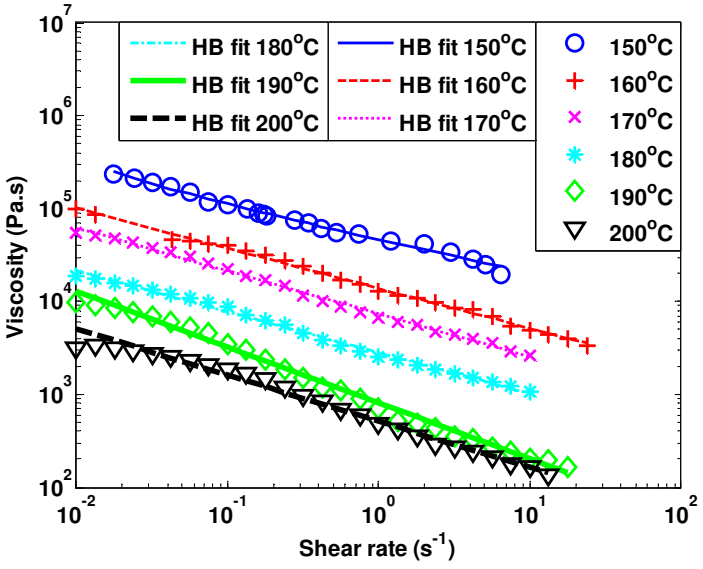

Figure 6.8: Herschel-Bulkley fit for MP110HT425 (C/H = 2.09, MC = 26%)

Table 6.10: Herschel-Bulkley model parameters for MP110HT425 (C/H = 2.09, MC = 26%)

Temperature (°C)	τ_0 (Pa)	K_2 $(Pa.s^n)$	n (-)
150	1.14×10^3	4.53×10^4	0.65
160	2.27×10^{-1}	1.38×10^4	0.57
170	0	7.36×10^3	0.54
180	0	2.82×10^2	0.56
190	0	8.03×10^2	0.40
200	0	5.12×10^2	0.50

Good fits are observed for MP110HT425. At temperatures 150 °C and 160 °C there is variation in all three Herschel-Bulkley parameters, however at higher temperatures this simplifies to the power-law equation. With other anisotropic MP110 samples, this behaviour continues; at some temperatures the Herschel-Bulkley equation fits and at other temperatures, it simplifies to the power-law equation parameters. A caveat of this technique, is that although yield-stress values are calculated for some flow curves, the sample shows no real yielding; the shape of the curve tends towards high and low shear plateaus. For samples with calculated yield stresses, the power-law index calculated fits the shear-thinning region at high shear-rate as it tends towards the high shear plateau. This model does not seem appropriate for helping to understand the underlying microstructure, whereby it would appear that particle break up occurs.

With higher mesophase samples (MP110HT425T6 and MP110HT437T6), behaviour transitions towards a more monotonically decreasing viscosity with shear. These curves are fitted much more appropriately with the power-law model as is shown in Figure 6.9. This is likely the case as the sample microstructure is in the process of drastic change; this will be caused by a likely softer mesophase and higher mesophase content. Due to the dramatic change in structure, an equally dramatic change in viscosity is measured.

The power-law model gives an overall easily interpretable manner of describing the material behaviour. The fit of this model to the data does not always give the best fit to the curve (or an indication of the shape); it does give an average quantifiable parameter with which the samples may be compared.

The Mittal pitch samples were curve-fitted by optimising for the power-law consistency and behaviour indices. This was done for the entire temperature range for the samples. The power-law behaviour index, n, for a sample over a range of temperatures generally has little deviation for the Mittal pitch. The consistency index however is a strong function of temperature. It will follow the same trend as the temperature dependance of the viscosity itself (which was modelled earlier using Arrhenius). The average n values can be seen in Figure 6.10(a).

There is a strong trend of decreasing n with the severity of thermal treatment. This helps describe the extent of shear-thinning of the samples. It shows a significant increase

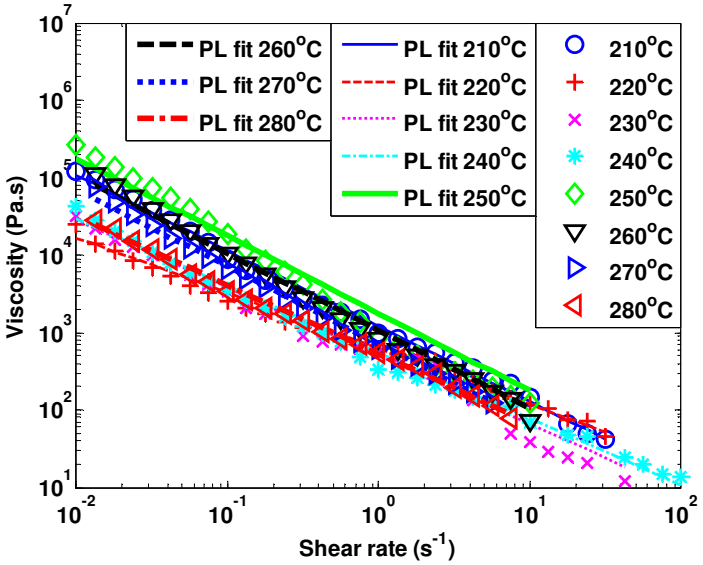

Figure 6.9: Power law model fit for MP110HT437T6 (C/H = 2.20, MC = 49%)

in shear-thinning for measurements made in the same viscosity range. The model shows that the isotropic samples are indeed isoviscous, with an index of almost one and little deviation. This confirms the visual trend observed.

The anisotropic samples show a significant decrease in the power-law index; from n of almost 0.5 to nearly 0. The drop of the parameter is much more significant for MP110HT425T6 and MP110HT437T6. The index quantifies the extent of the reorganisation of the structure, and with such a low index, it is a major change. It should be noted that the range of temperatures over which measurements are made also play a vital role, Figure 6.10(b). The decrease in behaviour index, is also accompanied by an increase in the range of $T - T_g$. Simultaneously, there is an increase in content of mesophase in the anisotropic pitch samples. Increased shear-thinning is a result of higher content and more softer mesophase in a lower viscosity continuous fluid. This would also explain the change in behaviour from an isotropic pitch, to a suspension, to an emulsion, as the C/H ratio and the measurement temperatures increases.

This behaviour is not observed for the anisotropic SASOL pitches. Figure 6.11 is a fit of the Herschel-Bulkley equation to SPHT400 (C/H = 1.55, MC = 9%), and its associated parameters are shown in Table 6.11.

SPHT400 shows an excellent fit at all temperatures. It is able to describe the change of shear behaviour over the different temperatures. Power-law behaviour is observed at lower temperatures; at higher temperatures the behaviour transitions to Herschel-Bulkley based behaviour which often reduces to that of a Bingham plastic.

For the range of shear-rates investigated, the lower temperature data, does not yield a high shear viscosity plateau. Within this region, the shear-thinning behaviour is dominant and the power-law equation best describes it. At higher temperatures, the low-shear data

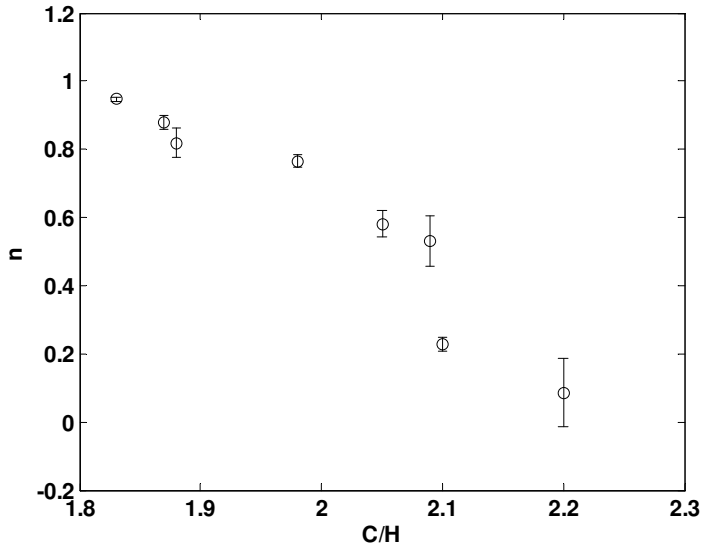

(a) Power law model parameter change for MP110 pitches

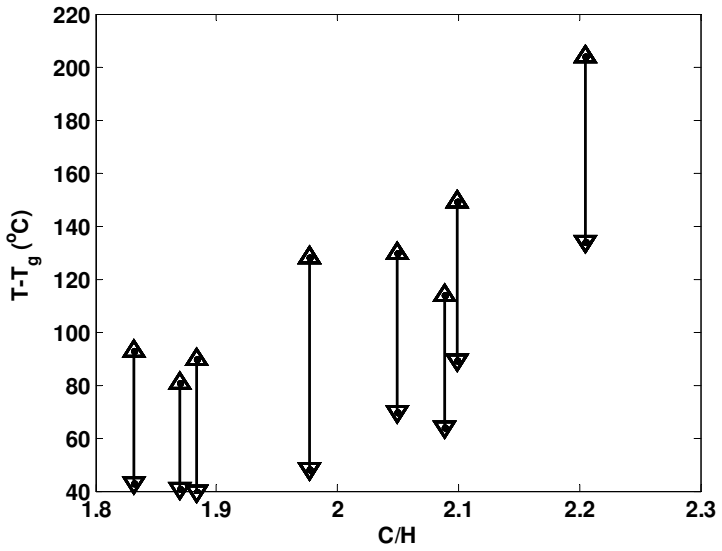

(b) Relative measurement temperatures for different Mittal samples

Figure 6.10: Power-law behaviour index variation of Mittal pitches

Table 6.11: Herschel-Bulkley model parameters for SPHT400 (C/H = 1.55, MC = 9%)

Temperature (°C)	τ_0 (Pa)	K_2 $(Pa.s^n)$	n (-)
150	0	5.38×10^4	0.63
160	0	1.24×10^4	0.68
170	1.27×10^2	2.22×10^3	0.91
180	7.32×10^1	5.52×10^2	0.98
190	5.90×10^1	1.54×10^2	1.03
200	4.21×10^1	4.06×10^1	1.05
210	2.61×10^1	2.20×10^1	1.00

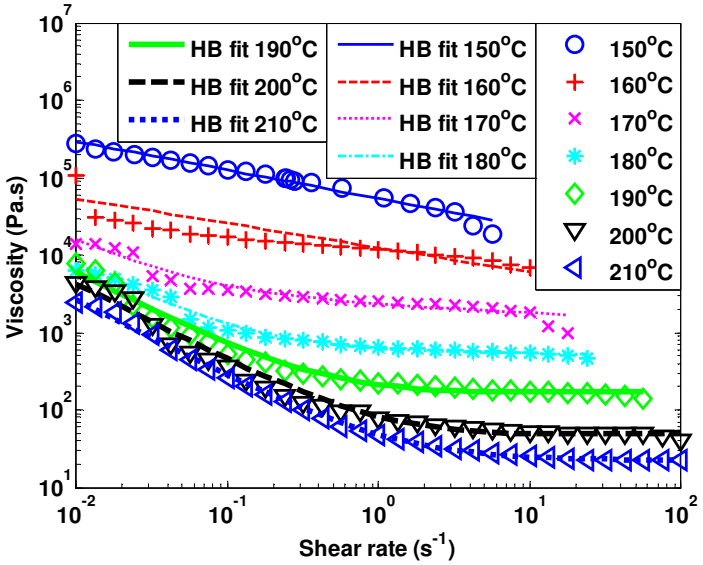

Figure 6.11: Herschel-Bulkley fit for SPHT400 (C/H = 1.55, MC = 9%)

is well described by the yield stress, whereupon at higher shear, the isoviscous behaviour is dominant. The fit of this Bingham plastic behaviour is shown in Figure 6.12.

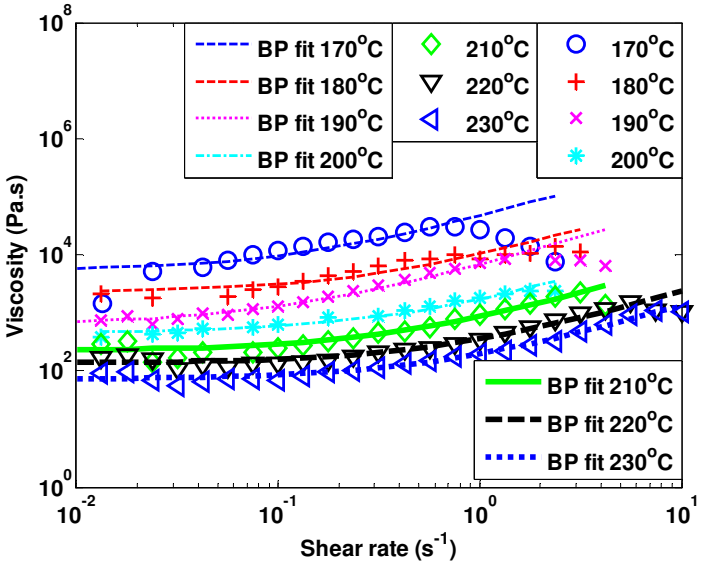

Figure 6.12: Flow curves for SPHT412 pitch with Bingham model fit

The appreciable yielding is a result of changing of the microstructure towards a secondary ordered state under shear. This is likely movement of the mesophase clusters or breakdown of gel-like structure. This behaviour is also observed for SPHT425, although at a higher temperature range.

A deviation in shape of flow curves is observed for SPHT420T3 (C/H = 1.76, MC = 59%), instead of a transition from a yield stress thinning to a an isoviscous material, there is a transition to a power-law shear-thinning fluid. These curves are shown in Figure 6.13.

The parameters of the SASOL anisotropic pitch samples, SPHT420T3 apart, are

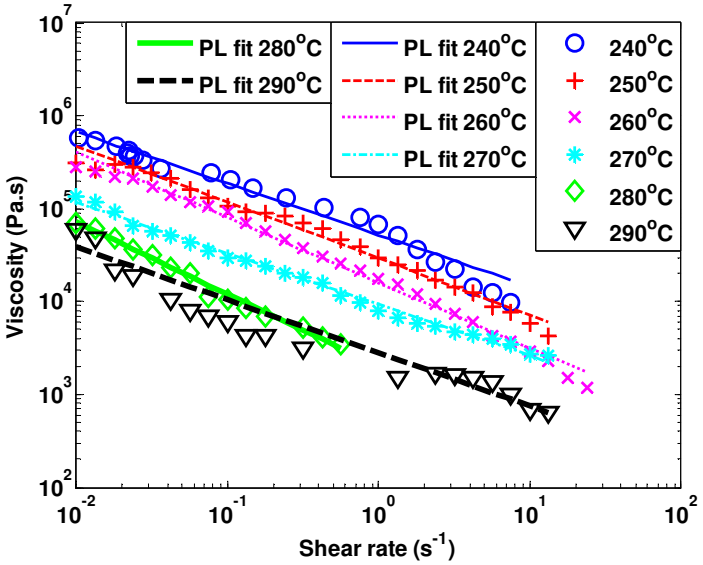

Figure 6.13: Power law model fit for SPHT420T3 (C/H = 1.76, MC = 59%)

shown in Figure 6.14. This indicates a higher required force to cause initial movement of the sample, and this is expected due to the change in microstructure. A larger difference is observed at lower plastic viscosity where the effect of microstructure is much more visible, and further supports the notion of gel-like structure.

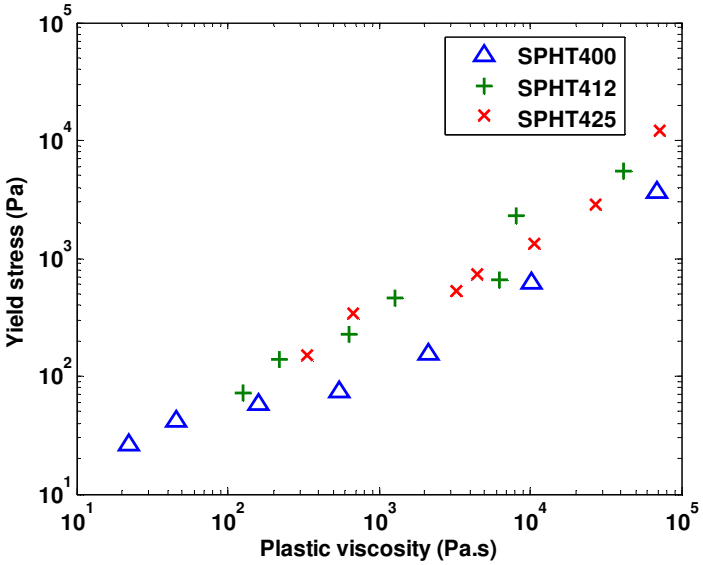

Figure 6.14: Bingham model parameters for the SASOL pitches

6.3 Suspension/Emulsion Rheology

The isotropic MP110 pitches (including MP110HT400 with low mesophase content) behave like suspensions. The isotropic samples are predominantly isoviscous with approximately 8 % particulate matter (by volume).

The initial, most relevant, and widely applied model for concentrated suspensions is the Krieger-Dougherty model (Krieger, 1972). This model is robust, and explains rheology over a wide range of volume fraction of filler; it however does not consider particle interaction. In general, this semi-empirical equation describes the rigid repulsion of particles quite successfully. The model used in this chapter assumes a hard-sphere suspension with random packing in a Newtonian fluid.

$$\eta = \eta_s \left(1 - \frac{\phi}{\phi_m}\right)^{-[\eta]\phi_m} \tag{2.30}$$

η is viscosity of the fluid with filler and ϕ representing the volume filler fraction in the suspension. Intrinsic viscosity,$[\eta]$, is a property of the system, and has experimentally been determined as 2.5 for a hard sphere suspension of unimodal distribution; this value was used in our models. This was determined by Einstein as often referred to as the Einstein coefficient. The maximum packing fraction,ϕ_m, used was 0.63, that of random packing for spheres.

The influence of the particulates on the viscosity of the fluid is shown in Figures 6.15, 6.16 and 6.17. The suspension viscosity is measured, and the volume fraction of filler was approximated, and the isotropic fluid viscosity was calculated. The density of amorphous carbon is in the range of $1.8-2.1\,\mathrm{g\,cm^3}$ with mesophase/pitch material approximately $1.3-1.4\,\mathrm{g\,cm^3}$. The difference in density between the mesophase and isotropic phase is different, but not large in comparison to that of amorphous carbon. The density of amorphous carbon was approximated as $2\,\mathrm{g\,cm^3}$ and this was used to convert the mass percentage of the particulates to the volume fraction. The particulate mass fractions are shown in Table 4.20.

All three figures show the relative decrease of viscosity (from suspension) to the isotropic fluid due to the presence of particulates. The change in viscosity is not drastic; and the change observed is merely a vertical displacement (decrease to calculated viscosity). This type of behaviour is expected, and the predominantly isoviscous behaviour of the suspension is therefore also characteristic of the isotropic pitch. Due to the low dispersed phase content, the fixed volume fraction approximated is a valid assumption as significant particle interaction (deagglomeration) does not appear to be a dominant feature of this system. For samples that show incremental increase in shear dependent behaviour, deagglomeration of particulates is the likely cause.

MP110HT400 is a sample that is largely isoviscous but does contain some mesophase. Due to the dominant isoviscous nature (compared to the higher mesophase content samples), the behaviour implies that the major contributor is still the isotropic pitch. The major difference, between MP110HT400 and the isotropic pitch samples, is that the mixture contains a higher content of dispersed phase; the particulates (8 %) and mesophase (13 %). Figure 6.18 shows the change in viscosity with different volumes of

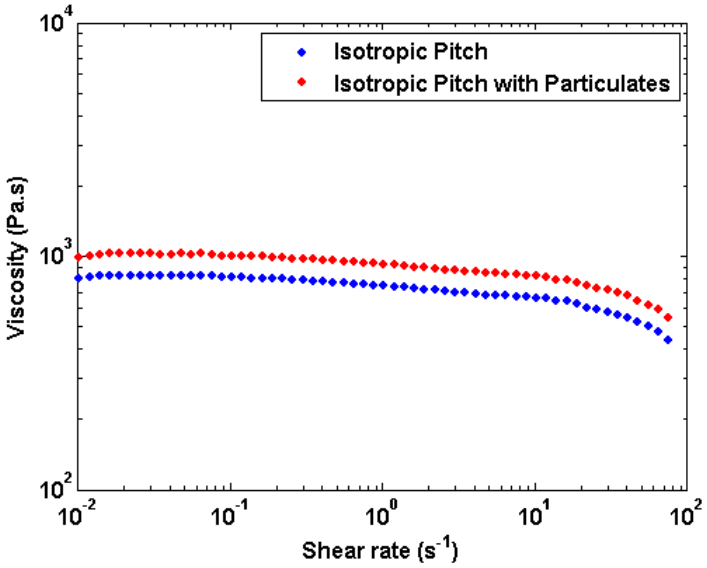

Figure 6.15: Krieger-Dougherty model applied to MP110 at 110 ℃

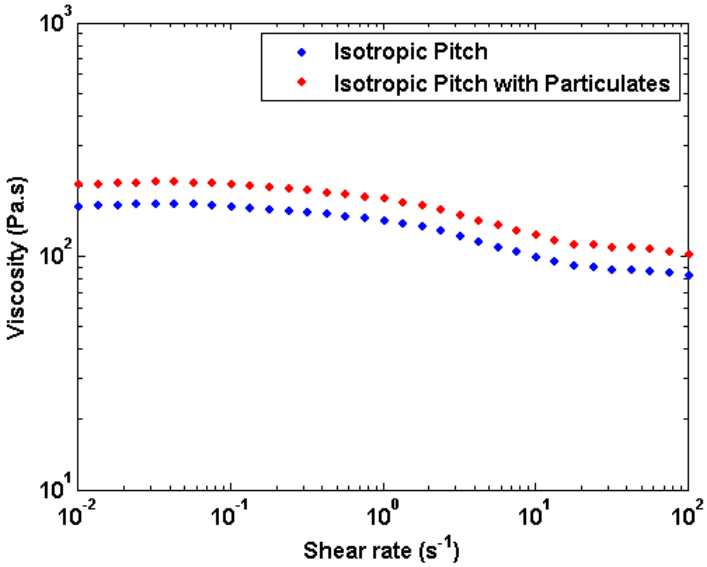

Figure 6.16: Krieger-Dougherty model applied to MP110HT350 at 140 ℃

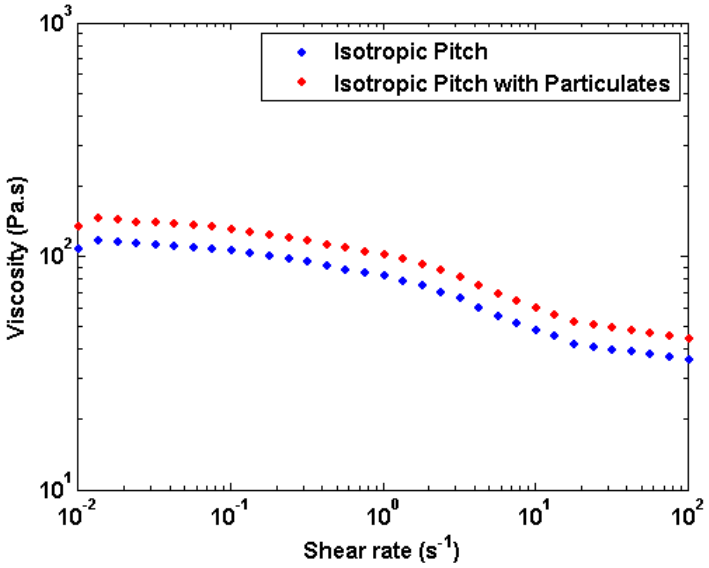

Figure 6.17: Krieger-Dougherty model applied to MP110HT375 at 150 °C

dispersed phase used: 8 % ($pitch - particulates$), 13 % ($pitch - mesophase$) and 21 % ($pitch - (particulates + mesophase)$). A slightly shear-thinning flow curve is predicted for the underlying fluid; this is similar to the behaviour observed by Blanco et al. (1999). It was expected that the shear-thinning behaviour would be caused by deagglomeration of the dispersed phase material, and to some extent this is true. Non-Newtonian fluid shear-thinning behaviour however was also shown to be the behaviour of separated isotropic pitch without particulate content; so predicted non-Newtonian flow curves can be used for further analysis.

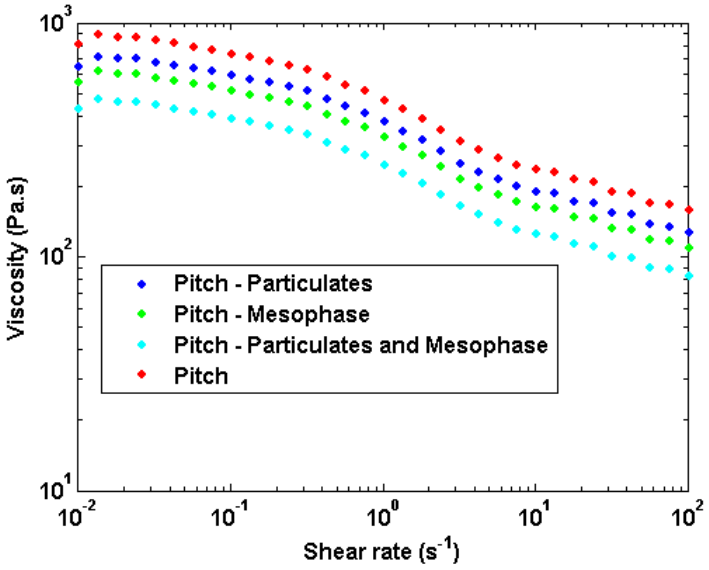

Figure 6.18: Krieger-Dougherty model applied to MP110HT400 at 160 °C

The calculated points on the curve correspond to different underlying mixtures: isotropic pitch ($\phi = 0.21$), isotropic pitch with particulates ($\phi = 0.13$) and isotropic pitch with

mesophase ($\phi = 0.08$). The trend observed is that of decreased mixture viscosity with higher ϕ content, which is to be expected.

Samples MP110HT437, MP110HT425, MP110HT425T6 to MP110HT437T6 are Mittal pitches that all contain significant amounts of mesophase material. The assumption of the material to behave similar to that of a suspension is thus not unexpected and has previously been proposed (Blanco et al., 1999). Here we will attempt to model such mixtures.

As described in Chapter 5, the temperature of measurement is important; especially with respect to the glass transition temperature. To attain the type of mixture, and thus applicable model, it is necessary to attain the point at which the mixture behaves either as a suspension or as an emulsion. This is done by making use of the capillary number and viscosity ratio (Grace, 1982)(Jansen et al., 2001). No interfacial surface tension data is available and therefore no mean field capillary numbers were calculated; however, the mean field viscosity ratio was calculated. For this scenario however, the viscosity of the mesophase is required.

Due to the lack of knowledge in the behaviour of the separate phases, alternative approaches were required. Separation was attempted, but ultimately proved unsuccessful, although separation is known to be possible (Blanco et al., 2000) (Singer et al., 1987). Khandare et al. (2000) predicted the mesophase viscosity using the WLF equation. This is used to predict the viscosity of the dispersed phase required for this analysis. For use of this approximation, a T_g is required, and this was done by making use of the $\tan(\delta)$ and the relationship it has with T_g for the other pitches. The approximate glass transition value calculated was 92 ℃, and the C_1 and C_2 values used were 14.6 and 43 respectively.

The mean field viscosity ratio calculated varied between 1 and 24. The critical capillary number is not known, and this is where low mean field viscosity ratios were calculated. At ratios above 4, droplet break up is unlikely but at low shear-rate there is a possibility it might occur. It should be noted that there is still a high interfacial tension caused by the particulate material.

In this system, the mesophase has a significantly higher viscosity than the isotropic phase; this would be shown by the appreciable change in the $\tan(\delta)$ values obtained for the two phases. This high viscosity mesophase is expected to behave similarly to a solid in this mixture and thus the application of Krieger-Dougherty model was implemented on our data.

The suspension model was implemented on MP110HT437. This was justified given the similarity of these curves to those showed of hard-sphere suspensions as described by Genovese (2012), shown in Figure 6.19 where increase in the Peclet number has an accompanying increase in fluid velocity. The continuous fluid behaviour was described from the data obtained from MP110HT400. For the model, the assumption was made, that because of the greatly similar glass transition temperature obtained from the isotropic

(amorphous) fraction, similar behaviour would have been expected for both isotropic fractions from the respective samples. It was not possible to carry out similar modelling of the MP110HT425 and MP110HT425T6 as there was no appropriate model to describe the continuous phase viscosity.

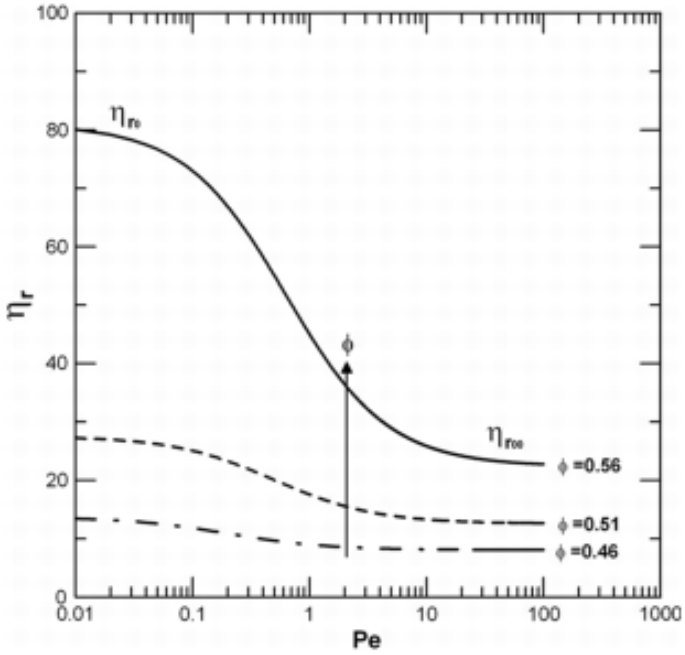

Figure 6.19: Viscosity relationship with increase in concentration (Genovese, 2012)

Sample MP110HT400 does however still contain a small amount of mesophase, as well as some particulate material (initial QI). As such, the behaviour of the isotropic pitch must be obtained via some analysis. The continuum fluid for the mixture of mesophase is assumed to be pure isotropic material. Using the Krieger-Dougherty suspension model, the effective volume fraction (ϕ_{eff}) was calculated for MP110HT437. Figure 6.20 shows the experimental data for the two pitches, the approximated isotropic pitch viscosity and the calculated volume fraction.

The isotropic pitch viscosity is shown to be much lower than that measured for MP110HT437. This implies that there is a significant volume of dispersed phase in the suspension; this is observed in the ϕ_{eff} calculated. The major outcome from this model is that the volume is not constant, with higher volumes observed at lower shear rate. The volume fractions obtained at several temperatures can be seen in Figure 6.21.

This figure shows us that the effective volume fraction decreases with shear rate. It implies that there is agglomeration of the mesophase particles (spheres) prior to shear, and that the particles de-agglomerate, or particle break-up occurs, with the increase in shear-rate (as is shown in Figure 6.22). It is also possible that the mesophase spheres becomes soft enough that they start to deform; however the stabilised spheres (via particulate) are likely to behave in this manner at higher temperatures.

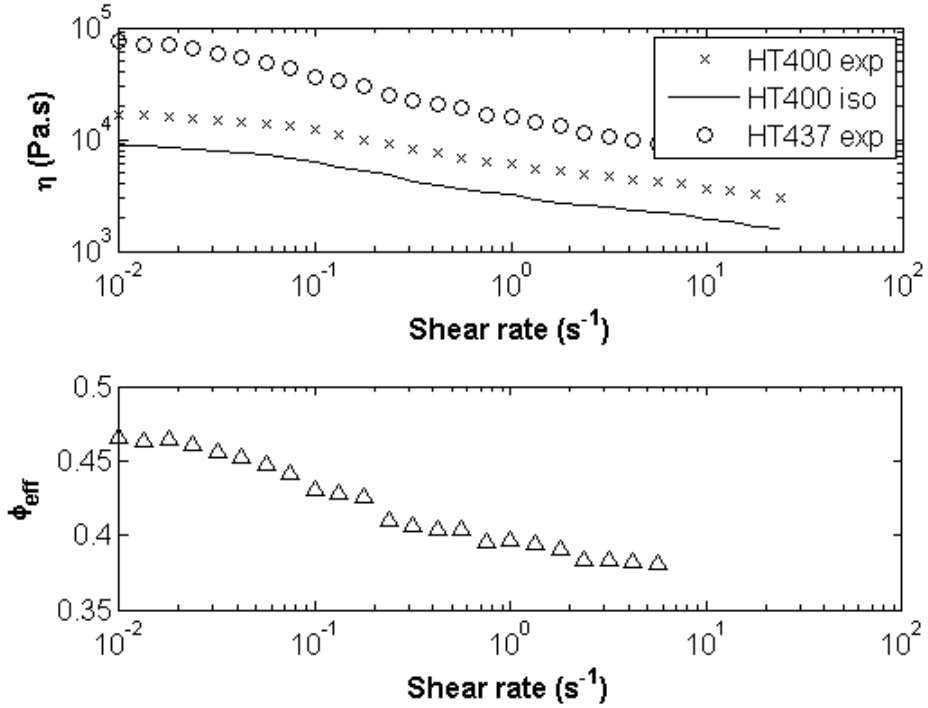

Figure 6.20: Viscosty of different fluids and corresponding ϕ_{eff} calculated from Krieger-Dougherty at 140 ℃

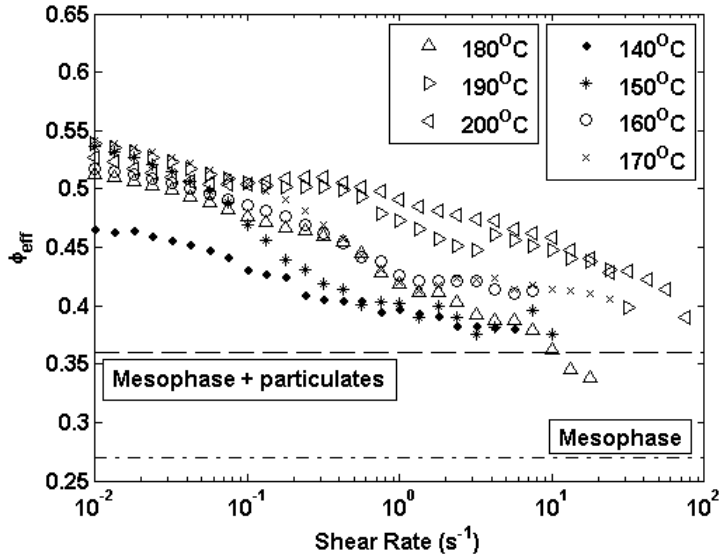

Figure 6.21: ϕ variation with shear for MP110HT437 using Krieger-Dougherty equation

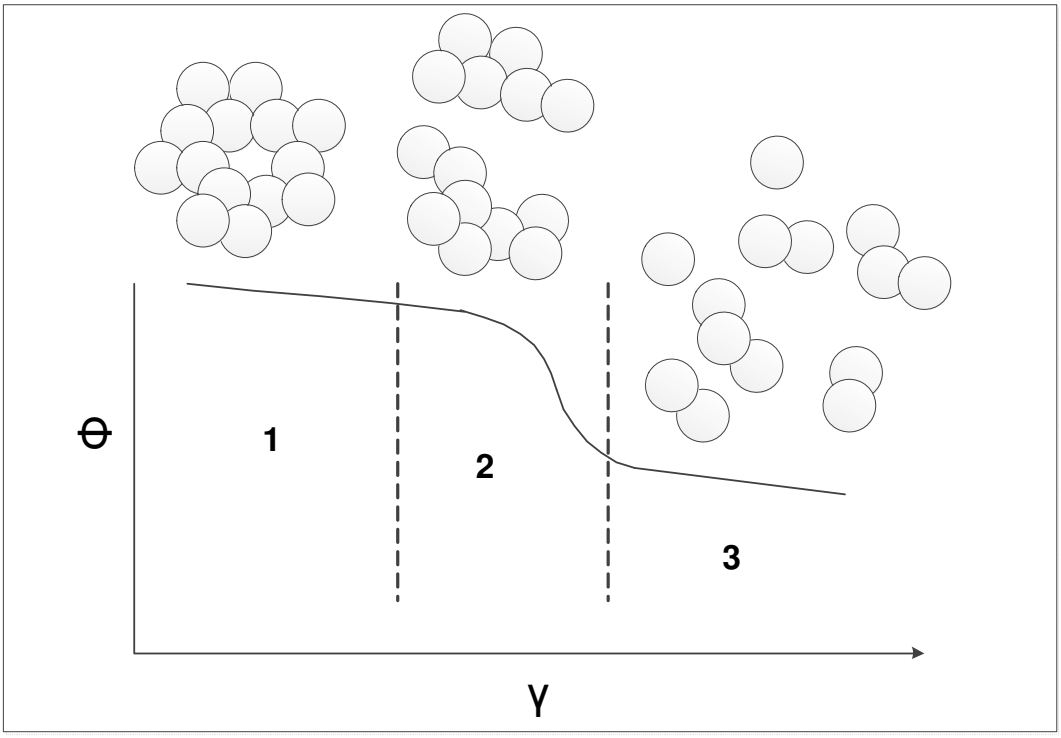

Figure 6.22: Evolution of mesophase particle change upon shear

The model also shows that the effective volume fraction tends towards 0.36 (with some deviation), which is approximately the volume fraction of mesophase (27 %) and particle matter (9 %) combined . The deviation from 0.36 at the higher shear-rates is not unexpected; some samples will have higher mesophase content and others lower due to the slight inhomogeneity of the sample.

The low shear volume calculated is approximately 52 %, and this is significantly higher than that expected of the mesophase and particulate material. This suggests that the mesophase act as larger particles, causing increased resistance to flow, and having a larger influence on the hydrodynamic flow of the fluid. A reason for the agglomeration is not known, and therefore a mechanism for this is not postulated. It is clear however that the formation of larger particles is predicted, and is a likely explanation for the behaviour of the material.

The modified Kriger-Dougherty equation for emulsions was also applied to MP110HT437. The viscosity ratio (K) varied between 150 and 9 over the temperature range from 140 °C to 200 °C.

Figure 6.23 shows the variation in effective volume fraction from the emulsion model. The trend is almost the same as that of the standard suspension model but with minor deviation to the effective volume fractions calculated. This suggests that the mesophase behaves like an agglomerated hard sphere suspension; this is likely due to the stabilising effect of the particulate QI. Deformation may occur, but the agglomeration is the dominant effect for these samples.

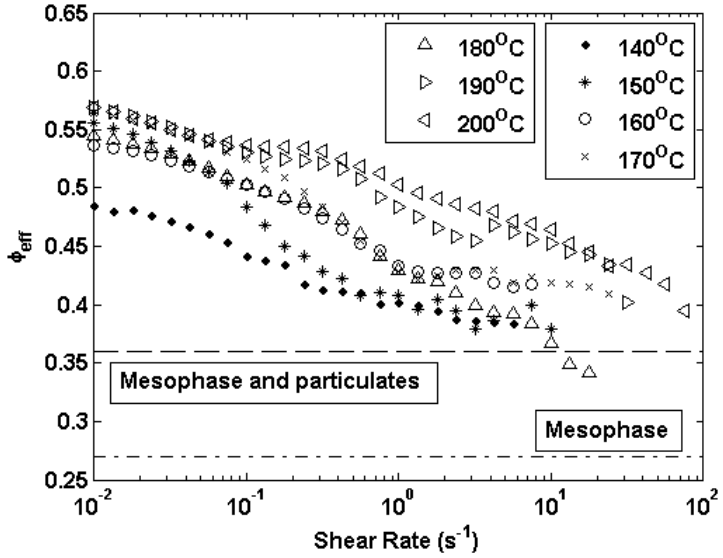

Figure 6.23: ϕ variation with shear for MP110HT437 using Krieger-Dougherty emulsion equation

Modelling of MP110HT425 and MP110HT425T6 as an emulsion or suspension would have been attempted but an approximate manner of predicting the continuous phase viscosity was not attainable. The behaviour of MP110HT425 sample is expected to behave in a similar manner to that of MP110HT437, with mesophase particle agglomerates breaking up upon shear.

MP110HT425T6 and MP110HT437T6 with higher mesophase volume fractions could only be measured at higher $T - Tg$. These samples show enhanced shear-thinning. The assumption of hard-sphere suspension may not be appropriate at these temperatures. To ascertain the behaviour expected of the emulsion, the mean field capillary number should be calculated. However, not all the appropriate parameters are available for the calculation (ie. surface tension). The mean viscosity ratio however can be calculated. For MP110HT437T6 with mesophase content of 49% the mean viscosity ratio varied between 1×10^{-4} and 1 at temperatures between 210 °C and 280 °C. Depending on the shear rate, the critical mean capillary number may indeed have been exceeded. This value of the mean capillary number is dependent on the surface tension. If indeed this is the case, which is likely, shear induced break up of the mesophase could occur; especially at higher shear-rates. Flow curves of MP110HT437T6, figure 5.12, resembles the curves observed for droplet break up showed by Jansen et al. (2001).

6.4 Summary and Discussion

The two-plateau models described all the samples extremely well. They were chosen as the models that would best suit the shape of flow curves for samples MP110HT425

and MP110HT437. This behaviour was expected due to possible mesophase particle agglomeration and break up. There was no significant change in the accuracy of the three models. The R^2 values of almost unity show the good fit and the difficulty to separate the effectiveness of the different models. Unfortunately no interpretation of microstructure via parameters was possible.

The anisotropic SASOL pitch behaviour is interesting given that it shows shear-thinning as well as yielding. SPHT400 and SPHT412 have approximately 9% mesophase. The yield stress observed in these samples is pronounced at higher temperatures of measurement. At the lower temperatures, only data from a limited range is visible; it is thus likely that a a complete picture of these samples for those temperatures is not necessarily possible. At these temperatures, the curves do resemble that of a viscoelastic liquid. At higher temperatures though, it is entirely likely that the initial yielding observed is as a result of the reorganisation of the mesophase clusters to a stable sheared state. This may be mesophase cluster alignment or breakup. It is clear however, that the curves are tending towards a high shear viscosity plateau; a complete transition has taken place. This is more clear in SPHT400, as opposed to SPHT412 and SPHT425 (17% mesophase). At the temperatures where measurements were made, it is also possible that the isotropic and mesophase material might have reached a low enough viscosity to be measured more easily. Droplet deformation after cluster break up may thus also be a possibility. These flow curves bear a strong resemblance to those of weak-gel networks such as has been shown by Saravanakumar et al. (2012) for a micellar ionic liquid with salt in Figure 6.24. Similarly, the authors show that at lower temperatures, the material behaves as a viscoelastic liquid. This behaviour is also observed here.

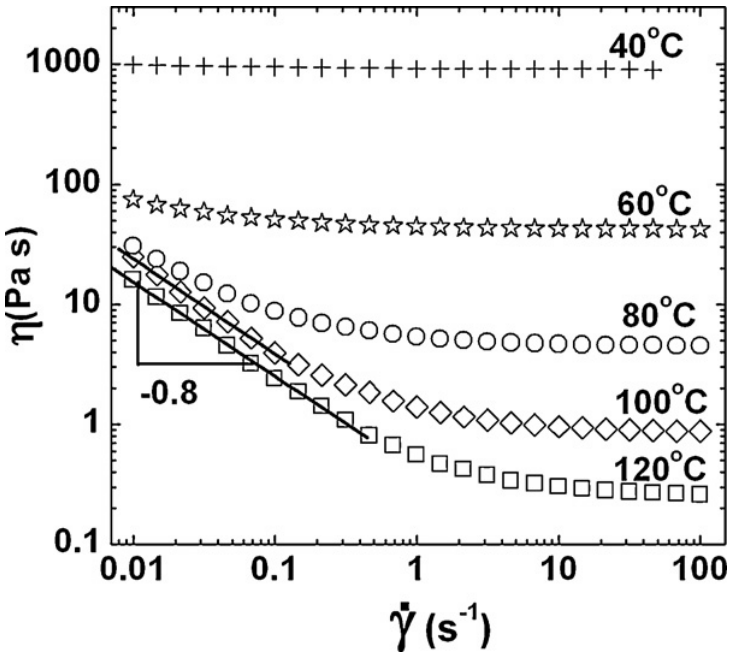

Figure 6.24: Flow curves of weak-gel as investigated by Saravanakumar et al. (2012)

For SPHT420T3 power-law shear-thinning behaviour continues over the entire shear-rate range measured. Given that the microstructure is similar to that of gelled networks, a breaking up of the network is a likely scenario. Depending on the viscosity of the mesophase, coalescence and continuous flow orientation may also occur. These curves are similar to those of gelled networks as studied by Lee & Lucey (2006), Figure 6.25.

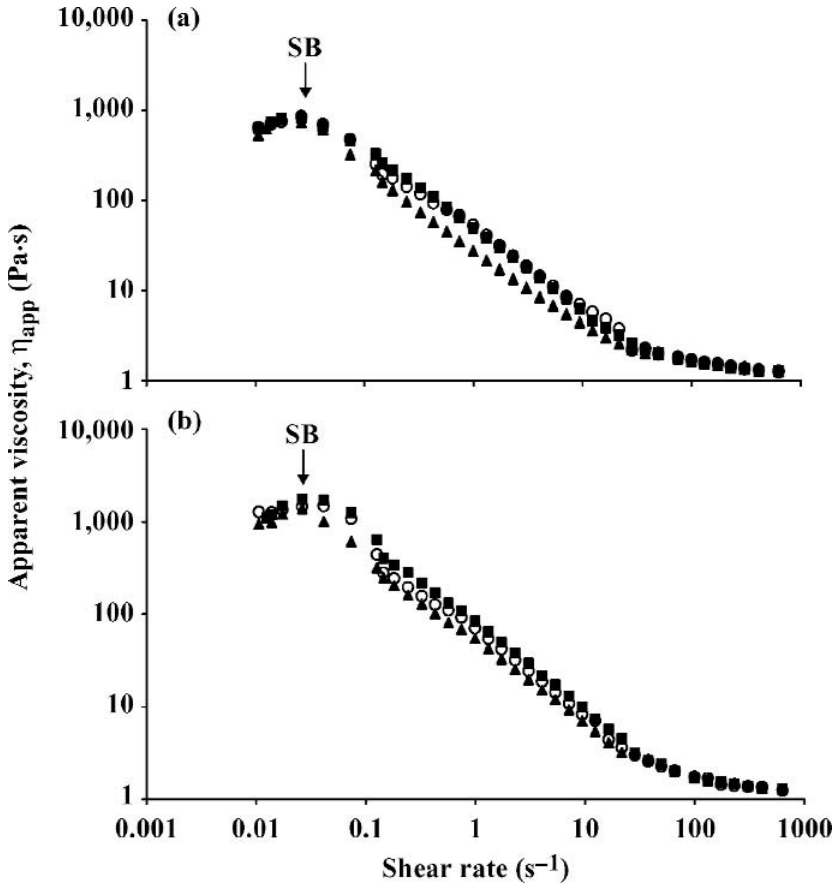

Figure 6.25: Flow curves of yogurt gels as investigated by Lee & Lucey (2006)

A summary of some of the characteristics is shown in Table 6.12

The Herschel-Bulkley model proved the best model to use for both fitting the rotational data and for understanding its behaviour via easily interpretable parameters. This would be the model that would aid best in interpreting and fitting of rotational shear data in future work. It however should be used with caution as the shape of the curves determine the best fit, and having some background into the possible behaviour would aid in the choice of model.

Table 6.12: Summary of pitch behaviour

Sample Description	Comment
Isotropic Pitch (Both sources)	Predominantly isoviscous samples at all temperatures Can be fitted by all models
MP110HT437 and MP110HT425	Best fitted by the two-plateau models Good fit with power-law 27% and 26% mesophase suspension
MP110HT425T6	Transition from two-plateau models to power-law model 38% mesophase transition from suspension to emulsion
MP110HT437T6	Best fitted by power-law model (Shear-thinning) 49% mesophase emulsion
SPHT400, SPHT412 and SPHT425	Low temperature - power-law fit viscoelastic liquid High temperature - Bingham plastic weak-gel 9%, 9% and 17% mesophase
SPHT420T3	Best fitted by power-law model (Shear-thinning) 59% mesophase viscoelastic liquid based gel

CHAPTER 7

RESULTS: OSCILLATORY RHEOMETRY

In Chapters 5 and 6 rotational shear behaviour was investigated and modelled. It was established that the isotropic pitches exhibit predominantly isoviscous Newtonian behaviour. The anisotropic pitches from both SASOL and Mittal sources were non-Newtonian. The partially anisotropic Mittal pitches show suspension/emulsion behaviour where particle breakup and droplet deformation are dominant characteristics. The anisitropic SASOL pitches show a strong Bingham plastic behaviour (ie. yield stress); strong shear-thinning and structure reorganisation at higher mesophase content (and change in gel-like structure) was also observed. In this chapter identification of the behaviour of the pitches via oscillation will be investigated; this behaviour will be compared to that observed during rotation.

7.1 Isotropic Pitch

In polymers the limit of acceptable strain is whereupon a deviation of 5 % of the moduli is exceeded; this is used as a guideline for this work. Figure 7.1 is loss and storage modulus data for MP110. From these experiments an amplitude of less then 0.1 % was needed and chosen for the frequency sweeps.

MP110 oscillatory behaviour was investigated at the following temperatures: 70 °C, 80 °C, 90 °C, 100 °C, 110 °C, 120 °C, 130 °C and 140 °C. Loss and storage modulus data for MP110 are obtained at these temperatures and are shown in Figures 7.2 and 7.3.

The storage modulus at all temperatures, decreases with lower frequencies. The magnitude of storage modulus also decreases as the temperature increases.

The loss modulus data has a different shape with respect to frequency as compared to the storage modulus. At 70 °C and 80 °C there is a maximum in the curve. At higher temperatures, the loss modulus decreases monotonically with (decreasing) frequency. The

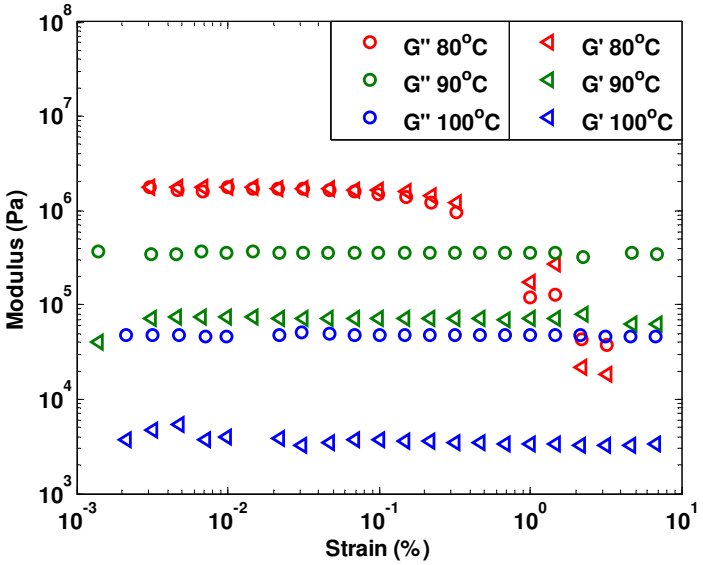

Figure 7.1: Amplitude strain sweep for MP110

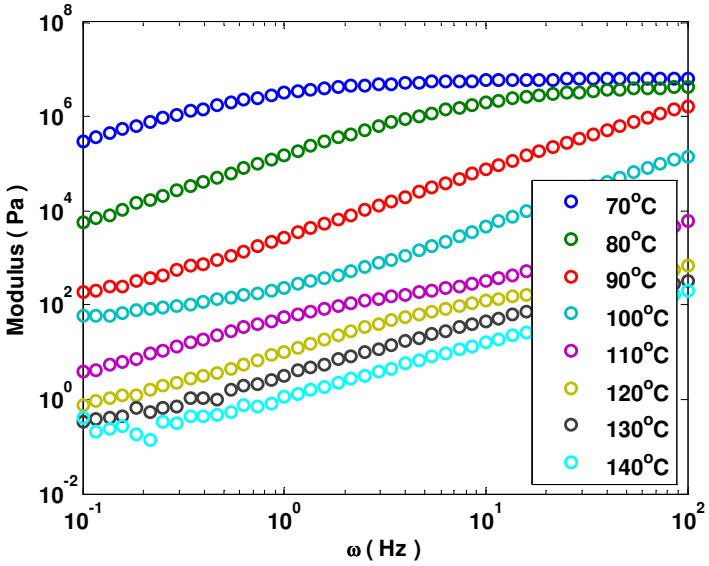

Figure 7.2: Elastic modulus data for MP110

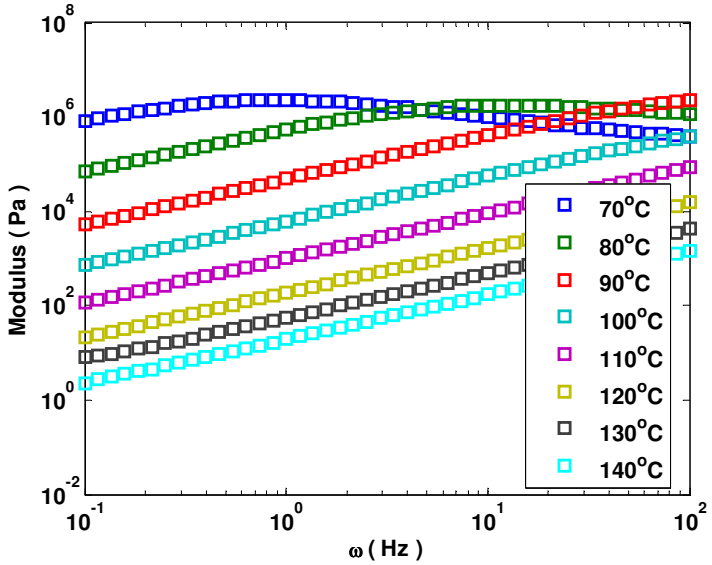

Figure 7.3: Loss modulus data for MP110

shape of these higher temperature curves are distinctly different from the elastic modulus.

For both curves, the data at a specific frequency and temperature, coincide with data at a different frequency and temperature. This behaviour leads to the possibility of employing time-Temperature-superposition to better understand the behaviour of the material. A technique similar to Turpin et al. (1994) was employed. Loss and storage modulus were adjusted; based on the temperature at which data were obtained and the temperature used as reference for the mastercurve. Density (at the corresponding temperatures) was not used to adjust the data as Py et al. (1997) proved this change made an insignificant change. After manipulation, the shift factors (a_t) were obtained from loss modulus data to produce mastercurves. Using time-Temperature-superposition, mastercurves were produced at 100 ℃ for MP110; this is shown in Figure 7.4.

Mastercurves of MP110HT350, MP110HT375 and MP110HT400 are also similar to that of MP110. These samples are qualitatively the same shape. Given that the chemical and physical properties, and structure, of MP110HT350 and MP110HT375 are similar, the rheological properties are expected to follow the same trend; this is indeed the case. Mastercurves for MP110HT350 were produced from data from temperatures 80 ℃ to 140 ℃. The mastercurves of the loss and storage modulus are shown in Figure 7.5. The mastercurves for MP110HT375 were produced from data obtained from 90 ℃ to 140 ℃ and is shown in Figure 7.6. Oscillatory data for MP110HT400 was combined to form mastercurves which are shown in Figure 7.7. The frequency sweeps were obtained from experiments from 110 ℃ to 160 ℃.

From the mastercurves produced, it is clear that at high frequency the storage modulus is higher than the loss modulus. This shows that the material is more solid than liquid. As the frequency decreases the two moduli intersect. At this point the material moves

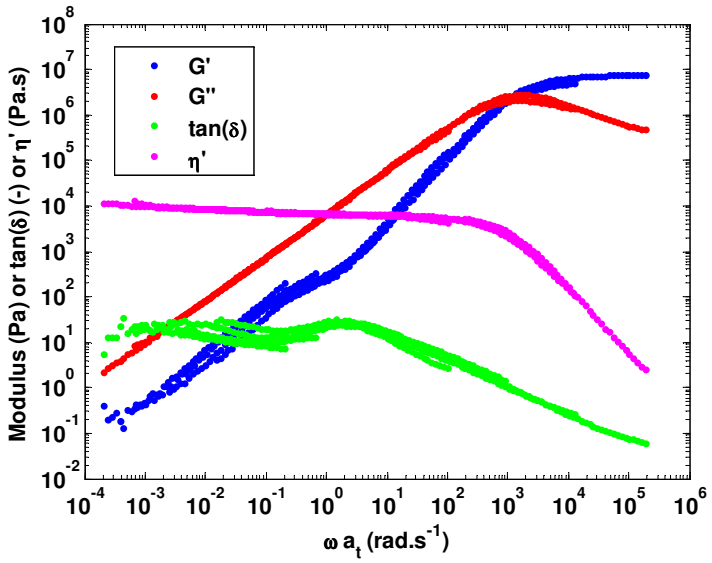

Figure 7.4: Mastercurves of MP110 reduced to a temperature of 100℃

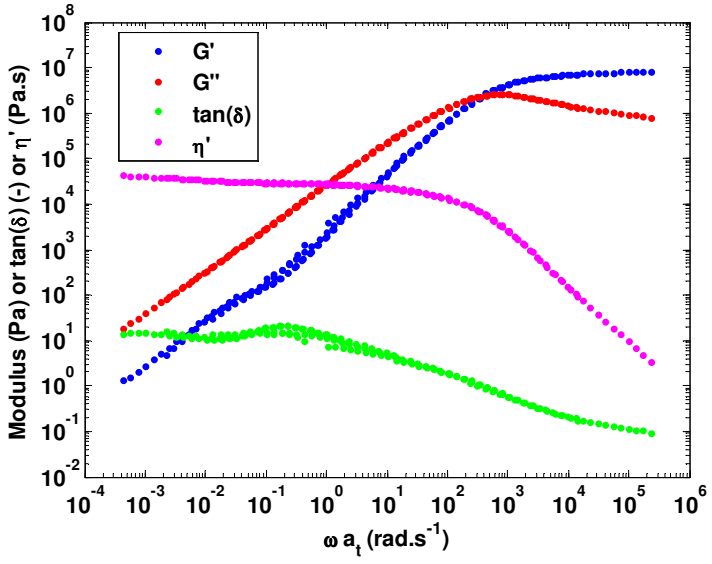

Figure 7.5: Mastercurves of MP110HT350 reduced to a temperature of 110℃

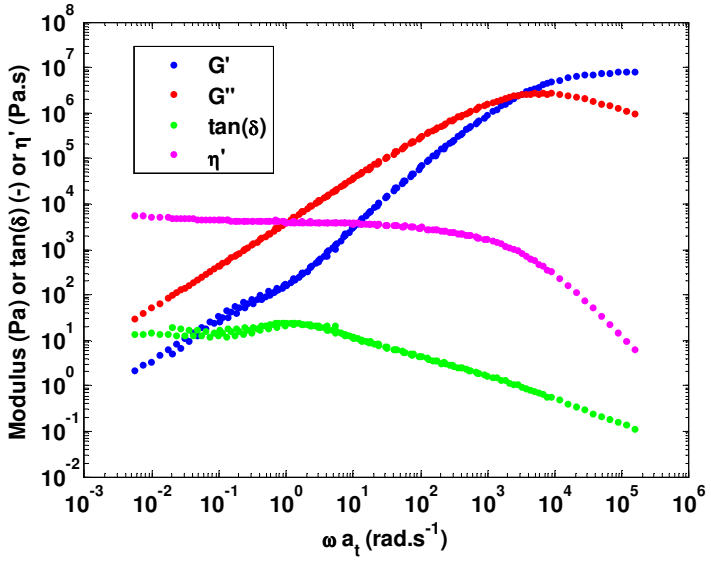

Figure 7.6: Mastercurves of MP110HT375 reduced to a temperature of 120℃

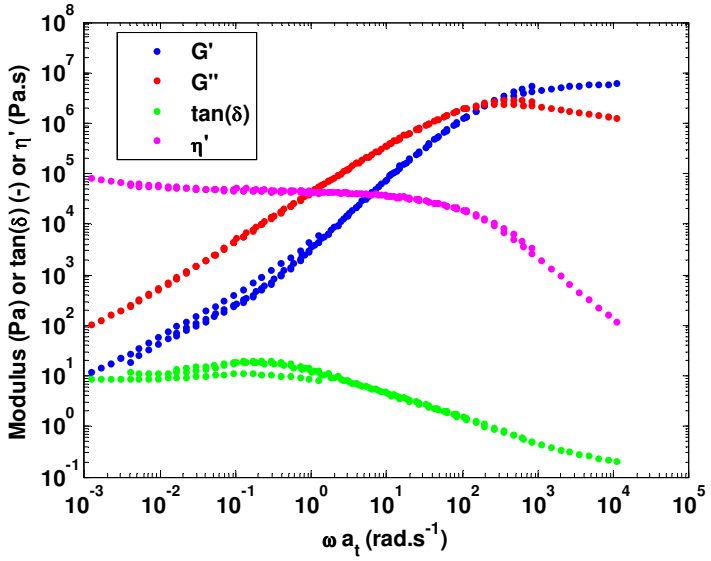

Figure 7.7: Mastercurves of MP110HT400 reduced to a temperature of 140℃

from a more solid structure to a more fluid structure. This is termed the crossover point. At lower frequencies these curves diverge. This shows the transition of the material into a more fluid state. This transition region has a log-log gradient of ≈ 1 in G'' and ≈ 1.5 for G'. At even lower frequencies, both moduli share the same gradient of ≈ 1.

Samples MP110, MP110HT350 and MP110HT375 contains approximately 10 % particulate material. The particulates present cause a stiffer structure. This would lead to higher than expected values for elastic modulus. The effect of increased stiffness might not necessarily be seen at lower temperatures (higher frequencies) closer to the glass transition, but a change at higher temperatures is visible. This would be the case when the material is sufficiently fluid that the particulates affect the low elasticity of the sample. If the particulates had no effect on the elasticity, the storage modulus would continue to drop and diverge from the loss modulus at low frequency.

The qualitative nature of the two moduli of MP110HT400 are similar to samples with lower aromaticity; this is a little surprising since a greater change would have been expected since it has a greater change in T_g and there is initial formation of small mesophase spheres. A difference in elasticity would have been expected due to some interaction between the two phases, this is however not the case. This thus indicates that the sample still acts as a near-Newtonian suspension. The mesophase formed acts as a non-interacting dispersed medium. The greater scatter at lower frequencies would then be attributed to the higher concentration of solid type material, particulate QI and mesophase spheres. $\tan(\delta)$ at the low frequencies tends towards 10.

The $\tan(\delta)$ curve for all these samples however shows a peak and plateau; this implies that the sample has an intermediate state where its behaviour is dominated by liquid properties (even if it is a high viscous liquid), and thereafter maintains this state of fluidity. This is achieved not by a change in liquid-like behaviour, but by the solid-type behaviour expressed via elasticity. The dynamic viscosity calculated shows low viscosity at high frequency, steadily increasing with frequency, and plateauing to a near-isoviscous region. The low viscosity at higher frequencies is not a true indication of the true viscosity of the sample. It is a reflection of the nature of the material, as it is not fluid, and the dominant property is the solid-like behaviour. The near-isoviscous value measured suggests that the fluid property of the material is not strongly influenced by shear (in oscillation). It also indicates that at a temperature of 100 °C (for MP110), the dynamic viscosity is approximately 1×10^4 Pa s. The $\tan(\delta)$ and dynamic viscosity curves also show similar shapes in the mastercurves of the other MP110 pitches.

It appears that there are 3 regions for the mastercurves of moduli for these samples (frequencies of regions are based on mastercurves of MP110):

- 1st region - solid material ($\omega \geq 10^3$)
- 2nd region - crossover to liquid-like behaviour and continued decreasing moduli

$(10^0 \leq \omega \leq 10^3)$

- 3rd region - liquid dominated material, however the elastic modulus ceases diverging. This is not often the case, similar results were seen by Daji et al. (1999), with large amounts of scatter at these reduced frequencies $(10^0 \leq \omega)$

Following the rotational behaviour, the oscillatory results are similar to the extent that there is no considerable change in the behaviour of the MP110 isotropic pitches. Since the rotational and oscillatory results are congruent for the aforementioned MP110 pitches, similar results would be expected from the various SASOL pitches.

Oscillatory experiments were also attempted on the SASOL pitches. SPAR oscillation results were extremely difficult to obtain. This is likely a result of strong Newtonian-like behaviour around room temperature. The sample is thus not a viscoelastic material; but instead is a highly viscous liquid.

This was not the case for SPHT350. Oscillatory frequency sweeps were conducted at 5 °C intervals from 60 °C to 110 °C. The mastercurves produced from these results are shown in Figure 7.8.

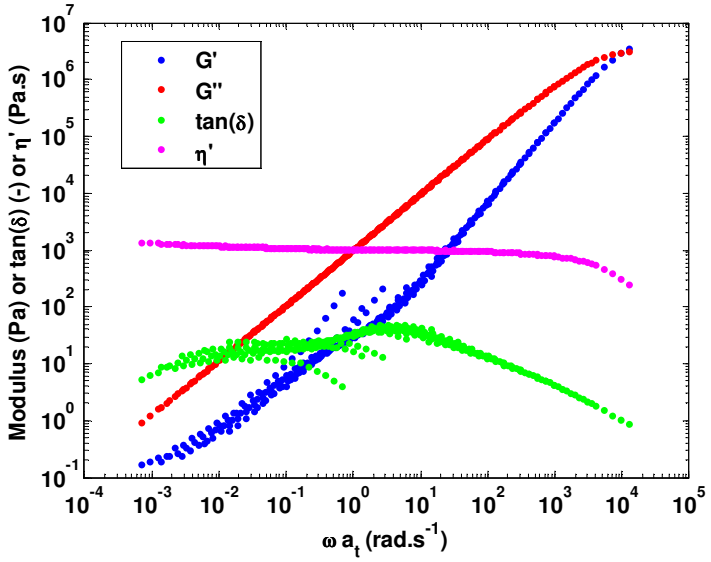

Figure 7.8: Mastercurves of SPHT350 reduced to a temperature of 80°C

This shows the typical crossover and diverging nature of the moduli. At high temperature, low frequency data shows some scatter with respect to elastic modulus. In general more scatter is observed in results with low magnitude elastic modulus. The moduli seem to also cease diverging and now maintain a constant offset (on logarithmic scale). The reason for this behaviour is unknown, no particulates are in the sample and no real mesophase is present. Diverging of the moduli was expected, towards a completely Newtonian fluid (no elasticity, $\delta = 90$).

Viscosity and tan(δ) curves are similar to those seen in the Mittal pitches. The low tan(δ) values at high frequency are indicative of a more elastic structure, which is

expected being measured close to the glass transition temperature. The peak and plateau, was not expected, but is as a result of the change in behaviour of the elasticity. It could be argued that there is a small decrease in $\tan(\delta)$ at extremely low frequencies, which is as a result of an increase in elastic properties. The viscosity curve shows little fluidity at higher frequencies and isoviscous behaviour at lower frequencies; this is expected of glassy materials.

Oscillatory mastercurves produced from frequency data for SPHT375 from temperatures 80 ℃ to 140 ℃ are shown in figure 7.9. The oscillatory mastercurves were difficult to obtain for SPHT400T3. The frequency data were quite scattered. The curve produced however is shown in Figure 7.10. This curve was constructed from data obtained at temperature from 140 ℃ to 170 ℃.

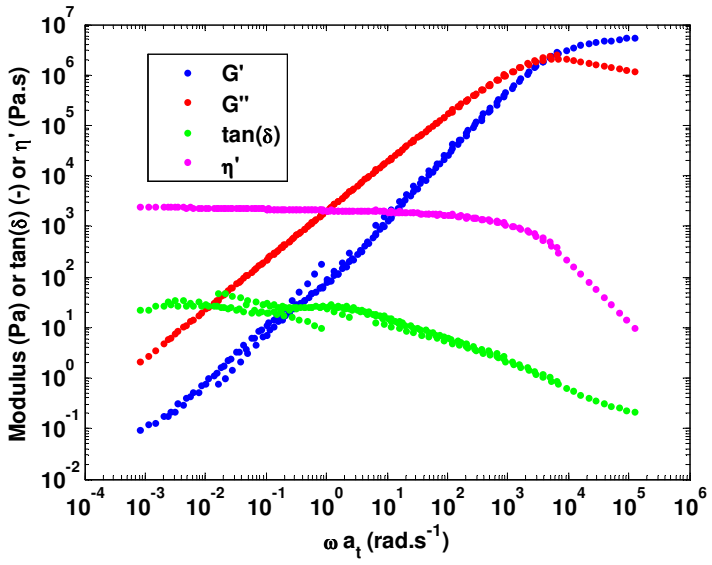

Figure 7.9: Mastercurves of SPHT375 reduced to a temperature of 110℃

The mastercurves of SPHT375 bear similarity to those of SPHT350. Qualitatively it shows the crossover, divergence and slight cessation (in magnitude) of the moduli with scatter. This is expected since all the other properties are in the vicinity of the measurements of SPHT350. For SPHT400T3 the mastercurves cover only a narrow temperature range. From this, only qualitative behaviour from the crossover to divergence is visible. The shape of curve and difficulty in obtaining usable data in itself is indicative of a material which is not completely homogenous. This sample still remains predominantly isoviscous.

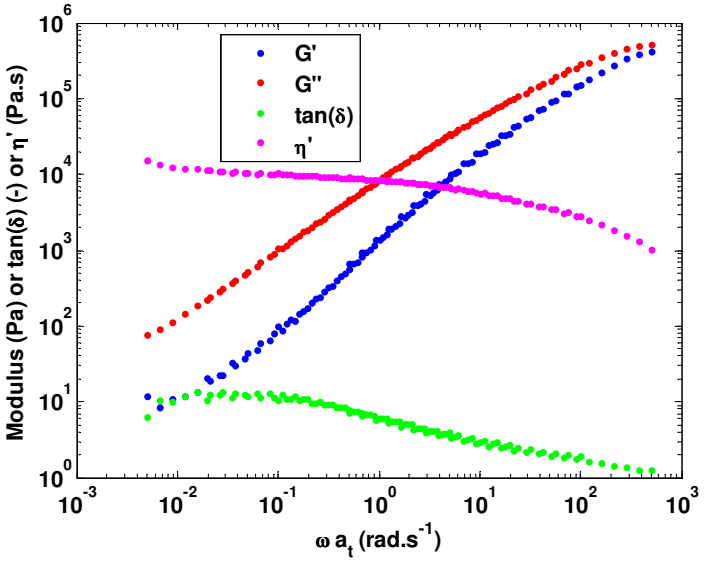

Figure 7.10: Mastercurves of SPHT400T3 reduced to a temperature of 150°C

7.2 Anisotropic Pitch

7.2.1 Mittal Pitches

Oscillatory behaviour of the anisotropic Mittal pitches were investigated. The amplitude sweeps from MP110HT437, MP110HT425, MP110HT425T6 and MP110HT437T6 can be seen in Figures 7.11, 7.12, 7.13 and 7.14.

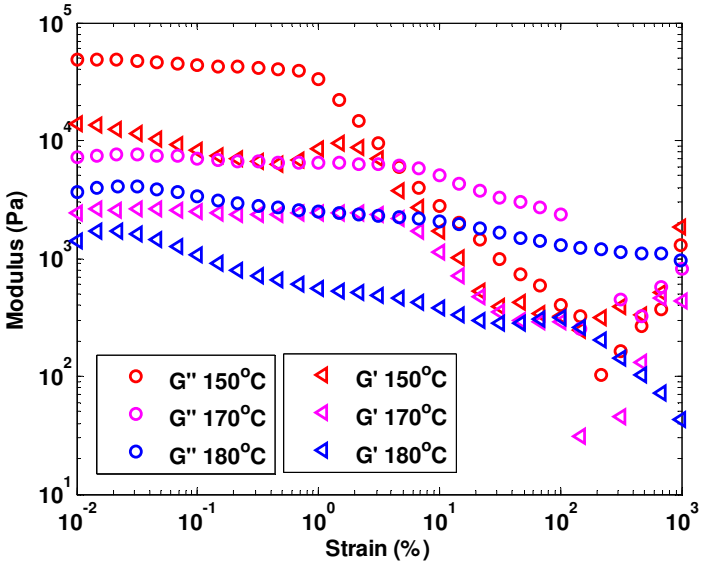

Figure 7.11: Amplitude strain sweep for MP110HT437

From these figures, there is deviation from linear viscoelasticity. For MP110HT437 and MP110HT425 the deviation is more evident in the storage modulus. MP110HT425T6 and MP110HT437T6 show further divergence from linearity.

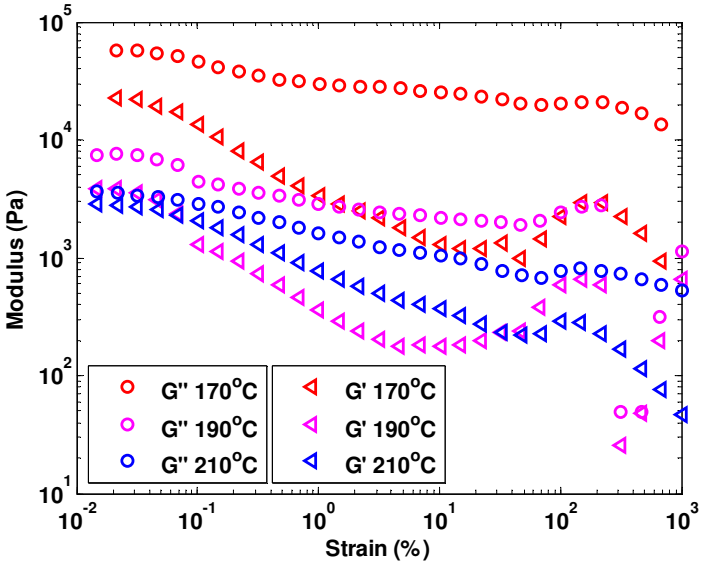

Figure 7.12: Amplitude strain sweep for MP110HT425

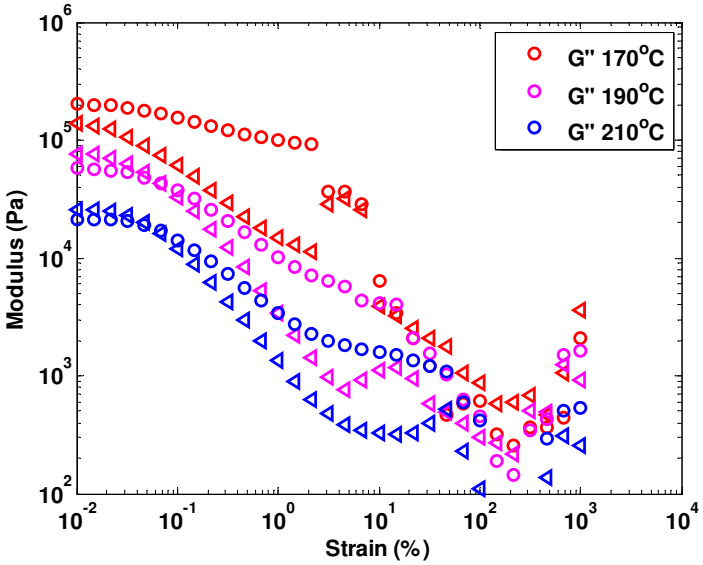

Figure 7.13: Amplitude strain sweep for MP110HT425T6

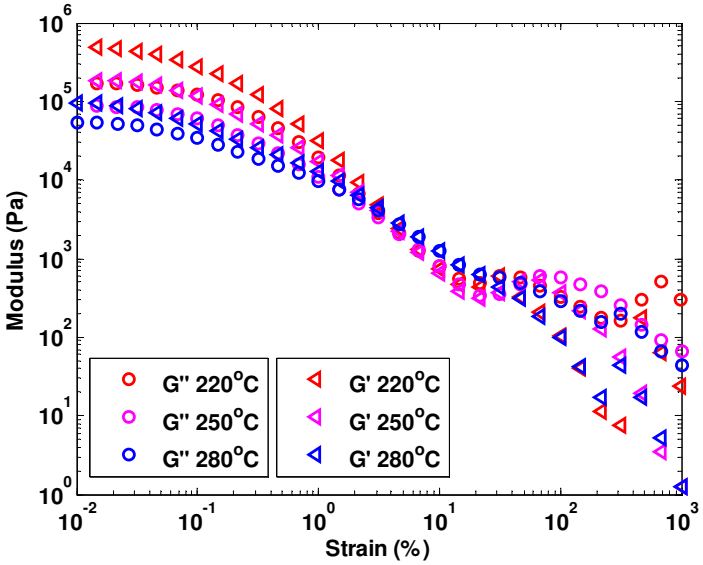

Figure 7.14: Amplitude strain sweep for MP110HT437T6

The micrographs of sample MP110HT425 show the presence of mesophase. DMTA results confirm some type of mesophase relaxation at approximately 140 °C. For MP110HT425, DMTA was not able to easily obtain the shoulder or second tan(δ) peak of the mesophase. Despite this, it is a fair assumption that the mesophase present in this sample is likely to have similar relaxation behaviour as with other Mittal pitches containing significant mesophase. At temperatures above 140 °C some form of softening of the mesophase should occur. The mesophase softening will affect the modulus and therefore data obtained during the amplitude strain sweep. A gradual drop of modulus was observed at high amplitude; this is believed to be as a result of the softening of the mesophase. The amplitude strain of 0.01% was used for the frequency sweep of all of these samples. This was done to try and ensure to being as close to the linear region as possible; least possible disturbance to the sample. The softening of the mesophase will thus also affect the frequency sweep data in some way.

The frequency sweep data of MP110HT437 seen in Figure 7.15. Compared to other Mittal pitch samples with lower C/H ratio, the behaviour is quite different. Major differences occur at lower frequencies; the moduli converge irrespective of the measurement temperature. No time-temperature-superposition was possible. At higher frequencies convergence and divergence is observed without crossover. This is likely the transition of the material from a suspension to an emulsion; caused by the softening of the mesophase.

The results obtained from the frequency sweeps on MP110HT425 can be seen in Figure 7.16. There is consistently a minimum in the curve observed (or change towards a minimum) at these temperatures at low frequencies. The increase occurs in both loss and storage modulus, and also an increase in tan(δ). This change in data is thought to be the result of a slow relaxation behaviour. This is observed at a temperature higher above

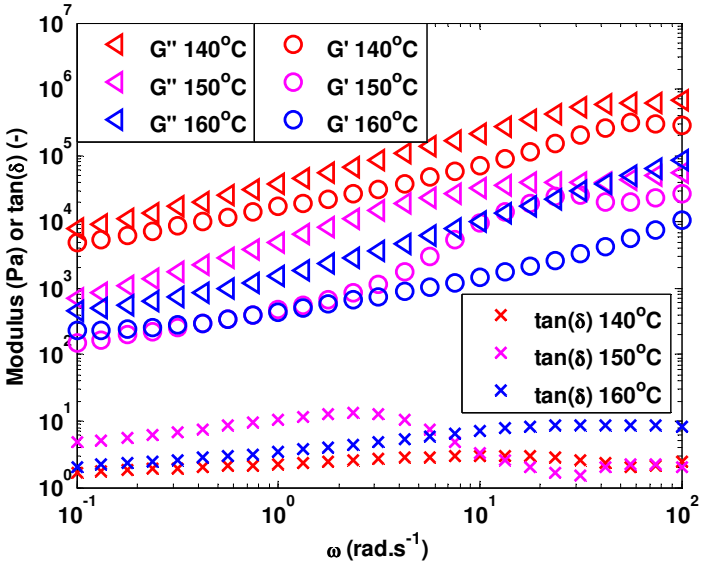

Figure 7.15: Frequency sweeps for MP110HT437

mesophase softening. The low frequency convergence is accentuated from that observed by MP110HT437 at lower temperatures.

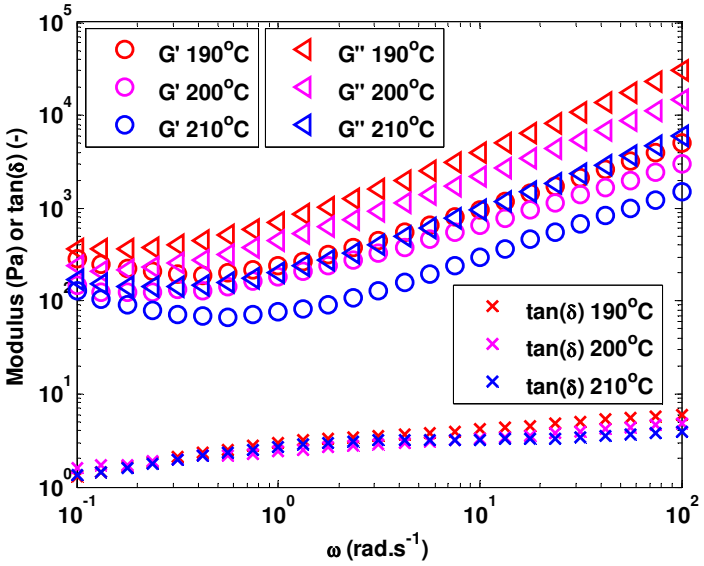

Figure 7.16: Frequency sweeps for MP110HT425

The behaviour of the sample also indicates that low frequency is necessary to show this relaxation. A low frequency would imply a slow relaxation. Very little disturbance is required to observe this phenomenon and thereby it is a sensitive process. The material relaxing is different from the amorphous pitch, but not grossly different (due to lack of drastic change in behaviour). At low frequency the mesophase has a significant effect, and at high frequency the isotropic phase is dominant.

Frequency based data of MP110HT425T6 can be seen in Figure 7.17. It exhibits decreasing modulus with lower frequencies as expected of viscoelastic material . No trend

could be observed, at low frequency, this suggests a more drastic change in the underlying structure occurs at these temperatures for this composition material (mesophase content), via the mesophase softening.

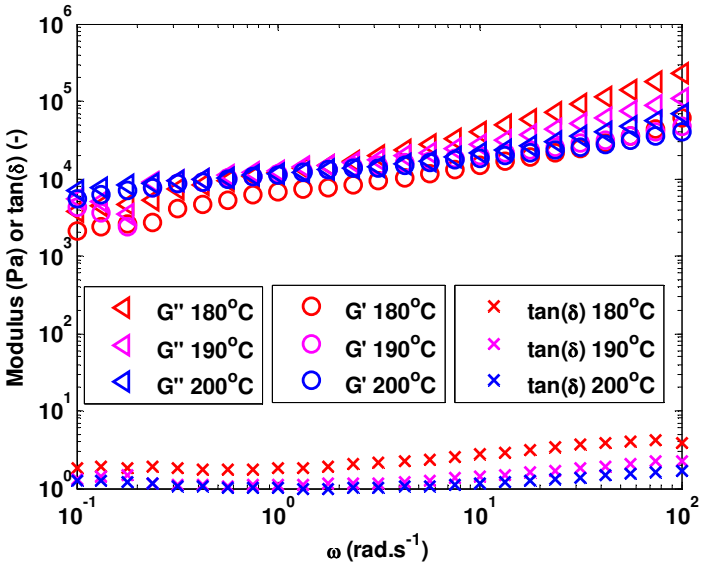

Figure 7.17: Frequency sweeps for MP110HT425T6

Frequency sweep results for MP110HT437T6 are shown in Figure 7.18. The moduli are indicative of a much more elastic material, especially at high frequencies. The values of storage modulus are higher than loss modulus at high frequencies, but decrease in tan(δ) indicates higher elasticity. As the frequency decreases, the loss modulus approaches the elastic modulus. Temperature also does not play such a significant role in this sample, as considerable change of modulus magnitude is not observed (over 60 °C interval).

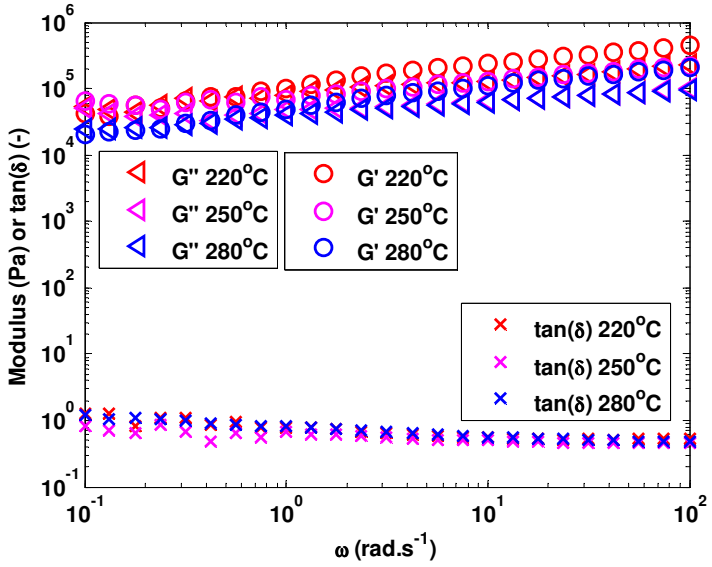

Figure 7.18: Frequency sweeps for MP110HT437T6

The modulus curves are similar for all the temperature range investigated. This is

the same behaviour showed for the rotational shear rheometry data; where the sample changes very little with respect to temperature.

MP110HT437T6 is expected to behave as an emulsion. The lack of major change in modulus leads to the conclusion that the continuous phase is weakly affected by temperature (in this range). This is suspected to be fluid behaviour far from its glass transition. Given that there is still a strong elastic component, the dispersed phase is thus the major contributor to the behaviour of the sample. For MP110HT437T6, this is the high content of mesophase. The mesophase is either a continuous dominant phase, or more likely a dispersed droplet system (where continuous domains are not as prevalent). A closely packed system is envisioned where the fluidity is effectively disrupted due to motion and as the sample relaxes at low frequencies, the mesophase relaxes into a state where both phases are more fluid. A similar conclusion was made during rotation.

For the anisotropic Mittal pitches, it is clear that the $\tan(\delta)$ tends towards 1 for all the low frequency data; hence convergence of moduli. Even though the samples are measured at different $T - T_g$, this phenomenon persists. Similarly as the mesophase content increasess, the $T - T_g$ increases. This shows that the sample has strong elasticity, and continues to do so over a wide range of temperatures, at different phase viscosity and at different mesophase concentration.

7.2.2 SASOL Pitches

The linear viscoelastic region for SPHT400 at an angular frequency of $10\,\mathrm{rad\,s^{-1}}$ can be seen in Figure 7.19. The frequency sweep information gathered and shown in Figure 7.20; it inferred that the time-Temperature-superposition (tTs) was not possible, and hence mastercurves were not produced. SPHT412 showed similar behaviour.

This would indicate a phenomenon whereby the material is sensitive to small disturbances. At both low shear rotation and oscillation, this behaviour was seen; at higher shears the resultant microstructure would be changed and in a different state.

The inability of the sample to follow tTs and associated linearity is not completely understood. The data can not be assembled together. It is seen at lower frequencies (for all temperatures), the moduli cease diverging. This is similar to the behaviour previously shown for the Mittal pitches. The SASOL and Mittal pitches have developed very different microstructures, and yet the samples still exhibit similar rheological properties. For The Mittal samples, it was understood that the mesophase is softening and hence influences the rheology. The interaction of the mesophase and isotropic phase of these SASOL pitches and anisotropic microstructure must then affect the rheology in a different way. The curves observed do appear to be those in a state of transition from viscoelastic liquid system to that of a weak gel (Saravanakumar et al., 2012). Similar behaviour was observed by Kundu & Ogale (2007), and also proposed that it is similar to that of a gelled

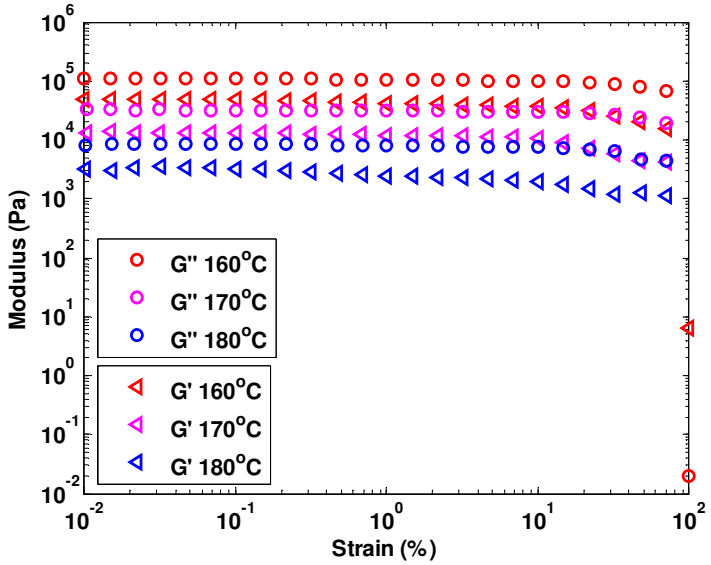

Figure 7.19: Linear viscoelastic region for SPHT400

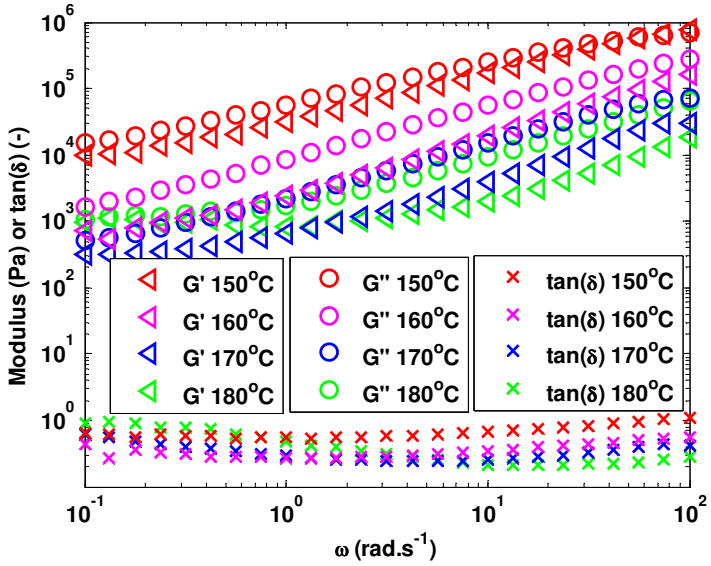

Figure 7.20: Oscillation frequency sweep for SPHT400

liquid. DMTA behaviour of these two samples, showed possible relaxation around 140 ℃ although this was not conclusive. If this possible relaxation is significant, it would thus also affect the structure and measured values of modulus obtained during the frequency sweep.

Oscillation frequency sweeps of SPHT425 were conducted and tTs was possible, the mastercurves produced are shown in Figure 7.21. This was unexpected since all previous anisotropic samples did not produce such data. The shape of these curves are different to that of the previous successful mastercurves. The temperatures over which frequency data was obtained is from 190 ℃ to 270 ℃. This is significantly higher than the measured glass transition of 83 ℃.

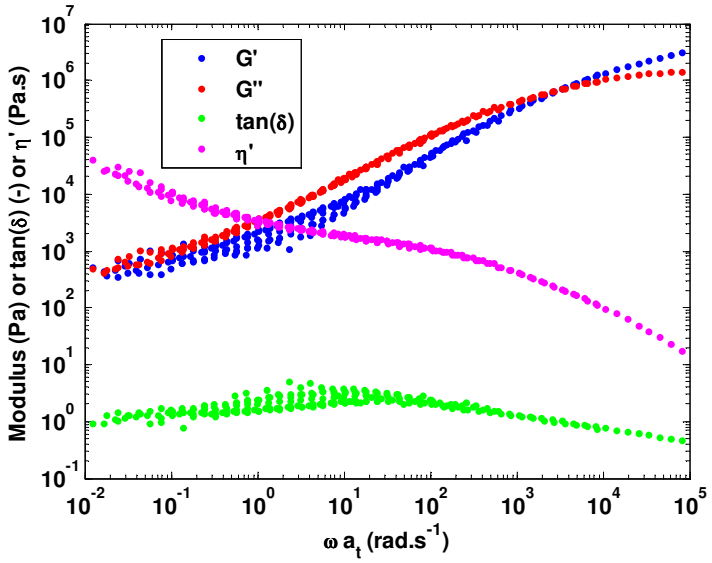

Figure 7.21: Mastercurves of SPHT425 reduced to a temperature of 260℃

It is observed that there is a crossover at high frequency, followed by divergence (of the moduli). The extent of divergence is not as pronounced as for the previous samples investigated, thus maintaining strong elastic properties. At higher temperatures, lower frequencies, convergence starts to occur; there is some scatter. The tan(δ) curve also does not deviate significantly from 1, showing that the loss and storage modulus have close to equal magnitude throughout the range of temperatures.

The shape of the curve is similar to those shown by Cheung et al. (1995) for mesophase pitches. Given that this sample contains 17% mesophase content, this is slightly surprising. However, a strong association between the components and phases in this mixture has been proposed, and the formation of a gel-like network suggested. Given the shape of the curves and the temperature of measurement above glass transition, this supports the postulated gel network hypothesis.

Figure 7.22 shows the mastercurves of SPHT425 when data only from temperatures 190 ℃ to 230 ℃ are used. This results in a much more continuous mastercurve which

illustrates initial convergence without significant scatter.

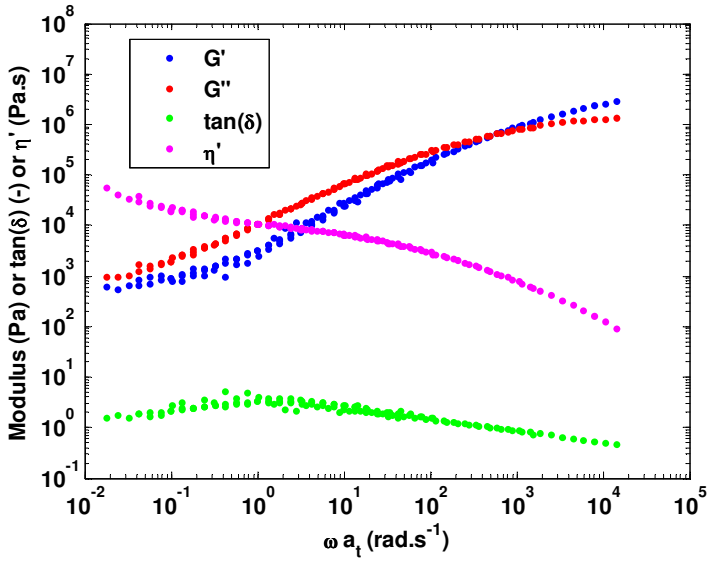

Figure 7.22: Mastercurves of low temperature SPHT425 data reduced to a temperature of 230℃

Figure 7.23 shows mastercurves of SPHT425 using data from 240 ℃ to 270 ℃. This figure shows better tTs than the original mastercurve, however scatter is still observed. This scatter could be attributed to the strong convergent nature of the data. The extent of such moduli convergence has previously not been observed (in pitch material).

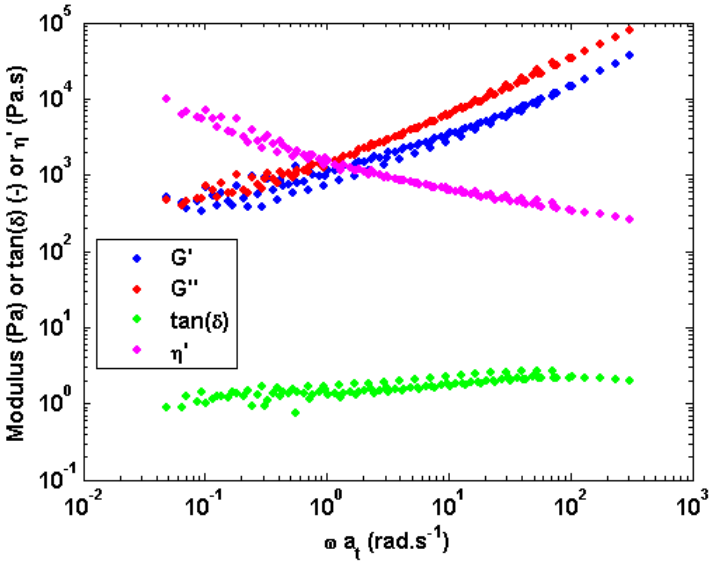

Figure 7.23: Mastercurves of high temperature SPHT425 reduced to a temperature of 270℃

Oscillatory frequency experiments on SPHT420T3 were conducted from 240 ℃ to 280 ℃. The mastercurves produced as a result are visible in Figure 7.24. This figure continues the trend observed from the mastercurve of SPHT425. In this case, the mas-

tercurves produced did not contain data that was as erratic as SPHT425 (especially with respect to the high temperature data). SPHT420T3 mastercurve moduli diverge after crossover and then convergence (with decreasing frequency). This suggests that the resultant increase in elasticity is attributable to the mesophase material and its contribution to the structure of the mixture. The moduli still do not differ by more than a decade of magnitude (on this scale); this shows that elasticity is maintained at higher temperatures.

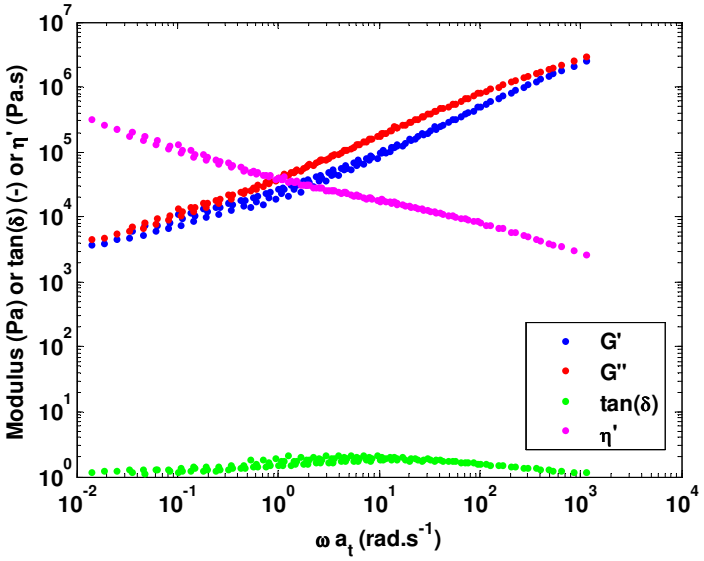

Figure 7.24: Mastercurves of SPHT420T3 reduced to a temperature of 280°C

For samples SPHT425 and SPHT420T3, it is also observed that there is also very little change in $\tan(\delta)$ as a function of frequency. This implies that the ratio of the two moduli do not differ significantly. The fact that the curve is steady around $\tan(\delta) = 1$, confirms the result of the samples maintaining an almost equal contribution of both elastic and fluid properties throughout the experiments.

The dynamic viscosity mastercurve continuously decreases as the experimental frequency is increased. This is a similarly shaped mastercurve to that obtained by Cheung et al. (1995). The dynamic viscosity curve is indicative of a material that has shear-thinning properties. This supports the postulate of interacting components and phases of a two phase weakly-gelled emulsion, whose structure breaks down upon increased shear.

7.3 Williams-Landel-Ferry (WLF) fit

The shift factors used for time-Temperature superposition were fitted using the WLF equation. Samples were shifted to use each of the data sets at different temperatures tested, as reference temperature. Figure 7.25 show the fit of such data to MP110, where Table 7.1 shows the associated parameters from WLF fit and associated equation derived by Fulcher, Tammamm and Hesse (related to Doolittle). This type of analysis was

conducted by Turpin et al. (1994), and a similar technique is applied here.

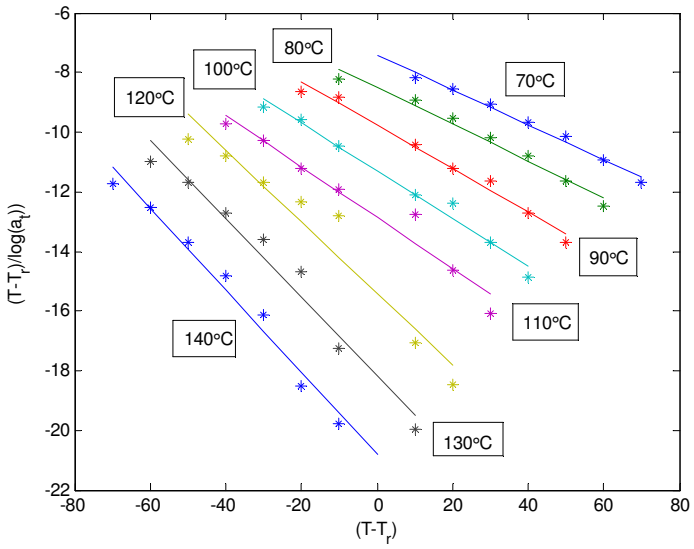

Figure 7.25: WLF plot for MP110 (* = experimental data, – = WLF fit)

Table 7.1: WLF Properties of Sample MP110AR

Temperature (°C)	Slope (-)	Intercept (K)	R^2 (-)	C_1 (-)	C_2 (K)	B (K)	T_∞ (K)
70	-0.0581	-7.4248	0.9876	17.2033	127.7308	2197.4	215.4192
80	-0.0615	-8.502	0.9738	16.2471	138.133	2244.3	215.017
90	-0.0731	-9.7606	0.9847	13.6785	133.5104	1826.2	229.6396
100	-0.0798	-11.2905	0.9823	12.5337	141.5116	1773.7	231.6384
110	-0.0857	-12.8692	0.9551	11.6635	150.1007	1750.7	233.0493
120	-0.12	15.4075	0.9375	8.3366	128.4459	1070.8	264.7041
130	-0.1313	-18.1672	0.9673	7.6134	138.3136	1053	264.8364
140	-0.1372	-20.7986	0.9773	7.2866	151.5519	1104.3	261.5981

Turpin et al. (1994) showed that the C_1 and C_2 parameters of the WLF fit could be easily obtained when a plot of $\frac{(T-T_r)}{log(a_t)}$ vs $T-T_r$ is produced. A linear curve-fitting regression would lead to the calculation of parameters as $C_1 = -\frac{1}{slope}$ and $C_2 = \frac{intercept}{slope}$. The parameters were calculated at every temperature where experimental data was obtained, and each temperature used as reference.

The Fulcher, Tammamm and Hesse equation is:

$$\log(\eta) = A + \frac{B}{T - T_0}$$

$$where \qquad C_1 = \frac{B}{T_r - T_\infty}$$

$$and \qquad C_2 = T_r - T_\infty$$

Here a base temperature of $T_0 = T_\infty$ is chosen, and this temperature is the point where no relaxation of the material is possible. This is done since both the WLF and Fulcher, Tammamm and Hesse equations require a temperature of reference. Choosing this temperature of T_∞ will hopefully give some understanding into the nature of the material. By manipulation of the WLF parameters, the Fulcher, Tammamm and Hesse equation parameters (B and T_∞) can be calculated. This is done when noting that $\log(a_t) = \frac{B}{T-T_0}$. The regression of the WLF equation and the parameters calculated as a result are shown in Table 7.1.

From the regression, it is evident that the WLF equation fits the data of time-Temperature-superposition well; this is observed via the R^2 of almost unity for all the reference temperatures. The C_1 value decreases continuously with higher reference temperature, whereas C_2 shows no easily observable order.

From Figure 7.25 and Table 7.1, it appears that the lines fall into three groups based on gradient. The slope of 70 °C and 80 °C is one group. 90 °C, 100 °C and 110 °C have similar slopes, and 120 °C, 130 °C and 140 °C are the final group. This would indicate that the material starts to behave slightly differently based on the temperature which is used as reference for construction of the mastercurves; showing that the underlying behaviour is not necessarily due to any single feature.

In the case of MP110, there is a good regression and the calculation of T_∞ was possible. The average T_∞ for MP110 is 240 K. This implies that the temperature of zero relaxation is −33 °C, considerably lower than any of the measured glass transition temperatures. The temperatures calculated also follow the trend of the three groups of gradient; thus there are three groups of similar T_∞. These temperatures, based on increasing reference temperature, are 215 K, 231 K and 263 K. This indicates, that based on this technique, the higher reference temperatures allow components with higher T_∞ (at these temperatures) to dominate.

It should also be noted that technically, WLF behaviour is only valid at temperatures above the glass transition (Arrhenius type gradient is observed). Below glass transition different mechanisms are dominant and therefore extrapolations to these temperatures are not necessarily accurate, however a qualitative indication of zero relaxation should be possible. A more accurate description is given by Ferry (1980: 284).

The calculated B and T_∞ can also be used to predict the shift factors (a_t). This is showed by Turpin et al. (1994) and the equation to be used is:

$$\log(a_t) = -\frac{B\cdot(T - T_r)}{(T - T_\infty)\cdot(T_r - T_\infty)} \tag{7.1}$$

The WLF plot for MP110HT350 is shown in Figure 7.26. The observable information that can be garnered is that there is a relatively good fit of the data to the WLF equation. The gradient appears to decrease with higher reference temperature. Above 100 °C,

the gradients seems to remain constant. The WLF and Fulcher, Tammamm and Hesse equation parameters for MP110HT350 are shown in Table 7.2.

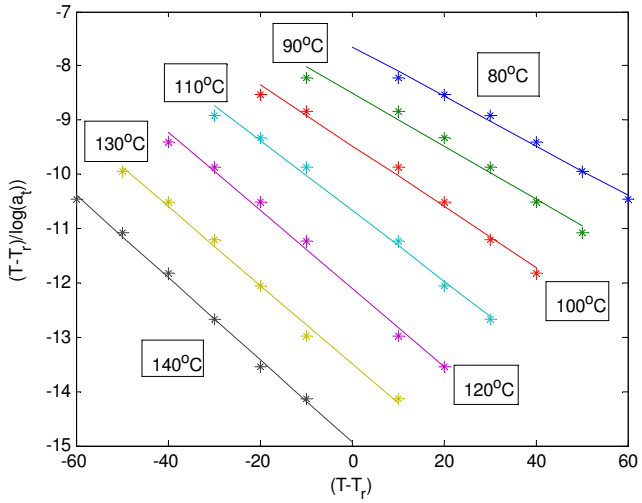

Figure 7.26: WLF plot for MP110HT350 (* = experimental data, – = WLF fit)

Table 7.2: WLF Properties of Sample MP110HT350

Temperature (°C)	Slope (-)	Intercept (K)	R^2 (-)	C_1 (-)	C_2 (K)	B (K)	T_∞ (K)
80	-0.0459	-7.6491	0.9903	21.7861	166.6444	3630.5	186.5056
90	-0.0493	-8.4912	0.982	20.2892	172.281	3495.5	190.869
100	-0.0564	-9.4758	0.9902	17.7194	167.906	2975.2	205.244
110	-0.0648	-10.6789	0.9927	15.4223	164.6939	2540	218.4561
120	-0.0729	-12.0947	0.9942	13.7227	165.9719	2277.6	227.1781
130	-0.0731	-13.506	0.9939	13.6745	184.6883	2525.5	218.4617
140	-0.0779	-15.0307	0.9978	12.8381	192.966	2477.3	220.184

For MP110HT350, high R^2 values, confirm good regression. The T_∞ is still not constant, but does show a trend of low reference temperature having a low T_∞, and higher reference temperature having high T_∞. It is also noticeable that the average T_∞ for MP110HT350, 208 K, is lower than that of MP110. This was unexpected, as a similar trend to the glass transition was expected.

For other isotropic pitches, MP110HT375, MP110HT400 and SPHT350, the WLF plots, Figures 7.27, 7.28 and 7.29, also show good regression; hence the WLF or Fulcher, Tammamm and Hesse constants can be used to predict shift factors and produce mastercurves. These parameters can be seen in Tables A.1, A.2 and B.1.

These samples, MP110HT375, MP110HT400 and SPHT3350, have an average T_∞ of 289 K, 306 K and 231 K respectively. A trend is observed that samples with higher glass transition temperature have higher T_∞, MP110HT350 apart.

The other two isotropic SASOL pitch samples, SPHT375 and SPHT400T3, produced

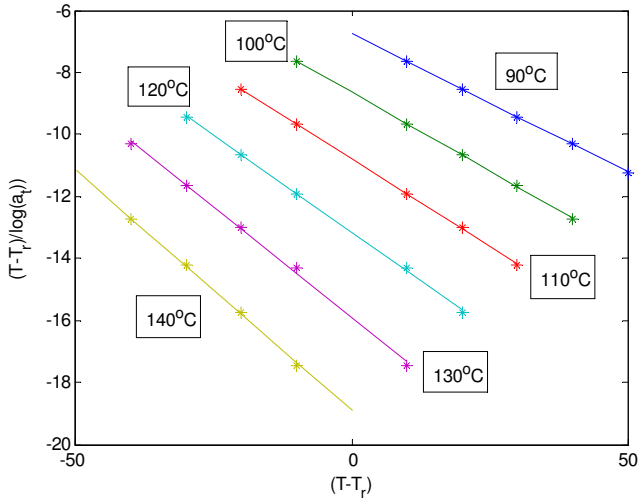

Figure 7.27: WLF plot for MP110HT375 (* = experimental data, – = WLF fit)

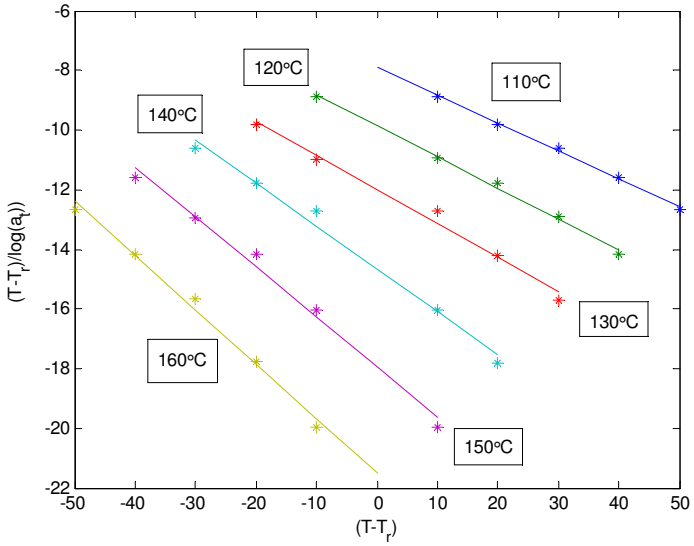

Figure 7.28: WLF plot for MP110HT400 (* = experimental data, – = WLF fit)

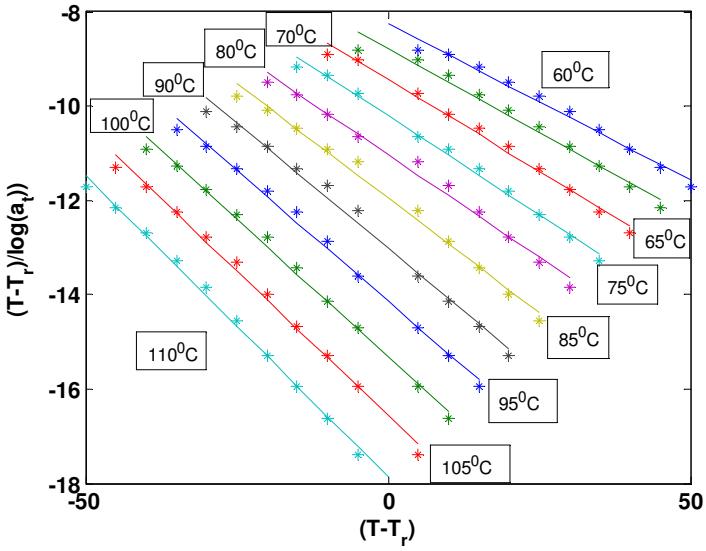

Figure 7.29: WLF plot for SPHT350 (* = experimental data, – = WLF fit)

mastercuves via time-Temperature-superposition, but do not follow Williams-Landel-Ferry behaviour. This is observed via the WLF plots produced, Figures 7.30 and 7.31. The poor regression was unexpected as the MP110 isotropic pitches showed such good correlation. Confirmation of this is observed in the R^2 values showed in Table 7.3.

SPHT350 does not change significantly from SPAR, and likely has similar components. At the higher thermal treatment temperatures, the composition changes slightly and thus could cause minor changes in the behaviour; it still essentially remains a single phase material.

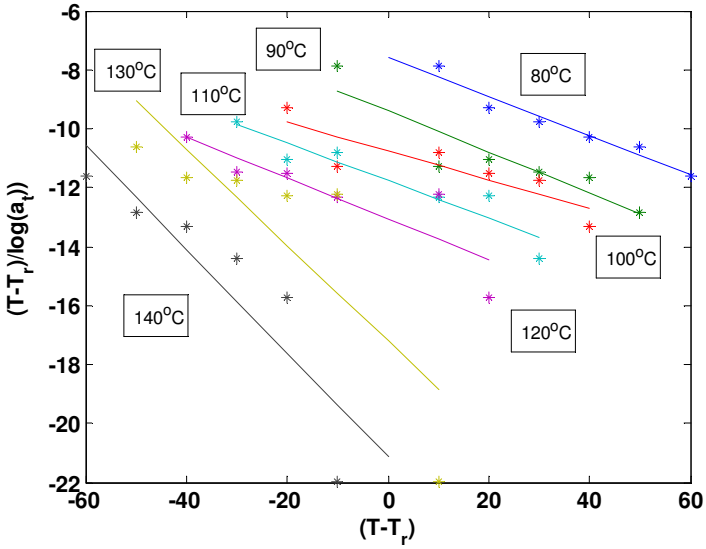

Figure 7.30: WLF plot for SPHT375 (* = experimental data, – = WLF fit)

As shown in section 7.2, all the anisotropic Mittal pitch samples did not follow time-Temperature-superposition. SPHT400 and SPHT412 similarly cannot produce master-

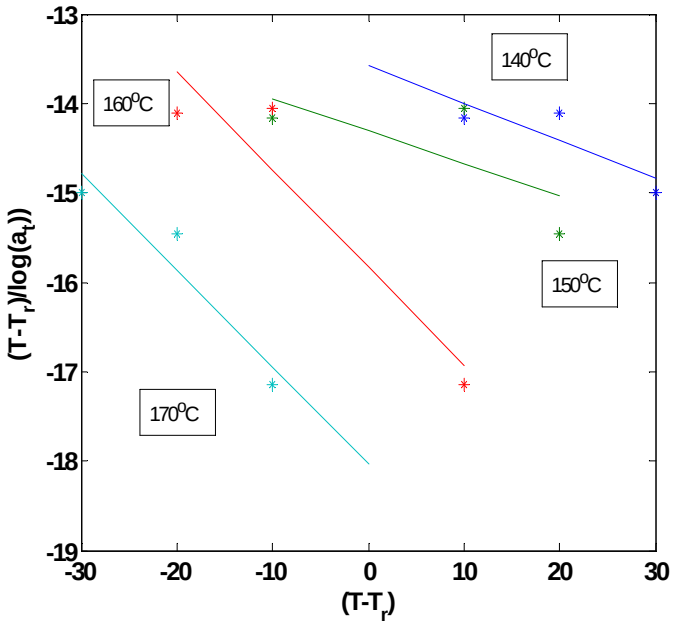

Figure 7.31: WLF plot for SPHT400T3 (* = experimental data, – = WLF fit)

Table 7.3: WLF Properties of SPHT375

Temperature (℃)	Slope (-)	Intercept (K)	R^2 (-)	C_1 (-)	C_2 (K)	B (K)	T_∞ (K)
80	-0.0665	-7.5800	0.9526	15.0431	114.0260	1715.3	239.1240
90	-0.0697	-9.3991	0.8204	14.3517	134.8930	1935.9	228.2570
100	-0.0491	-10.7568	0.7562	20.3798	219.2203	4467.7	153.9297
110	-0.0641	-11.7717	0.8834	15.6105	183.7623	2868.6	199.3877
120	-0.0693	-13.0654	0.7564	14.4283	188.5118	2719.9	204.6382
130	-0.1630	-17.2185	0.6942	6.1340	105.6185	647.9	297.5315
140	-0.1754	-21.1100	0.7891	5.7023	120.3743	686.4	292.7757

curves. As such no WLF data is possible. SPHT425 and SPHT420T3, do follow tTs and there WLF plots are shown in Figures 7.32 and 7.33. It is observed that these two samples do not follow the WLF-type behaviour. The R^2 values in Tables7.4 and B.3 confirm this.

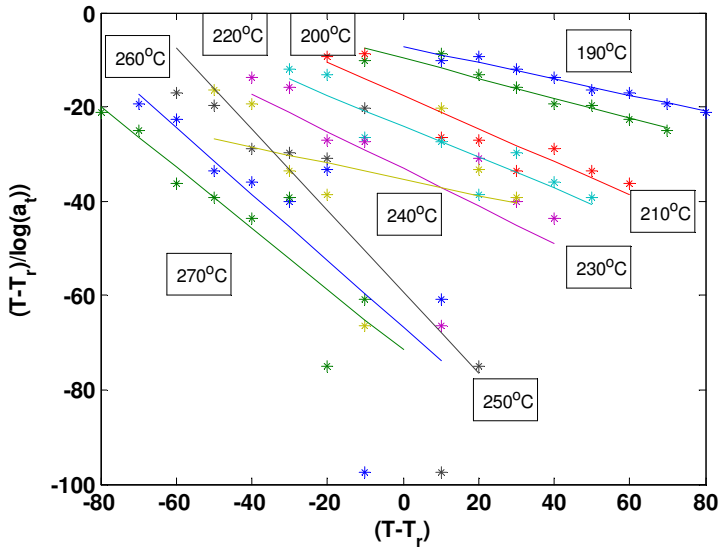

Figure 7.32: WLF plot for SPHT425 (* = experimental data, – = WLF fit)

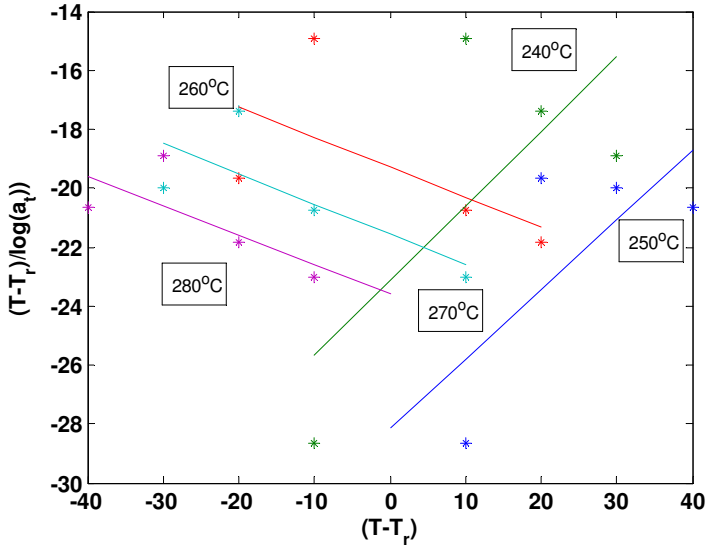

Figure 7.33: WLF plot for SPHT420T3 (* = experimental data, – = WLF fit)

Sample SPHT425 also produced mastercurves for both the higher and lower temperatures. The WLF plots for these samples are shown in Figures 7.34 and 7.35. Unsurprisingly Figure 7.34 is similar to Figure 7.32. The high temperature mastercurves however have shift factors that follow the WLF equation. This is verified by the R^2 values shown in Table 7.5. This indicates that the free volume change during this portion of the mastercurve is linear and predictable, even if it is over a narrow temperature range.

Table 7.4: WLF Properties of SPHT425

Temperature (°C)	Slope (-)	Intercept (K)	R^2 (-)	C_1 (-)	C_2 (K)	B (K)	T_∞ (K)
190	-0.1627	-7.4006	0.9580	6.1453	45.4789	279.5	417.6711
200	-0.1976	-9.7075	0.8989	5.0610	49.1302	248.6	424.0198
210	-0.3374	-17.6511	0.8087	2.9638	52.3147	155.1	430.8353
220	-0.2999	-23.7188	0.7416	3.3349	79.1004	263.8	414.0496
230	-0.3943	-33.8150	0.3168	2.5360	85.7546	217.5	417.3954
240	-0.1207	-35.3892	0.0310	8.2836	293.1494	2428.3	220.0006
250	-0.3876	-39.7713	0.7376	2.5802	102.6166	264.8	420.5334
260	-0.5108	-52.3510	0.8070	1.9576	102.4835	200.6	430.6665
270	-0.5691	-64.6240	0.8515	1.7571	113.5486	199.5	429.6014

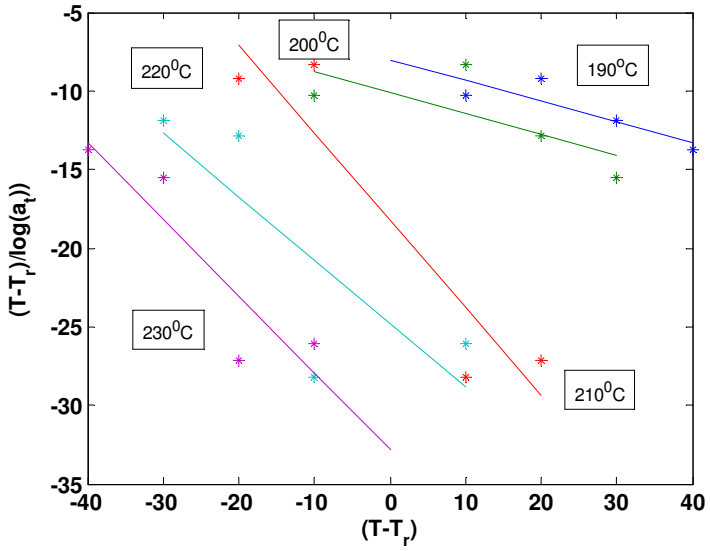

Figure 7.34: WLF plot for SPHT425 at low temperature (* = experimental data, – = WLF fit)

Table 7.5: WLF Properties of SPHT425 at high temperatures

Temperature (°C)	Slope (-)	Intercept (K)	R^2 (-)	C_1 (-)	C_2 (K)	B (K)	T_∞ (K)
240	-0.7155	-13.8627	0.9989	1.3976	19.3740	27.1	493.7760
250	-1.1030	-32.3379	0.9955	0.9066	29.3189	26.6	493.8311
260	-1.2546	-55.0083	0.9899	0.7971	43.8470	35.0	489.3030
270	-1.5817	-83.4825	0.9915	0.6322	52.7813	33.4	490.3687

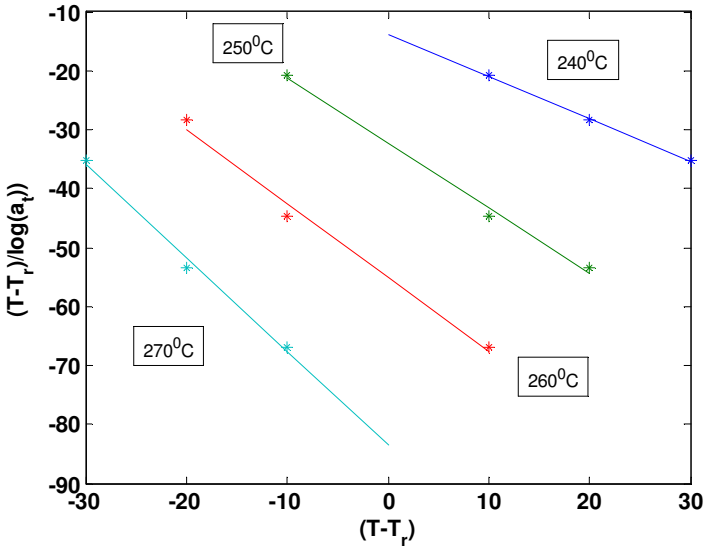

Figure 7.35: WLF plot for SPHT425 at high temperature (* = experimental data, – = WLF fit)

7.4 Discussion

Figures 7.4, 7.5, 7.6, 7.7, 7.8, 7.9 and 7.10 are mastercurves of isotropic pitches using the time-Temperature-superposition. All of these curves show similar behaviour when reduced to a temperature around softening. A solid material at low frequency, crossover from a viscoelastic solid to a viscoelastic liquid and then a liquid dominant material. Scatter is observed at lower frequencies. For MP110, MP110HT350 and MP110HT375 this is likely be the effect of the particulate material on the storage modulus in a fluid dominant system. For the SASOL pitches the cause for this behaviour is unknown.

Figures 7.21 and 7.24 shows the mastercurve of sample SPHT425 and SPHT420T3 at temperatures much higher than softening. The loss and storage modulus show the solid dominant and crossover regions as described before, but the third is slightly different. This area of the storage modulus curve does show a cessation in divergence, but also shows convergence (with decreasing frequency). This shape suggests increased elasticity of the sample. It as also indicative of the shape of coal-tar and heat treated pitches as investigated by (Daji et al., 1999).

Figures 7.36 and 7.37 represent comparative loss and storage moduli of the data shifted to a reference temperature of 110 °C. These mastercurves were produced using average B and T_∞ values calculated and shift factors predicted by equation 7.1.

Both figures show shift to lower frequencies with increased thermal treatment, or increased C/H ratio. This is indicative of the change in glass transition temperatures. As the T_g increases the mastercurves continuously shift to lower frequencies. This is observed for all the isotropic pitches. The most significant shift to lower frequency is observed for MP110HT400, this is the sample with a significantly higher T_g (with 13 % mesophase

content).

It shows the variation of the behaviour of the material. It is clearly visible that MP110HT400 has a significant increase in elasticity as compared to the other samples, whereas not much deviation is visible in the data of the loss moduli.

The storage modulus also shows the effect of the particulate QI matter with change in slope. This is most evident in MP110, whose effect is reduced with thermal treatment.

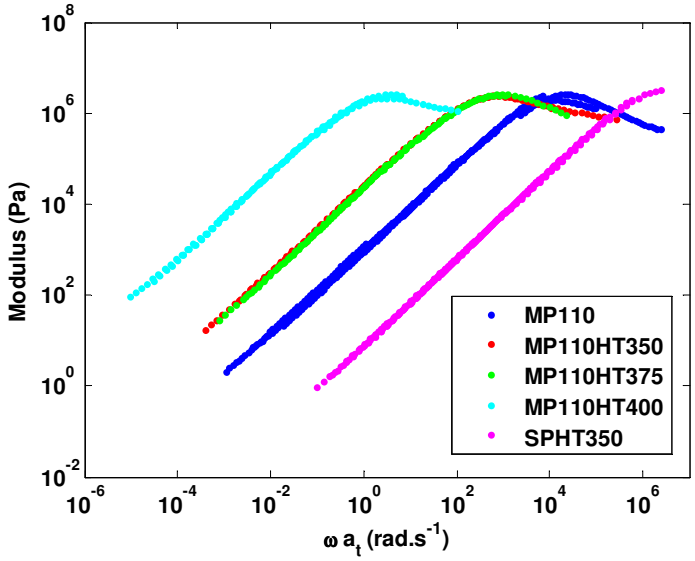

Figure 7.36: Mastercurves comparing loss modulus of isotropic pitches

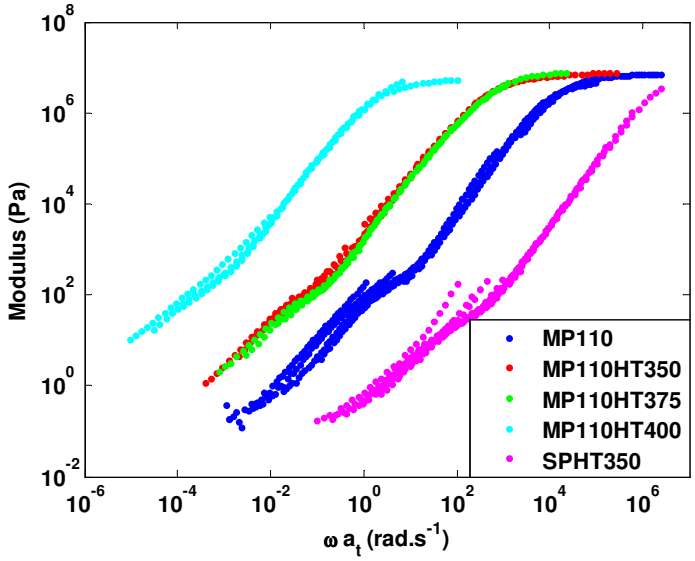

Figure 7.37: Mastercurves comparing storage modulus of isotropic pitches

The tan(δ) curves confirm the behaviour described from the loss and storage modulus, and can be seen in Figure 7.38. The combined viscosity curves, Figure 7.39, allows easy comparison of the samples with respect to their glass transition temperatures. The higher

the viscosity of the sample, the closer the reduced temperature of 110 ℃ is to T_g. The difference in the viscosity, at a fixed temperature, effectively expresses the fluidity and ability of the materials to be processed.

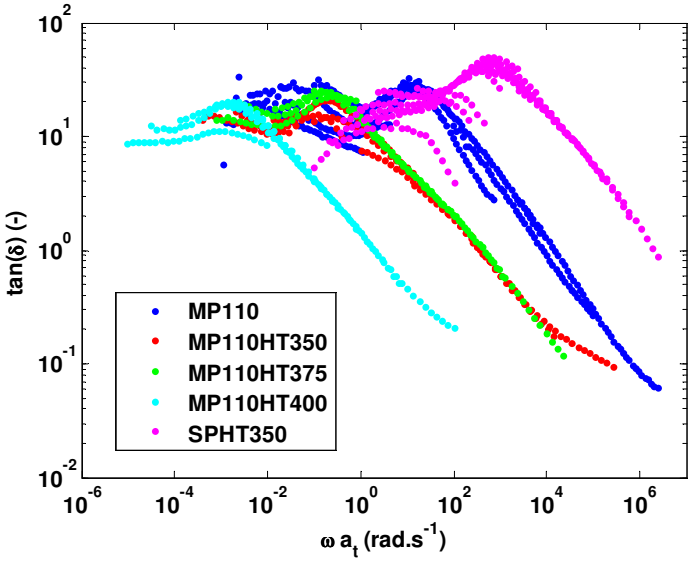

Figure 7.38: Mastercurves comparing tan(δ) of isotropic pitches

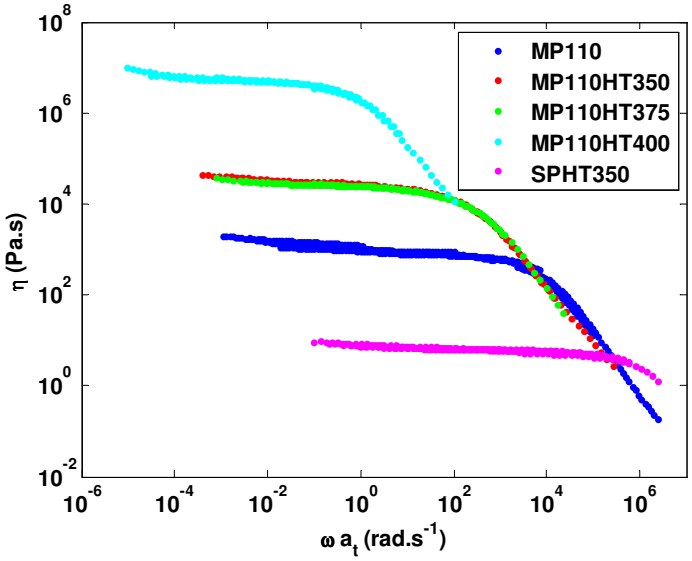

Figure 7.39: Mastercurves comparing dynamic viscosity of isotropic pitches

Figures 7.36, 7.37, 7.38 and 7.39 show that the WLF equation can be used to predict the shift factor and produce mastercurves in a limited temperature range. Regression to calculate these parameters may not always yield useful results. This is due to the sensitivity of the equation. The slightest change in experimental shift factor will yield WLF constants which are not be usable. A weary approach must be taken as the material used for the various oscillatory experiments might induce minor changes in behaviour; and

therefore also the magnitude of shift factors, and use of any prediction tools. Extrapolation to lower temperatures (via Fulcher-Tammam-Hesse equation) yield inconsistent and erroneous results and hence cannot be used to conclusively indicate characteristics of the material.

The anisotropic pitches show different behaviour. Mittal samples MP110HT437, MP110HT425, MP110HT425T6 and MP110HT437T6 all exhibit breakdown of structure during determination of the LVER. The frequency sweeps, with lowest possible strain, yielded results associated with change in microstructure. Frequency sweeps of these samples, at frequencies lower than $1\,\mathrm{rad\,s^{-1}}$, loss and storage moduli cease decreasing as would be expected (with decreasing frequency); in most cases, the moduli began increasing. For the Mittal pitches, this is easily attributed to the softening of the mesophase, or substantial change in mesophase properties in an emulsion.

SPHT400 and SPHT412 exhibited similar frequency sweep results to those of the Mittal pitches. The reason for their behaviour is not as clear. The transition from a viscoelastic liquid to a weak gel structure has been postulated for these samples.

SPHT425 and SPHT420T3 mastercurves were produced; and these were obtained at temperatures significantly above softening. These curves differ significantly from those observed for the isotropic pitches. SPHT425 mastercurves has a strong resemblance to those observed of mesophase pitches investigated by Cheung et al. (1995). This is surprising since it has 17% mesophase content. SPHT420T3 shows slightly stronger elastic dominated behaviour than SPHT425 at temperature of measurement; therefore this behaviour is more pronounced than that observed for mesophase pitch.

The $\tan(\delta)$ mastercurve values are substantially lower than those pitches previously investigated. These $\tan(\delta)$ curves are almost constant at 1, therefor $G' = G''$. This indicated that the system maintains similar levels of elasticity to fluidity; this being the case while there is a continuous shear-thinning viscosity with increase in frequency. This is the same behaviour as that observed for rotational rheometry with increasing shear-rates.

CHAPTER 8

CONCLUSIONS

The aim of this study was to produce pitches at different stages of transformation to mesophase and understand its behaviour. This was achieved by producing several heat treated isotropic pitches and pitches with varying mesophase content. An insight into the behaviour is achieved by first identifying the composition and structure of the material.

Thermal treatment resulted in the following changes in the pitch material:

- Increase in aromaticity, carbon yield, quinoline and toluene insolubles and mesophase content with the thermal treatment
- Change in composition resulted in a corresponding change in T_g and T_s
- TMA provided the most accurate value of true T_g
- DMTA proved to be a robust method to obtain the most relevant relaxation information
- C/H and MC can help to identify pitch properties, but only in a localised environment (therefore not unique globally)

Other details with respect to these pitches do not conform for both sources. This was expected and a description of some of these characteristics for the two pitches are shown in Table 8.1.

One of the most important aspects in characterising the pitches is the determination of T_g (and/or T_s). This proved true, as measurements of rheological properties were obtained at different temperatures. The relation of the measurement temperature to the T_g help interpret the behaviour of the material.

The isotropic pitches of both sources showed similar behaviour when characterised via rheometry (at temperatures around softening), these are:

Table 8.1: Summary of pitch characteristics

Topic	Mittal Pitches	SASOL Pitches
Composition	Aromatic	Aliphatic
Particulates	High particulate content	No particulate material
Mesophase Temperature Window	Between 400 °C and 440 °C	Between 400 °C and 430 °C
Mesophase	Formation of spheres No coalescence (particulates contribute to this behaviour)	Coalescence of mesophase Formation of clusters Fine mosaic appearance
Other	Mesophase relaxation was detected via DMTA with continuous isotropic phase	Continuous mesophase properties detected

- Near-Newtonian behaviour
- Near-isoviscous flow curves under rotational shear rheometry
- Isotropic pitch viscoelastic mastercurves during oscillatory shear rheometry (similar to Turpin et al. (1994) and Daji et al. (1999))
- Oscillatory behaviour shows glassy system behaviour close to glass transition temperatures
- Increased elasticity at higher temperatures
- Fits WLF described behaviour (for oscillation)
- Decrease in Arrhenius shear activation energy as T_g increases

For the isotropic pitches, all measurements were made within a temperature range of 100 °C above T_g. For these measurements the WLF technique was applied and resulted in satisfactory fits. This confirmed the glassy nature of the material around T_g.

For the anisotropic pitches however, the measurements were only possible at much higher temperatures, and further away from T_g. The anisotropic pitches show significantly different behaviour to the isotropic pitches. These pitches also showed different behaviour from their respective sources. Some of the general characteristics are:

- Non-Newtonian behaviour
- Measurements made at temperature ranges above T_s

- Microstructure (and change thereof) affects measurements

The anisotropic Mittal pitches were adequately described using suspension/emulsion models using the Krieger-Dougherty based equations. The viscosity of the anisotropic SASOL pitches were modelled using the continuum shear model based on Herschel-Bulkley derived equations.

For the Mittal pitches, as mesophase content increased, so did the measurement temperatures away from the T_g. As such, the Arrhenius activation energies determined are also at different temperatures away from T_g, which represent mixtures at different states as they change from suspension to emulsion. The technique of determining activation energy is still important, but its meaning should be taken into context with respect to structure and measurement temperature of the material.

The SASOL pitches have similarly complex behaviour. The measurement temperature is significantly further away from T_g than that of the Mittal pitches. This observation, provided proof of a strong interaction between the components, even at low to moderate mesophase content. The shape of the flow curve and its microstructure also support the hypothesis of gel-like behaviour.

It should be noted that due to the fact that sample measurements were being made at different temperatures, this would inevitably result in different behaviour of the pitches; this also means that samples are not always necessarily comparable.

Some of the rheological characteristics and structures of these pitches are described and summarised in Table 8.2.

From the analyses of the samples, different structures were observed: isotropic, suspension, emulsion, gel and mesophase. This shows an array of possible rheological outcomes from pitch material. The interaction of anisotropic pitch is thus a complex one and the study of sample rheology is an important and necessary characteristic. This thesis supports the use of rheometry to understand the behaviour of pitch, and that it should be used more often, but is currently often neglected.

Table 8.2: Summary of anisotropic pitch rheology characteristics

Topic	Mittal Pitches	SASOL Pitches
Structure	Suspension/emulsion	gel/mesophase
Low mesophase content - Rotation	Suspension Mesophase particle agglomeration Dispersed phase particle breakup	Weak-gel Yield stress Bingham plastic behaviour / Structure breakdown
High mesophase content - Rotation	Transition from suspension to emulsion Shear-thinning Power-law behaviour	Gel structure and mesophase structure Strongly shear-thinning characteristics Herschel-Bulkley and Power-law behaviour
Low mesophase content - Oscillation	Structure breakdown observed / no LVER Mesophase softening easily observed during frequency sweep	No LVER information Structural change at low frequency
High mesophase content - Oscillation		Elasticity observed at high temperatures Strong structure

8.1 Recommendations

Separation of the anisotropic pitch was attempted but proved unsuccessful; it is suggested to try and separate the anisotropic pitches into its component isotropic and mesophase phases. The method of separation as conducted by Singer et al. (1987) is recommended. The high temperature centrifugation also allows for an alternate manner of quantifying the mesophase content. The properties of the two phases can now be measured independently. This will provide an important insight into the properties of each phase; gaining the composition and structure of the separate phases provides a better understanding into the interaction of the material when they are measured as a mixture. All the techniques employed in this thesis and subsequent analysis should be sufficient. The possibility of modelling these systems will also provide a variety of additional work. Hurt & Hu (1999) and Hu & Hurt (2001) provide a strong basis for the thermodynamic modelling of such systems.

These mixtures were however limited to samples with fluid-dominant systems. The study should focus on processing to higher temperatures, closer to coking temperatures, and produce samples which have solid dominant characteristics. This being the transition from anisotropic pitch to coke. Observations of T_g, T_s and rheology being of importance. This can be achieved by the use of DMTA. For this study, much preparation and care will be needed to produce specimens for the instrument. Brittle samples will be difficult to

study and a microstructure which is rich in defects will break easily. This work will then provide a pitch-mesophase-carbon transformation diagram, similar to that as produced by Benn (1989).

BIBLIOGRAPHY

Alcan, J. and Inorga, A. (2001) "Characterisation of coal tar pitches by thermal analysis , infrared spectroscopy and solvent fractionation", *Fuel, 80*.

Azami, K.; Yokono, T.; Sanada, Y. and Uemera, S. (1989) "Studies on the early stage of petroleum pitch by means of high-temperature and ESR", *Carbon, 27* (2), 177–183.

Balduhn, R. and Fitzer, E. (1980) "Rheological properties of pitches and bitumina up to temperatures of 500", *Carbon, 18*, 155–161.

Barnes, H. (2003) "A review of the rheology of filled viscoelastic systems", *Rheology Reviews,* pages 1–36.

Barnes, H. (1994) "Rheology of emulsions–a review", *Colloids and Surfaces A: Physicochemical and Engineering Aspects, 91*, 89–95.

Barr, J. and Lewis, I. (1982) "Characterisation of pitches by differential scanning calorimetry", *Thermochimica Acta, 52*, 297–304.

Benn, M. (1989) *Pitch-Mesophase-Carbon Transformation Diagrams and the Fabrication of Carbon Materials*, PhD thesis, University of Sheffield,.

Bermejo, J.; Menéndez, R.; Figueiras, A. and Granda, M. (1995) "The role of low-molecular-weight components in the pyrolysis of pitches", *Fuel, 74* (12), 1792–1799.

Bhatia, G.; Aggarwal, R.; Chari, S. and Jain, S. (1977) "Rheological characteristics of coal tar and petroleum pitches with and without additives", *Carbon, 15*, 219–223.

Bhatia, G.; Fitzer, E. and Kompalik, D. (1986) "Mesophase formation in defined mixtures of coal tar pitch fractions", *Carbon, 24* (4), 489–494.

Blanco, C.; Fleurot, O.; Menendez, R.; Santamaria, R.; Bermejo, J. and Edie, D. (1999) "Contribution of the isotropic phase to the rheology of partially anisotropic coal-tar pitches", *Carbon, 37*, 1059–1064.

Blanco, C.; Lu, S.; Appleyard, S. and Rand, B. (2002)a "Micro-thermal analysis as a technique for in situ characterisation of the softening behaviour of the isotrpic phase and mesophase in thermally treated pitches", *Carbon,* pages 132–135.

Blanco, C.; Prada, V.; Santamaria, R.; Bermejo, J. and Menendez, R. (2002)b "Pyrolysis behaviour of mesophase and isotropic phases isolated from the same pitch", *Journal of Analytical and Applied Pyrolysis, 63*, 251–265.

Blanco, C.; Santamaria, R.; Bermejo, J. and Menendez, R. (2000) "Separation and characterisation of isotropic phase and co-existing mesophase in thermally treated coal-tar pitches", *Carbon, 38*, 1169–1176.

Braga, C. P.; de Castro Dutra, C. H. M.; de Castro, L. D. and de Andrade, C. T. (2009) "Influence of heat and pressure treatment on the rheological behaviour of petroleum pitches", *Fuel, 88*, 853–860.

Brooks, J. D. and Taylor, G. H. (1965) "The formation of graphitizing carbons", *Carbon, 3*, 185–193.

Burchell, T. (1999) *Carbon materials for advanced technologies*, Pergamon, first edition.

Cato, A. D. and Edie, D. D. (2003) "Flow behaviour of mesophase pitch", *Carbon, 41*, 1411–1417.

Cato, A. D.; Edie, D. D. and Harrison, G. M. (2005) "Steady state and transient rheological behaviour of mesophase pitch, Part I: Experiment", *Journal of Rheology, 49* (1), 161–174.

Chandrashekhar, S. (1992) *Liquid Crystals*, Cambridge University Press, second edition.

Cheung, T.; Turpin, M. and Rand, B. (1995) "Controlled stress, oscillatory rheometry of mesophase-pitches", *Carbon, 33* (12), 1673–1679.

Chhabra, R. and Richardson, J. (2008) "Chapter 1 - Non-Newtonian Fluid Behaviour", in *Non-Newtonian Flow and Applied Rheology*, Second edition.

Collett, G. W. and Rand, B. (1978)a "Rheological investigation of coal-tar pitch during its transformation to mesophase", *Fuel, 57*, 162–170.

Collett, G. W. and Rand, B. (1978)b "Thixotropic changes occurring on reheating a coal tar pitch containing mesophase", *Carbon, 16* (6), 477–479.

Cross, M. (1965) "Rheology of non-Newtonian fluids: a new flow equation for pseudo-plastic systems", *Journal of Colloid Science, 437* (20), 417–437.

Daguerre, E.; Nauguier, F. and Py, X. (1998) "Alpha-relaxation of a coal tar pitch and temperature-density effects on the viscoelastic parameters analysis", *Carbon, 36* (7-8), 1099–1105.

Daguerre, E.; Nauguier, F. and Py, X. (1999) "The molecular scaling of raw pitches by oscillatory rheometry", *Carbon, 37*, 1189–1197.

Daji, J.; Rand, B. and Turpin, M. (1999) "Viscoelastic behaviour of a heat treated isotropic pitch", *Carbon, 36*, 1406–1409.

Dealy, J. and Larson, R. (2006) *Structure and Rheology of Molten Polymers*, Hanser, .

Delhaes, P. (2001) *Graphite and Precursors*, Gordon and Breach Science Publishers, .

Derkach, S. R. (2009) "Rheology of emulsions", *Advances Colloid and Interface Science, 151*, 1–23.

Dumont, M.; Courges, M. A.; Pailler, R. and Bourrat, X. (2003) "Mesophase pitch for 3D-carbon fibre preform densification: rheology and processability", *Fuel, 82*, 1523–1529.

Edwards, W.; Jin, L. and Thies, M. (2003) "MALDI-TOF mass spectrometry: Obtaining reliable mass spectra for insoluble carbonaceous pitches", *Carbon, 41*, 2761–2768.

Ferry, J. (1980) *Viscoelastic Properties of Polymers*, John Wiley and Sons, Inc, third edition.

Fitzer, E.; Kompalik, D. and Yudate, K. (1987) "Rheological characteristics of coal-tar pitches", *Fuel, 66*, 1504–1511.

Genovese, D. B. (2012) "Shear rheology of hard-sphere, dispersed, and aggregated suspensions, and filler-matrix composites", *Advances in colloid and interface science, 171-172*, 1–16.

Grace, H. P. (1982) "Dispersion phenomena in high viscosity immiscible fluid systems and application of static mixers as dispersion devices in such systems", *Chemical Engineering Communications, 14* (3-6), 225–277.

Greinke, R. and Singer, L. (1988) "Constitution of coexisting phases in mesophase pitch during heat treatment: mechanism of mesophase formation", *Carbon, 26* (5), 665–670.

Herschel, W. and Bulkley, R. (1926) "Konsistenzmessungen von gummi-benzollösungen", *Kolloid-Zeitschrift, 39* (4), 291–300.

Hu, Y. and Hurt, R. H. (2001) "Thermodynamics of carbonaceous mesophase II . General theory for nonideal solutions", *Carbon, 39*, 887–896.

Hurt, R. H. and Hu, Y. (1999) "Thermodynamics of carbonaceous mesophase", *Carbon, 37*, 281–292.

Ito, O. (1993) "UV-visible and near-IR spectra of heat-treated pitches during mesophase formation", *Carbon, 31* (3), 401–406.

Jansen, K. M. B.; Agterof, W. G. M. and Mellema, J. (2001) "Droplet breakup in concentrated emulsions", *Journal of Rheology, 45* (1), 227.

Khandare, P.; Zondlo, J. and Pavlovic, A. (1996) "The measurement of the glass transition temperature of mesophase pitches using a thermomechanical device", *Carbon, 34* (5), 663–669.

Khandare, P. M.; Zondlo, J. W.; Stansberry, P. B. and Stiller, A. H. (2000) "Rheological investigations of pitch material Part II: viscosity measurement of A240 and ARA-24 pitches using a high-temperature high-pressure rheometer", *Carbon, 38*, 889–897.

Kim, C.; Ryu, S. and Rhee, B. (1993) "Properties of coal tar pitch-based mesophase separated by high-temperature centrifugation", *Carbon, 31* (5), 833–838.

Krieger, I. (1972) "Rheology of monodisperse latices", *Advances in Colloid and Interface Science, 3* (2), 111–136.

Kundu, S. and Ogale, A. A. (2006) "Rheostructural studies on a synthetic mesophase pitch during transient shear flow", *Carbon, 44*, 2224–2235.

Kundu, S. and Ogale, A. A. (2007) "Microstructural effects on the dynamic rheology of a discotic mesophase pitch", *Rheologica Acta, 46*, 1211–1222.

Kundu, S. and Ogale, A. A. (2010) "Rheostructural studies of a discotic mesophase pitch at processing flow conditions", *Rheologica Acta, 49* (8), 845–854.

Larson, R. (1999) *The structure and rheology of complex fluids*, Oxford University Press, New York.

Lee, W.-J. and Lucey, J. A. July (2006) "Impact of gelation conditions and structural breakdown on the physical and sensory properties of stirred yogurts.", *Journal of dairy science, 89* (7), 2374–85.

Liedtke, V. and Huttinger, K. (1996) "Mesophase pitches as matrix precursor of carbon fiber reinforced carbon: I. Mesophase pitch preparation and characterisation", *Carbon, 34* (9), 1057–1065.

Marsh, H.; Gomez, C.; Salazar, D. and Palazon, E. R. (2000) "Pyrolysis of petroleum residues II . Chemistry of pyrolysis", *38*, 535–546.

Marsh, H.; Martinez-Escandell, M. and Rodriguez-Reinoso, F. (1999) "Semicokes from pitch pyrolysis: mechanisms and kinetics", *Carbon, 37*, 363–390.

Marsh, H. and Menendez, R. (1988) "Carbons from pyrolysis of pitches, coals and their blends", *Fuel Processing Technology, 20*, 269–296.

Menendez, R.; Fleurot, O.; Blanco, C.; Santamaria, R.; Bermejo, J. and Edie, D. (1998) "Chemical and rheological characterization of air-blown coal-tar pitches", *Carbon, 36* (7-8), 973–979.

Mochida, I.; Korai, Y.; Ku, C.-h.; Watanabe, F. and Sakai, Y. (2000) "Chemistry of synthesis, structure, preparation and application of aromatic-derived mesophase pitch", *Carbon, 38*, 305–328.

Mochida, I.; Yoon, S.-h. and Korai, Y. (2002) "Mesoscopic Structure and Properties of Liquid Crystalline Mesophase Pitch and Its Transformation into Carbon Fiber", *Forum American Bar Association,* pages 81–101.

Mokoena, K.; Van der Walt, T.; Morgan, T.; Herod, A. and Kandiyoti, R. May (2008) "Heat treatment of medium-temperature Sasol-Lurgi gasifier coal-tar pitch for polymerizing to higher value products", *Fuel, 87* (6), 751–760 ISSN 00162361.

Montes-Moran, M.; Crespo, J.; Young, R.; Garcia, R. and Moinelo, S. (2002) "Mesophase from a coal tar pitch: a Raman spectroscopy study", *Fuel Processing Technology, 77-78*, 207–212.

Nazem, F. F. (1980) "Rheology of carbonaceous mesophase pitch", *Fuel, 59*, 581–858.

Osswald, T. and Menges, G. (2003) *Materials Science of Polymers for Engineers*, Hanser Verlag, second edition.

Owens, R. and Phillips, T. (2002) *Computational Rheology*, Imperial College Press, London.

Pal, R. (2001) "Novel viscosity equations for emulsions of two immiscible liquids", *Journal of Rheology, 45* (2), 509–520.

Panaitescu, C. and Predeanu, G. (2001) "Microstructural characteristics of toluene and quinoline-insolubles from coal-tar pitch and their cokes", *International Journal of Coal Geology, 71*, 448–454.

Papole, G. J. (2012) "Characterization of medium temperature gasifier pitch", Master's thesis, University of Pretoria,.

Parks, T.; Cross, L. and Lynch, L. (1991) "An {NMR} method for quantitative determination of the carbonaceous mesophase content of a petroleum pitch", *Carbon, 29* (7), 921 – 927.

Perez, M.; Granda, M.; Garcia, R.; Santamaria, R.; Romero, E. and Menendez, R. (2002) "Pyrolysis behaviour of petroleum pitches prepared at different conditions", *Journal of Analytical and Applied Pyrolysis, 63* (2), 223–239.

Py, X.; Daguerre, E.; Guillot, A. and Spinner, B. (1997) "Alpha-relaxation of an isotropic petroleum pitch: A controlled stress and strain oscillatory rheometry study", *Carbon, 35*, 1013–1021.

Rand, B. (1987) "Pitch precursors for advanced carbon materials - rheological aspects*", *Fuel, 66*, 1491–1503.

Rand, B.; Yardim, S. and Ferhat, M. (2001) *Design and Control of Structure of Advanced Carbon Materials for Enhanced Performance*, NATO Science Series Kluwer Academic Publishers, first edition.

Royall, P. G.; Huang, C.-y.; Tang, S.-w. J.; Duncan, J.; Van-de Velde, G. and Brown, M. B. September (2005) "The development of DMA for the detection of amorphous content in pharmaceutical powdered materials.", *International journal of pharmaceutics, 301* (1-2), 181–91.

Sakai, M. (1979) "Viscoelastic properties of a pitch and coke-pitch disperse system", *Carbon, 17*, 139–144.

Sakai, M. and Inagaki, M. (1981) "Determination of viscoelastic properties of pitches by torsional creep", *Carbon, 9*, 37–43.

Saravanakumar, K.; Tata, B. and Aswal, V. (2012) "Thermoreversible viscoelastic to weak gel transition in a micellar ionic liquid with salt", *Colloids and Surfaces A: Physicochemical and Engineering Aspects, 414*, 359–365.

Sima, L.; Blanco, C.; Santamaria, R.; Granda, M.; Slaghuis, H. and Menendez, R. (2003) "Relationship between chemical composition and pyrolysis behaviour of a medium temperature pitch (or Lurgi-gasifier pitch)", *Fuel Processing Technology, 84*, 63–77.

Singer, L.; Riffle, D. and Cherry, A. (1987) "High temperature centrifugation: Application to mesophase pitch", *Carbon, 25* (2), 249–257.

Stephen, M. and Straley, J. (1974) "Physics of liquid crystals", *Reviews of Modern Physics, 46* (4).

Turpin, M.; Cheung, T. and Rand, B. (1994) "Controlled stress, oscillatory rheometry of a petroleum pitch", *Carbon, 32*, 225–230.

Vieira, F.; de Castro Dutra, C. H. M. and de Castro, L. (2011) "Determining the anisotropic content in a petroleum pitch - Comparison of centrifugation and optical microscopy techniques", *Fuel, 90*, 908–911.

Ward, I. and Sweeney, J. (2004) *An Introduction to the Mechanical Properties of Solid Polymers*, John Wiley and Sons, Ltd, second edition.

Wildemuth, C. and Williams, M. (1984) "Viscosity of suspensions modeled with a shear-dependent maximum packing fraction", *Rheologica Acta, 23* (6), 627–635.

Williams, M.; Landel, R. and Ferry, J. (1955) "The temperature dependence of relaxation mechanisms in amorphous polymers and other glass-forming liquids", *J. Am. Chem. Soc, 679* (12).

Appendices

APPENDIX A

MP110 PITCH INFORMATION

A.1 Williams-Landel-Ferry Fit

Table A.1: WLF Properties of Sample MP110HT375

Temperature (℃)	Slope (-)	Intercept (K)	R^2 (-)	C_1 (-)	C_2 (K)	B (K)	T_∞ (K)
90	-0.0894	-6.7448	1	11.1897	75.472	844.5113	287.678
100	-0.1014	-8.6427	0.9999	9.8629	85.2418	840.7301	287.9082
110	-0.1133	-10.7849	0.9999	8.8275	95.2034	840.4064	287.9466
120	-0.1246	-13.1664	0.9994	8.0246	105.6548	847.8342	287.4952
130	-0.141	-15.9046	0.9991	7.0933	112.8166	800.2474	290.3334
140	-0.1544	-18.9092	0.9992	6.4783	122.5005	793.6005	290.6495

Table A.2: WLF Properties of Sample MP110HT400

Temperature (℃)	Slope (-)	Intercept (K)	R^2 (-)	C_1 (-)	C_2 (K)	B (K)	T_∞ (K)
110	-0.094	-7.8837	0.9979	10.6425	83.9026	892.9325	299.2474
120	-0.1038	-9.8724	0.9965	9.6331	95.102	916.1296	298.048
130	-0.1141	-11.9954	0.9876	8.764	105.1278	921.3431	298.0222
140	-0.1444	-14.6569	0.9882	6.9276	101.5363	703.3993	311.6137
150	-0.1682	-17.9686	0.9879	5.9457	106.8363	635.2184	316.3137
160	-0.1827	-21.5226	0.9905	5.474	117.8137	644.9076	315.3363

APPENDIX B

SASOL PITCH INFORMATION

B.1 Williams-Landel-Ferry Fit

Table B.1: WLF Properties of SPHT350

Temperature (℃)	Slope (-)	Intercept (K)	R^2 (-)	C_1 (-)	C_2 (K)	B (K)	T_∞ (K)
60	-0.0663	-8.2473	0.9870	15.0642	124.2403	1871.6	208.9096
65	-0.0706	-8.7904	0.9776	14.1543	124.4222	1761.1	213.7278
70	-0.0777	-9.4376	0.9906	12.8704	121.4664	1563.3	221.6836
75	-0.0834	-10.2115	0.9933	11.9842	122.3775	1466.6	225.7724
80	-0.0867	-11.0357	0.9880	11.5261	127.2002	1466.1	225.9498
85	-0.0969	-11.9499	0.9903	10.3185	123.3070	1272.4	234.8429
90	-0.1062	-13.0189	0.9909	9.4153	122.5773	1154.1	240.5726
95	-0.1110	-14.1388	0.9946	9.0074	127.3549	1147.1	240.7950
100	-0.1164	-15.3096	0.9953	8.5881	131.4810	1129.2	241.6690
105	-0.1225	-16.5578	0.9948	8.1622	135.1490	1103.1	243.0009
110	-0.1277	-17.8623	0.9957	7.8280	139.8279	1094.6	243.3221

Table B.2: WLF Properties of SPHT400T3

Temperature (℃)	Slope (-)	Intercept (K)	R^2 (-)	C_1 (-)	C_2 (K)	B (K)	T_∞ (K)
140	-0.0418	-13.5817	0.7044	23.8975	324.5695	7756.4	88.5805
150	-0.0362	-14.3124	0.5063	27.5987	395.0033	10901.6	28.1467
160	-0.1092	-15.8326	0.8839	9.1576	144.9878	1327.7	288.1622
170	-0.1080	-18.0251	0.9001	9.2613	166.9367	1546.1	276.2133

Table B.3: WLF Properties of SPHT420T3

Temperature (°C)	Slope (-)	Intercept (K)	R^2 (-)	C_1 (-)	C_2 (K)	B (K)	T_∞ (K)
240	0.2364	-28.1526	0.5023	-4.2298	-119.0794	503.7	632.2294
250	0.2528	-23.1294	0.5132	-3.9555	-91.4886	361.9	614.6386
260	-0.1019	-19.2843	0.3753	9.8151	189.2775	1857.8	343.8725
270	-0.1020	-21.5526	0.5619	9.8084	211.3961	2073.5	331.7539
280	-0.0990	-23.5734	0.5381	10.1043	238.1921	2406.8	314.9579

Table B.4: WLF Properties of SPHT425 at low temperatures

Temperature (°C)	Slope (-)	Intercept (K)	R^2 (-)	C_1 (-)	C_2 (K)	B (K)	T_∞ (K)
190	-0.1306	-8.0373	0.7263	7.6585	61.5535	471.4	401.5965
200	-0.1317	-10.1191	0.5228	7.5924	76.8284	583.3	396.3216
210	-0.5563	-18.2262	0.8668	1.7977	32.7646	58.9	450.3854
220	-0.4037	-24.8233	0.6463	2.4769	61.4843	152.3	431.6657
230	-0.4865	-32.7912	0.8133	2.0556	67.4051	138.6	435.7449